Towards Chemoresistance Reduction in Laryngeal Cancer: Development of a chemoresistant laryngeal cell culture model for evaluating chemosensitizing strategies

by

Christian Rafael Moya García, BME, M.Phil.

Department of Biomedical Engineering

Faculty of Medicine and Health Sciences

McGill University

February 2024

A thesis submitted in conformity with the requirements
for the degree of Ph.D. in Biological and Biomedical Engineering

Acknowledgments

I would like to begin this acknowledgment by expressing my heartfelt gratitude to all those who have played a significant role in my doctoral training, a journey that took me from my homeland in Guadalajara, Mexico to the vibrant city of Montreal. This incredible academic expedition has been a transformative experience, and I am humbled and deeply thankful for the steady support and encouragement I have received along the way.

First and foremost, I want to acknowledge the invaluable support of my family. My parents, María and Rafael, have been my pillars of strength throughout my life. Their unwavering belief in my dreams and their sacrifices have been the driving force behind my pursuit of higher education. Your love and guidance have made me who I am today, and I dedicate this achievement to you.

To my siblings, Liz, Jaz, and Ray, your encouragement and understanding during this demanding journey have been a constant source of motivation. Your belief in my abilities has been a guiding light, and I am truly grateful for your support.

I would also like to extend my sincere gratitude to my thesis supervisors, Prof. Nicole Li-Jessen and Prof. Maryam Tabrizian, for their invaluable guidance, mentorship, and support. Your expertise, patience, and dedication to my success have been instrumental in shaping the direction of my research and my growth as a scholar. Your belief in my potential has pushed me to strive for excellence.

The academic and entrepreneurial communities at McGill and the city of Montreal have become a second home for me. I am thankful for the friendships that have enriched my life. The diverse and inclusive atmosphere of Montreal has broadened my horizons and deepened my understanding of the world.

I must acknowledge the diligent efforts of my friends and colleagues who have stood by me, provided invaluable insights, and offered their encouragement. Your presence in my life has made this journey all the more meaningful.

Furthermore, I would like to express my appreciation to the funding agencies and scholarship programs, including National Sciences and Engineering Research Council of Canada and McGill's Department of Biomedical Engineering, for their financial support, which made my doctoral studies possible. Your investment in my education has had a profound impact on my academic journey.

I am truly blessed to have had such an incredible support system throughout my doctoral studies. The completion of this thesis marks not just my personal achievement but a collective accomplishment of all those who have believed in me. I am filled with gratitude for the love, support, and opportunities that have been bestowed upon me. I look forward to contributing positively to both academic and entrepreneurial communities as well as society overall.

With profound gratitude,
Chris

Thesis Organization

This thesis is written in a manuscript-based structure with seven chapters as outlined below.

Chapter 1: provides an outline of the motivations, reasoning, and underlying rationale behind the study design, in addition to specific research objectives.

Chapter 2: provides a literature review on challenges in laryngeal cancer treatment, molecular pathways of chemoresistance, and drug delivery nanocarriers.

Chapter 3: is a copy of a published review paper titled "*In vitro models for Head and Neck Cancer: Current Status and Future Perspective"*. This manuscript reviews distinct head and neck cancer's tumor microenvironment features, 2D/3D *in vitro* models and the future prospect of advanced *in vitro* models.

Chapter 4: is a copy of a published original research paper titled "*Chitosomes Loaded with Docetaxel as a Promising Drug Delivery System to Laryngeal Cancer Cells: An In Vitro Cytotoxic Study*." This paper is about characterizing the physio-chemical features of docetaxel-loaded chitosomes and to evaluate their biological effects on laryngeal cancer and stromal cell cultures.

Chapter 5: is a copy of an original research paper now in preparation on *Towards a chemoresistant laryngeal cancer cell model: Cell sensitization study via transcriptomic analysis and tumor-on-a-chip devices*. This paper is about developing an in-house docetaxel-resistant laryngeal cancer cell model. RNA-sequencing and biological functional analyses were performed to validate this cell line model. A chemosensitizing study using metformin and docetaxel-loaded chitosomes was further tested on 2D culture and laryngeal-tumor-on-a-chip models composed of the resistant laryngeal cancer cells and stromal vocal fold fibroblasts.

Chapter 6: presents an overall discussion of research findings, study limitations and future prospects related to both docetaxel-resistant cell and laryngeal-tumor-on-a-chip models.

Chapter 7: summarizes the research contributions and directions in preclinical de-escalation strategies for laryngeal cancer treatment.

Table of Contents

List of Tables

List of Figures

List of Abbreviations

Akt – Serine/threonine-specific protein kinase B

DTX – Docetaxel

EMT – Epithelial to mesenchymal transition

DLS – Dynamic light scattering

DR-LSCC – DTX-resistant laryngeal squamous cell carcinoma

FTIR – Fourier-transform infrared spectroscopy

HIF-1α – Hypoxia-inducible factor 1-alpha

HNC – Head and Neck Cancer

HNSCC – Head and Neck Squamous Cell Carcinoma

HPV – Human papilloma virus

HVFF – Human vocal fold fibroblast

LA-HNSCC – Locally advanced head and neck squamous cell carcinoma

LC – Laryngeal Cancer

LSCC – Laryngeal squamous cell carcinoma

LSEC – Laryngeal squamous epithelial cell

mTOR – Mammalian target of rapamycin

NTA – Nanoparticle Tracking Analysis

PI3K – phosphatidylinositol 3-kinase

SEM – Scanning electron microscopy

TEM – Transmission electron microscopy

TNM – Tumor-lymph Node-Metastasis

TPF – Taxane, platinum-based and 5-fluoruracil

Abstract

The goal of this thesis project was to reduce the chemoresistance of laryngeal cancer cells to docetaxel drugs with an adjuvant treatment of metformin. Laryngeal squamous cell carcinoma (LSCC) is a subtype of head and neck cancer that critically affects daily activities of speaking, swallowing, and breathing. LSCC accounts for over 30% of all head and neck cancer cases globally on an annual basis, ranking second in prevalence after oral cancer. First-line chemotherapy for LSCC includes docetaxel, cisplatin, and 5-fluorouracil. Yet, chemoresistance remains a major challenge for patients with LSCC not associated with human papilloma virus infection, with about 50% of a 5-year overall survival rate. Systemic delivery of chemotherapeutics, either via a vein or an artery, is prone to induce deleterious side effects including high toxicities and locoregional extravasation. De-escalation strategies like the use of chemosensitizers were proposed to reduce long-term toxicities while increasing drug bioavailability at the tumor site. Metformin, an antiglycemic agent, was shown to inhibit cancer cells' metabolic activity via the mammalian target of rapamycin; thus, enhances chemotherapy effects on tumor reduction.

First, we proposed to load docetaxel into lipid nanocarriers to shield docetaxel, a lipophilic drug, from early degradation that led to increased drug availability. A chitosan mucoadhesive coating on lipid nanocarriers was used to enhance drug retention within tumors. Such a coating was crucial because interstitial fluids can rapidly wash away drugs. The mucoadhesive coating helped retain docetaxel within the tumor, facilitating localized treatment. Study results confirmed that chitosan-coated lipid nanocarriers, i.e., chitosomes, were successfully taken up into the cytoplasm of human LSCC, demonstrating effective docetaxel delivery by the nanocarriers. Docetaxel-loaded chitosomes exhibited significantly higher cytotoxicity in LSCC when compared to stromal laryngeal fibroblasts (30% vs. 10%; $p < 0.05$). No hemolytic effects were observed on human red blood cells and thus support potential intra-arterial delivery of these chitosan-based nanocarriers.

Next, considering the resistant nature of laryngeal cancer, we developed a docetaxel-resistant LSCC model by using an in-house docetaxel escalating exposure protocol for 4 months. Cells were compared with known chemoresistance genotypes and phenotypes via transcriptomic and functional analyses. Compared to control groups, chemoresistant-specific pathways of PI3K/mTOR and autophagy were upregulated in docetaxel-exposed LSCC, which matched the

literature of chemoresistance development in aggressive tumors. Functional cytotoxic experiments were further performed by subjecting the cells to docetaxel treatments. Results confirmed that the cells showed 36% more viability compared to the LSCC, indicating these cells acquired chemoresistance and were less responsive to the drug.

Finally, we evaluated the effect of combined metformin and docetaxel therapy in a microfluidic system. We developed a 2-channel laryngeal-tumor-on-a-chip model by co-culturing docetaxel-resistant LSCC and stromal laryngeal fibroblasts. With the dynamic perfusion, hypoxic gradient was created within the chips as *in vivo* laryngeal tumor core. The migration of stromal laryngeal fibroblasts into chemoresistant LSCC was observed toward the hypoxic gradient. Moreover, the proposed chip cultures were exposed to metformin and docetaxel-loaded chitosomes. Increased cell death was observed in stromal fibroblasts and cancer cells, compared to drug alone controls (55% vs. 15%; $p < 0.05$) 5 days after the treatment. Chitosome uptake was noticed after 6-hr inspection in both cell groups. This thesis presented a reliable and representative *in vitro* model of chemoresistant laryngeal cancers that will contribute to developing new therapeutic strategies for reducing drug resistance and tumor recurrence.

Résumé

L'objectif de cette thèse a été de réduire la chimiorésistance des cellules cancéreuses du larynx aux médicaments à base de docétaxel et la metformine. Le carcinome épidermoïde du larynx (CELC) est un sous-type du cancer de la tête et du cou qui affecte gravement les activités quotidiennes telles que parler, avaler et respirer. Le CELC représente plus de 30% de tous les cas de cancer de la tête et du cou dans le monde par an La chimiothérapie pour le CELC comprend le docétaxel, le cisplatine et le 5-fluorouracile. Cependant, la chimiorésistance demeure un défi majeur pour les patients atteints de CELC non associé à une infection par le virus du papillome humain, avec 50% de taux de survie globale à cinq ans. L'administration systémique de la chimiothérapie, par voie veineuse ou artérielle, est susceptible d'entraîner des effets secondaires, notamment des toxicités élevées et une extravasation locorégionale. L'utilisation de chimiosensibilisants a été proposée pour réduire les toxicités à long terme tout en augmentant la biodisponibilité des médicaments dans la tumeur. La metformine a été démontrée pour inhiber l'activité métabolique des cellules cancéreuses liée à la mTOR, améliorant ainsi l'efficacité de la chimiothérapie dans les tumeurs.

Nous avons proposé de charger le docétaxel dans des nanovecteurs lipidiques pour le protéger de la dégradation précoce. Un revêtement mucoadhésif en chitosane sur les nanovecteurs a été utilisé pour améliorer la rétention du docétaxel dans les tumeurs. Le revêtement mucoadhésif a aidé à maintenir le docétaxel dans la tumeur, facilitant le traitement localisé. Les résultats de l'étude ont confirmé que les nanovecteurs lipidiques enrobés de chitosane, c'est-à-dire les «chitosomes», étaient efficacement pris dans le cytoplasme du CELC humain. Les chitosomes chargés de docétaxel ont montré une cytotoxicité plus élevée dans le CELC par rapport aux fibroblastes du larynx (30% vs. 10%; $p < 0.05$). Aucun effet hémolytique n'a été observé sur les globules rouges humains, soutenant ainsi une éventuelle administration intra-artérielle de ces chitosomes.

Ensuite, nous avons généré un CELC résistant au docétaxel en utilisant un protocole d'exposition progressive au docétaxel pendant 4 mois. Les cellules ont été comparées à des phénotypes de chimiorésistance connus par les analyses transcriptomiques et fonctionnelles. Par rapport aux groupes témoins, les voies spécifiques de la chimiorésistance du PI3K/mTOR et de l'autophagie ont été surexprimées dans le CELC exposé au docétaxel. Des expérimentations cytotoxiques ont ensuite été réalisées en soumettant les cellules à des traitements au docétaxel. Les résultats ont

confirmé que les cellules avaient acquis une chimiorésistance et étaient 36% moins sensibles au médicament.

Enfin, nous avons évalué l'effet de la thérapie combinée de metformine et de docétaxel avec des systèmes microfluidiques. Nous avons développé des modèles de cancer du larynx sur puce à 2 canaux en co-cultivant des CELC résistants au docétaxel et des fibroblastes du larynx. Grâce à la perfusion dynamique, un gradient hypoxique a été créé dans les puces simulant le noyau tumoral laryngé *in vivo*. La migration des fibroblastes vers les CELC résistants a été observée en direction du gradient hypoxique. De plus, une perfusion de 12 minutes de chitosomes chargés de docétaxel a été réalisée pour imiter l'administration intra-artérielle comme en pratique clinique. Une augmentation de la mort cellulaire des fibroblastes et CELC résistants ont été observé après les injections combines de metformine et de chitosomes par rapport aux témoins medicamenteux seuls (55% contre 15% ; $p < 0,05$) 5 jours après le traitment. Les chitosomes ont été intériorisé par les deux types cellulaires. Cette thèse a présenté un nouveau modèle *in vitro* des cancers du larynx résistants à la chimiothérapie, visant à améliorer les approches thérapeutiques ciblant la résistance aux médicaments et la récurrence tumorale.

Contribution to original knowledge

This thesis provides, for the first time, the development of chitosomes to enhance DTX's bioavailability for laryngeal cancer treatment. To test the DTX-loaded chitosomes and chemosensitizing strategies, we developed a DTX-resistant laryngeal cancer cell model using a step-wise intermittent protocol that experimentally induce drug resistance. From analyzing such a model via RNA-sequencing, we identified potential molecular mechanisms associated with DTX resistance that can potentially be anti-resistant drug targets in the future. Finally, we developed a laryngeal-tumor-on-a-chip platform that emulated tumor hypoxia via the co-culture of in-house DTX-resistance cancer cells and vocal fold stromal fibroblasts. This *in vitro* study provided initial evidence on the benefit of a chemosensitizing agent, namely, metformin, that could potentially help restore the tumor sensitivity to DTX drug.

Contribution of Authors

Publications:

1. Published Review Article: *In vitro models for head and neck cancer: Current status and future perspective.*

   This manuscript was published in Frontier in Oncology on the 3rd of August 2022. DOI: doi.org/ 10.3389/fonc.2022.960340

   Christian R. Moya-Garcia, Hideaki Okuyama, Nader Sadeghi, Jianyu Li, Maryam Tabrizian, and Nicole Y. K. Li-Jessen.

   C.M.-G.: Conceptualization, visualization, writing-original draft, reviewing and editing.

   H.O.: visualization, writing-reviewing and editing.

   N.S.: writing-reviewing and editing.

   J.L.: writing-reviewing and editing.

   M.T.: Conceptualization, visualization, writing-original draft, reviewing and editing, supervision.

   N.L.-J.: Conceptualization, visualization, writing-original draft, reviewing and editing, supervision, funding acquisition.

   All authors contributed to the article and approved the submitted version.

2. Published Original article: *Chitosomes Loaded with Docetaxel as a Promising Drug Delivery System to Laryngeal Cancer Cells: An In Vitro Cytotoxic Study.*

   This manuscript was published in the International Journal of Molecular Sciences on the 8th of June 2023. DOI: doi.org/ 10.3390/ijms24129902

   Christian R. Moya-Garcia, Nicole Y. K. Li-Jessen, and Maryam Tabrizian.

   C.R.M.-G.: conceptualization, visualization, writing-original draft, and writing-reviewing and editing.

   N.Y.K.L.-J.: conceptualization, visualization, writing-original draft, writing-reviewing and editing, supervision, funding acquisition, and project administration.

   M.T.: conceptualization, visualization, writing-original draft, reviewing and editing, supervision, funding acquisition, and project administration.

   All authors have read and agreed to the published version of the manuscript.

3. Submitted Original article: *Establishment of a Chemoresistant Laryngeal Cancer Cell Model to Study Chemoresistance and Chemosensitization Responses Via Transcriptomic Analysis and a Tumor-On-A-Chip Platform*

   This manuscript is now in preparation.

   Christian R. Moya-Garcia, Meghana Munipalle, Alain Pacis, Nader Sadeghi, Maryam Tabrizian, and Nicole Y. K. Li-Jessen

   C.R.M.-G.: conceptualization, data plotting, visualization, writing-original draft, and writing-reviewing and editing.

   M.M.: reviewing and editing.

   A.P.: data plotting, visualization, reviewing and editing.

   N.S. reviewing and editing.

   M.T.: conceptualization, visualization, writing-original draft, reviewing and editing, supervision, funding acquisition, and project administration.

   N.Y.K.L.-J.: conceptualization, visualization, writing-original draft, writing-reviewing and editing, supervision, funding acquisition, and project administration.

Chapter 1. Thesis Motivation and Aims

The primary causes of head and neck cancers (HNC) that are not associated with human papilloma virus infection, which affects the oral cavity, hypopharynx, larynx, and oropharynx are typically alcohol and tobacco misuse [1]. Due to the widespread exposure of epithelium in the aerodigestive tract to these carcinogens [1], individuals with HNC face the potential of having multiple primary tumors simultaneously in this region [1]. Treatment of HNC causes toxic side effects when chemotherapy is administered intra-venously or -arterially especially for those who are overtreated [2]. The projected cost of HNC worldwide is calculated to be $535 billion USD for incidents occurring between 2018 and 2030 [3]. Patients with laryngeal cancer (LC) not only bear cancer-related challenges but also emotional hurdles leading to suicidal risk [4]. For patients with locally advanced LC, a combined approach of surgery and chemotherapy has been proposed for patient survival and surgical laryngeal preservation [1, 5]. To treat LC, health care professionals follow established guidelines for primary treatment as those described by Pfister *et al* [1, 5]. However, existing challenges with chemotherapy in HNC treatment relate (1) to de-escalating the cytotoxic overtreatment of systemic/locoregional chemotherapy and potential extravasation, and (2) overcoming chemoresistance in patients [2]. Chemosensitizing strategies have been sought as a de-escalation strategy for cancer patients [6]. Particularly, inhibitor agents that target mTOR were proposed to sensitize resistant cancer cells and improve chemotherapy, which results in tumor size reduction in HNC [6].

1.1 Thesis Rationale

To circumvent the problem with chemotherapy drugs being washed away by tumoral interstitial flow, we proposed to implement mucoadhesive chitosomes as drug carriers to improve the bioavailability of docetaxel (DTX) in the tumor, facilitating localized treatment. Chemosensitizing strategies have been sought as a de-escalation strategy for cancer patients [5]. Particularly, inhibitor agents that target mTOR were proposed to restore the drug sensitivity of resistant cancer cells, which results in a reduction of tumor size and improved treatment outcome for patients with HNC [6]. We thus proposed to metformin (MTF) that is an FDA-approved mTOR inhibitor drug for diabetes treatment, meaning its use is safe for repurposing it as chemosensitizer. Since there is not a chemoresistant laryngeal cancer cell model available, we proposed an in-house docetaxel stepwise exposure protocol to induce DTX resistance in a commercially available laryngeal cancer

cell line. Lastly, given that 2D conventional monocultures are inadequate to emulate *in vivo* conditions, we proposed to leverage microfluidic culture techniques, tumor-on-a-chip micro-physiological systems, to mimic the hypoxic tumor core and deliver our proposed combination therapies of MTF and DTX.

1.2 Thesis Aims

The overall goal of this thesis was to develop a new *in vitro* model to investigate a de-escalation strategy on chemoresistant laryngeal cancer (**Figure 1-1**). To achieve this goal, an integration of biological and biomedical engineering concepts was used to: (1) encapsulate and characterize DTX into chitosomes as cytotoxic treatment for laryngeal cancer cells; (2) develop and characterize a DTX-resistant laryngeal cancer cell model for genotypic profiling and therapy testing; (3) study the sensitivity of the resistant cancer cell model to the combined MTF/DTX-loaded chitosomes therapy via laryngeal-tumor-on-a-chip inspections.

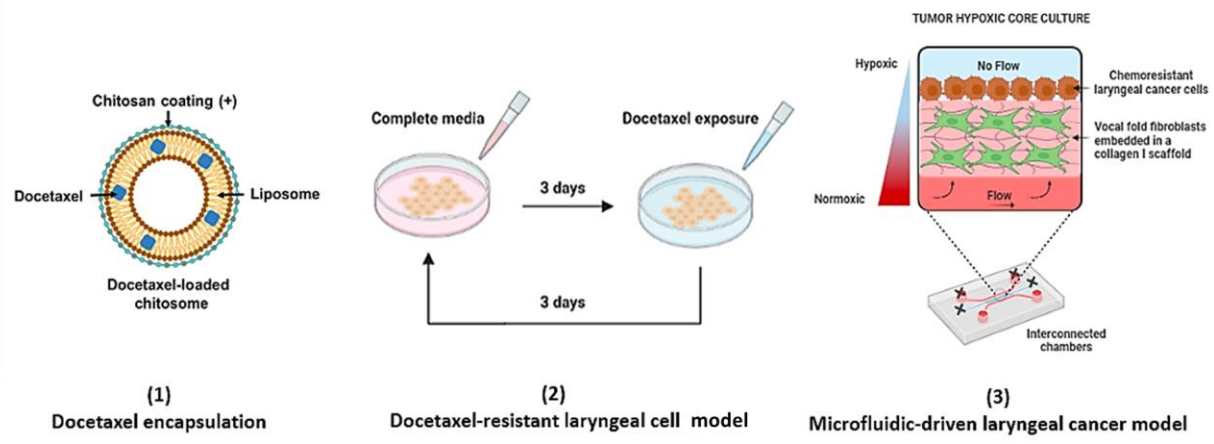

Figure 1-1. Overview and Specific Aims of the Thesis Project.

Aim 1. Encapsulate DTX into mucoadhesive chitosomes

We proposed to coat chitosan onto DTX-loaded nano-liposomes to improve mucoadhesiveness and DTX drug release profile for localized mucoadhesive laryngeal treatment. Transmission electron microscopy, nanoparticle tracking analysis, Fourier transform infrared spectroscopy were used for physicochemical characterization of nano-liposomes. Chitosan coating was evaluated using immersion analysis into mucin solution and its absorbance readouts. Cytotoxic studies were

assessed via LIVE/DEAD staining and absorbance analysis. We expected that DTX-loaded chitosomes would show higher toxicity to laryngeal cancer cells compared to that of free-form DTX treatment.

Aim 2. Develop and characterize an in-house DTX-resistant laryngeal cell line

We proposed to use a step-wise intermittent protocol to experimentally induce DTX resistance in a commercially available laryngeal cancer cell line. RNA-sequencing and functional analysis were used to characterize the presumed chemoresistance in this new in-house laryngeal cancer cell line. A chemosensitizing study using MTF was performed on 2D cultures to verify the presumed resistant phenotype in this resistant cancer cell line.

Aim 3. Evaluate a chemosensitizing strategy using laryngeal-tumor-on-a-chip platforms

The in-house DTX-resistant cancer cells and vocal fold stromal fibroblasts were co-cultured on a microfluidic device to mimic the hypoxic tumor core. The laryngeal tumor-on-a-chip was a 2-channel microfluidic system and was subjected to a priming of MTF sensitization followed by DTX drug exposures. Stromal cells migration, expression of hypoxic and oxidative stress markers, and cell viability were evaluated using microscopy and biochemical assays. We expected that such a platform would enable a better understanding of tumor-stromal interactions related to drug sensitivity, as well as, testing new drug strategies for reducing chemoresistance.

1.3 References

1. Pfister DG, Spencer S, Adelstein D, et al. Head and neck cancers, version 2.2020. JNCCN J Natl Compr Cancer Netw. 2020;18(7):873-898. doi:10.6004/jnccn.2020.0031

2. Aigner KR, Selak E, Aigner K. Short-term intra-arterial infusion chemotherapy for head and neck cancer patients maintaining quality of life. J Cancer Res Clin Oncol [Internet]. 2019;145(1):261–8. Available from: http://dx.doi.org/10.1007/s00432-018-2784-4

3. Patterson RH, Fischman VG, Wasserman I, Siu J, Shrime MG, Fagan JJ, Koch W, Alkire BC. Global burden of head and neck cancer: economic consequences, health, and the role of surgery. Otolaryngology–Head and Neck Surgery. 2020 Mar;162(3):296-303.

4. Saghafi E, Andås CA, Bernson J, Kjeller G. Patients' experiences of adverse symptoms, emotions, and coping strategies in connection to treatment of head and neck cancer - an interview study. BMC Oral Health. 2023;23(1):1–13.

5. Pfister, D.G., Ang, K.K., Brizel, D.M., Burtness, B.A., Cmelak, A.J., Colevas, A.D., Dunphy, F., Eisele, D.W., Gilbert, J., Gillison, M.L. and Haddad RI. Head and neck cancers. JNCCN J Natl Compr Cancer Netw. 2011;9(6):596–650. doi:10.6004/jnccn.2008.0051

6. Maloney SM, Hoover CA, Morejon-Lasso L V., Prosperi JR. Mechanisms of taxane resistance. Cancers (Basel). 2020;12(11):1–57.

Chapter 2. Introduction

Head and neck cancer (HNC) is the 6th most common type of cancer [1]. Laryngeal cancer (LC), a sub-type of HNC only preceded by that of oral cancer [2]. LC had an annual incidence rate of 177,422 worldwide in 2019 [2] that is estimated to increase 43% by 2035 [3]. The classification of LC cancer stage is based on the invasiveness of the tumor using the Tumor-lymph Node-Metastasis scheme (**Table 2-1**) [4,5]**.** Depending on the stage of the tumor, surgery, radiation therapy, chemotherapy and immunotherapy may be prescribed to HNC patients (**Table 2-2**).

Table 2-1. Tumor-lymph Node-Metastasis (TNM) classification of LC (glottis).

T	Description	N	Description	M	Description
Tx	Carcinoma cannot be evaluated	**Nx**	Lymph node cannot be evaluated		
Tis	Carcinoma in situ	**N0**	No regional lymph node metastasis	**M0**	No distant metastasis
T1	Tumor limited to VFs	**N1**	Ipsilateral lymph node metastasis, <3cm, ENE (-)		
T1a	One fold				
T1b	Both folds				
T2	Expansion to supra/sub glottic levels	**N2**	Lymph node metastasis, <6cm, ENE (-)		
		N2a	Single ipsilateral node metastasis, <6cm, ENE (-)		
		N2b	Multiple ipsilateral nodes metastases, <6cm, ENE (-)		
		N2c	Bilateral or contralateral lymph nodes metastases, <6cm, ENE (-)		
T3	Vocal fold fixation (invasion of lymph nodes and paraglottic space)				
T4	Further invasion	**N3**	Lymph node metastasis, >6cm		
T4a	Anterior invasion	**N3a**	Lymph node metastasis, >6cm, ENE (-)		

T4b	Posterior invasion	**N3b**	Lymph node metastasis, >6cm, ENE (+)		
T4c	Other organs			**M1**	Distant metastasis

Extra-nodal Extension (ENE), combination of TNM stages may be present depending on the patient's clinical and pathological case

The standardized mortality rate, ratio of deaths, of LC is 2.6% in males and 0.3% in females [4]. Also, the 5-year survival rate of HPV^- HNC/LC remains less than 50% for the past three decades [3,6]. Further, chemoresistance, which causes the cancer relapse and metastasis, severely hampers the improvement of clinical outcome in patients with HNC/LC. Various novel strategies such as combinatorial approaches using cancer vaccine platforms with novel immunomodulatory methods and standard-of-care [7,8] have been proposed to improve the survival rate for patients with cancers [9]. In particular, biomaterials are proposed to deliver chemotherapy drugs to the tumor microenvironment in a controlled and sustained manner overcoming the impediment of chemoresistance and systemic toxicity [10,11] .

Table 2-2. Current therapeutic approaches of laryngeal cancer.

Treatment	Approach	General Impression	Complications
Surgery	Cordectomy	Applied to precancerous lesions [4] Reduced morbidity [2]	Inadequate final margin [19]
	Transoral surgery	Applied to early-stage cancers [12] Organ preservation [12]	Inadequate final margin [19]
	Total laryngectomy	Applied to advance-stage cancers [4] High restoration after procedure [2]	Tested in older patients only [13] Significant morbidity [12]
Radiotherapy	Dose 60-70 Gy	Aim to preserve vocal quality [4] Applied to early-stage cancers [13] Organ preservation [12] Adjuvant treatment [13]	Cost [4] Edema [4] Inflammation, fibrosis [4,14]
Chemotherapy	Induction (Laryngeal conservation program), concomitant	Applied to advance-stage cancers [4] Adjuvant treatment [13]	Systemic treatment [2,15] High toxicity [13]

	(patients refusing total laryngectomy), exclusive (under study) chemotherapy		
Immunotherapy	Cetuximab (anti-EGFR)	Applied to recurrent/metastatic LC [14,16]	Cetuximab - Skin allergic reaction [14]
	Pembrolizumab and Nivolumab (anti-PD1, checkpoint inhibition)		Checkpoint inhibitor - Patients may not overcome the disease after checkpoint inhibition treatment[16]. Inflammation found in other organs, diarrhea, physical fatigue and skin rash. [17]

2.1 Locally advanced laryngeal cancer: clinical challenges and emerging treatments

For the surgical approaches of locally advanced head and neck squamous cell carcinoma (LA-HNSCC) comprising the resection of whole larynx were used to ensure patient survival as the primary intention [18]. On the other hand, radiotherapy and chemotherapy are used in combination with cold knife surgery to preserve the larynx and its functionality [18–20]. Patients with unresectable HNC/LC, chemotherapy has been shown to make initially unresectable carcinomas operable [21,22] and thus may ease the surgical margin decision for larynx preservation [23,24].
For induction chemotherapy, drugs are usually administered intravenously. Despites its benefits for metastatic treatment, chemotherapy carry risks of overtreatment, and subcutaneous/perivascular extravasation [25,26]. As note, the median time of survival after locoregional recurrence or metastatic disease is only six months [27]. Thus, locoregional intra-arterial administration of chemotherapeutics was suggested to address the adverse effects experienced systemically by delivering the drug directly into tumor supplying arteries, instead of distributing the chemotherapeutic agents throughout the entire body [28–30]. However, the intra-arterial delivery may still cause high toxic extravasation damage in the surrounding tumor region [29,30].

Induction chemotherapy application on LA-HNSCC (stage T3/T4) relies on the use of taxane, platinum-based and 5-fluorouracil, in which this drug combination is known as TPF [21,31]. Docetaxel (DTX) alongside with paclitaxel are part of taxane family drugs whose tubulin-directed antimitotic and lipophilic effects hinder the mitotic spindle development by stabilizing pre-existing microtubules [32]. Platinum-based drugs, such as cisplatin, are alkylating and slightly hydrophilic

agents that suppress DNA synthesis and mitosis by interacting with N7 sites on purines leading to apoptotic cell death [33]. 5-fluorouracil drug is an antimetabolite and slightly hydrophilic agents that merge with DNA and RNA strands leading to apoptotic cell death [34].

TPF drugs can kill fast-proliferating cells but carry risks of systemic toxicity. To overcome this toxicity, adjuvant multimodality treatments such as sequential and concurrent chemoradiotherapies may be considered to improve the efficacy of chemotherapy. For example, DTX has been used in combination with cisplatin as a neo-adjuvant chemotherapy treatment for HPV^+ oral squamous cell carcinomas [35]**.** Pathological complete remission (absence of cancer in sample) at the primary (72%) and nodal (57%) oral squamous cell carcinoma tumors were reported, which has potential of improving the complete surgical resection with clear-of-cancer resection margins. In case, docetaxel extravasation occurs due to intravenous infusion causing tissue necrosis and bullae (large blisters of the skin), intralesional steroids as hydrocortisone with topical betamethasone are recommended [26].

In addition to induction chemotherapy, concurrent chemo-radiotherapy is considered as a standard-of-care for LA-HNSCC [36]. This regimen may improve the locoregional outcome in comparison to the sole induction chemotherapy [37]. For instance, TPF/concurrent chemo-radiotherapy regimen was reported to improve the progression free survival in LA-HNSCC patients [38]. Unfortunately, systemic toxicity is still associated with concurrent chemo-radiotherapy implementation [36]. As such, instead of using an intravenous delivery method, a locoregional intra-arterial administration may serve one viable option to reduce systematic cytotoxicity and chemoresistance in order to improve the safety and efficacy of current HNC/LC chemotherapy.

2.2 Molecular mechanisms associated with chemoresistance

Hypoxia and epithelial to mesenchymal transition (EMT) are two of molecular mechanisms known to chemoresistance in HNSCC tumors [39,40]. Regarding hypoxia, tumor cells that adapt to hypoxic environments become more aggressive and present radio- and chemo-resistant phenotypes [41]. The PI3K/Akt/mTOR and hypoxia-inducible factor 1 (HIF-1α) signaling pathways are central in the role of tumor hypoxia [42–45]. PI3K/Akt/mTOR pathway is involved in protein synthesis, cell proliferation, survival, multiple drug resistance mechanisms and hypoxia in cancer cells [46] (Figure 2-1). HIF-1α pathway is related to mitochondrial activity, antagonized apoptosis and

autophagy that promotes a hypoxic environment in tumor [41]. In addition, hypoxia leads to the aberrant angiogenesis in tumor microenvironment [42,47]. The poor vasculature state has implications in limiting oxygen and nutrient supply, as well as decreasing lipophilic chemotherapy drug delivery that restricts chemotherapy response.

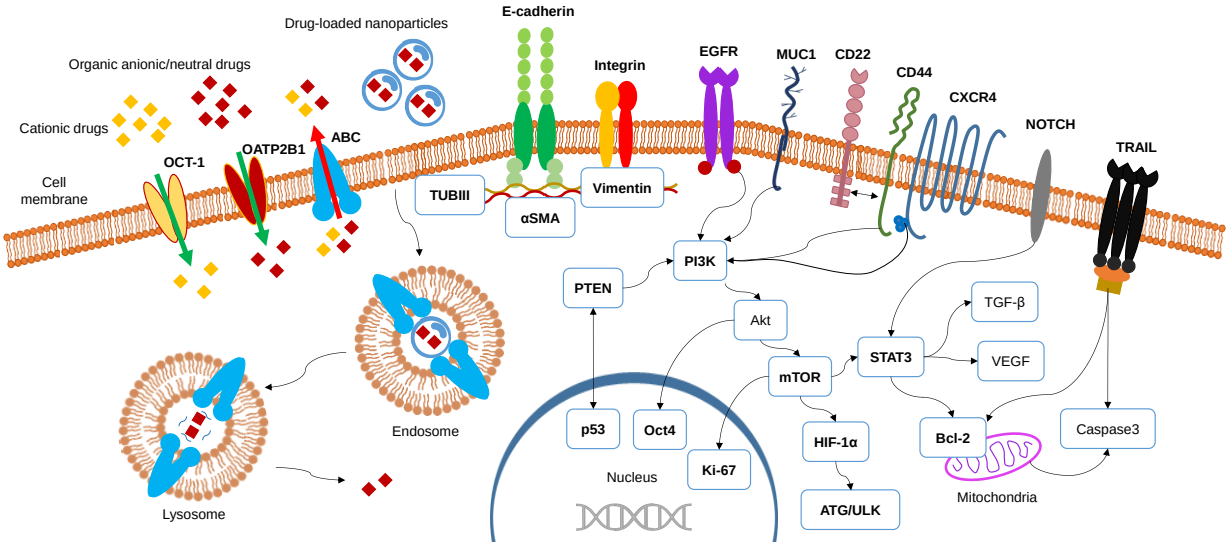

Figure 2-1. Chemoresistance markers related to the mTOR pathway.

EMT may also have a role in promoting chemoresistance. During cancer progression, epithelial cells shift into a mesenchymal phenotype [48]. Endothelial cells secrete epidermal growth factor that enhances tumorous motility and stemness [49]. Fibroblasts may differentiate from endothelial and epithelial cells during EMT and involve in the growth and maintenance of tumor through autocrine and paracrine signaling [48,50]. One clinical study showed that tumor hypoxia promoted laryngeal cancer cell invasion through EMT [51]. Again, activation of PI3K/Akt/mTOR signaling pathway may contribute to the EMT-hypoxia relation [51,52].

Aside from EMT-hypoxia relation, the PI3K/Akt/mTOR signaling pathway promotes drug resistance via autophagy, which is a cytoplasmatic proteolytic process of macromolecules and organelles [53,54]. Autophagy deters taxane treatment via activation of HIF1-α in cancer cells [55]. In particular to LC, increased autophagy relates to a poor clinical prognosis [54]. Upregulated autophagy may be suppressed by inhibiting the mTOR complex that in turn downregulates

autophagy-related ATG13 and ULK1 genes [53]. For that reason, impaired autophagy is an intracellular process to regulate to improve taxane treatment in LC.

Further, the upregulation of the ATP-binding cassette (ABC) transporters is another molecular mechanism of chemoresistance in HNSCC [56,57] linked to upregulated PI3K/Akt/mTOR pathway [58]. ABC transporters, i.e., ABCB1, are drug efflux pumps that reduce intracellular drug concentrations causing treatment failure [56,58]. Specific to DTX and paclitaxel, ABCC3 overexpression is associated to low treatment response in oral squamous cell carcinoma and other types of cancers [59]. To improve prognosis, upregulated ABC transporters may be downregulated by inhibition of the mTOR pathway [58].

Besides, mucin pathway induces chemoresistance in concordance to enhanced expression of ABC transporters [60] and increased hypoxia in HNSCC [61]. Mucins are O-glycoproteins whose role relates to cellular adhesion, differentiation, and protection/immunity of epithelial cells [60]. Mucin-related genes, i.e., MUC1 and MUC4, are aberrantly expressed in LSCC associated with treatment resistance and invasiveness [62]. MUC1 activates the PI3K/Akt/mTOR pathway via the glycolytic flux intrinsic in metabolic homeostasis [63]. Thus, a target therapy of PI3K/Akt/mTOR pathway, linked to EMT-hypoxia-autophagy and mucin-related molecular mechanisms, may help circumvent chemoresistance in locally advanced HNC/LC.

2.3 Potential use of chemosensitizer to reduce chemoresistance

Activation of PI3K/Akt/mTOR signaling pathway is associated with radio- and chemo-resistance in HNSCC patients [64–66]. Recently, inhibition of the PI3K/Akt/mTOR signaling pathway has been investigated to chemosensitize and de-escalate current HNSCC chemotherapy overtreatment [64]. For example, metformin (MTF) is a mammalian target of rapamycin (mTOR) inhibitor and an FDA-approved drug for patients with type 2 diabetes [67]. Although MTF was originally prescribed for diabetic patients, MTF was evaluated of its potential as a cancer drug. MTF anti-cancer effect may be attributable to the inhibition of the mTOR and activation of the AMPK signaling pathways (**Figure 2-2**). In particular, at 1-20mM dose of MTF, the drug promoted the apoptosis of esophageal squamous cell carcinomas [68] and inhibited the proliferation of oral squamous cell carcinoma in vitro [69]. MTF was also used to sensitize laryngeal cancer cells to 5-fluorouracil, denoting the potential as adjuvant treatment [70]. Although discrepancy regarding

the effect of MTF on non-diabetic cancer patients exist [71], a higher dose of MTF may be required to adjust for anti-chemoresistance purposes [72]. MTF regimen may have potentials of reducing chemoresistance in taxane treatment [73,74]. Clinical trial data suggested the positive efficacy of MTF chemosensitizing effect of DTX treatment on resistant metastatic prostate [75], and gastric [76] cancers.

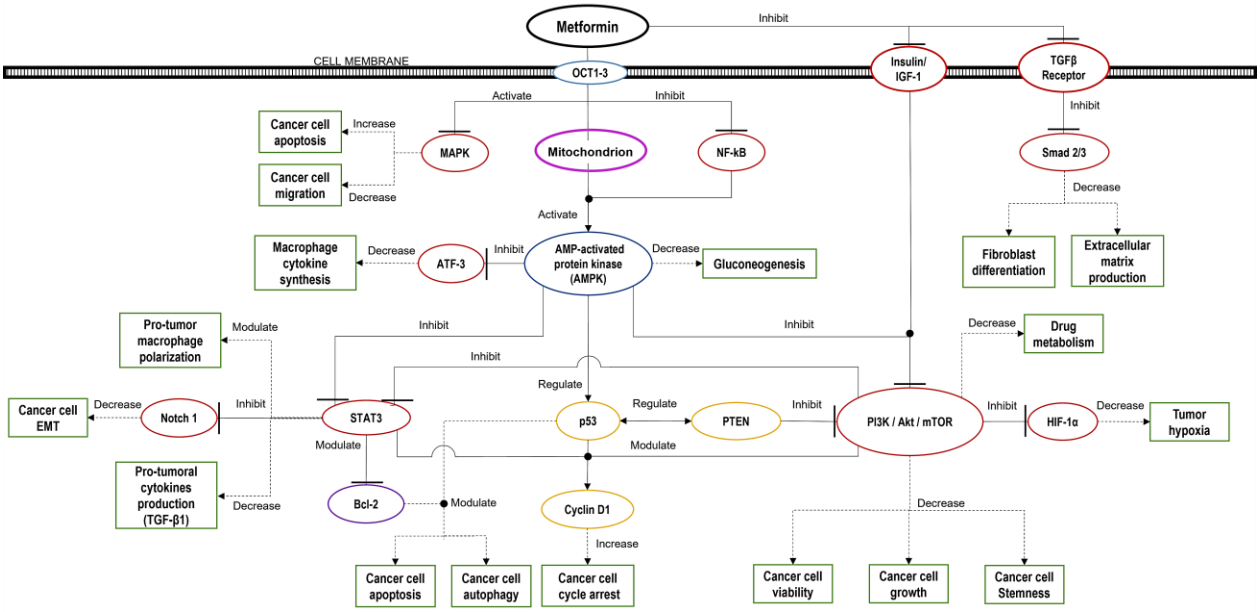

Figure 2-2. MTF was reported to inhibit mTOR through the AMPK activation and the transcription factor NF-κB suppression. mTOR is a key molecule in the PI3K/Akt and AMPK pathways. mTOR is a serine/threonine kinase that is important in cell metabolism, growth, proliferation and survival [78]. Oncogenic-mutated mTor molecules were found to promote cancer progression [78]. MTF indirectly causes an anti-tumor effect by lowering the glucose and insulin metabolism resulting in suppressing the tumor cell growth [79,80]. Inhibitions of the mTOR and NF-κB have been reported *in vitro* and *in vivo* studies of cutaneous squamous cell [81] and primary hepatocellular cell [82] carcinomas. MTF was reported of its potential of inhibiting cancer cell growth in gastric [83], breast [84] and pancreatic [85] neoplasia in vivo and in vitro studies. Chowdhury et al. assessed the MTF effect on 19 cancer cell lines presenting Organic Cation Transporters 1–3 (OCT 1-3) [86]. Their results showed reduced hypoxic tumor fractions in all cell lines after MTF treatment. MTF has potential of mitigating the gene expression of HIF-1α and proliferative activity in oral squamous cell carcinoma [87,88]. Low concentrations of MTF were reported to downregulate stemness markers on oral squamous cell carcinoma [80]. Furthermore, MTF is likely to reverse the EMT on breast [89] and thyroid [90] cancers though inhibition of the mTOR pathway.

Aside from hypoxia-related chemoresistance markers, EMT and stemness markers (**Table 2-3**) such as Notch1 has a role in taxane resistant in HNSCC [65]. As observed in both *in vitro* and *in*

vivo setting HNSCC expressing upregulated Notch1 demonstrated increased resistance to both DTX and paclitaxel. MTF has also shown potential of improving chemotherapy treatment through mitigating EMT and stemness mechanism on oral squamous cell carcinomas [77]. For those reasons, adjuvant MTF may benefit the treatment of laryngeal cancer.

Table 2-3. Chemoresistance markers of all cancers. EMT - Epithelial-mesenchymal transition

Molecule		**Location**	**Chemoresistance association**	**Regulation**
Akt[43,45,52,64,65,91]	Serine/threonine protein kinase B	Nucleoplasm - microtubule	Autophagy / Stemness / EMT / Tumor hypoxia	Upregulated
Bcl-2[45,65,91]	B-cell lymphoma 2	Mitochondrial membrane	Apoptosis / Autophagy / Stemness / Tumor hypoxia	Downregulated
Bcl-xL[45,65,91]	B-cell lymphoma extra large	Mitochondrial membrane	Apoptosis / Autophagy / Stemness / Tumor hypoxia	Upregulated
Beclin 1[91]		Cytoplasm	Apoptosis / Autophagy / Stemness / Tumor hypoxia	Downregulated
CD44[52,65,91]	Cluster of differentiation 44	Cell membrane	Stemness	Upregulated
CD133[91]	Cluster of differentiation 133	Cell membrane	Epithelial-mesenchymal transition	Upregulated
CD147[91]	Cluster of differentiation 147	Cell membrane	Epithelial-mesenchymal transition	Upregulated
Cyclins [45,65,92]		Nucleoplasm	Epithelial-mesenchymal transition	Upregulated
CYP3A5[65]	Cytochrome P450 family / enzyme	Cytoplasm	Tumor hypoxia / Drug metabolism	Upregulated
E-cadherin[52,65,91,92]		Cell junctions	Epithelial-mesenchymal transition	Downregulated

EGFR[43,45,52,64,65,91]	Epidermal growth factor receptor	Cell membrane	Tumor hypoxia	Upregulated
Erk1/2[45,65,91]	Extracellular signal-regulated kinase	Cytoplasm	Tumor hypoxia	Upregulated
GLUT-1[43]	Glucose transporter 1	Cell membrane	Tumor hypoxia	Upregulated
HIF-1α [43,45,52,57,65,91]	Hypoxia-inducible factor 1α	Nucleoplasm	Tumor hypoxia	Upregulated
JNK[43,45,65,91]	c-Jun N-terminal kinase	Cytoplasm	Tumor hypoxia	Upregulated
Ki-67[43,45,92]		Nucleoplasm	Tumor hypoxia	Upregulated
MAPK[45,64,65,91]	Ras-mitogen-activated protein kinase	Cytoplasm	Tumor hypoxia	Upregulated
mTOR[43,45,52,64,65,91]	Mammalian target of rapamycin	Cytoplasm	Autophagy / stemness / EMT / Tumor hypoxia	Upregulated
Nanog[52,65,91]		Nucleoplasm	Epithelial-mesenchymal transition	Upregulated
N-cadherin[91]		Cell junctions	Epithelial-mesenchymal transition	Upregulated
NFκB[65,91]	Nuclear factor κB	Intracellular	Tumor hypoxia	Upregulated
Notch1[52,65,91]	single-pass transmembrane receptor	Cell membrane	Stemness / EMT	Upregulated
p53[43,52,65,91]	Tumor suppressor p53	Intracellular	Tumor hypoxia	Upregulated
PI3k[43,45,52,64,65,91]	Phosphatidylinositol 3-kinase	Intracellular	Autophagy / Stemness / EMT / Tumor hypoxia	Upregulated
P-gp (MDR1, ABCB1, ABCC10)[57,65,91]	P-glycoprotein (Multidrug resistance protein 1, ATP-binding cassette families)	Cell membrane	EMT / Tumor hypoxia	Upregulated
PTEN[43,45,52,64,65,91]	Tumor suppressor PTEN		Stemness / Tumor hypoxia	Downregulated

STAT3[52,65,93]	Signal transducer and activator of transcription 3	Intracellular	Tumor hypoxia	Upregulated
Survivin[65,91]		Mitotic structure	Stemness	Upregulated
TGF-β[43,52,65,91]	Transforming growth factor β	Cytoplasm	Stemness / EMT/ Tumor hypoxia	Upregulated
TUBB3[65]	β-tubulin III	Microtubules	EMT / Tumor hypoxia	Upregulated
Vimentin[52,65,91,92]		Intermediate filaments	Epithelial-mesenchymal transition	Upregulated
VEGF[43,45,91]	Vascular endothelial growth factor	Intracellular	Tumor hypoxia	Upregulated
ZEB1[52,65,91]	zinc-finger e-box binding homeobox1	Nucleoplasm	Stemness / EMT	Upregulated

EMT - Epithelial-mesenchymal transition

2.4 Enhance the delivery of chemotherapeutics with liposome nanocarriers

Controlled local release of chemotherapeutic drugs in the tumor microenvironment may provide more effective treatment of hypoxic tumor regions while circumventing the undesirable side effects of systemic administration. Implantable and injectable biomaterials were proposed to improve the outcome of chemotherapy by localizing the treatment at the site of interest (**Table 2-4**). Biomaterials' physico-chemical properties can be tuned to incorporate nano-carriers of chemotherapy [94-97]. Liposomes made of phospholipids and cholesterol are among those nano-carriers that have been extensively used as a vehicle for localized drug delivery due to their similarity to phospholipid bi-layer of cell membrane [98].

Table 2-4. Biomaterial Approaches for Cancer Treatment.

Type	Cases	Objective	Pros	Cons
Macroscale biomaterials	PLGA, PEG, PVA	Drug delivery	Biodegradable [99,100]	Potential inflammation and pH drop [100]
	Collagen, HA, fibrin, chitosan, and alginate hydrogels	Tissue regeneration and Drug delivery	Highly biocompatible and	Poor mechanical strength [101]

			biodegradable [99,100]	
	DNA biomaterials	Inherent immunogenicity	Natural immunogenicity [99]	Enzyme contamination [99]
	Peptide-based materials	Cell and drug delivery	Tunable and biocompatible [99,102]	Limited structure [102]
Implantable biomaterials	Macroscale porous scaffolds combined with immunotherapies	Release of immunotherapy molecules	Functionalized scaffolds and minimally invasive [99]	Failure to thrive in implantation site [99]
Injectable biomaterials	Cryogels	Fluid macroscale biomaterial that releases chemo- and immuno-therapy molecules	Localized where a needle can reach [99]	cannot be placed in surgically inaccessible locations or volume-sensitive areas [99]
	Hydrogels			
	Nanomaterials	Drug delivery	Penetrating, tunable release factor [103]	Side effects, potential toxicity (CDN STING [99]) [103]

Poly (lactide-co-glycolide) (PLGA), poly (ethylene glycol) (PEG) and poly (vinyl alcohol) (PVA), Hyaluronic acid (HA), cyclic dinucleotides (CDNs), Stimulator of interferon genes (STING)

In addition, the physico-chemical features of liposomes are suitable for drug delivery. Liposomes ranging in size of 100-200 nm have a long circulation performance in blood vessels [104]. Such liposomal dimensions, allows liposomes to extravasate, which promote passive targeting in hypoxic tumors by exploiting the enhanced permeability and retention effect [104,105]. Hypoxic tumor micro-vessels have an aberrant and leaky conformation that likely enable extravasation of macromolecules and liposomes in the tumor extracellular fluid. This aberrant vasculature may create a *cul de sac* for probable liposome accumulation and further endocytosis by tumor cells [105]. In addition, liposomes being lipid-based nano-carriers provide lipophilic drugs, as DTX [106], dispersion capabilities in the aberrant hypoxic vasculature [104,105,107].

Generally, non-adhesive nanocarriers face difficulties in entering tumors due to high interstitial pressures [108]. Bioadhesive coatings can be applied to the surface of liposomes to enhance their physical and colloidal stability, improve bioavailability, and increase the amount of drug they can hold [109-117]. For example, chitosan coating can be applied on anionic nanoliposomes to make

them mucoadhesive and to improve the drug retention and their uptake by target tumors [109,111–113,115,118]. Chitosan-coated liposomes, commonly referred as chitosomes, have been shown to interact electrostatically with glycoproteins in oral mucin [118,119] leading to increased retention of nanocarriers in tumor sites. This characteristic is particularly beneficial for mucin-rich mucosae commonly found in head and neck tumors. Additionally, chitosomes exhibit reduced aggregation in the blood and liver, and enhance both transcellular and paracellular drug transport, resulting in prolonged drug release [119]. More importantly, the mucoadhesive property of chitosomes would prevent the drug further migrating around the tumor after local laryngeal injection.

In sum, challenges and emerging trends in H&N research relates to (1) chemoresistance is common in H&N, (2) chemosensitizing is an emerging strategy to reduce chemoresistance, and (3) enhancing bioavailability of drugs (either chemosensitizer or DTX) is needed to maximize drug efficacy. Ongoing research is needed to better understand the nature of chemoresistance in H&N and to develop new treatment strategies in reducing chemoresistance .

2.5 References

1. Leemans CR, Braakhuis BJM, Brakenhoff RH. The molecular biology of head and neck cancer. Nat Rev Cancer. 2011;11(1):9–22.

2. Cramer JD, Burtness B, Le QT, Ferris RL. The changing therapeutic landscape of head and neck cancer. Nat Rev Clin Oncol [Internet]. 2019;16(11):669–83. Available from: http://dx.doi.org/10.1038/s41571-019-0227-z

3. Lin C, Cheng W, Liu X, Li H, Song Y. The global, regional, national burden of laryngeal cancer and its attributable risk factors (1990–2019) and predictions to 2035. Eur J Cancer Care (Engl). 2022;31(6):1–10.

4. Schultz P. Vocal fold cancer. Eur Ann Otorhinolaryngol Head Neck Dis [Internet]. 2011;128(6):301–8.]

5. Amin, Mahul B., Edge, Stephen, Greene, Frederick, Byrd, David R., Brookland, Robert K., Washington, Mary K., Gershenwald JE. AJCC Cancer Staging Form Supplement. Ajcc Cancer Staging Manual, Eighth Ed. 2018;(June):1–80.

6. Bose P, Brockton NT, Dort JC. Head and neck cancer: From anatomy to biology. Int J Cancer. 2013;133(9):2013–23.

7. Saxena M, van der Burg SH, Melief CJM, Bhardwaj N. Therapeutic cancer vaccines. Nat Rev Cancer [Internet]. 2021;21(6):360–78.

8. Kim CG, Sang YB, Lee JH, Chon HJ. Combining cancer vaccines with immunotherapy: Establishing a new immunological approach. Int J Mol Sci. 2021;22(15).

9. Barnett CME, Broit N, Yap PY, Cullen JK, Parsons PG, Panizza BJ, et al. Optimising intratumoral treatment of head and neck squamous cell carcinoma models with the diterpene ester Tigilanol tiglate. Invest New Drugs. 2019;37(1):1–8.

10. Norouzi M, Nazari B, Miller DW. Injectable hydrogel-based drug delivery systems for local cancer therapy. Drug Discov Today [Internet]. 2016;21(11):1835–49.

11. Ta HT, Dass CR, Dunstan DE. Injectable chitosan hydrogels for localised cancer therapy. J Control Release. 2008;126(3):205–16.

12. Mell LK, Vitzthum L. How I Manage Early-Stage Laryngeal Cancer [Internet]. Clinical Oncology News. 2017 [cited 2019 Dec 1]. Available from: https://www.clinicaloncology.com/Other-Solid-Tumors/Article/12-17/How-I-Manage-EarlyStage-Laryngeal-Cancer/46470

13. Salvador-Coloma C, Cohen E. Multidisciplinary Care of Laryngeal Cancer. J Oncol Pract. 2016;12(8):717–24.

14. Rapidis AD, Wolf GT. Immunotherapy of head and neck cancer: Current and future considerations. J Oncol. 2009;2009.

15. Oosting SF, Haddad RI. Best practice in systemic therapy for head and neck squamous cell carcinoma. Front Oncol. 2019;9(AUG):1–9.

16. Bauman JE, Cohen E, Ferris RL, Adelstein DJ, Brizel DM, Ridge JA, et al. Immunotherapy of head and neck cancer: Emerging clinical trials from a National Cancer

Institute Head and Neck Cancer Steering Committee Planning Meeting. Cancer. 2017;123(7):1259–71.

17. Dong H, Markovic SN. Therapeutic Targets of FDA-Approved Immunotherapies in Oncology. In: The Basics of Cancer Immunotherapy. 2018. p. 21–38.

18. Megwalu UC, Sikora AG. Survival outcomes in advanced laryngeal cancer. JAMA Otolaryngol - Head Neck Surg. 2014;140(9):855–60.

19. Hinni ML, Ferlito A, Brandwein-Gensler, M. S., Takes, R. P., Silver, C. E., Westra, W. H., ... & Hunt JL. Surgical margins in head and neck cancer: A contemporary review. Head Neck. 2012;35(9):1362–70.

20. Cosetti M, Yu GP, Schantz SP. Five-year survival rates and time trends of laryngeal cancer in the US population. Arch Otolaryngol - Head Neck Surg. 2008;134(4):370–9.

21. Vermorken JB, Remenar E, Van Herpen C, Gorlia T, Mesia R, Degardin M, et al. Cisplatin, fluorouracil, and docetaxel in unresectable head and neck cancer. N Engl J Med. 2007;357(17):1695–704.

22. Schmaltz H, Borel C, Ciftci S, Takeda-Raguin C, Debry C, Schultz P, et al. Induction chemotherapy before surgery for unresectable head and neck cancer. B-ENT. 2016;12(1):29–32.

23. Baddour HM, Magliocca KR, Chen AY. The importance of margins in head and neck cancer. J Surg Oncol. 2016;113(3):248–55.

24. Thomas Robbins K, Triantafyllou A, Suárez C, López F, Hunt JL, Strojan P, et al. Surgical margins in head and neck cancer: Intra- and postoperative considerations. Auris Nasus Larynx. 2019;46(1):10–7.

25. Sharour LA. Oncology nurses' knowledge about exploring chemotherapy related - Extravasation care: A cross-sectional study. Clin Epidemiol Glob Heal [Internet]. 2020;8(3):780–4.

26. Roman JW, Ojemuyiwa MA, Cordes LM, Madan RA, Sperling L. Docetaxel extravasation: Pathologic correlation and treatment with intralesional steroids. JAAD Case Reports [Internet]. 2017;3(4):322–5.

27. Murdoch D. Standard, and novel cytotoxic and molecular-targeted, therapies for HNSCC: An evidence-based review. Curr Opin Oncol. 2007;19(3):216–21.

28. Aigner KR, Selak E, Aigner K. Short-term intra-arterial infusion chemotherapy for head and neck cancer patients maintaining quality of life. J Cancer Res Clin Oncol [Internet]. 2019;145(1):261–8.

29. Kuan CH, Chung MJ, Hong RL, Tseng TY, Tai HC, Cheng NC, et al. The impacts of intra-arterial chemotherapy on head and neck microvascular reconstruction. J Formos Med Assoc [Internet]. 2020;119(10):1524–31.

30. Heianna J, Makino W, Hirakawa H, Agena S, Tomita H, Ariga T, et al. Therapeutic efficacy of selective intra-arterial chemoradiotherapy with docetaxel and nedaplatin for fixed bulky nodal disease in head and neck cancer of unknown primary. Eur Arch Oto-Rhino-Laryngology [Internet]. 2022;279(6):3105–13.

31. Fabregas JC, Loaiza-Bonilla A, Talebi TN, Warsch S, Fernandez G, Raez LE, et al. Concurrent chemoradiotherapy versus induction chemotherapy followed by chemoradiotherapy (sequential approach) in the management of head and neck cancer. Expert Rev Anticancer Ther. 2013;13(9):1065–72.

32. Marzo I, Naval J. Antimitotic drugs in cancer chemotherapy: Promises and pitfalls. Biochem Pharmacol [Internet]. 2013;86(6):703–10.

33. Shaloam D, Tchounwou PB. Cisplatin in cancer therapy: Molecular mechanisms of action. Eur J Pharmacol. 2014;740:364–78.

34. Matuo R, Sousa FG, Escargueil AE, Soares DG, Grivicich I, Saffi J, et al. DNA repair pathways involved in repair of lesions induced by 5-fluorouracil and its active metabolite FdUMP. Biochem Pharmacol. 2010;79(2):147–53.

35. Sadeghi N, Khalife S, Mascarella MA, Ramanakumar A V., Richardson K, Joshi AS, et al. Pathologic response to neoadjuvant chemotherapy in HPV-associated oropharynx cancer. Head Neck. 2020;42(3):417–25.

36. Tishler RB. Concurrent chemotherapy and radiation for head and neck cancer. In: Radiation Medicine Rounds. 2011. p. 183–200.

37. Gyawali B, Shimokata T, Honda K, Ando Y. Chemotherapy in locally advanced head and neck squamous cell carcinoma. Cancer Treat Rev [Internet]. 2016;44:10–6.

38. Kim R, Hahn S, Shin J, Ock CY, Kim M, Keam B, et al. The effect of induction chemotherapy using docetaxel, cisplatin, and fluorouracil on survival in locally advanced head and neck squamous cell carcinoma: A meta-analysis. Cancer Res Treat. 2016;48(3):907–16.

39. Gammon L, Mackenzie IC. Roles of hypoxia, stem cells and epithelial-mesenchymal transition in the spread and treatment resistance of head and neck cancer. J Oral Pathol Med. 2016;45(2):77–82.

40. Joseph JP, Harishankar MK, Pillai AA, Devi A. Hypoxia induced EMT: A review on the mechanism of tumor progression and metastasis in OSCC. Oral Oncol [Internet]. 2018;80(February):23–32.

41. Jing X, Yang F, Shao C, Wei K, Xie M, Shen H, et al. Role of hypoxia in cancer therapy by regulating the tumor microenvironment. Mol Cancer. 2019;18(1):1–15.

42. Wang JC, Li GY, Li PP, Sun X, Li WM, Li Y, et al. Suppression of hypoxia-induced excessive angiogenesis by metformin via elevating tumor blood perfusion. Oncotarget. 2017;8(43):73892–904.

43. Bredell MG, Ernst J, El-Kochairi I, Dahlem Y, Ikenberg K, Schumann DM. Current relevance of hypoxia in head and neck cancer. Oncotarget. 2016;7(31):50781–804.

44. Doktorova H, Hrabeta J, Khalil MA, Eckschlager T. Hypoxia-induced chemoresistance in cancer cells: The role of not only HIF-1. Biomed Pap. 2015;159(2):166–77.

45. Marquard FE, Jücker M. PI3K/AKT/mTOR signaling as a molecular target in head and neck cancer. Biochem Pharmacol [Internet]. 2020;172:113729.

46. Jiang B-H, Liu L-Z. Role of mTOR in anticancer drug resistance: perspectives for improved drug treatment Bing-Hua. Drug Resist Updat. 2008;11(3):63–76.

47. Kurelac I, Umesh Ganesh N, Iorio M, Porcelli AM, Gasparre G. The multifaceted effects of metformin on tumor microenvironment. Semin Cell Dev Biol [Internet]. 2020;98(May 2019):90–7.

48. Peltanova B, Raudenska M, Masarik M. Effect of tumor microenvironment on pathogenesis of the head and neck squamous cell carcinoma: A systematic review. Mol Cancer. 2019;18(1):1–24.

49. Zhang Z, Dong Z, Lauxen IS, Filho MSA, Nör JE. Endothelial cell-secreted EGF induces epithelial to mesenchymal transition and endows head and neck cancer cells with stem-like phenotype. Cancer Res. 2014;74(10):2869–81.

50. Utispan K, Koontongkaew S. Fibroblasts and macrophages: Key players in the head and neck cancer microenvironment. J Oral Biosci [Internet]. 2017;59(1):23–30. Available from: http://dx.doi.org/10.1016/j.job.2016.11.002

51. Zuo J, Wen J, Lei M, Wen M, Li S, Lv X, et al. Hypoxia promotes the invasion and metastasis of laryngeal cancer cells via EMT. Med Oncol. 2016;33(2):1–9.

52. Singh A, Settleman J. EMT, cancer stem cells and drug resistance: An emerging axis of evil in the war on cancer. Oncogene. 2010;29(34):4741–51.

53. Qin Y, Ashrafizadeh M, Mongiardini V, Grimaldi B, Crea F, Rietdorf K, et al. Autophagy and cancer drug resistance in dialogue: Pre-clinical and clinical evidence. Cancer Lett. 2023;570(June).

54. Kang X, Chen Y, Yi B, Yan X, Jiang C, Chen B, et al. An integrative microenvironment approach for laryngeal carcinoma: The role of immune/methylation/autophagy signatures on disease clinical prognosis and single-cell genotypes. J Cancer. 2021;12(14):4148–71.

55. Mosca L, Ilari A, Fazi F, Assaraf YG, Colotti G. Taxanes in cancer treatment: Activity, chemoresistance and its overcoming. Drug Resist Updat [Internet]. 2021;54(November 2020):100742.

56. Kanno Y, Chen CY, Lee HL, Chiou JF, Chen YJ. Molecular Mechanisms of Chemotherapy Resistance in Head and Neck Cancers. Front Oncol. 2021;11(May):1–13.

57. Azharuddin M, Roberg K, Dhara AK, Jain MV, Darcy P, Hinkula J, et al. Dissecting multi drug resistance in head and neck cancer cells using multicellular tumor spheroids. Sci Rep. 2019;9(1):1–12.

58. Hua H, Kong Q, Zhang H, Wang J, Luo T, Jiang Y. Targeting mTOR for cancer therapy. J Hematol Oncol. 2019;12(1):1–19.

59. Ramírez-Cosmes A, Reyes-Jiménez E, Zertuche-Martínez C, Hernández-Hernández CA, García-Román R, Romero-Díaz RI, et al. The implications of ABCC3 in cancer drug resistance: can we use it as a therapeutic target? Am J Cancer Res [Internet]. 2021;11(9):4127–40.

60. Reynolds IS, Fichtner M, McNamara DA, Kay EW, Prehn JHM, Burke JP. Mucin glycoproteins block apoptosis; promote invasion, proliferation, and migration; and cause chemoresistance through diverse pathways in epithelial cancers. Cancer Metastasis Rev. 2019;38(1–2):237–57.

61. Utispan K, Koontongkaew S. Mucin 1 regulates the hypoxia response in head and neck cancer cells. J Pharmacol Sci [Internet]. 2021;147(4):331–9.

62. Sipaul F, Birchall M, Corfield A. What role do mucins have in the development of laryngeal squamous cell carcinoma? A systematic review. Eur Arch Oto-Rhino-Laryngology. 2011;268(8):1109–17.

63. Marimuthu S, Rauth S, Ganguly K, Zhang C, Lakshmanan I, Batra SK, et al. Mucins reprogram stemness, metabolism and promote chemoresistance during cancer progression. Cancer Metastasis Rev. 2021;40(2):575–88.

64. Galstyan A, Cho J, Johnson DE, Grandis JR. Modulation of the PI3K/mTOR pathways. Improv Ther Ratio Head Neck Cancer. 2020;89–105.

65. Maloney SM, Hoover CA, Morejon-Lasso L V., Prosperi JR. Mechanisms of taxane resistance. Cancers (Basel). 2020;12(11):1–57.

66. Bouland C, Eynden X Vanden, Lalmand M, Buset T, Yanni A, Javadian R, et al. Preventive and Therapeutic Effect of Metformin in Head and Neck Cancer : A Concise Review. J Clin Med. 2023;12(9):6195.

67. Eikawa S, Nishida M, Mizukami S, Yamazaki C, Nakayama E, Udono H. Immune-mediated antitumor effect by type 2 diabetes drug, metformin. Proc Natl Acad Sci U S A. 2015;112(6):1809–14.

68. Feng Y, Ke C, Tang Q, Dong H, Zheng X, Lin W, et al. Metformin promotes autophagy and apoptosis in esophageal squamous cell carcinoma by downregulating Stat3 signaling. Cell Death Dis. 2014;5(2):1–12.

69. Luo Q, Hu D, Hu S, Yan M, Sun Z, Chen F. In vitro and in vivo anti-tumor effect of metformin as a novel therapeutic agent in human oral squamous cell carcinoma. BMC Cancer. 2012;12.

70. Barlak N, Sanli F, Capik O, Tuysuz E, Aydın Karatas E, Turkez H, et al. Metformin Treatment Sensitizes Human Laryngeal Cancer Cell Line Hep- 2 to 5-Fluorouracil. Clin Cancer Drugs. 2019;7(1):16–24.

71. Chen K, Li Y, Guo Z, Zeng Y, Zhang W, Wang H. Metformin: Current clinical applications in nondiabetic patients with cancer. Aging (Albany NY). 2020;12(4):3993–4009.

72. Cai H, Everett RS, Thakker DR. Efficacious dose of metformin for breast cancer therapy is determined by cation transporter expression in tumours. Br J Pharmacol. 2019;176(15):2724–35.

73. Mayer MJ, Klotz LH, Venkateswaran V. Evaluating Metformin as a Potential Chemosensitizing Agent when Combined with Docetaxel Chemotherapy in Castration-resistant Prostate Cancer Cells. Anticancer Res. 2017;37(12):6601–7.

74. dos Santos Guimarães I, Ladislau-Magescky T, Tessarollo NG, dos Santos DZ, Gimba ERP, Sternberg C, et al. Chemosensitizing effects of metformin on cisplatin- and paclitaxel-resistant ovarian cancer cell lines. Pharmacol Reports [Internet]. 2018;70(3):409–17.

75. Zaidi S, Gandhi J, Joshi G, Smith NL, Khan SA. The anticancer potential of metformin on prostate cancer. Prostate Cancer Prostatic Dis [Internet]. 2019;22(3):351–61.

76. Fatehi-Agdam M, Vatankhah MA, Panahizadeh R, Jeddi F, Najafzadeh N. Efficacy of Metformin and Chemotherapeutic Agents on the Inhibition of Colony Formation and Shh/Gli1 Pathway: Metformin/Docetaxel Versus Metformin/5-Fluorouracil. Drug Res (Stuttg). 2021;71(1):17–25.

77. Siddappa G, Kulsum S, Ravindra DR, Kumar V V., Raju N, Raghavan N, et al. Curcumin and metformin-mediated chemoprevention of oral cancer is associated with inhibition of cancer stem cells. Mol Carcinog. 2017;56(11):2446–60.

78. Guri Y, Nordmann TM, Roszik J. mTOR at the transmitting and receiving ends in tumor immunity. Front Immunol. 2018;9(MAR):1–8.

79. Lei Y, Yi Y, Liu Y, Liu X, Keller ET, Qian CN, et al. Metformin targets multiple signaling pathways in cancer. Chin J Cancer. 2017;36(1):1–9.

80. Patil S. Metformin treatment decreases the expression of cancer stem cell marker CD44 and stemness related gene expression in primary oral cancer cells. Arch Oral Biol [Internet]. 2020;113(March):104710.

81. Chaudhary SC, Kurundkar D, Elmets CA, Kopelovich L, Athar M. Metformin, an antidiabetic agent reduces growth of cutaneous squamous cell carcinoma by targeting mTOR signaling pathway. Photochem Photobiol. 2012;88(5):1149–56.

82. Zheng L, Yang W, Wu F, Wang C, Yu L, Tang L, et al. Prognostic significance of AMPK activation and therapeutic effects of metformin in hepatocellular carcinoma. Clin Cancer Res. 2013;19(19):5372–80.

83. Kato K, Gong J, Iwama H, Kitanaka A, Tani J, Miyoshi H, et al. The antidiabetic drug metformin inhibits gastric cancer cell proliferation in vitro and in vivo. Mol Cancer Ther. 2012;11(3):549–60.

84. Zhuang Y, Miskimins WK. Metformin induces both caspase-dependent and poly(ADP-ribose) polymerase-dependent cell death in breast cancer cells. Mol Cancer Res. 2011;9(5):603–15.

85. Klubo-Gwiezdzinska J, Jensen K, Costello J, Patel A, Hoperia V, Bauer A, et al. Metformin inhibits growth and decreases resistance to anoikis in medullary thyroid cancer cells. Endocr Relat Cancer. 2012;19(3):447–56.

86. Chowdhury S, Yung E, Pintilie M, Muaddi H, Chaib S, Yeung MT, et al. MATE2 expression is associated with cancer cell response to metformin. PLoS One. 2016;11(12):1–18.

87. Guimarães TA, Farias LC, Santos ES, Fraga CA de C, Orsini LA, Teles L de F, et al. Metformin increases PDH and suppresses HIF-1a under hypoxic conditions and induces cell death in oral squamous cell carcinoma. Oncotarget. 2016;7(34):55057–68.

88. Sanada Y, Sasanuma H, Takeda S, Tano K, Masunaga SI. Disruption of Hif-1α enhances cytotoxic effects of metformin in murine squamous cell carcinoma. Int J Radiat Biol [Internet]. 2018;94(1):88–96.

89. Qu C, Zhang W, Zheng G, Zhang Z, Yin J, He Z. Metformin reverses multidrug resistance and epithelial-mesenchymal transition (EMT) via activating AMP-activated protein kinase (AMPK) in human breast cancer cells. Mol Cell Biochem. 2014;386(1–2):63–71.

90. Han B, Cui H, Kang L, Zhang X, Jin Z, Lu L, et al. Metformin inhibits thyroid cancer cell growth, migration, and EMT through the mTOR pathway. Tumor Biol. 2015;36(8):6295–304.

91. Zheng HC. The molecular mechanisms of chemoresistance in cancers. Oncotarget. 2017;8(35):59950–64.

92. da Silva SD, Morand GB, Alobaid FA, Hier MP, Mlynarek AM, Alaoui-Jamali MA, et al. Epithelial-mesenchymal transition (EMT) markers have prognostic impact in multiple primary oral squamous cell carcinoma. Clin Exp Metastasis. 2015;32(1):55–63.

93. Li Z, Liao A, Liu M, Zhang S, Feng Z, Wang G, et al. Synthesis of poly(amidoamine)-poly(ethyleneglycol)-poly(amidoamine) and preparation of its hydrogel solution containing doxorubicin. 2016;1(3):1–6.

94. Elkhoury K, Koçak P, Kang A, Arab-Tehrany E, Ward JE, Shin SR. Engineering smart targeting nanovesicles and their combination with hydrogels for controlled drug delivery. Pharmaceutics. 2020;12(9):1–24.

95. Laomeephol C, Ferreira H, Kanokpanont S, Neves NM, Kobayashi H, Damrongsakkul S. Dual-functional liposomes for curcumin delivery and accelerating silk fibroin hydrogel formation. Int J Pharm [Internet]. 2020;589(September):119844.

96. Li R, Lin Z, Zhang Q, Zhang Y, Liu Y, Lyu Y, et al. Injectable and in Situ-Formable Thiolated Chitosan-Coated Liposomal Hydrogels as Curcumin Carriers for Prevention of in Vivo Breast Cancer Recurrence. ACS Appl Mater Interfaces. 2020;12(15):17936–48.

97. Wang W, Zhang P, Shan W, Gao J, Liang W. A novel chitosan-based thermosensitive hydrogel containing doxorubicin liposomes for topical cancer therapy. J Biomater Sci Polym Ed. 2013;24(14):1649–59.

98. Bozzuto G, Molinari A. Liposomes as nanomedical devices. Int J Nanomedicine. 2015;10:975–99.

99. Leach DG, Young S, Hartgerink JD. Advances in immunotherapy delivery from implantable and injectable biomaterials. Acta Biomater. 2019;88:15–31.

100. Mariani E, Lisignoli G, Borzì RM, Pulsatelli L. Biomaterials: Foreign bodies or tuners for the immune response? Vol. 20, International Journal of Molecular Sciences. MDPI AG; 2019.

101. Vats A, Tolley NS, Polak JM, Gough JE. Scaffolds and biomaterials for tissue engineering: A review of clinical applications. Clin Otolaryngol Allied Sci. 2003;28(3):165–72.

102. Chow D, Nunalee ML, Lim DW, Simnick AJ, Chilkoti A. Peptide-based biopolymers in biomedicine and biotechnology. Mater Sci Eng R Reports. 2008;62(4):125–55.

103. Li XD, Gao JY, Yang Y, Fang HY, Han YJ, Wang XM, et al. Nanomaterials in the application of tumor vaccines: Advantages and disadvantages. Onco Targets Ther. 2013;6:629–34.

104. Mizrahy S, Peer D. Polysaccharides as building blocks for nanotherapeutics. Chem Soc Rev. 2012;41(7):2623–40.

105. Gabizon AA, Shmeeda H, Zalipsky S. Pros and cons of the liposome platform in cancer drug targeting. J Liposome Res. 2006;16(3):175–83.

106. Pereira S, Egbu R, Jannati G, Al-Jamal WT. Docetaxel-loaded liposomes: The effect of lipid composition and purification on drug encapsulation and in vitro toxicity. Int J Pharm [Internet]. 2016;514(1):150–9.

107. Kalyane D, Raval N, Maheshwari R, Tambe V, Kalia K, Tekade RK. Employment of enhanced permeability and retention effect (EPR): Nanoparticle-based precision tools for targeting of therapeutic and diagnostic agent in cancer. Mater Sci Eng C [Internet]. 2019;98(August 2018):1252–76.

108. de Lázaro I, Mooney DJ. Obstacles and opportunities in a forward vision for cancer nanomedicine. Nat Mater. 2021;20(11):1469–79.

109. Sun X, Xu H, Huang T, Zhang C, Wu J, Luo S. Simultaneous delivery of anti-miRNA and docetaxel with supramolecular self-assembled “chitosome” for improving chemosensitivity of triple negative breast cancer cells. Drug Deliv Transl Res. 2020;11(2021):192–204.

110. Megahed MA, El-sawy HS, Reda AM, Abd-allah FI, Abu SK, Lila AE, et al. Effect of nanovesicular surface-functionalization via chitosan and / or PEGylation on cytotoxicity of tamoxifen in induced-breast cancer model. Life Sci. 2022;307(May):120908.

111. Alomrani A, Badran M, Harisa GI, ALshehry M, Alhariri M, Alshamsan A, et al. The use of chitosan-coated flexible liposomes as a remarkable carrier to enhance the antitumor efficacy of 5-fluorouracil against colorectal cancer. Saudi Pharm J [Internet]. 2019;27(5):603–11.

112. Dawoud M. Chitosan coated solid lipid nanoparticles as promising carriers for docetaxel. J Drug Deliv Sci Technol [Internet]. 2021;62(November 2020):102409.

113. Shukla SK, Chan A, Parvathaneni V, Gupta V. Metformin-loaded chitosomes for treatment of malignant pleural mesothelioma – A rare thoracic cancer. Int J Biol Macromol [Internet]. 2020;160:128–41.

114. Lai WF, Wong WT, Rogach AL. Molecular design of layer-by-layer functionalized liposomes for oral drug delivery. ACS Appl Mater Interfaces. 2020;12(39):43341–51.

115. AlQahtani SA, Harisa GI, Alomrani AH, Alanazi FK, Badran MM. Improved pharmacokinetic and biodistribution of 5-fluorouracil loaded biomimetic nanoerythrocytes decorated nanocarriers for liver cancer treatment. Colloids Surfaces B Biointerfaces [Internet]. 2021;197(October 2020):111380.

116. Zhang E, Xing R, Liu S, Li K, Qin Y, Yu H, et al. Vascular targeted chitosan-derived nanoparticles as docetaxel carriers for gastric cancer therapy. Int J Biol Macromol [Internet]. 2019;126:662–72.

117. Singh I, Swami R, Jeengar MK, Khan W, Sistla R. p-Aminophenyl-α-d-mannopyranoside engineered lipidic nanoparticles for effective delivery of docetaxel to brain. Chem Phys Lipids [Internet]. 2015;188:1–9.

118. Pandey M, Choudhury H, Ying JNS, Ling JFS, Ting J, Ting JSS, et al. Mucoadhesive Nanocarriers as a Promising Strategy to Enhance Intracellular Delivery against Oral Cavity Carcinoma. Pharmaceutics. 2022;14(4):1–19.

119. Collado-González M, Espinosa YG, Goycoolea FM. Interaction between Chitosan and Mucin: Fundamentals and applications. Biomimetics. 2019;4(2):1–20.

Chapter 3. Review article

In vitro models for head and neck cancer: Current status and future perspective

This manuscript was published in Frontiers in Oncology (2022). DOI: doi: 10.3389/fonc.2022.960340

Christian R. Moya-Garcia[1], Hideaki Okuyama[2,3], Nader Sadeghi[4,5], Jianyu Li[1,6], Maryam Tabrizian[1,7*], Nicole Y. K. Li-Jessen[1,2,4,5*]

[1]Department of Biomedical Engineering, McGill University, Canada
[2]School of Communication Sciences and Disorders, McGill University, Canada
[3]Department of Otolaryngology – Head & Neck Surgery, Kyoto University, Japan
[4]Department of Otolaryngology – Head and Neck Surgery, McGill University, Canada
[5]Research Institute of McGill University Health Center, McGill University, Canada
[6]Department of Mechanical Engineering, McGill University, Canada
[7]Faculty of Dental Medicine and Oral Health Sciences, McGill University, Canada
*Correspondence to: maryam.tabrizian@mcgill.ca; nicole.li@mcgill.ca

Abstract: The 5-year overall survival rate remains approximately 50% for head and neck (H&N) cancer patients, even though new cancer drugs have been approved for clinical use since 2016. Cancer drug studies are now moving toward the use of three-dimensional culture models for better emulating the unique tumor microenvironment (TME) and better predicting in vivo response to cancer treatments. Distinctive TME features, such as tumor geometry, heterogenous cellularity, and hypoxic cues, notably affect tissue aggressiveness and drug resistance. However, these features have not been fully incorporated into in vitro H&N cancer models. This review paper aims to provide a scholarly assessment of the designs, contributions, and limitations of in vitro models in H&N cancer drug research. We first review the TME features of H&N cancer that are most relevant to in vitro drug evaluation. We then evaluate a selection of advanced culture models, namely, spheroids, organotypic models, and microfluidic chips, in their applications for H&N cancer drug research. Lastly, we propose future opportunities of in vitro H&N cancer research in the prospects of high-throughput drug screening and patient-specific drug evaluation.

3.1 Introduction

Cancer drug research and development (R&D) are considered as one of the most expensive expenditures among drug development as compared to that of all other diseases (1). The global spending on oncology drugs reached $164 billion in 2020 and an estimated $269 billion by 2025 even as annual growth rates ease to approximately 10% (2). Mailankody and Prasad from National Cancer Institutes in the United States critically pointed out that new cancer drugs may not necessarily help to increase the survival rate in cancer patients despite the expensive investments in cancer drug R&D (3). In 2016, the Food and Drug Administration (FDA) approved the chemotherapy drug hydroxyurea for the treatment of locally advanced head and neck (H&N) cancer as well as the immunotherapy drugs pembrolizumab and nivolumab for recurrent/metastatic H&N cancer (4). Since, the role of these three drugs in the H&N cancer primary treatment has not been properly elucidated, the 5-year overall survival of H&N cancer patients remains less than 50% (5) with 30% of them experiencing cancer relapse and resistance to treatment (6).

The R&D pipeline for new drug discoveries starts with in vitro models, followed by preclinical/animal testing and clinical trials. In vitro platforms often represent a first milestone to reach the evaluation of drug cytotoxicity, dose, resistance, and sensitivity as well as the identification of the target molecular mechanisms of prognostic markers (7). Specific to cancer drug screening and discovery, in vitro models are often designed to mimic the tumor microenvironment (TME) of interest (8, 9). For instance, an overexpression of epithelial growth factor receptors (EGFRs) were noted in almost 90% of patients with H&N tumors (10, 11). To reflect this environment, in one of the very early in vitro studies with H&N squamous cell carcinoma cultures collected from larynx, retromolar trigone, cervical lymph node, and the floor of mouth, the inhibition of the EGFR was assessed by incorporating two anti-EGFR monoclonal antibodies (MAbs 425 and 528) based on in vitro models (12). Cell viability results showed that the two anti-EGFR antibodies reduced cancer cell growth by up to 97% compared to healthy mucosal epithelial cells after a 5-day exposure. Further, in vitro and in vivo studies on monoclonal antibodies against EGFR led to the discovery of cetuximab, which was approved by the FDA for colon cancer treatment in 2004 and in 2011 for the treatment of recurrent/metastatic H&N cancer (13).

The recent evolution of in vitro cancer models has been focused on emulating the tissue-specific TME as much as possible to recapitulate drug resistance and uptake in specific tumor tissues. Advances in spheroid/organoid bioengineering and their culturing methods, as well as microfluidic technologies, are harnessed to enable physiologically and clinically relevant in vitro cancer models. Distinctive TME features, namely, three-dimensional (3D) tumor geometry, heterogeneous cell populations, and fenestrated tumor vasculature, have been incorporated into in vitro models, such as breast (14), lung (15), and liver (16) cancers. However, tissue-specific TME features have not been fully applied to in vitro H&N cancer model designs, which might explain the slow advancement of effective drug discovery and longitudinal drug evaluation for H&N cancers.

To survey the current implementation of 3D in vitro models for H&N cancer, we performed a search for original research papers published on The National Center for Biotechnology Information (NCBI) PubMed® between January 2017 and April 2022 using the following combined terms, namely, "head and neck cancer," "spheroid," "organoid," "microfluidic," and "organotypic" (**Figure 3-1**). The search generated 71 research studies. Spheroid cultures (34%; N = 24) and scaffold models (22%; N = 16) were the two most common 3D culture models in H&N cancer research. To understand the uptake of 3D in vitro models for H&N cancer drug discovery, a search was performed on the original studies of 12 common cancers including H&N (17) published on NCBI PubMed® between January 2017 and April 2022 using the following combined terms: "in vitro", "drug discovery", "breast", ''lung'', ''colorectal'', ''glioblastoma'', ''prostate'', ''melanoma'', ''lymphoma'', ''pancreatic'', ''cervical'', ''head and neck'', "thyroid", "oral", "laryngeal", ''bladder'', ''renal'', and "cancer". The search generated 489 results. Among the 12 organs searched, approximately 27.6% (N = 135) were related to breast cancer while only 2.2% (N = 11) were associated with H&N cancer. Further search on drug discovery–related publication for H&N cancer showed that only 3 out of the 11 results used 3D in vitro models. In other words, approximately 4.2% [(3 out of 11)/71] of 3D in vitro models were applied in the study of cancer drug discovery. The aforesaid statement described the need for more H&N cancer research using advanced 3D in vitro models instead of conventional 2D cultures for developing new anticancer drugs.

In this paper, we review the unique TME characteristics in H&N cancers and their relevance to the tumor tissue aggressiveness and drug resistance. We present the design principles of in vitro models to mimic key TME features relevant to H&N cancer. We then report on several state-ofthe-art culturing models, namely, spheroids, 3D scaffolds, organotypic models, and microfluidic devices that have contributed to the H&N cancer therapeutic R&D. Finally, we provide a perspective on more reproducible and robust in vitro H&N cancer models for high-throughput drug screening and patient-specific drug development.

3.2 Tumor microenvironment in head and neck cancers

A typical TME in H&N cancer is heterogeneously composed of neoplastic cells, endothelial cells, and fibroblasts, as well as tumor-infiltrating immune cells from the mucosae of the oral, nasal and paranasal cavities, larynx, and pharynx (6, 17) (**Figure 3-2**). Approximately 90% of H&N cancer cells are considered as squamous cell carcinomas (6, 18). The H&N carcinomas present an air–liquid interface conformation since the apical TME is in contact with the air from the cavity lumen whereas the basal TME interacts with blood (6, 18, 19). In particular, these fish scale–like/squamous epithelial neoplastic cells exhibit an aggressive abnormal cell proliferation crossing the boundaries of surrounding cells in concert with endothelial cells and fibroblasts (18). Extracellular matrix (ECM) proteins as collagen, elastin, fibronectin, and laminin provide a structural support that plays a part in cell adhesion and migration in the TME of H&N (19).

H&N squamous cell carcinomas may present oncogenes associated with human papillomavirus (HPV) infection (18, 20), largely p16 followed by p18 genes (20). A classification of H&N squamous cell carcinoma relies on the presence of HPV-associated oncogenes that are normally referred to as HPV+ or HPV- H&N cancer (20). In particular, the mutation and down- or upregulation of molecular mechanisms such as PI3K/Akt/ mTOR (mammalian target of rapamycin), TP53, NOTCH, EGFR, JAK/STAT, Ras/MEK/ERK, and MET pathways are found to be associated with the progression of H&N squamous cell carcinoma (20) (**Figure 3-2D**). For example, the PI3K/Akt/mTOR pathway is upregulated in more than 90% of H&N squamous cell carcinomas, resulting in an increased resistance to chemotherapy and radiotherapy and cancer progression (21).

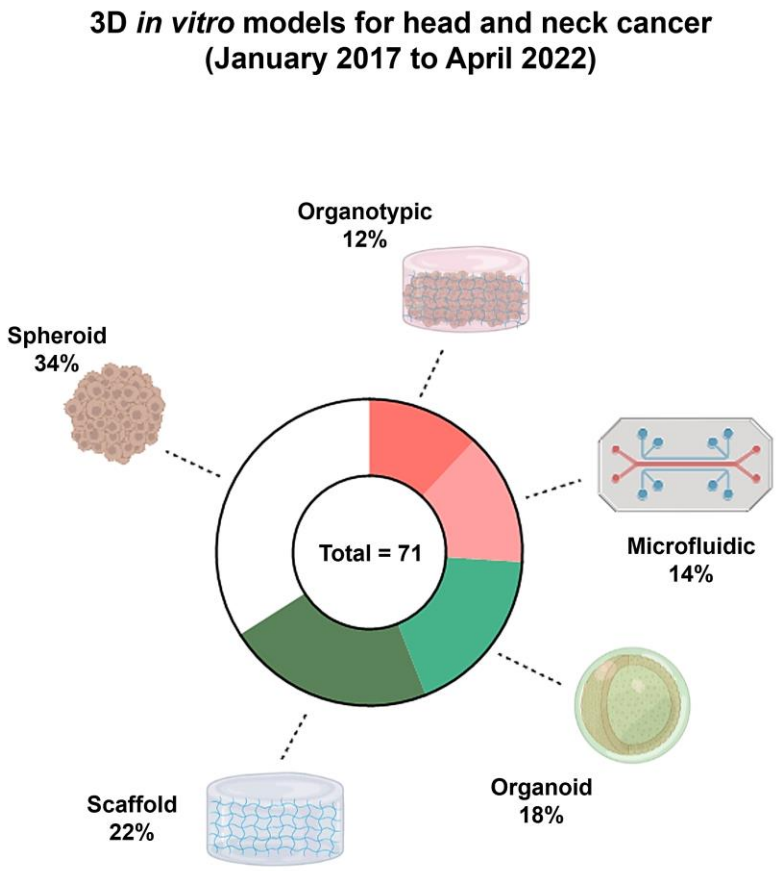

Figure 3-1. Culturing models in head and neck (H&N) cancers. Pie graph of published articles between 2017 and 2022 using the NCBI PubMed®. Related publications of three-dimensional (3D) in vitro models in H&N cancer with spheroids being the most abundant type of culture model. Figure created with BioRender.com and GraphPad Prism 9.3.1.

Similar to other cancer progressions, in H&N cancer, epithelial, mesothelial, and endothelial cells shift from a basal to mesenchymal phenotype that allows these cells to acquire mobility and protect tumor cells from anoikis, a programmed cell death (19). These phenomena are commonly known as epithelial, mesothelial, and endothelial mesenchymal transitions, respectively. Cancer-associated fibroblasts may differentiate from resident fibroblasts and from epithelial, mesothelial, and endothelial cells during respective mesenchymal transitions. Cancer-associated fibroblasts play important roles in tumor growth and maintenance through secreting autocrine and paracrine signaling molecules such as IL-1a, IL-1b, IL-6, IL33, HGF, VEGF, TNF-a, TGF-b, CCL-2, CXCL-12, CXCR-4, MMP-2, and Snail (17, 19, 22). Cancer-associated fibroblasts in concert with

endothelial cells secrete EGF that enhances tumorous motility and stemness (23, 24). In addition, stromal cells such as fibroblasts produce ECM proteins (e.g., collagen, elastin, and fibronectin) that create the fibrous architectural conformation of the tumorous body (19, 25). This structural fibrous network contributes to cell adhesion, cell proliferation, and cell migration, which, in turn, leads to tumor progression and reduced response to treatment (18, 19, 25).

Specific to the H&N cancer, the TME aggressiveness and resistance to treatment are linked to two primary mechanisms, namely, the dysregulation of the immune system and tumor hypoxia (20). With respect to the dysregulated immune system, a plethora of immune cells including T cells (cytotoxic and regulatory phenotypes), B cells, natural killers, tumor-associated macrophages (anti- and pro-tumor phenotypes), tumor-associated neutrophils, myeloid-derived suppressor cells, and mast cells are found within the TME of H&N tumors (6, 26). Checkpoint markers, including programmed cell death 1 (PD-1) and its ligand PD-L1, were found upregulated on exhausted T cells and myeloid-derived suppressor cells in the H&N TME (6). As a result, two PD-1 inhibitor drugs, pembrolizumab and nivolumab, were developed and approved for H&N cancer treatment in 2016, for unresectable and cisplatin-resistant recurrent/metastatic H&N cancer (4, 27, 28).

Tumor hypoxia is another well-recognized factor contributing to the aggressive tumor behavior and drug resistance in H&N cancer (19, 20, 29). The fenestrated tumor vessels result in aberrant tumor blood flow to the under-perfused areas of the solid tumor (**Figures 3-2E, F**). In particular, oxygen, nutrients, and drugs are restricted to reach the cells in certain tumor areas, leading to some high-level hypoxic regions within the TME (18, 20). Pro-tumor/anti-inflammatory macrophages are reported to secrete excessive angiogenic cytokines such as VEGF, IL-6, IL-8, CCL-2, and MMP-9, which results in aberrant angiogenesis and the hypoxic H&N-specific TME in vitro and in vivo (6, 17, 18, 30, 31).

3.3 Design principles of in vitro head and neck cancer models

Like many other in vitro models mimicking the TME, a representative in vitro H&N tumor model is expected to sufficiently recapitulate: (I) a 3D tumor-like geometry for cell– cell and cell–ECM interactions; (II) the heterogeneous cell types such as squamous cell carcinomas, stromal, and immune cells in the TME; and (III) the aberrant and fenestrated vasculature for the high-level hypoxic TME (**Figure 3-2**). These principles are further elaborated in the following paragraphs.

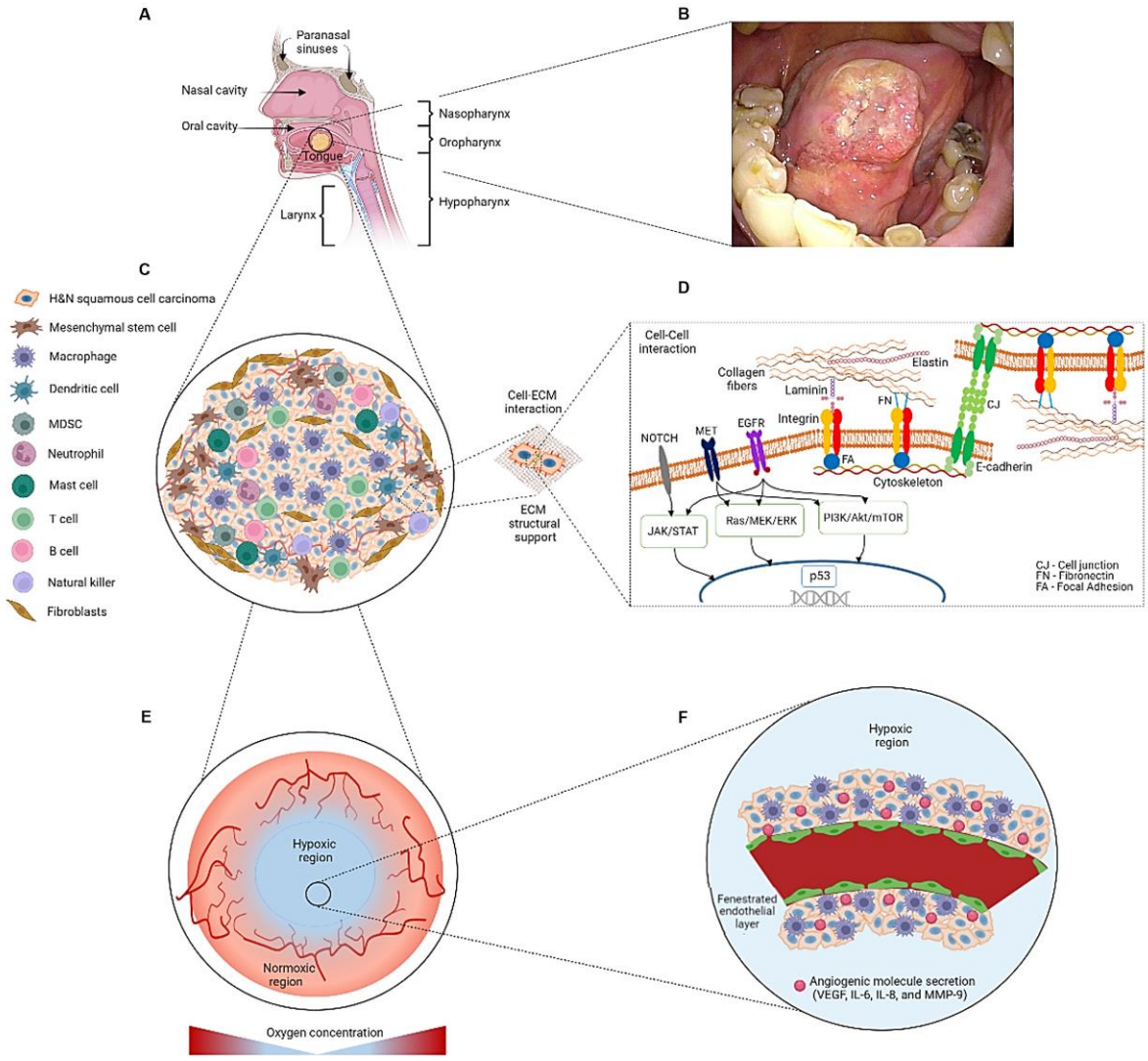

Figure 3-2. Schematic representation of the potential tumor location and tumor microenvironment (TME) in H&N cancer. (A) H&N cancer may be found at oral, nasal, and paranasal cavities, larynx, and pharynx anatomical sites. (B) Clinical image of stage 2 tongue cancer (<4 cm) provided by Drs. Yo Kishimoto and Hideaki Okuyama's research team at the Kyoto University Hospital with patient's consent. (C) Heterogeneous cell populations are resided within an H&N squamous cell carcinoma. Stromal cells including mesenchymal stem cells and fibroblasts are commonly found in the outer layer of the tumorous body. Tumor-infiltrating immune cells including macrophages and T cells among others are found within the tumor. (D) The extracellular matrix provides structural support and biochemical cues to the TME via cell–cell/–ECM interactions. Mutation of pathways PI3K/Akt/mTOR, TP53, NOTCH, EGFR, JAK/STAT, Ras/MEK/ERK, and MET relate to H&N cancer development. (E) The hypoxic region is located at the center of the tumor, which is characterized by aberrant vasculature. (F) This fenestrated vasculature hampers the proper supply of nutrients, oxygen, and therapeutics. ECM, extracellular matrix; IL, interleukin; MDSC, myeloid-

derived suppressor cell; MMP, metalloproteinase; VEGF, vascular epithelial growth factor. Figure created with BioRender.com.

3.3.1 Three-dimensional tumor geometry

Tumors are 3D sphere-like solid structures with unique physical and biochemical boundaries, in which they need to be considered for cancer drug screening and evaluation. First, the physical geometry of the tumor affects drug disposition, diffusion, and absorption (32–34). For instance, the flat two-dimensional (2D) monolayer geometry exposes the drug application to the entire cell monolayer, making the cells more susceptible to the applied drug compared to that of 3D geometry (35, 36). Advanced in vitro cancer models have incorporated 3D spherical geometries to make the drug diffusion and uptake by cellular targets more similar to the in vivo settings of solid H&N tumors. Second, the 3D tumor geometry is a key parameter in the organization of cell membrane receptors and the remodeling of ECM constituents, which, in turn, modulate autocrine and paracrine signaling mechanisms in the TME. For example, E-cadherin adhesion proteins were found to be upregulated in 12 individual spheroid cultures made from each H&N cancer cell line (FaDu, HLaC78, Hep-2, Hep-2-Tax, HLaC79, HLaC79-Tax, HPaC79, HSmC78, CAL-27, PE/CA-PJ41, SCC4, HNO210) but not in any of the corresponding 2D monolayer controls (32). As such, 3D sphere-like culture models, as of spheroids, are essential to emulate the physical and biochemical characteristics of the solid tumor shape in the evaluation of cell–cell/–ECM crosstalk and pharmacokinetics of cancer drugs (32, 33).

3.3.2 Heterogeneous cell types

Recently, multicellular in vitro models have been developed for lung (37), breast (38), and pancreatic (39) cancer research. Such model is particularly useful to study the crosstalk between cells in response to cancer drugs. For example, a triple coculture pancreatic model was developed to create a hetero-, multicellular tumor spheroid consisting of pancreatic cancer cells, fibroblasts, and endothelial cells for the investigation of the TME response to chemotherapy (39). To mimic the heterogenous TME in H&N cancer, cell lines such as CAL-27, CAL-33, Detroit 562, Hep2, Hep3, FaDu, SCC-4, UM-SCC-3, UM-SCC-4, and UM-SCC17A, among others, are widely used in in vitro 2D and 3D H&N cancer models (40).

Being able to model a heterogeneous cell population in vitro is key to understand the complex interactions of cancer, stromal, and immune cells, and their collective response to the testing drugs within the TME (**Figures 3-2C, D**). For instance, a cisplatin sensitivity study used a simple 2D transwell system with Boyen's chambers to coculture patient-derived CAFs and pharyngeal cancer cell lines (FaDu and Detroit 562) (41). Clonogenic survival and gene inspection showed that CAFs notably affected the colony-forming and cisplatin-sensitizing capabilities of pharyngeal cancer cells through the paracrine signaling of VEGFA, PGE2S, COX2, EGFR, and NANOG. As 2D transwell systems can incorporate two cell types at most, enhancing the complexity of in vitro models is a necessary step to better mimic the 3D tumor cell heterogeneity in H&N and other tumors. However, one major challenge of multicellular coculture models is the cross-contamination of culture media (42). To address this challenge, microfluidic platforms can be used to compartmentalize heterogeneous cell populations within the same culture platform (43, 44). One plausible strategy is to culture individual cell populations in separate compartments sharing a constantly irrigated channel with cultured media. The shared media will then contain paracrine factor secretion aiding the multicellular interactions of the individual cellular compartments.

3.3.3 Hypoxic environment and fenestrated vasculature

Tumor hypoxia is a notable factor of avascular solid tumor cores and micrometastases in cancer development (45). The TME of H&N cancer may have regions with oxygen levels as low as <5 mmHg at hypoxic sites (46). Fenestrated vasculature in hypoxic niches leads to vessel leakage, which limits an effective supply of oxygen, nutrients, and therapeutics to the tumor core. Hypoxic cues, namely, oxygen deprivation and irregular irrigation, are thus two key parameters to be considered in the design of effective in vitro H&N cancer models (**Figures 3-2E, F**).

Regarding oxygen deprivation, hypoxic gradients can be created by utilizing 3D in vitro culture geometry (47) or hypoxic culture chambers with microfluidics (48). For instance, spheroid cultures have been created to generate three geometrical regions with distinctive hypoxic gradients, namely, (I) an outer high-oxygen/nutrient-proliferative region, (II) a middle medium-oxygen/nutrient senescence region, and (III) a low-oxygen/ nutrient necrotic region found in the spheroid core (36, 45).

Concerning irregular irrigation, static cultures do not translate the capillary supply as of in vivo systems (49). To this end, microfluidic technologies hold great promises to mimic the irregular blood supply of tumors by precisely controlling and monitoring the flow rate of media (ranging in microliters per minute) with integrated microchannels and a sensing element into the culturing platform (50). Hypoxic profiles can also be tuned by integrating spheroid models into microfluidic platforms. The cellular uptake of chemotherapy drugs can then be imaged along specific hypoxic gradients with real-time microscopy (51).

3.4 Advanced in vitro models for head and neck cancer drug screening and evaluation

The most common evaluation platform for drug development in H&N cancer is conventional 2D in vitro models thus far due to their low cost, high reproducibility, and potential coculture capability (52). However, 2D in vitro models are unable to (I) mimic the physical geometry of tumor, (II) avoid the cross-contamination of culture media in multicellular models, and (III) mimic the oxygen deprivation and irregular irrigation of the hypoxia region, which are key factors in the evaluation of tumor progression, chemoresistance, and treatment response (35, 36, 52). Advanced in vitro systems, including spheroids, 3D scaffolds, and microfluidic devices, have thus been developed to overcome these barriers (53). Although the application of these culture platforms to model H&N cancer microenvironment and its drug discovery is still in its infancy, recent research on H&N cancer has been using 3D in vitro models to advance the growing need of these systems for clinical translation (**Figure 3-3**).

3.4.1 Spheroid models

Spheroids are functional aggregations of cells that are generally formed via forced floating aggregation, hanging drop, or organotypic hydrogel embedment methods (52). The forced floating aggregation methods are most commonly used in H&N cancer models (32–34, 54–57) (**Table 3-1, Figure 3-4).** The forced floating method is to use low-attachment well-plates that hinder the cell–substrate interaction and promote cell self-aggregation. In addition, hanging drop and hydrogel embedment methods were also used to fabricate H&N cancer spheroids. The hanging drop methodology is to place a drop of cell suspension on the underside of culture plates that cells can aggregate and form spheroids at the drop tip (58, 59). For the organotypic hydrogel embedment

approach, cell suspensions are pipetted into an ECM-based hydrogel for cellular support, self-assembly, and spheroid formation (60, 61).

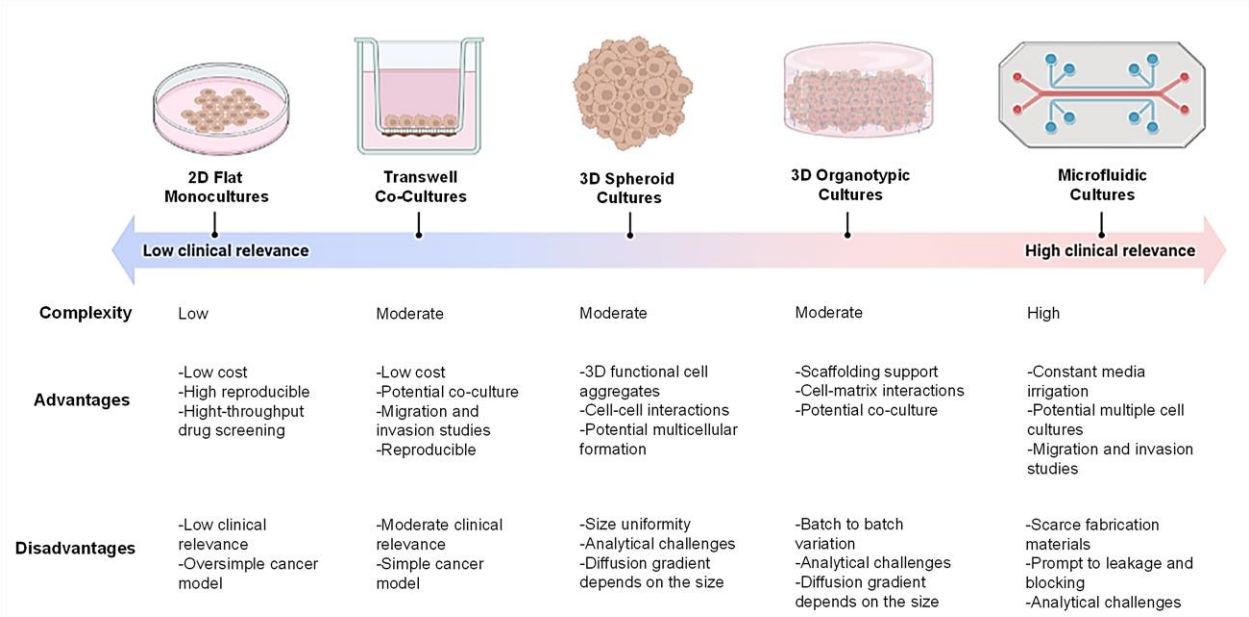

Figure 3-3. Common in vitro cancer models. Two-dimensional (2D) flat monolayer cell cultures grown on plastic or glass surfaces. Transwell systems with Boyden's chamber inserts for cellular cocultures. 3D spheroid-based systems by forced aggregation of cells into a 3D construct. 3D organotypic systems by culturing cells within a matrix such as a hydrogel. Microfluidic-based culture systems by culturing cells within a microchannel with fluid circulation. Figure created with BioRender.com.

With the introduction of spheroid H&N models, researchers were able to better decipher the epithelial–mesenchymal transition (EMT) mechanism under a hypoxic environment with or without cancer drugs (62). For example, Melissaridou et al. (33) compared 2D and 3D cell cultures from five H&N squamous cell carcinoma–derived cell lines in their expression of EMT and stemness markers as well as response to cetuximab and cisplatin drugs. EMT-associated and stem cell markers including CDH1, NANOG, and SOX2 were upregulated in 3D spheroid groups but not in 2D monolayer controls. In addition, the spheroid groups showed increased resistance to cisplatin and cetuximab treatments compared to 2D monolayer cultures. Essid et al. (48) developed spheroids from a human tongue cell line to investigate the relationship between EMT and hypoxia. These spheroids were grown in hypoxic chambers subjected to 1% O2 for 30 days. Results showed an increased mRNA expression in E-cadherin and N-cadherin as well as carbonic anhydrase 9, a hypoxic marker, in the spheroid hypoxic cores.

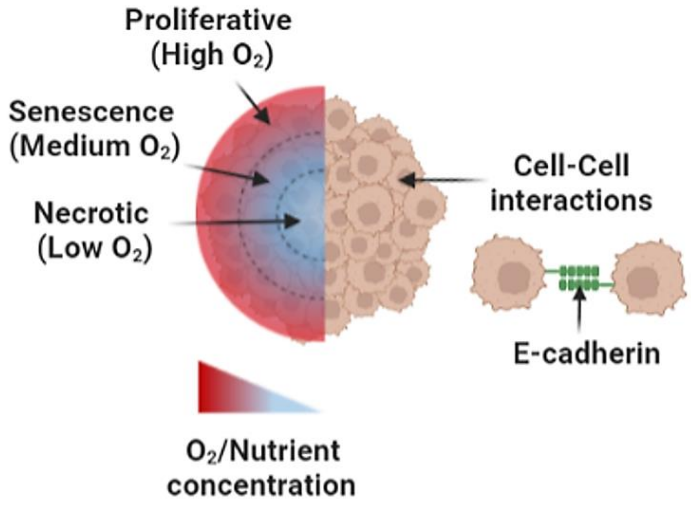

Figure 3-4. An illustration of spheroid culture model. Hypoxic gradients within spheroid cultures comprise an outer high-oxygen/nutrient region, a middle medium-oxygen/nutrient region, and a low-oxygen/nutrient region. In addition, cell–cell interactions take place in the spheroid model via functional cell aggregation and E-cadherin binding. Figure created with BioRender.com.

To further investigate the effect of hypoxia on the treatment response in H&N cancers (**Figure 3-4**), Basheer et al. (47) analyzed protein expression on five H&N cancer cell lines under normoxia and hypoxia in both OSC-19 spheroid cultures and monolayer controls using Western blot, flow cytometry, and immunofluorescence staining. The protein expression of CCR7, a chemokine receptor associated with hypoxia, was found significantly higher in the hypoxic core of the spheroid cultures compared to monolayer and normoxic controls. All in all, previously mentioned results pointed to the importance of tumor-like geometries as presented in spheroid models for the evaluation of drug sensitivity and cytotoxicity.

Future prospects

New 3D bioprinting techniques such as inkjet-based, pressure-assisted, and laser-assisted approaches (63) hold new promises for fabricating complex organotypic tumor spheroids in terms of cellularity and architecture (64). To fabricate multicellular spheroids, bioprinting allows the layer-by-layer precise assembly of 3D biological constructs. Synthetic polymers (e.g., polycaprolactone) and naturally derived polymers (e.g., alginate) are commonly used as bioinks to resemble the tissue-specific ECM (65, 66). Bioinks can also be printed with multiple cell types

(squamous cell carcinomas, CAFs, and pro-tumor macrophages of H&N tumors) by using pressure-assisted and laser-assisted printing approaches (63). The incorporation of cancer stem cells may further mirror the aggressive H&N TME (55, 67) in the bioprinted construct due to the self-renewal and differentiation capabilities of these cell types. In addition, physiological cues such as 3D tumor geometry, cell heterogeneity, and normoxic-to-hypoxic strata can thus be recreated to induce cell–cell/–ECM interactions as expected in the H&N TME (68).

Further, a multi- and heterogeneous-layer geometry of the tumor spheroids can be bioprinted by implementing cell-laden bioink deposition with zone-specific techniques, for example, by varying pore-size and interconnectivity (63, 66, 69). As a result, each layer of the organotypic spheroid can have individual TME cell populations and ECM compositions to better mimic hypoxic niches within the tumor-like in vitro models (63). Within the 3D organotypic models, organoids that are specific3Dcell–embedded models consisting of stem or patient-specific cells and ECM constituents in the form of a multilayer geometry are very desirable H&N TME models (70). The future perspective of organoids is further discussed in the Future Outlook section.

Table 3-1. Spheroid models in head and neck (H&N) cancer research.

Author	Aim	Drug Stimulant	Culture Model Design and Components				Analytic Outputs	Main Findings
			Single vs Multi-cellular Cultures	Primary vs Cell Lines	2D vs 3D Geometry	Hypoxic Cues		
Schmidt *et al.* [111]	To compare the effect of 2D and 3D culture methods regarding gene expression in terms of cell junctions, cell adhesion, cell cycle and metabolism	NS	Single	**Primary:** NS **Cell lines:** - FaDu -HLaC78 -Hep-2 -Hep-2-Tax -HLaC79 -HLaC79-Tax -HPaC79 -HSmC78 -CAL-27 -PE/CA-PJ41 -SCC4 -HNO210	**2D:** Monolayer control **3D:** Forced floating method	NS	-RNA extraction -RNA quality control -Microarray analysis -Real-time PCR -Scanning electron microscopy	-Spheroid tight formation was dependant on upregulation of E-cadherin (cell adhesion) and downregulation Ki67 (cell proliferation) in comparison to monolayer controls
Melissaridou *et al.* [112]	To compare the effect of 2D and 3D culture methods on cell	-Cetuximab -Cisplatin	Single	**Primary:** NS	**2D:** Monolayer control	NS	-Clonogenic assay -Tunel staining	-Spheroids presented a cancer stem cell-like phenotype

	proliferation, response to anti-cancer drugs and EMT profiles			**Cell lines:** -LK0858B -LK0902 -LK0917 -LK1108 -LK1122	**3D:** Forced floating method		-CellTiter 96® Proliferation Assay -Western blotting -RT-qPCR	(upregulation of EMT-associated proteins). -Drug effects were significantly different on spheroids compared to monolayer control.
Azharuddin *et al.* [83]	To compare the effect of 2D and 3D culture methods regarding chemoresistance	-Cisplatin -Doxorubicin -Methotrexate	Tri-culture (cancer cells)	**Primary:** NS **Cell lines:** -LK0902 -LK0917 -LK1108	**2D:** Monolayer control **3D:** Forced floating method	NS	-CellTiter 96® Proliferation Assay -Live-cell imaging calcein-AM -Ros DCFDA assay -Flow cytometry	-Drug vulnerability and potential chemoresistance was predicted by analyzing efflux pump (ABC pump) activities. -Comparative response of multi-drug resistance, drug efflux capability, and reactive oxygen species on treated cells.

Essid *et al.* [113]	To compare the effect of 2D and 3D culture methods on EMT, cancer stem cell, and hypoxia markers	Hypoxia 1% O_2 chamber (monolayer)	Single	**Primary:** NS **Cell lines:** CAL-33	**2D:** Monolayer control **3D:** Forced floating method	✓	-Clonogenic assay -Western blotting -Immunofluorescence staining -RT-PCR	-Serum in media was reported to revert EMT, cancer stem cell, and hypoxia phenotype. -Spheroids cultured under hypoxia (1% O_2) showed increased carbonic anhydrase IX, vimentin, N-cadherin, glioma-associated oncogene homolog 1, and decreased E-cadherin.
Basheer *et al.* [114]	To compare the effect of hypoxic and normoxic culture methods on HIF-1α – CCR7 correlation	Hypoxia, low O_2 or $CoCl_2$ to cell culture medium	Multi-cellular	**Primary:** NS **Cell lines:** -OSC-19 -FaDu -SCC-4 -A-253 -Detroit-562	**2D:** Monolayer control **3D:** Spheroid formation Not Specified	✓	-Immunofluorescence staining -Immunoblotting -Flow cytometry	-HIF-1α expression (hypoxia) was associated with the expression of CCR7 (migration marker). -Correlation between HIF-1 α and CCR7 was noted in early histological xenograft cancer samples

Hagemann *et al.* [115]	To compare 2D and 3D methods as chemotherapy and radiotherapy testing platforms	-Cisplatin -5-FU -2Gy radiation	Single	**Primary:** -Tumor biopsy from H&N squamous cell carcinoma **Cell lines:** -CAL-27 -FaDu -PiCa	**2D:** Monolayer control **3D:** -Forced floating and -Hanging drop methods	NS	-WST-8 assay -ELISA	-Forced floating method was reported to be safer and more reliable than the hanging drop method. -Proof-of-concept data concerning spheroids as therapy screening platform. -Spheroid growth was reduced after chemoradiation treatment. Significant negative impact was noted with the cisplatin + radiation treatment compared to cisplatin alone.
Goričan *et al.* [116]	To evaluate a 3D model as therapy testing platform	All-trans retinoic acid (ATRA)	Single	**Primary:** NS **Cell lines:** FaDu	**2D:** NS **3D:** Forced floating method	NS	-Immunofluorescence staining -qPCR -Flow cytometry -Western blotting -HTS	-A new cancer stem cell-enriched spheroid model adaptable for HTS of anti-cancer stem cell compounds -ATRA treatment was reported to reduce cancer stem cell markers.

Magan *et al.* [117]	To evaluate a 3D model as chemotherapy and immunotherapy testing platform	-Cisplatin -Cetuximab	Two-culture	**Primary:** Patient-derived cancer-associated fibroblasts **Cell lines:** -LK0902 -LK0917 -LK1108	**2D:** NS **3D:** Forced floating method		-Immunofluorescence staining -TUNEL assay -RT-qPCR - CellTiter 96® Proliferation Assay	-Cancer-associated fibroblasts increased cancer cell proliferation and EGFR expression in co-cultured tumor spheroid -EGFR-overexpressed spheroids showed increased response towards cetuximab after 72h exposure -Ki67 overexpression was noted in tumor cells treated with cisplatin for 72h
Kochanek *et al.* [118]	To evaluate a 3D model as chemotherapy testing platform	-Doxorubicin	Single	**Primary:** NS **Cell lines:** -FaDu -CAL-27	**2D:** NS **3D:** Forced floating method	NS	-Immunofluorescence staining -Widefield microscopy -LIVE/DEAD staining -Proliferation assay -Mitochondrial mass and membrane potential assay	-Cells at the outer layer of the spheroid showed higher drug uptake compared to cores after 1-day exposure -Spheroid morphology was altered after 1-day drug exposure

-CAL-33

-OSC-19

-Detroit-562

-BIRC-56

-PCI-13

-PCI-52

-UM-SCC-1

UM-22B

-SCC-9

-HET-1A

3.4.2 Organotypic models

Organotypic models provide intracellular communication between cells embedded in ECM-based scaffolds (71–74) (**Figure 3-5**). A 3D scaffold-based in vitro model aims at recapitulating the native tissue's ECM microenvironment in terms of mechanical stability and structural architecture in the support of cell signaling, migration, survival, and growth (75). The materials used to make biological scaffolds are mostly obtained from natural or synthetic polymers, often in aqueous form. To convert the aqueous materials to a gel-like scaffold, crosslinking methods such as UV radiation, enzymatic reactions, and temperature changes have been adopted for sol–gel transitions in most in vitro cancer model developments (76).

To date, organotypic H&N models comprise the use of patient-derived H&N squamous cells together with decellularized extracellular matrix (dECM) (77–80)or synthetic ECM substitutes (60, 61, 81–83) as the most common constituent materials (**Table 3-2**). In particular, dECM scaffolds are often selected for cancer modeling, owing to their retained bioactive molecules (e.g., collagen, proteoglycans, and glycoproteins) (75) to support H&N cancer and TME cells for organoid formation. In addition, synthetic ECM substitutes such as the commercially available Matrigel®, which is derived from mice sarcoma (84), are also used for fabricating organotypic H&N cancer models (60, 77, 80). However, Matrigel® is reported with single-batch variations that cause a significant concern on mechanical inconsistency, especially in fabricating reproducible organoids even when using the same batch of the product (84).

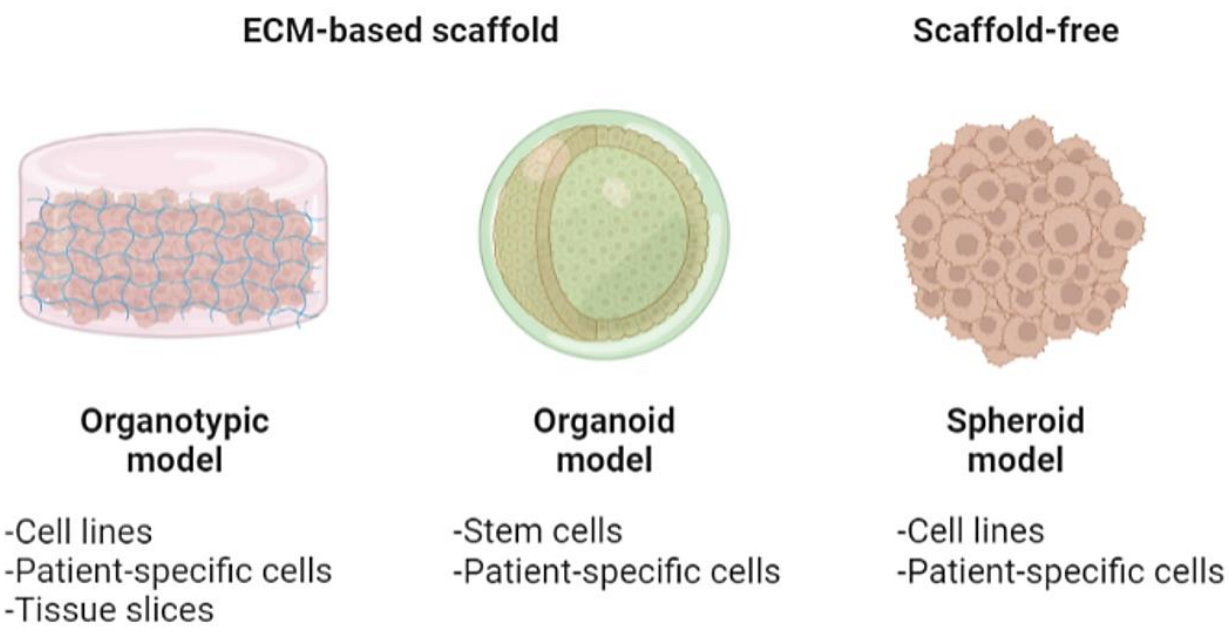

Figure 3-5. An illustration of organotypic culture models. Organotypic models provide cell–cell/ECM interactions within the culture model. Organotypic models are 3D in vitro platforms comprising the embedment of disaggregated cells/tissues in ECM-based scaffolds. Particularly, organoids are those organotypic models derived specifically from stem or patient-specific cells. Spheroids may be fabricated using one or multiple conventional cell lines or patient-derived cells, with or without the use of ECM-based embedment. Figure created with BioRender.com.

In an effort of developing patient-specific organotypic models, Tanaka et al. (60) combined an epithelial cell sheet, the Matrigel®, and individual squamous cell carcinomas derived from 43 biopsies of H&N cancer patients. The organotypic models were subjected to the exposure of cisplatin and docetaxel for eight consecutive days (60). Results showed that these models displayed a patient-specific chemoresistant response. For example, the MDA-HN-2C organoid group developed resistance to cisplatin and docetaxel, corresponding to that of the individual patient donor with recurrent H&N cancer. In addition, the organoid-like models showed increased resistance to both drugs in comparison to that of 2D monolayer controls. The proposed patient-derived organoid (PDO) platform served a notable step toward the application of predicting patient-specific H&N drug sensitivity in vitro.

One advancement of the cancer organotypic model is to approximate the heterogeneity of tissue strata as seen in the tumor architecture. For instance, in H&N tumor, tissue strata mostly comprise

squamous epithelia, basal strata, stroma, and lamina propria. Zhao et al. (77) investigated whether the tissue sources of dECM would result in a specific stratum architecture of the scaffold that might, in turn, affect the drug response of cancer cells. Mouse, rat, and pig tongue tissue samples were decellularized and used to fabricate scaffolds with patient- specific cancer-associated fibroblasts and CAL-27 cells. Hematoxylin & eosin staining, scanning electron microscopy, and transmission electron microscopy showed a similar histological stratum architecture of the three dECM scaffolds. Further investigation using a mouse dECM scaffold showed that the elastic modulus of mouse dECM scaffolds was comparable to that of native mouse tongue tissue (0.503 MPa vs. 0.567 MPa).

Compared to monolayer non-scaffold controls, mouse-derived dECM scaffolds showed improved cell adhesion, proliferation, and survival after 14 and 28 days of cultures in the absence of drug exposure. After a 2-day exposure of cisplatin, an apoptotic marker, namely, caspase 8, showed distinctive staining patterns across the strata of mouse-derived dECM scaffolds. For instance, cancer cells at the muscle fiber layer of the scaffold expressed stronger caspase 8 expression than those at the basal layer of the scaffold, possibly owing to the drug-penetration gradients.

Aside from the evaluation of dECM sources, Ayuso et al. (79) compared 3 culture models, namely, (I) 2D monolayer cocultures with primary cancer-associated fibroblasts and H&N cancer cell lines (UM-SCC-1 and UM-SCC-47), (II) 3D collagen hydrogel scaffolds seeded with H&N cancer cells, and (III) 3D H&N cancer cell spheroids of their responses to cetuximab and an mTOR inhibitor. Cell cytotoxicity results indicated a stronger drug resistance response in the coculture (1.4-fold increase) and 3D culture groups (2.6-fold increase) compared to 2D monocultures. No statistical comparison was reported between the two 3D culture groups. Nevertheless, the differentiated drug resistance between the 2D and the 3D culture groups may be associated with the geometry-induced drug impediment.

High-throughput screening (HTS) with organotypic models is one critical advancement of scaffold models for immune- oncology and drug discovery (85). Using 384-well plates, Tuomainen et al. (80) evaluated the effect of 19 immunotherapy drugs on 12 H&N cancer cell lines seeded within 3D scaffolds inserted in those plates. The 19 immuno- drugs were inhibitors of 5 EGFR (gefitinib, erlotinib, cetuximab/erbitux, canertinib, and afatinib), 6 MEK (trametinib, TAK-733, selumetinib,

refametinib, pimasertib, and binimetinib), and 8 mTOR (temsirolimus, sirolimus, ridaforolimus, PF-04691502, omipalisib, everolimus, dactolisib, and apitolisib). The testing scaffolds included Matrigel® and human-derived leiomyoma referred to as Myogel. Compared to Matrigel®, cells embedded in Myogels showed significantly lower EGFR and MEK inhibition activity after 72 h of drug inspection. Normalized HTS drug response profiles consisted off our activity levels based on a drug-sensitivity score (DSS) and artificial cutoff points: inactive DSS < 5, low 5 ≥ DSS < 10, moderate 10 ≥ DSS < 15, and high DSS ≥ 15 (80). Overall, a low activity of mTOR inhibitors was consistently found in most of the cell lines from both Matrigel® and Myogel scaffold models. Results from this study provided early evidence of the reliability and predictability of using HTS organoid platforms in the evaluation of cancer therapeutics.

In addition to chemotherapy drug–related studies, Young et al. (81) developed a 3D tissue construct of a collagen and cellulose tissue roll scaffold "TRACER" for radiation therapy screening. The FaDu cell line and primary cancer–associated fibroblasts, stromal cells, were transfected with green fluorescent protein and mCherry, respectively. Both cells were seeded into the cellulose layer (cancer-associated fibroblasts in layer 1 and FaDu in layer 3) with or without a central collagen/agarose layer to separate the coculture. The cell-seeded TRACER was rolled onto an acrylic core placed into custom-made 50-ml Falcon tubes and then subjected to 5- or 10-Gray radial arc radiations. Clonogenic results indicated that no radioprotective behavior from the CAFs was observed in the cocultures regardless of the presence of the central layer after 24-h culture. In a separate study, x-ray radiation (0–15 Gray) was found to downregulate HeLa cancer cell proliferation, cell viability, vinculin, and a- tubulin expression in 2% agarose hydrogels with 250 μm of diameter compared to 2D flat counterparts (86). Although results from these two radiation studies were not fully corroborated, 3D tissue constructs with cocultures showed the potentials of elucidating epithelial–stromal interactions of tumor response to radiation exposure.

Future prospects

Organotypic models have demonstrated great possibilities for approximating the TME and supporting the HTS cancer drug platform. Several technical challenges remain to adapt the organotypic models to fulfill the two aforesaid promises. Organotypic fabrication is complex, especially considering the scaffold embedment that influences the therapeutic response based on

the scaffold's composition and network (87). For instance, these models have not been fully designed to incorporate the irrigation features of tumor modeling. One possibility is to place the scaffolds into microfluidic channels to recapitulate the constant irrigation features of native tumor or healthy tissues with bioprinting and electrospinning techniques (88). Electrolyte-assisted electrospinning can further help to fabricate nanofibrous membranes through electrostatic forces to draw charged threads of dissolved polymers to a grounded electrolyte solution (89). These nanofiber membranes can be located inside microfluidic channels for tissue-engineered scaffolds (89). By integrating electrospinning and microfluidic technologies, scaffold-based models can better meet the functionality of continuous monitoring and irrigation of cancer therapeutics.

Table 3-2. Organotypic Models in Head and Neck Cancer Research. NS = Not Studied

Author	Aim	Drug Stimulant	Culture Model Design and Components				Analytic Outputs	Main Findings
			Single vs Multi-cellular Cultures	Primary vs Cell Lines	2D vs 3D Geometry	Hypoxic Cues		
Tanaka *et al.* [119]	To compare 2D vs 3D methods as chemotherapy sensitivity platform	-Cisplatin -Docetaxel	Single	**Primary:** -Tumor biopsy from H&N squamous cell carcinoma **Cell lines:** -MDA-HN2016-2 -MDA-HN2016-18 -MDA-HN2016-21	**2D:** Monolayer control **3D:** Forced floating method and then transferred into Matrigel®	NS	-DNA extraction -STR profiling -Western blotting -Clonogenic assay	-Patient-derived organotypic model were useful as testing platforms for chemotherapy agents. -Seven 2D cell lines and 13 organoid cell lines produced after this study -Obtained cell lines presented chemoresistance cues as tissue source
Driehuis *et al.* [120]	To compare 2D vs 3D methods as photodynamic therapy testing platform	Photosensitizer (binds EGFR) for photodynamic therapy	Single	**Primary:** -Tumor biopsy from H&N squamous cell carcinoma	**2D:** Monolayer control **3D:**	NS	-qPCR -Flow Cytometry -Immunofluorescence staining -PDT Assay	-Patient-derived organotypic model had similar EGFR expression as tissue source. -These models were useful as testing platforms for EGFR-targeted therapy.

				Cell lines: - UM-SCC-14C -CRL-1555 -human cervical carcinoma cell line HeLa (CCL-2) -human embryonal kidney cell line HEK293T (CRL-3216)	Basement Membrane Extract type 2 (an ECM mimetic agent) in media			
Zhao *et al.* [121]	To compare 2D vs 3D methods as chemotherapy screening and regenerative platform	Cisplatin	Single	**Primary:** -Patient-derived tongue squamous cell carcinoma and cancer-associated fibroblasts **Cell lines:** -CAL-27	**2D:** Monolayer control **3D:** Decellularized tongue extracellular matrix from mice, pig and rat	NS	-Immunohistochemistry and immunofluorescence staining -Scanning electron microscopy -Transmission electron microscopy -Atomic force microscopy -DNA quantification -Proteomic analysis	-3D scaffold derived from tongue squamous cell carcinoma as *in vitro* culture support and migration -3D ECM-like platform for drug testing -Mouse-derived dECM scaffold showed increased cell adhesion, survival, and differentiation compared to control -Cisplatin exposure data showed heterogeneity of cisplatin response within the muscle and basal layers of the mouse-derived dECM scaffold via cell cytotoxicity and caspase 8 positive staining compared to monolayer control.

					-collagen I/Matrigel® matrix		-MTT assay -Scratch assay	
Burghartz *et al* [122]	To compare 2D vs 3D methods as *in vitro* support model	**NS**	Single	**Primary:** Human salivary gland epithelial cells **Cell lines:** -CAL-27	**2D:** Monolayer control **3D:** decellularized porcine jejunum matrix	NS	-Immunofluorescence staining -Scanning electron microscopy -Transmission electron microscopy -Amylase Assay Kit -RT-PCR	-3D ECM-like platform for potential radiotherapy use -Gene expression of α-amylase was higher in 3D mono- and coculture compared to 2D monoculture
Ayuso *et al.* [123]	To compare 2D vs 3D methods as dual drug screening platform	-AZD8055 (mTOR inhibitor) -Cetuximab (Erbitux)	Two-culture	**Primary:** -Patient-derived cancer-associated fibroblasts **Cell lines:** -UM-SCC-1 -UM-SCC-47	**2D:** Monolayer control **3D:** Spheroid hanging drop	NS	- CellTiter 96® Proliferation Assay -Immunofluorescence staining	-3D ECM-like platform as co-culture setup for drug testing and EGFR pathway analysis -Cell cytotoxicity data showed higher drug resistance response in the co-culture (1.4-fold increase) and 3D culture groups (2.6-fold increase) compared to 2D monocultures

					(cultured without fibroblasts) 3D collagen hydrogel (cultured without fibroblasts)			
Tuomainen *et al*. [124]	To compare 2D vs 3D methods as drug screening platform	-EGFR (Gefitinib, Erlotinib, Cetuximab, Canertinib, and Afatinib) -MEK (Trametinib, TAK-733, Selumetinib, Refametinib, Pimasertib, and Binimetinib) -mTOR (Temsirolimus, Sirolimus, Ridaforolimus, PF-04691502, Omipalisib, Everolimus,	Single	**Primary:** NS **Cell lines:** -UT-SCC-8 -UT-SCC-14 -UT-SCC-24A -UT-SCC-24B -UT-SCC-28 -UT-SCC-42A -UT-SCC-42B -UT-SCC-40	**2D:** Monolayer control **3D:** Matrigel® and a leiomyoma–derived matrix “Myogel”	NS	**-**Drug sensitivity and resistance testing **-** CellTiter 96® Proliferation Assay -Meta-analysis of Clinical Data -Immunoblot analysis	-3D ECM-like platform for drug testing and pathway analyses -Cells seeded in Myogels showed significantly lower EGFR and MEK inhibition activity -Cells seeded in both scaffolds showed a low mTOR inhibition activity in most of the cell lines

		Dactolisib, and Apitolisib)		-UT-SCC-44 -UT-SCC-73 -UT-SCC-81 -T-SCC-106A				
Young *et al.* [125]	To compare 2D vs 3D methods as radiotherapy screening platform	5 or 10 Gray	Two-culture	**Primary:** -Patient-derived Cancer-associated fibroblasts **Cell lines:** -CAL-27	**2D:** Monolayer control **3D:** Tissue Roll for the Analysis of Cellular Environment and Response (TRACER) construct a collagen gel and cellulose scaffold	✓	-MTT assay -Immunofluorescence staining -Hypoxia (EF5) staining -Live/Dead staining -Cell migration -Clonogenic assay	-3D ECM-like platform as co-co-culture setup for radiotherapy and hypoxia analysis -Increased cell migration and invasion of tumor-stroma co-cultures within the layers of the tissue roll construct -No significant radiation resistance of tumor-stroma co-cultures within the layers of the tissue roll construct
Lee *et al.* [126]	To compare 2D vs 3D methods as chemotherapy testing platform	-Cisplatin -Docetaxel	Two-culture	**Primary:** -Tumor biopsy/explants from H&N	**2D:** Monolayer control	✓	-Cell counting kit-8 (CCK-8) -LIVE/DEAD assay using	-Tumor explants were reported to present hypoxic cues, and drug screening sensitivity

				squamous cell carcinoma **Cell lines:** NS	**3D:** Dissociated epithelial cells seeded on a mixture of solidified fibrin glue and tumor explants		-LOX-1 a hypoxia probe	-Tumor explants in fibrin matrix survived over 10 days while those explants without the matrix survived less than 8 days
Engelmann *et al*. [127]	To compare HPV-associated organotypic explants as radiotherapy testing platform	2 Gray	Multi-cellular	**Primary:** -Tumor biopsy/explants from H&N squamous cell carcinoma **Cell lines:** NS	**2D:** NS **3D:** Dermal equivalents from viscose fiber fabric embedded with fibroblast for ECM production H&N tissue slices	NS	-H&E staining -Immunohistochemical staining -Immunofluorescence staining -PCR -Motility and invasiveness analysis -Cell viability, proliferation, and apoptosis assays	-3D ECM-like platform for radiotherapy use -Radioresistant tumor cells and morphological variations were noted after 5-day fractionated irradiation exposure -Tumor slices/explants in dermal equivalents remained viable for up to 21-day cultures

3.4.3 Microfluidic platforms

Microfluidic platforms are micromanufactured devices with interconnected chambers, membranes, and grooves that share low volumes of fluids (**Figure 3-6**), which have been widely applied for in vitro modeling such as organ-on-a-chip models (49, 90–95) and point-of-care systems (96). In cancer research, microfluidic platforms are mostly fabricated using lithography and surface micromatching techniques with polydimethylsiloxane, silicon, glass, polycarbonate, and polymethylmethacrylate as main materials (49, 91–93, 97–99). Flow mechanisms can be implemented through a passive or an active approach within the microfluidic device. Passive flow can be driven by gravity, hydrostatic pressure, surface tension, or osmotic pumps (93). Active flow mechanism, which is commonly used in H&N microfluidic devices, involves the use of peristaltic (2 µl/min to 10 L/min), syringes (0.012 nl/min to 0.3 L/min), and pressure- driven pumps (nl/min to ml/min) (49, 91, 93, 96–100).

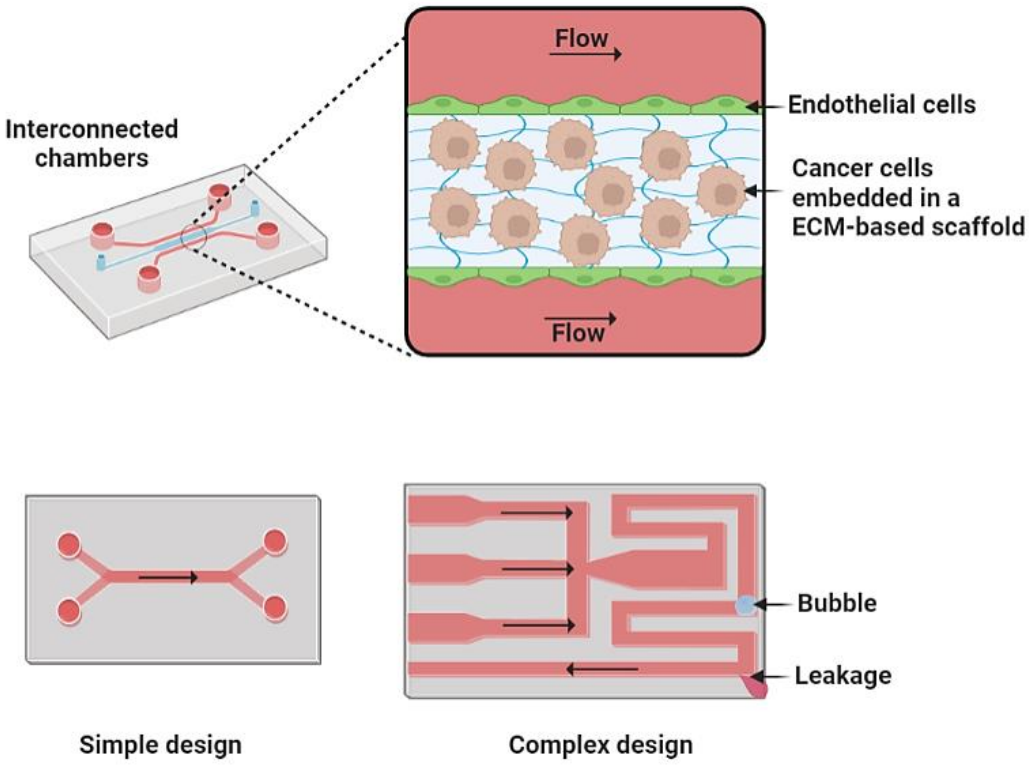

Figure 3-6. An illustration of microfluidic culture models. Microfluidic devices comprise the interconnection of chambers and grooves sharing low volumes of liquids. A more complex design with more channels and chambers can enhance its physiological representation but may also increase the chance of challenges as bubble blocking and liquid leakage. Figure created with BioRender.com.

Microfluidic platforms support simultaneous compartmentalization of multiple cancer cell populations with constant culture media irrigation (90). This compartmentalization with dynamic flow features allows for the programmatic control and real-time monitoring of cancer cell–vasculature interplay through the interconnected cellular compartments of the platform (49, 91, 101). Most chemotherapy drugs are also delivered intravenously that flow dynamically through blood vessels to the tumor vasculature and extravascular tissues (102). The dynamic flow feature of microfluidic devices can thus resemble the transportation of intravenous systemic treatment and help to evaluate its pharmacokinetics in a more precise, controllable manner. Chemotherapy drugs, such as paclitaxel, cisplatin, and 5-fluorouracil, have been tested with microfluidic devices in H&N cancer research (**Table 3-3**).

The first microfluidic device for H&N cancer drug screening was designed by Hattersley et al. via lithography in polydimethylsiloxane and a syringe pump (49). Primary H&N squamous cell carcinoma biopsies (~3-mm3 size) placed in the microfluidic device equipped with a syringe pump were exposed to cisplatin and 5-flourouracil continuous flow up to 7 days. Results showed decreases in cell viability and proliferation on drug-exposed groups compared to unexposed controls. In addition, the sandwich ELISA results of cytochrome c, a key compound in cell apoptosis, were found higher in the culture media in the treated groups compared to untreated controls. This study represented an important step of evaluating the personalized treatment of patient's tumor biopsies under constant drug irrigation.

Riley et al. (91) further advanced the design of microfluidic platforms for personalized H&N drug screening. This platform was fabricated with two polyether–ether–ketone support plates, a silicone gasket as a tissue well, and a syringe pump. Such platform was applied to evaluate the effect of a combined JNK inhibitor and etoposide drug treatment on thyroid cancer biopsies (~5-mm diameter) from 23 individual patients. After 4 days of drug exposure, increased cell death was found in the thyroid cancer biopsy group compared to the unexposed group although no patient-specific drug responses were observed in this study.

Interconnected compartmentalization strategies within microfluidic devices for H&N cancer modeling were first implemented by Jin et al. (103). Their microfluidic platforms were made of

two layers of polydimethylsiloxane interconnected by a porous polycarbonate membrane and flow applied via a double syringe pump. This membrane allowed the nutrient/drug exchange between the top chamber (i.e., more cell death) to cisplatin/5-fluorouracil treatment whereas patient-specific spheroids (SCC-1 group) were more sensitive to cisplatin/paclitaxel treatment.

Future prospects

H&N cancer drug studies with microfluidic models emphasized the importance of using patient-derived biopsies from oral cavity, pharynx, larynx, lymph nodes, and thyroid for patient-specific prediction of drug response (49, 91, 94), echoing those as in the review of organoid models. Patient-derived tissue biopsies preserve key cellular heterogeneity and geometry of the tumor, which are important variables for drug screenings. However, the use of tissue/tumor biopsies for microfluidic platforms is hampered by the technical challenge of on-chip imaging and off-chip analysis (104). Milliscale tissues as tumor biopsies usually give raise to culture challenge concerning the complex tissue preservation during long-term culture times (105). Fortunately, advances in microfluidic platforms make the long-term culture of thick tissue samples possible with an effective nutrient and oxygen supply through a dynamic flow of culture medium (49, 91). In particular, pump-free microfluidic devices were shown to be able to maintain 2-mm human organotypic models for a 75-day continuous culture of human brain organoids (106).

Other advances in microfluidic technology, such as dismantable/open and droplet-based formats, also facilitate the development of tumor-on-a-chip devices (104) (**Figure 3-7**). The dismantable/open-layer feature of microfluidic platforms allows for the direct retrieval of the analyzed samples by taking apart the top layer of the device (104). Cultured materials can then be easily accessible for off-chip analysis as the histological staining of biopsies and biopsy-like tissues. The fabrication of tumor-on-a- chip platforms can be complicated due to the necessity of having a microscale cell culture environment and chamber flow interconnection, which often requires high manual skill sets. The use of 3D printing for creating the on-chip microcomponents such as chambers, membranes, and grooves is therefore a very wise option to save labor and costs compared to conventional lithography and polydimethylsiloxane molding (107–111).

Table 3-3. Microfluidic Devices in Head and Neck Cancer Research. NS = Not Studied

Author	Aim	Drug Stimulant	Culture Model Design and Components				Analytic Outputs	Main Findings
			Single vs Multi-cellular Cultures	Primary vs Cell Lines	2D vs 3D Geometry	Hypoxic Cues		
Hattersley *et al*. [128]	A dynamic culture method as chemotherapy screening platform	-5-FU -Cisplatin	Single	**Primary:** Patient-derived H&N squamous cell carcinoma **Cell lines:** NS	**2D:** Unexposed control Dynamic flow **3D:** Multi-micro-channels Dynamic flow Syringe pump	NS	-H&E staining -Lactose dehydrogenase release -WST-1 metabolism -Trypan blue -Cytochrome C analysis	-Preclinical model for personalized medicine and testing -H&E staining showed retention of multi-layer tissue strata -Combination therapy presented higher levels of cytochrome C compared to untreated control
Riley *et al*. [129]	A dynamic culture method as drug screening platform	-Etoposide (topoisomerase II inhibitor) -SP600125 (JNK inhibitor)	Single	**Primary:** Human thyroid tissue samples **Cell lines:**	**2D:** Unexposed control Dynamic flow **3D:**	NS	-Hematoxylin and eosin -Flow cytometry -Trypan blue -Immunohistochemistry staining -Functional analysis	-Preclinical model for personalized medicine and testing -H&E staining showed retention of multi-layer tissue strata -Thyroid biopsies were considered functional due to the production of T4 during the culture period -Increased apoptosis on thyroid samples after perfusion of both drugs in comparison to untreated control

				NS	Tissue chamber Dynamic flow Syringe pump		- Lactose dehydrogenase release -TUNEL assay -Immunoblot analysis	
Al-Samadi *et al.* [130]	A dynamic culture method as drug screening platform	-PDL1 antibody -IDO1 inhibitor	Single	**Primary:** Primary H&N squamous cell carcinomas, T cells, B cells, NK cells, monocytes, and dendritic cells **Cell lines:** HSC-3	**2D:** Unexposed control Dynamic flow **3D:** Chambers coated with ECM substitute Dynamic flow Unspecified pump	NS	-Migration assay -Immunofluorescence staining - CellTiter 96® Proliferation Assay -Cell Trace kit	-Preclinical organotypic model for personalized medicine and testing -IDO 1 inhibitor influence immune cell migration to cancer cells -Therapy response was reported to be patient-dependant
Bower *et al.* [131]	A dynamic culture method as maintenance platform	NS	Single	**Primary:** Human biopsies of laryngeal,	**2D:** Unexposed control	NS	-H&E staining -Trypan blue	-Patient-derived samples were viable for 48h after placement in the microfluidic chip

				oropharyngeal or oral cavity tumors staged at T2–T4 **Cell lines:** NS	Dynamic flow **3D:** Biopsy chamber Dynamic flow Syringe pump		-Flow cytometry -MTS proliferation assay	-No significance difference concerning average proliferation of samples pre- and post-cultured in the chip
Lugo-Cintrón *et al*. [132]	A dynamic culture method as angiogenesis platform	NS	Two-culture	**Primary:** Human tubular lymphatic vessels and cancer-associated fibroblasts **Cell lines:** -HLEC2500 -HOrF2640	**2D:** Unexposed control Dynamic flow **3D:** Collagen hydrogel adhesion chamber Dynamic flow Syringe pump	NS	-H&E staining -Immunofluorescence staining -Immunohistochemistry staining -Proliferation assay -Migration and permeability assay -RT-qPCR -Multiphoton microscopy	-Preclinical organotypic model for personalized medicine and testing -Cancer-associated fibroblasts increased the gene expression of pro-lymphangiogenic factors in the lymphatic-like vessels

Sharafeldin *et al*. [133]	A dynamic culture method as biomarker detection platform	NS	Single	**Primary:** NS **Cell lines:** -HN12 -HN13 -HN30 -CAL-27	**2D:** Subtract biomarker control signal **3D:** Sonic-assisted chemical lysis chambers Dynamic flow peristaltic micropump	NS	-Biomarker quantification (desmoglein 3, VEGF-A,VEGF-C, β-Tub)	-Biomarker detection model for cancer metastasis diagnostic -Limit of detection was below 0.20fg/mL of the analyzed analyte in 20min evaluation
Jin *et al*. [134]	A dynamic culture method as chemotherapy screening platform	-Paclitaxel -Cisplatin -5-FU	Two-culture	**Primary:** Patient-derived tumor cells from squamous cell carcinoma and salivary gland adenoid cystic carcinoma	**2D:** NS **3D:** Transwell-like channels -Bottom chambers	NS	-Hoechst 33342 and propidium iodide -Immunofluorescence staining	-Preclinical organotypic model for personalized medicine and testing -High concentration of drugs did not provide a therapeutic effect as HUVEC cells were killed. A lower concentration was recommended to provide a therapy to kill cancer cells (over 50% apoptosis) and low HUVEC cytotoxicity (over 50% viability) -Therapy response was reported to be patient-dependant concerning different low drug concentrations

	coated with
Cell lines:	ECM substitute
-ACC-M	
	Dynamic flow
-UM-SCC-6	
	Double syringe
-HUVEC	pump

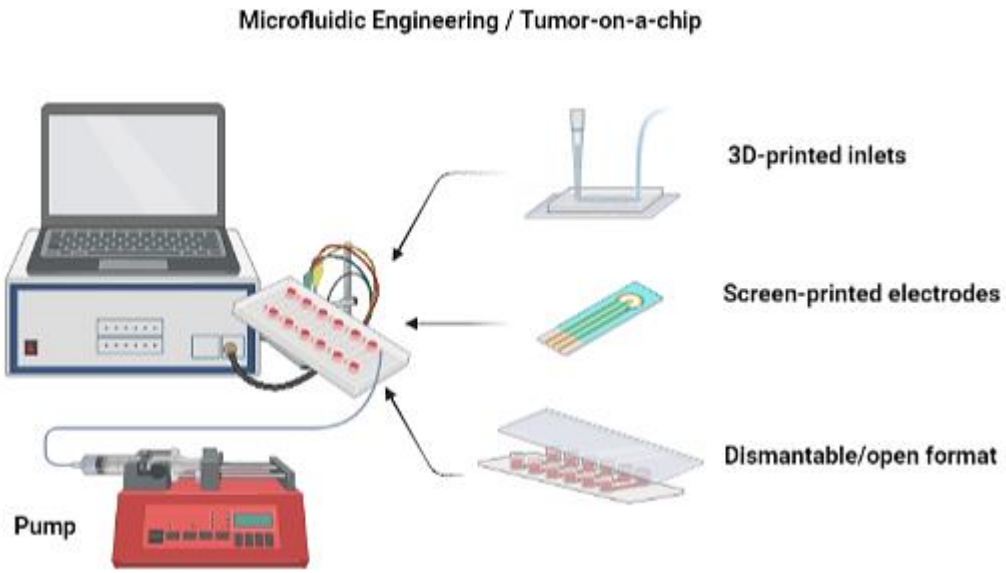

Figure 3-7. Advances in microfluidic technology. Microfluidic devices as tumor-on-a-chip may incorporate 3D-printed components and a dismantable/ open format. Figure created with BioRender.com.

Lastly, combined chemotherapy drugs, namely, cisplatin and docetaxel, have already been tested as a tumor reduction strategy in HPV+ oropharynx cancer patients (112). The multicompartments of microfluidic devices can be harnessed for screening multiple therapeutics in parallel, mimicking various combinations of cancer drug treatments like dual chemotherapy drugs or even the combination of chemoradiotherapy (105).

3.5 Future Outlook

The development of multicellular tumor spheroid systems that are compatible for preclinical studies, as HTS drug screening (113), is one important milestone of advancing personalized cancer medicine (114). As a result, PDOs became increasingly used to preserve part of the structural features and genome, epitome, transcriptome, proteome, and metabolome information of an individual's H&N tumorigenesis is for anticancer drug studies (115–117). Certain challenges such as suboptimal reproducibility and high manufacturing costs are well-known barriers with advanced culturing systems. In particular, the development of microfluidic devices requires specialized microfabrication and operation skills. Below, we further present specific challenges with PDOs in their adaptation for HTS with respect to their sourcing, fabrication, and culturing life span (**Figure 3-8**).

3.5.1 Overcoming the limited source of patient-derived organoids

Tumor tissue biopsies are needed from cancer patients to generate PDOs, but the source is often limited and unpredictable with clinical samples (**Figure 3-8A**). Fortunately, PDOs can be replicated and cryopreserved in specialized facilities, known as living biobanks, without losing cell-type specificity (87, 118). For example, intraductal papillary mucinous neoplasms were collected from patients with pancreatic cancer (119). The tumor tissues were first digested with a proteolytic enzyme for cell retrieval. The recovered cancer cells were then seeded in Matrigel® and stored as PDOs in a living biobank (119). The gene analysis data of key markers KRAS, PTEN, PIK3CA, GNAS, RNF43, and BRAF showed a similar expression between PDO and the patient's tumor tissue biopsy, which confirmed the preservation of patient samples' genome in living biobanks.

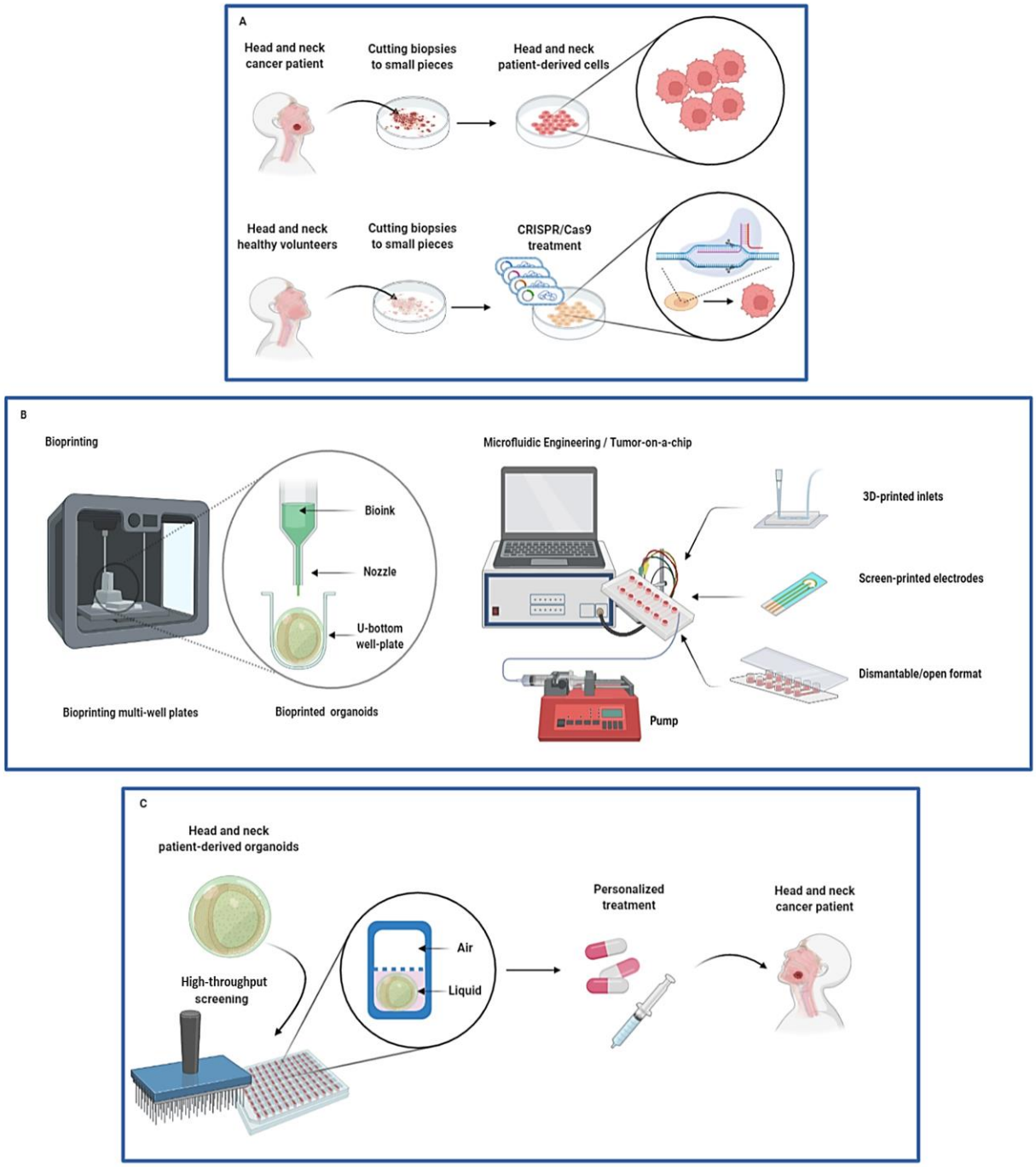

Figure 3-8. Future outlook of in vitro H&N cancer patient-derived organoid (PDO) models. (A) Sourcing of H&N PDO models using the tumor biopsies of cancer patients and CRISPR DNA–modified healthy cells. (B) Fabrication of H&N PDO models using bioprinting. (C) H&N PDO model life span used as air–liquid interface in HTS for personalized medicine purposes. Figure created with BioRender.com.

The stock of PDOs from living biobanks can be further expanded with the method of patient-derived xenografts (PDXs) (120–122). A PDX is to first insert PDOs in animals and then amplify the PDOs within the host. The derived PDXs (i.e., cloned PDOs) are then cryopreserved and stored in living biobanks, preserving cell–cell interactions as those of parent tumor. Of note, the genome copy number alterations of PDX- expanded PDOs may change after extensive passaging due to possible host reactions to the implant (123–125). As such, if a high passage (>P10) is used in treatment, caution needs to be exercised as PDOs and PDX-expanded PDOs may display a differentiated response to drug therapeutics. Furthermore, PDX models are time consuming and expensive, the engraftment efficiencies may be different among the TME types, and finally, the immune response cannot be properly evaluated due to the immunodeficiency of host strains (126). As a result, additional cancer model strategies are thus required.

3.5.2 Patient-derived organoids from cancer and healthy stem cells

In addition to tissue biopsies, organoids can be grown from cancer or healthy stem cells (115, 116, 120, 123, 127–133)although their use in cancer research is still in its infancy (128, 133–135). PDOs from cancer stem cells possess metastatic, chemotherapy, and radiotherapy resistance features, while healthy stem cells do not present those intrinsic characteristics (133, 136). At the same time, cancer stem cells are criticized of their limited clonal heterogeneity (133). A plethora of cancer-associated markers such as CD133, CD44, ABCG2, aldehyde dehydrogenase, octamer binding transcriptional factor 4, SOX2, and NANOG have been reported in cancer stem cells (134, 135, 137). However, marker expression does not necessarily translate into a cancer stem cell phenotype without transplantation assays (138). These assays are necessary to verify and characterize the tumor-initiating and -regenerating capabilities of such cells on implanted hosts.

Conversely, healthy adult stem cells like mesenchymal stem cells (139) and induced pluripotent stem cells (140) are another option of PDOs in cancer research. Human-induced pluripotent stem cells from healthy adults were proposed to generate PDOs for liver cancer studies (140). For instance, induced pluripotent stem cell reprogramming from human fibroblasts was successfully directed toward a hepatic endoderm-like phenotype via differentiation media containing activin A, bFGF, and BMP4 after 8 days of exposure (141). Then, the exposure of differentiation media with NOTCH activator agents to generate liver tumoroids or NOTCH inhibitors for liver organoids was performed after 2–3 weeks (140). The aforesaid methodology could be adjusted, following the

generation protocol of vocal fold mucosae from human-induced pluripotent cells (142). At that point, the PDO fabrication protocol for H&N cancer may implement the upregulation of Snail, the downregulator of epithelial markers and the upregulator of mesenchymal markers (143), and exposure to FGFs to generate stratified squamous epithelia (139, 144).

In more detail, induced pluripotent stem cell–based cancer modeling can be used as follows (145): (I) genetic alterations can be engineered into normal human-induced pluripotent stem cells using transcription activator-like effector nucleases (TALENs) or CRISPR/Cas9 (146). These stem-derived cells with engineered cancer-associated mutations can be used to acquire the initial cancer molecular events to then emulate cancer progression (145). (II) Induced pluripotent stem cells can be used to reprogram patient-specific somatic cells with cancer predisposition syndromes such as Li–Fraumeni syndrome (147). (III) Induced pluripotent stem cells can be engineered as cancer-specific cells by targeting tumor suppressors such as SMAD4, Rb/P16, BRCA1, CDKN1A, and CDKN2A (145). The previously mentioned stem cell strategies may help advance PDO research on H&N cancer.

Lastly, human embryonic stem cells were implemented as organoids for metastatic brain cancer modeling using induced pluripotency stem cell strategy (148). However, the use of embryonic stem cells possesses ethical concern, low immune compatibility and potential rejection after clinical transplantation (149). Nevertheless, continuous in vitro validation such as phenotype analysis is warranted to ensure the safe use of healthy stem cells as PDO models for cancer research.

3.5.3 Patient-derived organoids from CRISPR/Cas9 DNA-modified healthy cells

CRISPR/Cas9 transgenesis technology has been proposed to genetically modify healthy biopsies into PDOs (115, 116, 120, 123). The technology of CRISPR/Cas9, simply put, involves activating/silencing a specific gene of target (**Figure 3-8A**). CRISPR/Cas9-mediated genome editing comprises the implementation of two components: (I) single-effector Cas9 protein to allow double-stranded breaks in the target DNA and (II) a single-guide RNA to guide the Cas9 complex to the targeted genomic zone (150, 151). The CRISPR/Cas9 technology has already been used to

fabricate human oncogenic organoids from healthy liver by editing PTEN/TP53 and from healthy colon by targeting APC/SMAD4/TP53/K ras/PIK3CA (152). Interestingly, human pluripotent stem cells can gain CRISPR/Cas9-mutated p53 with a critical functional evaluation of p53 to avoid double- strand break toxicities dependent on p53/TP53 (153). Furthermore, wild-type human gastric organoid cell lines with ARID1A, an early-stage gastric cancer marker, as a single mutant target has been modified through CRISPR/Cas9 technology (154). In H&N cancer, gene editing may target the EGFR/PI3K/Akt/ mTOR pathway for oncogenic organotypic fabrication.

One known limitation with CRISPR/Cas9 technology is related to the low specificities to the target genes (150, 152). For instance, the off-target effect is often observed at a rate ≥50% in RNA-guided endonuclease-induced mutations in unintended target zones (150, 155). In silico libraries as the sgDesigner tool can be used to optimize the design of novel plasmids by including both the single- guide RNA and the target site that was not used before (150). In addition, implementing Cas9 variants such as Cas9 nickase has also been used to induce single-stranded breaks combined with a single-guide RNA in order to produce double- stranded DNA breaks at the desired location (150).

3.5.4 Overcoming the fabrication complexity of patient-derived organoids

Organotypic models provide a superior potential in patient-specific cellular heterogeneity, molecular phenotypes, tissue–stratum architecture, and geometry (156). Bioprinting may help fabricate PDO fabrication in a more precise and automated manner compared to conventional PDO production. Specifically, the layer-by-layer strategy of bioprinting can help to generate spatial-specific cell distribution and ECM architecture in PDO fabrication (**Figure 3-8B**). This strategy is empowered by inkjet/extrusion, laser-assisted, and stereolithography bioprinting methods (120, 157–159). For example, a 3D digital light processing bioprinting/HTS study was conducted to bioprint hepatocellular carcinomas and HUVECs in 96-well plates (160). The bioprinted gelatin methacryloyl (GelMa)–based construct had the dimensions of 2.4 mm × 2.4 mm × 250 μm, highlighting the spatial precision of Digital light processing bioprinting (DLP) technology required for HTS.

Digital light processing bioprinting technology has enhanced the resolution (~10 times) of bioprinted PDOs, which has been one notable barrier with nozzle extrusion (159–162). In addition,

digital light processing bioprinting offers a shear stress–free advantage over extrusion bioprinting by reducing potential cell damage during organotypic assembly (66, 158, 162). This shear stress–free printing method achieves a cell viability of ≥90% within the 3D-printed construct, whereas that of extrusion bioprinting is 40%–80% (66). Concerning multiple gradients in the printed assembly, digital light processing bioprinting presents a dynamic gradient tunability needed for proper recapitulation of complex anatomical structures compared to that of extrusion bioprinting (163). In addition, a low amount of bioink waste is found while changing the gradients using digital light processing bioprinting combined with microfluidic technology (163). Digital light bioprinting also allows to swiftly produce photopolymerized 3D constructs via a projected light (66, 160–162) (**Figure 3-8B**). Typically speaking, the resolution of digital light processing bioprinting meets the need of organoid bioprinting (158, 159, 161).

For instance, the resolution for inkjet/extrusion and laser-assisted bioprinting is ~50–500 μm and ~100 μm, respectively, while digital light processing bioprinting can achieve as high as 50-μm resolution (161, 162, 164). In general, digital light processing bioprinting take up to 40 min to entirely bioprint a 96-well plate (160)at the speedof0.5–15 mm/s (164). Extrusion bioprinting has been reported to have longer fabrication times, 10–50 mm/s (165), because of the interaction between the bioink viscoelasticity and the extrusion nozzle size (166, 167). Given that the resolution necessary for the cell-laden tumor organotypic models is below 100 μm (161), the high-resolution capability of digital light processing bioprinting will allow precise fabrication of H&N PDO models without comprising the time cost. The increased resolution of 3D- printed organ-on-a-chip can also benefit the development of HTS platforms down the road (168).

The challenges of digital light processing bioprinting are the scarce number of photoinitiators such as Eosin Y, Irgacure 819, and lithium phenyl-2,4,6-trimethylbenzoylphosphinate (160, 164) and photo-crosslinking resins like GelMA, methacryloyl hyaluronic acid, and poly(ethylene glycol) diacrylate (159, 162, 164). A deficient concentration of photoinitiators within the construct provokes poor mechanical properties affecting the desired resolution and cell viability (159, 162). Because of that deficiency, proper standardization to balance the photoinitiator and resin concentrations will need to be carried out to achieve the reported cell viability ≥90% (66) and high resolution ≤50 mm (159, 162, 164). Another hurdle of digital light processing bioprinting is the limited incorporation of multiple materials within the 3D cell–based construct (159, 162, 164).

However, digital light processing bioprinting can incorporate a multimaterial structure combined with microfluidics to print multiple bioinks (163). Taken into consideration the bioink component accessibility, nozzle extrusion bioprinting remains the most popular bioprinting method for bioprinting (159, 167, 169).

3.5.6 Overcoming the long-term culturing of patient-derived organoids

Microfluidic chips allow the long-term culture of sizable biological micro-/milliscale samples such as PDOs with effective nutrient/waste exchange via the dynamic liquid flow within the chip (109). Recent airway-on-a-chip microfluidic platforms, especially those with air–liquid interface feature (170–173), are particularly suitable and adapted for H&N cancer modeling given that the H&N squamous cell carcinomas are constantly exposed to air. However, most airway-on-a-chip devices need pumps to perfuse air and liquid through the air–liquid interface channels, respectively (171–174). This pump requirement presents a critical challenge for the adaption of HTS arrays. To date, non-microfluidic air–liquid interface platforms may incorporate up to 96 individual Transwell plates (175), whereas microfluidic-based air–liquid interface systems are able to integrate up to 64 individual chambers at most (176). None of these are truly considered as high throughput, in which HTS is commonly known as testing hundreds of samples on one array.

That said, one most recent microfluidic platform, developed by Bircsak et al. (177), allowed to house tumor organoids cultures up to 200 individual chambers. This device comprised the use of a multiplexer fluid control, a perfusion rocker platform, and culture chambers overlayed by the three-lane fluid channels. One of the analyses of this liver-on-a-chip platform was to study the drug metabolism of five drugs: phenacetin, coumarin, diclofenac, terfenadine, and phenolphthalein. Adopting such a microfluidic platform with air–liquid interface and pump-free features will present a great leap of advancing in in vitro H&N cancer modeling for high-throughput drug screening (**Figure 3-8C**). Accomplishing the combination of human multiorgan-on-chips (178) and high- throughput testing could benefit personalized anti-cancer therapy screening and discovery to boot (179).

3.6 Conclusion

Geometry, multicellularity, and constant irrigation are key features for developing H&N-specific in vitro models for drug screening and discovery. Organotypic multicellular spheroid and organoid cultures are highly applicable to approximate cancer- specific TME by mirroring desired geometry and cell–cell/–ECM interactions as presented in vivo tumor tissues. Organotypic models can be further combined with microfluidic devices to evaluate the crosstalk between cells and barriers to the mass transport of oxygen, nutrients, and drug therapeutics. Ultimate in vitro H&N models can be achieved by incorporating PDOs, air–liquid interface, and high-throughput readouts for de novo oncology drug discovery and evaluation. The adoption of such a tumor-on-a-chip platform is expected to minimize the need of animal models and reduce the chance of failures in clinical trials for translational research.

Authors contributions

CM-G: Conceptualization, visualization, writing-original draft, reviewing and editing. NL-J: Conceptualization, visualization, writing-original draft, reviewing and editing, supervision, funding acquisition. MT: Conceptualization, visualization, writing-original draft, reviewing and editing, supervision. HO: visualization, writing-reviewing and editing. NS: writing-reviewing and editing. JL: writing-reviewing and editing. All authors contributed to the article and approved the submitted version.

Funding

This study was supported by the National Sciences and Engineering Research Council of Canada (RGPIN-2018–03843 and ALLRP 548623-19; PI: N.L.-J.), Canada Research Chair research stipend (J.Y.L., M.T., N.L.-J.) and the National Institutes of Health (R01 DC-018577-01A1). The presented content is solely the responsibility of the authors and does not necessarily represent the official views of the above funding agencies.

Acknowledgements

We thank Dr.S. Yo Kishimoto and HO’s team for their work in obtaining permission for the clinical figure.

Conflict of interest

The authors declare that the research was conducted in the absence of any commercial or financial relationships that could be construed as a potential conflict of interest.

Publisher's note

All claims expressed in this article are solely those of the authors and do not necessarily represent those of their affiliated organizations, or those of the publisher, the editors and the reviewers. Any product that may be evaluated in this article, or claim that may be made by its manufacturer, is not guaranteed or endorsed by the publisher.

3.7 References

1. Wouters OJ, McKee M, Luyten J. Estimated research and development investment needed to bring a new medicine to market, 2009-2018. JAMA J Am Med Assoc (2020) 323(9):844–53. doi: 10.1001/jama.2020.1166

2. IQVIA Institute for Human Data Science. Global trends in r & d: Overview through 2021. Available at: https://www.iqvia.com/insights/the-iqvia-institute/reports/global-trends-in-r-and-d-2022.

3. Mailankody S, Prasad V. Five years of cancer drug approvals: Innovation, efficacy, and costs. JAMA Oncol (2015) 1(4):539–40. doi: 10.1001/jamaoncol.2015.0373

4. National Cancer Institute. Drugs approved for head and neck cancer. National Cancer Institute (2021) National Institutes of Health, Maryland, USA. p. 1. Available at: http://www.cancer.gov/about-cancer/treatment/drugs/head-neck.

5. Kowalski LP, Coletta RD, Salo T, Maschietto M, Chojniak R, Lima JM, et al. Head and neck cancer: Emerging concepts in biomarker discovery and opportunities for clinical translation. Clin Transl Med (2020) 10(7):3–7. doi: 10.1002/ctm2.209

6. Chen SMY, Krinsky AL, Woolaver RA, Wang X, Chen Z, Wang JH. Tumor immune microenvironment in head and neck cancers. Mol Carcinog (2020) 59(7):766–74. doi: 10.1002/mc.23162

7. Jafri MA, Kalamegam G, Abbas M, Al-Kaff M, Ahmed F, Bakhashab S, et al. Deciphering the association of cytokines, chemokines, and growth factors in chondrogenic differentiation of human bone marrow mesenchymal stem cells using an ex vivo osteochondral culture system. Front Cell Dev Biol (2020) 7. doi:10.3389/fcell.2019.00380

8. Croston GE. The utility of target-based discovery. Expert Opin Drug Discov (2017) 12(5):427–9. doi: 10.1080/17460441.2017.1308351

9. Moffat JG, Vincent F, Lee JA, Eder J, Prunotto M. Opportunities and challenges in phenotypic drug discovery: An industry perspective. Nat Rev Drug Discov (2017) 16(8):531–43. doi: 10.1038/nrd.2017.111

10. Leemans CR, Braakhuis BJM, Brakenhoff RH. The molecular biology of head and neck cancer. Nat Rev Cancer (2011) 11(1):9–22. doi: 10.1038/nrc2982

11. Kalyankrishna S, Grandis JR. Epidermal growth factor receptor biology in head and neck cancer. J Clin Oncol (2006) 24(17):2666–72. doi: 10.1200/JCO.2005.04.8306

12. Grandis JR, Chakraborty A, Melhem MF, Zeng Q, Tweardy DJ. Inhibition of epidermal growth factor receptor gene expression and function decreases proliferation of head and neck squamous carcinoma but not normal mucosal epithelial cells. Oncogene (1997) 15(4):409–16. doi: 10.1038/
sj.onc.1201188

13. Cramer JD, Burtness B, Le QT, Ferris RL. The changing therapeutic landscape of head and neck cancer. Nat Rev Clin Oncol (2019) 16(11):669–83. doi: 10.1038/s41571-019-0227-z

14. Bahcecioglu G, Basara G, Ellis BW, Ren X, Zorlutuna P. Breast cancer models: Engineering the tumor microenvironment. Acta Biomater (2020) 106:1–21. doi: 10.1016/j.actbio.2020.02.006

15. Kim M, Mun H, Sung CO, Cho EJ, Jeon HJ, Chun SM, et al. Patient-derived lung cancer organoids as in vitro cancer models for therapeutic screening. Nat Commun (2019) 10(1):1–15. doi: 10.1038/s41467-019-11867-6

16. Broutier L, Mastrogiovanni G, Verstegen MMA, Francies HE, Gavarró LM, Bradshaw CR, et al. Human primary liver cancer-derived organoid cultures for disease modeling and drug screening. Nat Med (2017) 23(12):1424–35. doi:10.1038/nm.4438

17. Utispan K, Koontongkaew S. Fibroblasts and macrophages: Key players in the head and neck cancer microenvironment. J Oral Biosci (2017) 59(1):23–30. doi: 10.1016/j.job.2016.11.002

18. Curry JM, Sprandio J, Cognetti D, Luginbuhl A, Bar-Ad V, Pribitkin E, et al. Tumor microenvironment in head and neck squamous cell carcinoma. Semin Oncol (2014) 41(2):217–34. doi: 10.1053/j.seminoncol.2014.03.003

19. Peltanova B, Raudenska M, Masarik M. Effect of tumor microenvironment on pathogenesis of the head and neck squamous cell carcinoma: A systematic review. Mol Cancer (2019) 18(1):1–24. doi: 10.1186/s12943-019-0983-5

20. Alsahafi E, Begg K, Amelio I, Raulf N, Lucarelli P, Sauter T, et al. Clinical update on head and neck cancer: molecular biology and ongoing challenges. Cell Death Dis (2019) 10(8):1–17. doi: 10.1038/s41419-019-1769-9

21. Marquard FE, Jücker M. PI3K/AKT/mTOR signaling as a molecular target in head and neck cancer. Biochem Pharmacol (2020) 172:113729. doi: 10.1016/j.bcp.2019.113729

22. Fujii N, Shomori K, Shiomi T, Nakabayashi M, Takeda C, Ryoke K, et al. Cancer-associated fibroblasts and CD163-positive macrophages in oral squamous cell carcinoma: Their

clinicopathological and prognostic significance. J Oral Pathol Med (2012) 41(6):444–51. doi: 10.1111/j.1600-0714.2012.01127.x

23. Zhang Z, Dong Z, Lauxen IS, Filho MSA, Nör JE. Endothelial cell-secreted EGF induces epithelial to mesenchymal transition and endows head and neck cancer cells with stem-like phenotype. Cancer Res (2014) 74(10):2869–81. doi: 10.1158/0008-5472.CAN-13-2032

24. Álvarez-Teijeiro S, García-Inclán C, Villaronga MÁ, Casado P, Hermida-Prado F, Granda-Díaz R, et al. Factors secreted by cancer-associated fibroblasts that sustain cancer stem properties in head and neck squamous carcinoma cells as potential therapeutic targets. Cancers (Basel) (2018) 10(9):334. doi: 10.3390/cancers10090334

25. Saint A, Van Obberghen-Schilling E. The role of the tumor matrix environment in progression of head and neck cancer. Curr Opin Oncol (2021)33(3):168–74. doi: 10.1097/CCO.0000000000000730

26. Zhang X, Shi M, Chen T, Zhang B. Characterization of the immune cell infiltration landscape in head and neck squamous cell carcinoma to aid immunotherapy. Mol Ther Nucleic Acids (2020) 22:298–309. doi: 10.1016/j.omtn.2020.08.030

27. Pai SI, Zandberg DP, Strome SE. The role of antagonists of the PD-1:PD-L1/PD-L2 axis in head and neck cancer treatment. Oral Oncol (2016) 61:152–8.doi: 10.1016/j.oraloncology.2016.08.001

28. Larkins E, Blumenthal GM, Yuan W, He K, Sridhara R, Subramaniam S, et al. FDA Approval summary: Pembrolizumab for the treatment of recurrent or metastatic head and neck squamous cell carcinoma with disease progression on or after platinum-containing chemotherapy. Oncologist (2017) 22(7):873–8. doi: 10.1634/theoncologist.2016-0496

29. Curry JM, Sprandio J, Cognetti D, Luginbuhl A, Bar-Ad V, Pribitkin E, et al. Tumor microenvironment in head and neck squamous cell carcinoma. Semin Oncol (2014) 41(2):217–34. doi: 10.1053/j.seminoncol.2014.03.003

30. Schmieder A, Michel J, Schönhaar K, Goerdt S, Schledzewski K. Differentiation and gene expression profile of tumor-associated macrophages. Semin Cancer Biol (2012) 22(4):289–97. doi: 10.1016/j.semcancer.2012.02.002

31. Li B, Ren M, Zhou X, Han Q, Cheng L. Targeting tumor-associated macrophages in head and neck squamous cell carcinoma. Oral Oncol (2020) 106:104723. doi:10.1016/j.oraloncology.2020.104723

32. Schmidt M, Scholz CJ, Polednik C, Roller J. Spheroid-based 3-dimensional culture models: Gene expression and functionality in head and neck cancer. Oncol Rep (2016) 35(4):2431–40. doi: 10.3892/or.2016.4581

33. Melissaridou S, Wiechec E, Magan M, Jain MV, Chung MK, Farnebo L, et al. The effect of 2D and 3D cell cultures on treatment response, EMT profile and stem cell features in head and neck cancer 11 medical and health sciences 1112 oncology and carcinogenesis. Cancer Cell Int (2019) 19(1):1–10. doi: 10.1186/s12935-019-0733-1

34. Azharuddin M, Roberg K, Dhara AK, Jain MV, Darcy P, Hinkula J, et al. Dissecting multi drug resistance in head and neck cancer cells using multicellular tumor spheroids. Sci Rep (2019) 9(1):1–12. doi: 10.1038/s41598-019-56273-6

35. Langhans SA. Three-dimensional in vitro cell culture models in drug discovery and drug repositioning. Front Pharmacol (2018) 9:1–14. doi: 10.3389/fphar.2018.00006

36. Pinto B, Henriques AC, Silva PMA, Bousbaa H. Three-dimensional spheroids as in vitro preclinical models for cancer research. Pharmaceutics (2020) 12(12):1–38. doi: 10.3390/pharmaceutics12121186

37. Lamichhane SP, Arya N, Kohler E, Xiang S, Christensen J, Shastri VP. Recapitulating epithelial tumor microenvironment in vitro using three dimensional tri-culture of human epithelial, endothelial, and mesenchymal cells. BMC Cancer (2016) 16(1):1–12. doi: 10.1186/s12885-016-2634-1

38. Nash CE, Mavria G, Baxter EW, Holliday DL, Tomlinson DC, Treanor D, et al. Development and characterisation of a 3D multi-cellular in vitro model of normal human breast: A tool for cancer initiation studies. Oncotarget (2015) 6(15):13731–41. doi: 10.18632/oncotarget.3803

39. Lazzari G, Nicolas V, Matsusaki M, Akashi M, Couvreur P, Mura S. Multicellular spheroid based on a triple co-culture: A novel 3D model to mimic pancreatic tumor complexity. Acta Biomater (2018) 78:296–307. doi: 10.1016/j.actbio.2018.08.008

40. Lin CJ, Grandis JR, Carey TE, Gollin SM,Whiteside TL, KochWM, et al. Head and neck squamous cell carcinoma cell lines: established models and rationale for selection. Head Neck J Sci Spec Head Neck (2007) 29(2):163–88. doi: 10.1002/hed.20478

41. Peltanova B, Liskova M, Gumulec J, Raudenska M, Polanska HH, Vaculovic T, et al. Sensitivity to cisplatin in head and neck cancer cells is significantly affected by patient-derived cancer-associated fibroblasts. Int J Mol Sci (2021) 22(4):1–13. doi: 10.3390/ijms22041912

42. Vis MAM, Ito K, Hofmann S. Impact of culture medium on cellular interactions in in vitro Co-culture systems. Front Bioeng Biotechnol (2020) 8:1–8. doi: 10.3389/fbioe.2020.00911

43. Materne EM, Maschmeyer I, Lorenz AK, Horland R, Schimek KMS, Busek M, et al. The multi-organ chip - a microfluidic platform for long-term multi-tissue coculture. J Vis Exp (2015) 2015(98):1–11. doi: 10.3791/52526

44. De Vitis E, La Pesa V, Gervaso F, Romano A, Quattrini A, Gigli G, et al. A microfabricated multi-compartment device for neuron and schwann cell differentiation. Sci Rep (2021) 11(1):1–12. doi: 10.1038/s41598-021-86300-4

45. Rodrigues J, Heinrich MA, Teixeira LM, Prakash J. 3D In vitro model (R) evolution: Unveiling tumor–stroma interactions. Trends Cancer (2021) 7(3):249–64. doi: 10.1016/j.trecan.2020.10.009

46. Joseph JP, Harishankar MK, Pillai AA, Devi A. Hypoxia induced EMT: A review on the mechanism of tumor progression and metastasis in OSCC. Oral Oncol (2018) 80:23–32. doi: 10.1016/j.oraloncology.2018.03.004

47. Basheer HA, Pakanavicius E, Cooper PA, Shnyder SD, Martin L, Hunter KD, et al. Hypoxia modulates CCR7 expression in head and neck cancers. Oral Oncol (2018) 80:64–73. doi: 10.1016/j.oraloncology.2018.03.014

48. Essid N, Chambard JC, Elgaaïed AB. Induction of epithelial-mesenchymal transition (EMT) and Gli1 expression in head and neck squamous cell carcinoma (HNSCC) spheroid cultures. Bosn J Basic Med Sci (2018) 18(4):336–46. doi:10.17305/bjbms.2018.3243

49. Hattersley SM, Sylvester DC, Dyer CE, Stafford ND, Haswell SJ, Greenman J. A microfluidic system for testing the responses of head and neck squamous cell carcinoma tissue biopsies to treatment with chemotherapy drugs. Ann BioMed Eng (2012) 40(6):1277–88. doi: 10.1007/s10439-011-0428-9

50. Orcheston-Findlay L, Hashemi A, Garrill A, Nock V. A microfluidic gradient generator to simulate the oxygen microenvironment in cancer cell culture. Microelectron Eng (2018) 195:107–13. doi: 10.1016/j.mee.2018.04.011

51. Grist SM, Nasseri SS, Laplatine L, Schmok JC, Yao D, Hua J, et al. Longterm monitoring in a microfluidic system to study tumour spheroid response to chronic and cycling hypoxia. Sci Rep (2019) 9(1):1–13. doi: 10.1038/s41598-019-54001-8

52. Costa EC, Moreira AF, de Melo-Diogo D, Gaspar VM, Carvalho MP, Correia IJ. 3D tumor spheroids: an overview on the tools and techniques used for their analysis. Biotechnol Adv (2016) 34(8):1427–41. doi: 10.1016/j.biotechadv.2016.11.002

53. Pozzi S, Scomparin A, Israeli Dangoor S, Rodriguez Ajamil D, Ofek P, Neufeld L, et al. Meet me halfway: Are in vitro 3D cancer models on the way to replace in vivo models for nanomedicine development? Adv Drug Deliv Rev (2021) 175:113760. doi: 10.1016/j.addr.2021.04.001

54. Hagemann J, Jacobi C, Gstoettner S, Welz C, Schwenk-Zieger S, Stauber R, et al. Therapy testing in a spheroid-based 3D cell culture model for head and neck squamous cell carcinoma. J Vis Exp (2018) 2018(134):1–8. doi: 10.3791/57012

55. Goričan L, Gole B, Potočnik U. Head and neck cancer stem cell-enriched spheroid model for anticancer compound screening. Cells (2020) 9(7):1707. doi: 10.3390/cells9071707

56. Magan M, Wiechec E, Roberg K. CAFs affect the proliferation and treatment response of head and neck cancer spheroids during co-culturing in a unique in vitro model. Cancer Cell Int (2020) 20(1):1–11. doi: 10.1186/s12935-020-01718-6

57. Kochanek SJ, Close DA, Johnston PA. High content screening characterization of head and neck squamous cell carcinoma multicellular tumor spheroid cultures generated in 384-well ultra-low attachment plates to screen for better cancer drug leads. Assay Drug Dev Technol (2019) 17(1):17–36. doi: 10.1089/adt.2018.896

58. Hagemann J, Jacobi C, Hahn M, Schmid V, Welz C, Schwenk-Zieger S, et al. Spheroid-based 3D cell cultures enable personalized therapy testing and drug discovery in head and neck cancer. Anticancer Res (2017) 37(5):2201–10. doi: 10.21873/anticanres.11555

59. Santi M, Mapanao AK, Cappello V, Voliani V. Production of 3D tumor models of head and neck squamous cell carcinomas for nanotheranostics assessment. ACS Biomater Sci Eng (2020) 6(9):4862–9. doi: 10.1021/acsbiomaterials.0c00617

60. Tanaka N, Osman AA, Takahashi Y, Lindemann A, Patel AA, Zhao M, et al. Head and neck cancer organoids established by modification of the CTOS method can be used to predict in vivo drug sensitivity. Oral Oncol (2018) 87:49–57. doi: 10.1016/j.oraloncology.2018.10.018

61. Driehuis E, Spelier S, Beltrán Hernández I, de Bree R, M. Willems S, Clevers H, et al. Patient-derived head and neck cancer organoids recapitulate EGFR expression levels of respective tissues and are responsive to EGFR targeted photodynamic therapy. J Clin Med (2019) 8(11):1880. doi: 10.3390/jcm8111880

62. Jung AR, Jung CH, Noh JK, Lee YC, Eun YG. Epithelial-mesenchymal transition gene signature is associated with prognosis and tumor microenvironment in head and neck squamous cell carcinoma. Sci Rep (2020) 10 (1):1–11. doi: 10.1038/s41598-020-60707-x

63. Li J, Chen M, Fan X, Zhou H. Recent advances in bioprinting techniques: Approaches, applications and future prospects. J Transl Med (2016) 14(1):1–15. doi: 10.1186/s12967-016-1028-0

64. Kitaeva KV, Rutland CS, Rizvanov AA, Solovyeva VV. Cell culture based in vitro test systems for anticancer drug screening. Front Bioeng Biotechnol (2020) 8:1–9. doi: 10.3389/fbioe.2020.00322

65. Skardal A, Atala A. Biomaterials for integration with 3-d bioprinting. Ann BioMed Eng (2015) 43(3):730–46. doi: 10.1007/s10439-014-1207-1

66. Tiwari AP, Thorat ND, Pricl S, Patil RM, Rohiwal S, Townley H. Bioink: a 3D-bioprinting tool for anticancer drug discovery and cancer management. Drug Discovery Today (2021) 26(7):1574–90. doi: 10.1016/j.drudis.2021.03.010

67. Affolter A, Lammert A, Kern J, Scherl C, Rotter N. Precision medicine gains momentum: Novel 3D models and stem cell-based approaches in head and neck cancer. Front Cell Dev Biol (2021) 9:1–27. doi: 10.3389/fcell.2021.666515

68. Almela T, Tayebi L, Moharamzadeh K. 3D bioprinting for in vitro models of oral cancer: Toward development and validation. Bioprinting (2021) 22:e00132. doi: 10.1016/j.bprint.2021.e00132

69. Daly AC, Davidson MD, Burdick JA. 3D bioprinting of high cell-density heterogeneous tissue models through spheroid fusion within selfhealing hydrogels. Nat Commun (2021) 12(1):1–13. doi: 10.1038/s41467-021-21029-2

70. Chakraborty S, DePalma TJ, Skardal A. Increasing accuracy of In vitro cancer models: Engineering stromal complexity into tumor organoid platforms. Adv NanoBiomed Res (2021) 2100061:2100061. doi: 10.1002/anbr.202100061

71. Jacobi N, Seeboeck R, Hofmann E, Schweiger H, Smolinska V, Mohr T, et al. Organotypic three-dimensional cancer cell cultures mirror drug responses in vivo:Lessons learned from the inhibition of EGFR signaling. Oncotarget (2017) 8(64):107423–40. doi: 10.18632/oncotarget.22475

72. Watters KM, Bajwa P, Kenny HA. Organotypic 3D models of the ovarian cancer tumor microenvironment. Cancers (Basel) (2018) 10(8):1–10. doi: 10.3390/cancers10080265

73. De Gregorio V, Urciuolo F, Netti PA, Imparato G. In vitro organotypic systems to model tumor microenvironment in human papillomavirus (HPV)-related cancers. Cancers (Basel) (2020) 12(5):1150. doi: 10.3390/cancers12051150

74. Suryaprakash RTC, Kujan O, Shearston K, Farah CS. Three-dimensional cell culture models to investigate oral carcinogenesis: A scoping review. Int J Mol Sci (2020) 21(24):1–17. doi: 10.3390/ijms21249520

75. Ferreira LP, Gaspar VM, Mano JF. Decellularized extracellular matrix for bioengineering physiomimetic 3D in vitro tumor models. Trends Biotechnol (2020) 38(12):1397–414. doi: 10.1016/j.tibtech.2020.04.006

76. Nele V, Wojciechowski JP, Armstrong JPK, Stevens MM. Tailoring gelation mechanisms for advanced hydrogel applications. Adv Funct Mater (2020) 30(42):2002759. doi: 10.1002/adfm.202002759

77. Zhao L, Huang L, Yu S, Zheng J, Wang H, Zhang Y. Decellularized tongue tissue as an in vitro model for studying tongue cancer and tongue regeneration. Acta Biomater (2017) 58:122–35. doi: 10.1016/j.actbio.2017.05.062

78. Burghartz M, Lennartz S, Schweinlin M, Hagen R, Kleinsasser N, Hackenberg S, et al. Development of human salivary gland-like tissue In vitro. Tissue Eng Part A (2018) 24(3–4):301–9. doi: 10.1089/ten.tea.2016.0466

79. Ayuso JM, Vitek R, Swick AD, Skala MC, Wisinski KB, Kimple RJ, et al. Effects of culture method on response to EGFR therapy in head and neck squamous cell carcinoma cells. Sci Rep (2019) 9(1):1–9. doi: 10.1038/s41598-019-48764-3

80. Tuomainen K, Al-Samadi A, Potdar S, Turunen L, Turunen M, Karhemo PR, et al. Human tumor–derived matrix improves the predictability of head and neck cancer drug testing. Cancers (Basel) (2020) 12(1):1–15. doi: 10.3390/cancers12010092

81. Young M, Rodenhizer D, Dean T, D'Arcangelo E, Xu B, Ailles L, et al. A TRACER 3D Co-culture tumour model for head and neck cancer. Biomaterials (2018) 164:54–69. doi: 10.1016/j.biomaterials.2018.01.038

82. Lee J, You JH, Shin D, Roh JL. Ex vivo culture of head and neck cancer explants in cell sheet for testing chemotherapeutic sensitivity. J Cancer Res ClinOncol (2020) 146(10):2497–507. doi: 10.1007/s00432-020-03306-7

83. Engelmann L, Thierauf J, Laureano NK, Stark HJ, Prigge ES, Horn D, et al. Organotypic co-cultures as a novel 3d model for head and neck squamous cell carcinoma. Cancers (Basel) (2020) 12(8):1–20. doi: 10.3390/cancers12082330

84. Aisenbrey EA, Murphy WL. Synthetic alternatives to matrigel. Nat Rev Mater (2020) 5(7):539–51. doi: 10.1038/s41578-020-0199-8

85. Sivakumar R, Chan M, Shin JS, Nishida-Aoki N, Kenerson HL, Elemento O, et al. Organotypic tumor slice cultures provide a versatile platform for immunooncology and drug discovery. Oncoimmunology (2019) 8(12):e1670019. doi:10.1080/2162402X.2019.1670019

86. Qiu Y, Ning D, Zhang P, Curly S, Qiao Y, Ma L, et al. Three-dimensional microtissues as an in vitro model for personalized radiation therapy. Analyst (2017) 142(19):3605–12. doi: 10.1039/C7AN00794A

87. Gilazieva Z, Ponomarev A, Rutland C, Rizvanov A, Solovyeva V. Promising applications of tumor spheroids and organoids for personalized medicine. Cancers (Basel) (2020) 12(10):1–19. doi: 10.3390/cancers12102727

88. Akther F, Little P, Li Z, Nguyen NT, Ta HT. Hydrogels as artificial matrices for cell seeding in microfluidic devices. RSC Adv (2020) 10(71):43682–703. doi: 10.1039/D0RA08566A

89. Giannitelli SM, Costantini M, Basoli F, Trombetta M, Rainer A. Electrospinning and microfluidics: An integrated approach for tissue engineering and cancer. In: Electrofluidodynamic technologies (EFDTs) for biomaterials and medical devices: Principles and advances. Università Campus Bio-Medico di Roma, Rome, Italy: Elsevier Ltd (2018). p. 139–155 p. doi: 10.1016/B978-0-08-101745-6.00008-6

90. Fitzgerald AA, Li E, Weiner LM. 3D culture systems for exploring cancer immunology. Cancers (Basel) (2021) 13(1):1–19. doi: 10.3390/cancers13010056

91. Riley A, Green V, Cheah R, McKenzie G, Karsai L, England J, et al. A novel microfluidic device capable of maintaining functional thyroid carcinoma specimens ex vivo provides a new drug screening platform. BMC Cancer (2019) 19(1):1–13. doi: 10.1186/s12885-019-5465-z

92. Al-Samadi A, Poor B, Tuomainen K, Liu V, Hyytiäinen A, Suleymanova I, et al. In vitro humanized 3D microfluidic chip for testing personalized immunotherapeutics for head and neck cancer patients. Exp Cell Res (2019) 383 (2):111508. doi: 10.1016/j.yexcr.2019.111508

93. Duzagac F, Saorin G, Memeo L, Canzonieri V, Rizzolio F. Microfluidic organoids-on-a-chip: Quantum leap in cancer research. Cancers (Basel) (2021) 13(4):1–35. doi: 10.3390/cancers13040737

94. Bower R, Green VL, Kuvshinova E, Kuvshinov D, Karsai L, Crank ST, et al. Maintenance of head and neck tumor on-chip: Gateway to personalized treatment? Futur Sci OA (2017) 3(2):FSO174. doi: 10.4155/fsoa-2016-0089

95. Lugo-Cintrón KM, Ayuso JM, Humayun M, Gong MM, Kerr SC, Ponik SM, et al. Primary head and neck tumour-derived fibroblasts promote lymphangiogenesis in a lymphatic organotypic Co-culture model. EBioMedicine (2021) 73:103634. doi: 10.1016/j.ebiom.2021.103634

96. Sharafeldin M, Chen T, Ozkaya GU, Choudhary D, Molinolo AA, Gutkind JS, et al. Detecting cancer metastasis and accompanying protein biomarkers at single cell levels using a 3D-printed microfluidic immunoarray. Biosens Bioelectron (2021) 171:112681. doi: 10.1016/j.bios.2020.112681

97. Xie H, Appelt JW, Jenkins RW. Going with the flow: Modeling the tumor microenvironment using microfluidic technology. Cancers (Basel) (2021) 13(23):1–26. doi: 10.3390/cancers13236052

98. Yang Y, Wang H. Microfluidic technologies for head and neck cancer: from single-cell analysis to tumor-on-a-chip. In: Early detection and treatment of head & neck cancers (2021) Springer. p. 43–62.

99. Akgönüllü S, Bakhshpour M, Pişkin AK, Denizli A. Microfluidic systems for cancer diagnosis and applications. Micromachines (2021) 12(11):1349. doi: 10.3390/mi12111349

100. Roh JL, Park JY, Kim EH, Jang HJ, Kwon M. Activation of mitochondrial oxidation by PDK2 inhibition reverses cisplatin resistance in head and neck cancer. Cancer Lett (2016) 371(1):20–9. doi: 10.1016/j.canlet.2015.11.023

101. Shang M, Soon RH, Lim CT, Khoo BL, Han J. Microfluidic modelling of the tumor microenvironment for anti-cancer drug development. Lab Chip (2019) 19(3):369–86. doi: 10.1039/C8LC00970H

102. Dewhirst MW, Secomb TW. Transport of drugs from blood vessels to tumour tissue. Nat Rev Cancer (2017) 17(12):738–50. doi: 10.1038/nrc.2017.93

103. Jin D, Ma X, Luo Y, Fang S, Xie Z, Li X, et al. Application of a microfluidic based perivascular tumor model for testing drug sensitivity in head and neck cancers and toxicity in endothelium. RSC Adv (2016) 6(35):29598–607. doi: 10.1039/C6RA01456A

104. Bērziņa S, Harrison A, Taly V, Xiao W. Technological advances in tumor on-chip technology: From bench to bedside. Cancers (Basel) (2021) 13(16):4192. doi: 10.3390/cancers13164192

105. Eduati F, Utharala R, Madhavan D, Neumann UP, Longerich T, Cramer T, et al. A microfluidics platform for combinatorial drug screening on cancer biopsies. Nat Commun (2018) 9(1):1–13. doi: 10.1038/s41467-018-04919-w

106. Cho AN, Jin Y, An Y, Kim J, Choi YS, Lee JS, et al. Microfluidic device with brain extracellular matrix promotes structural and functional maturation of human brain organoids. Nat Commun (2021) 12(1):1–23. doi: 10.1038/s41467-021-24775-5

107. Kim SK, Kim YH, Park S, Cho SW. Organoid engineering with microfluidics and biomaterials for liver, lung disease, and cancer modeling. Acta Biomater (2021) 132:37–51. doi: 10.1016/j.actbio.2021.03.002

108. Velasco V, Shariati SA, Esfandyarpour R. Microtechnology-based methods for organoid models. Microsystems Nanoeng (2020) 6(1):1–13. doi: 10.1038/s41378-020-00185-3

109. Kurth F, Györvary E, Heub S, Ledroit D, Paoletti S, Renggli K, et al. Organs-on-a-chip engineering. In: Organ-on-a-chip Academic Press (2020). pp. 47–130.

110. Serex L, Bertsch A, Renaud P. Microfluidics: A new layer of control for extrusion-based 3D printing. Micromachines (2018) 9(2):86. doi: 10.3390/mi9020086

111. Bhattacharjee N, Urrios A, Kang S, Folch A. The upcoming 3D-printing revolution in microfluidics. Lab Chip (2016) 16(10):1720–42. doi: 10.1039/C6LC00163G

112. Sadeghi N, Khalife S, Mascarella MA, Ramanakumar AV, Richardson K, Joshi AS, et al. Pathologic response to neoadjuvant chemotherapy in HPV-associated oropharynx cancer. Head Neck (2020) 42(3):417–25. doi: 10.1002/hed.26022

113. Calpe B, Kovacs WJ. High-throughput screening in multicellular spheroids for target discovery in the tumor microenvironment. Expert Opin Drug Discov (2020) 15(8):955–67. doi: 10.1080/17460441.2020.1756769

114. Han SJ, Kwon S, Kim KS. Challenges of applying multicellular tumor spheroids in preclinical phase. Cancer Cell Int (2021) 21(1):1–19. doi: 10.1186/s12935-021-01853-8

115. Veninga V, Voest EE. Tumor organoids: Opportunities and challenges to guide precision medicine. Cancer Cell (2021) 39(9):1190–201. doi: 10.1016/j.ccell.2021.07.020

116. Wensink GE, Elias SG, Mullenders J, Koopman M, Boj SF, Kranenburg OW, et al. Patient-derived organoids as a predictive biomarker for treatment response in cancer patients. NPJ Precis Oncol (2021) 5(1):1–13. doi: 10.1038/s41698-021-00168-1

117. Signati L, Allevi R, Piccotti F, Albasini S, Villani L, Sevieri M, et al. Ultrastructural analysis of breast cancer patient-derived organoids. Cancer Cell Int (2021) 21(1):1–13. doi: 10.1186/s12935-021-02135-z

118. Gunti S, Hoke ATK, Vu KP, London NR. Organoid and spheroid tumor models: Techniques and applications. Cancers (Basel) (2021) 13(4):1–18. doi:10.3390/cancers13040874

119. Beato F, Reverón D, Dezsi KB, Ortiz A, Johnson JO, Chen DT, et al. Establishing a living biobank of patient-derived organoids of intraductal papillary mucinous neoplasms of the pancreas. Lab Investig (2021) 101(2):204–17. doi: 10.1038/s41374-020-00494-1

120. Qu J, Kalyani FS, Liu L, Cheng T, Chen L. Tumor organoids: synergistic applications, current challenges, and future prospects in cancer therapy. Cancer Commun (2021) 41(12):1–23. doi: 10.1002/cac2.12224

121. Nero C, Vizzielli G, Lorusso D, Cesari E, Daniele G, Loverro M, et al. Patient-derived organoids and high grade serous ovarian cancer: from disease modeling to personalized medicine. J Exp Clin Cancer Res (2021) 40(1):1–14. doi: 10.1186/s13046-021-01917-7

122. Takahashi N, Higa A, Hiyama G, Tamura H, Hoshi H, Dobashi Y, et al. Construction of in vitro patient-derived tumor models to evaluate anticancer agents and cancer immunotherapy. Oncol Lett (2021) 21(5):1–12. doi: 10.3892/ol.2021.12667

123. Rae C, Amato F, Braconi C. Patient-derived organoids as a model for cancer drug discovery. Int J Mol Sci (2021) 22(7):3483. doi: 10.3390/ijms22073483

124. Karakasheva TA, Kijima T, Shimonosono M, Maekawa H, Sahu V, Gabre JT, et al. Generation and characterization of patient-derived head and neck, oral, and esophageal cancer organoids. Curr Protoc Stem Cell Biol (2020) 53(1):1–27. doi: 10.1002/cpsc.109

125. Ben-David U, Ha G, Tseng YY, Greenwald NF, Oh C, Shih J, et al. Patient-derived xenografts undergo murine-specific tumor evolution. Nat Genet (2017) 49 (11):1567–75. doi: 10.1038/ng.3967

126. Murayama T, Gotoh N. Patient-derived xenograft models of breast cancer and their application. Cells (2019) 8(6):621. doi: 10.3390/cells8060621

127. Crespo M, Vilar E, Tsai SY, Chang K, Amin S, Srinivasan T, et al. Colonic organoids derived from human induced pluripotent stemcells formodeling colorectal cancer and drug testing. NatMed (2017) 23(7):878–84. doi: 10.1038/nm.4355

128. Azar J, Bahmad HF, Daher D, Moubarak MM, Hadadeh O, Monzer A, et al. The use of stem cell-derived organoids in disease modeling: An update. Int J Mol Sci (2021) 22(14):7667. doi: 10.3390/ijms22147667

129. Kim EJ, Kang KH, Ju JH. Crispr-cas9: A promising tool for gene editing on induced pluripotent stem cells. Korean J Intern Med (2017) 32(1):42–61. doi: 10.3904/kjim.2016.198

130. Matano M, Date S, Shimokawa M, Takano A, Fujii M, Ohta Y, et al. Modeling colorectal cancer using CRISPR-Cas9-mediated engineering of human intestinal organoids. Nat Med (2015) 21(3):256–62. doi: 10.1038/nm.3802

131. De Masi C, Spitalieri P, Murdocca M, Novelli G, Sangiuolo F. Application of CRISPR/Cas9 to human-induced pluripotent stem cells: From gene editing to drug discovery. Hum Genomics (2020) 14(1):1–12. doi: 10.1186/s40246-020-00276-2

132. Huang L, Holtzinger A, Jagan I, Begora M, Lohse I, Ngai N, et al. Ductal pancreatic cancer modeling and drug screening using human pluripotent stem cell and patient-derived tumor organoids. Nat Med (2015) 21(11):1364–71. doi: 10.1038/nm.3973

133. Pernik MN, Bird CE, Traylor JI, Shi DD, Richardson TE, McBrayer SK, et al. Patient-derived cancer organoids for precision oncology treatment. J Pers Med (2021) 11(5):423. doi: 10.3390/jpm11050423

134. Chen D, Wang C-Y. Targeting cancer stem cells in squamous cell carcinoma. Precis Clin Med (2019) 2(3):152–65. doi: 10.1093/pcmedi/pbz016

135. Mohan A, Raj Rajan R, Mohan G, Kollenchery Puthenveettil P, Maliekal TT. Markers and reporters to reveal the hierarchy in heterogeneous cancer stem cells. Front Cell Dev Biol (2021) 9. doi: 10.3389/fcell.2021.668851

136. Ukai S, Honma R, Sakamoto N, Yamamoto Y, Pham QT, Harada K, et al. Molecular biological analysis of 5-FU-resistant gastric cancer organoids; KHDRBS3 contributes to the attainment of features of cancer stem cell. Oncogene (2020) 39(50):7265–78. doi: 10.1038/s41388-020-01492-9

137. Yang L, Shi P, Zhao G, Xu J, Peng W, Zhang J, et al. Targeting cancer stem cell pathways for cancer therapy. In: Signal transduction and targeted therapy, vol. Vol. 5. Springer US (2020). doi: 10.1038/s41392-020-0110-5

138. Tang DG. Understanding cancer stem cell heterogeneity and plasticity. Cell Res (2012) 22(3):457–72. doi: 10.1038/cr.2012.13

139. Spencer H, Moshkbouymatin N, Webb WR, Joshi A, D'Souza A. Update on the role of emerging stem cell technology in head and neck medicine. Head Neck (2021) 43(6):1928–38. doi: 10.1002/hed.26674

140. Nguyen R, Da Won Bae S, Qiao L, George J. Developing liver organoids from induced pluripotent stem cells (iPSCs): An alternative source of organoid generation for liver cancer research. Cancer Lett (2021) 508:13–7. doi: 10.1016/j.canlet.2021.03.017

141. Takebe T, Zhang RR, Koike H, Kimura M, Yoshizawa E, Enomura M, et al. Generation of a vascularized and functional human liver from an iPSC-derived organ bud transplant. Nat Protoc (2014) 9(2):396–409. doi: 10.1038/nprot.2014.020

142. Lungova V, Thibeault S. Developmental derivation of vocal fold mucosa from human induced pluripotent stem cells. Protocolexchange (2019), 1:1–14. doi: 10.21203/rs.2.12611/v1

143. Ota I, Masui T, Kurihara M, Yook JI, Mikami S, Kimura T, et al. Snail induced EMT promotes cancer stem cell-like properties in head and neck cancer cells. Oncol Rep (2016) 35(1):261–6. doi: 10.3892/or.2015.4348

144. Lungova V, Chen X, Wang Z, Kendziorski C, Thibeault SL. Human induced pluripotent stem cell-derived vocal fold mucosa mimics development and responses to smoke exposure. Nat Commun (2019) 10(1):1–16. doi: 10.1038/s41467-019-12069-w

145. Zhang M, Vandana JJ, Lacko L, Chen S. Modeling cancer progression using human pluripotent stem cell-derived cells and organoids. Stem Cell Res (2020) 49:102063. doi: 10.1016/j.scr.2020.102063

146. Pu J, Frescas D, Zhang B, Feng J. Utilization of TALEN and CRISPR/Cas9 technologies for gene targeting and modification. Exp Biol Med (2015) 240(8):1065–70. doi: 10.1177/1535370215584932

147. Lee DF, Su J, Kim HS, Chang B, Papatsenko D, Zhao R, et al. Modeling familial cancer with induced pluripotent stem cells. Cell (2015) 161(2):240–54. doi: 10.1016/j.cell.2015.02.045

148. Choe MS, Kim JS, Yeo HC, Bae CM, Han HJ, Baek K, et al. A simple metastatic brain cancer model using human embryonic stem cell-derived cerebral organoids. FASEB J (2020) 34(12):16464–75. doi: 10.1096/fj.202000372R

149. Ho BX, Pek NMQ, Soh BS. Disease modeling using 3D organoids derived from human induced pluripotent stem cells. Int J Mol Sci (2018) 19(4):936. doi: 10.3390/ijms19040936

150. Uddin F, Rudin CM, Sen T. CRISPR gene therapy: Applications, limitations, and implications for the future. Front Oncol (2020) 10. doi: 10.3389/fonc.2020.01387

151. Asmamaw M. Biologics: Targets and therapy mechanism and applications of CRISPR / cas-9-Mediated genome editing. Biologics: Targets & Therap (2021) 15:353–61. doi: 10.2147/BTT.S326422

152. Ramakrishna G, Babu PE, Singh R, Trehanpati N. Application of CRISPRCas9 based gene editing to study the pathogenesis of colon and liver cancer using organoids. Hepatol Int (2021) 15(6):1309–17. doi: 10.1007/s12072-021-10237-z

153. Ihry RJ, Worringer KA, Salick MR, Frias E, Ho D, Theriault K, et al. P53 inhibits CRISPR-Cas9 engineering in human pluripotent stem cells. Nat Med (2018) 24(7):939–46.

doi: 10.1038/s41591-018-0050-6

154. Lo YH, Kolahi KS, Du Y, Chang CY, Krokhotin A, Nair A, et al. A crispr/cas9-engineered arid1a-deficient human gastric cancer organoid model reveals essential and nonessential modes of oncogenic transformation. Cancer Discovery (2021) 11(6):1562–81.
doi: 10.1158/2159-8290.CD-20-1109

155. Zhang XH, Tee LY, Wang XG, Huang QS, Yang SH. Off-target effects in CRISPR/Cas9-mediated genome engineering. Mol Ther Nucleic Acids (2015) 4(11):e264.
doi: 10.1038/mtna.2015.37

156. Zanoni M, Cortesi M, Zamagni A, Arienti C, Pignatta S, Tesei A. Modeling neoplastic disease with spheroids and organoids. J Haematol Oncol (2020) 0:1–15.
doi: 10.1186/s13045-020-00931-0

157. Brassard JA, Nikolaev M, Hübscher T, Hofer M, Lutolf MP. Recapitulating macro-scale tissue self-organization through organoid bioprinting. Nat Mater(2021) 20(1):22–9.
doi: 10.1038/s41563-020-00803-5

158. Daly AC, Prendergast ME, Hughes AJ, Burdick JA. Bioprinting for the biologist. Cell (2021) 184(1):18–32. doi: 10.1016/j.cell.2020.12.002

159. Sun W, Starly B, Daly AC, Burdick JA, Groll J, Skeldon G, et al. The bioprinting roadmap. Biofabrication (2020) 12(2):022002. doi: 10.1088/1758-5090/ab5158

160. Hwang HH, You S, Ma X, Kwe L, Victorine G, Lawrence N, et al. High throughput direct 3D bioprinting in multiwell plates. Biofabrication (2021) 13(2):025007.
doi: 10.1088/1758-5090/ab89ca

161. Li J, Parra-Cantu C, Wang Z, Zhang YS. Improving bioprinted volumetric tumor microenvironments in vitro. Trends Cancer (2020) 6(9):745–56. doi: 0.1016/j.trecan.2020.06.002

162. Huh JT, Moon YW, Park J, Atala A, Yoo JJ, Lee SJ. Combinations of photoinitiator and UV absorber for cell-based digital light processing (DLP) bioprinting. Biofabrication (2021) 13(3):034103. doi: 10.1088/1758-5090/abfd7a

163. Wang M, Li W, Mille LS, Ching T, Luo Z, Tang G, et al. Digital light processing based bioprinting with composable gradients. Adv Mater (2022) 34(1):2107038. doi: 10.1002/adma.202107038

164. Goodarzi Hosseinabadi H, Dogan E, Miri AK, Ionov L. Digital light processing bioprinting advances for microtissue models. ACS Biomater Sci Eng (2022) 8(4):1381–95. doi: 10.1021/acsbiomaterials.1c01509

165. Arslan-Yildiz A, El Assal R, Chen P, Guven S, Inci F, Demirci U. Towards artificial tissue models: Past, present, and future of 3D bioprinting. Biofabrication (2016) 8(1):014103. doi: 10.1088/1758-5090/8/1/014103

166. Lee B, Kim S, Ko J, Lee SR, Kim Y, Park S, et al. 3D micromesh-based hybrid bioprinting: multidimensional liquid patterning for 3D microtissue engineering. NPG Asia Mater (2022) 14(1):1–10. doi: 10.1038/s41427-022-00355-x

167. Suntornnond R, Tan EYS, An J, Chua CK. A mathematical model on the resolution of extrusion bioprinting for the development of new bioinks. Mater (Basel) (2016) 9(9):756. doi: 10.3390/ma9090756

168. Cui P, Wang S. Application of microfluidic chip technology in pharmaceutical analysis: A review. J Pharm Anal (2019) 9(4):238–47. doi: 10.1016/j.jpha.2018.12.001

169. Betancourt N, Chen X. Review of extrusion-based multi-material bioprinting processes. Bioprinting (2022) 25:e00189. doi: 10.1016/j.bprint.2021.e00189

170. Park JY, Ryu H, Lee B, Ha DH, Ahn M, Kim S, et al. Development of a functional airway-on-a-chip by 3D cell printing. Biofabrication (2019) 11(1):015002. doi: 10.1088/1758-5090/aae545

171. Si L, Bai H, Rodas M, Cao W, Oh CY, Jiang A, et al. A human-airway-on-a-chip for the rapid identification of candidate antiviral therapeutics and prophylactics. Nat BioMed Eng (2021) 5(8):815–29. doi: 10.1038/s41551-021-00718-9

172. Si L, Prantil-Baun R, Benam KH, Bai H, Rodas M, Burt M, et al. Discovery of influenza drug resistance mutations and host therapeutic targets using a human airway chip. BioRxiv (2019) 685552. doi: 10.1101/685552

173. Benam KH, Villenave R, Lucchesi C, Varone A, Hubeau C, Lee HH, et al. Small airway-on-a-chip enables analysis of human lung inflammation and drug responses in vitro. Nat Methods (2016) 13(2):151–7. doi: 10.1038/nmeth.3697

174. Shrestha J, Ryan ST, Mills O, Zhand S, Razavi Bazaz S, Hansbro PM, et al. A 3D-printed microfluidic platform for simulating the effects of CPAP on the nasal epithelium. Biofabrication (2021) 13(3):035028. doi: 10.1088/1758-5090/abe4c1

175. Bluhmki T, Bitzer S, Gindele JA, Schruf E, Kiechle T, Webster M, et al. Development of a miniaturized 96-transwell air–liquid interface human small airway epithelial model. Sci Rep (2020) 10(1):1–14. doi: 10.1038/s41598-020-69948-2

176. Jung O, Tung YT, Sim E, Chen YC, Lee E, Ferrer M, et al. Development of human-derived, three-dimensional respiratory epithelial tissue constructs with perfusable microvasculature on a high-throughput microfluidics screening platform. Biofabrication (2022) 14(2):025012. doi: 10.1088/1758-5090/ac32a5

177. Schuster B, Junkin M, Kashaf SS, Romero-Calvo I, Kirby K, Matthews J, et al. Automated microfluidic platform for dynamic and combinatorial drug screening of tumor organoids. Nat Commun (2020) 11(1):1–12. doi: 10.1038/s41467-020-19058-4

178. Ingber DE. Human organs-on-chips for disease modelling, drug development and personalized medicine. Nat Rev Genet (2022) 0123456789. doi: 10.1038/s41576-022-00466-9

179. Zuchowska A, Skorupska S. Multi-organ-on-chip approach in cancer research. Organs-on-a-Chip (2022) 4:100014. doi: 10.1016/j.ooc.2021.100014

Preface to Chapter 4

In Chapter 4, we proposed to encapsulate and characterize DTX in chitosomes as a cytotoxic treatment for laryngeal cancer cells (Aim 1). We conducted a series of in vitro experiments to evaluate (1) the loading of DTX into the chitosan-coated and non-coated liposomes, (2) mucoadhesive behavior of the chitosan coating on the DTX-loaded liposomes, (3) cytotoxic effect of DTX-loaded chitosomes on laryngeal cancer cell, laryngeal fibroblasts, and red blood cells.

This work included the development and characterization of mucoadhesive chitosan-coated anionic nanoliposomes, referred to as 'chitosomes', loaded with docetaxel to facilitate the targeted delivery of docetaxel to laryngeal cancer cells. The anionic liposomes had a diameter of about 100 nm and a zeta potential of -26 mV intended to have enhanced permeability and retention properties. The application of chitosan as a coating increased the liposome size by 20nm and the surface charge shifted to +25 mV. We confirmed the formation of DTX-loaded chitosomes through FTIR spectroscopy and mucoadhesive testing using an anionic mucin dispersion.

Both empty liposomes and chitosomes demonstrated no harmful effects on human laryngeal fibroblasts and cancer cells. Importantly, the chitosomes were efficiently taken up into the cytoplasm of laryngeal cancer cells, indicating their effectiveness as a nanocarrier for DTX delivery. Then, we proceeded with the respective DTX cytotoxic studies on coated and uncoated nanoliposomes. We observed significantly higher cytotoxicity of DTX-loaded chitosomes towards human laryngeal cancer cells compared to fibroblasts and control treatments. Furthermore, no damage to human red blood cells was observed after 3 hours of exposure, supporting the potential for intra-arterial administration of our proposed delivery system. This study indicated the promise of DTX-loaded chitosomes for locoregional chemotherapy delivery to laryngeal cancer cells.

This work is published in the International Journal of Molecular Sciences.
Moya-Garcia, C. R., Li-Jessen, N. Y. K., & Tabrizian, M. (2023). Chitosomes Loaded with Docetaxel as a Promising Drug Delivery System to Laryngeal Cancer Cells: An In Vitro Cytotoxic Study. *International Journal of Molecular Sciences*, *24*(12), 9902.

Chapter 4. First original article

Chitosomes loaded with docetaxel as a promising drug delivery system to laryngeal cancer cells: An in vitro cytotoxic study.

This manuscript was published in the International Journal of Molecular Sciences on the 8th of June 2023. DOI: doi.org/ 10.3390/ijms24129902

Christian R. Moya-Garcia[1], Nicole Y.K. Li-Jessen[1,2,3,4,†,*] and Maryam Tabrizian[1,5,†,*]

1 Department of Biomedical Engineering, Faculty of Medicine and Health Sciences, McGill University, 3775 Rue University, Montreal, QC H3A 2B4, Canada; christian.moyagarcia@mail.mcgill.ca

2 School of Communication Sciences and Disorders, McGill University, 2001 Av. McGill College #8, Montréal, QC H3A 1G1, Canada; nicole.li@mcgill.ca

3 Department of Otolaryngology – Head and Neck Surgery, McGill University Health Centre, 1001 Decarie Blvd., Montreal, Quebec, H4A 3J1, Canada

4 Research Institute of the McGill University Health Centre, 1001 Decarie Blvd, Montreal, QC H4A 3J1, Canada

5 Faculty of Dental Medicine and Oral Health Sciences, McGill University, 2001 Ave McGill College, Montreal, QC H3A 1G1, Canada

† Equal contribution

* Corresponding author: nicole.li@mcgill.ca and maryam.tabrizian@mcgill.ca

Abstract: Current delivery of chemotherapy, either intra-venous or intra-arterial, remains suboptimal for patients with head and neck tumors. The free form of chemotherapy drugs, as docetaxel, has non-specific tissue targeting and poor solubility in blood that deters treatment efficacy. Once reaching tumors, these drugs can also be easily washed away by the interstitial fluids. Liposomes have been used as nanocarriers to enhance docetaxel bioavailability. Yet, they are affected by potential interstitial dislodging due to insufficient intratumoral permeability and retention capabilities. Here, we developed and characterized docetaxel-loaded anionic nanoliposomes coated with a layer of mucoadhesive chitosan (chitosomes) for the application of chemotherapy drug delivery. Anionic liposomes had 99.4 ± 1.5 nm in diameter with a zeta potential of -26 ± 2.0 mV. The chitosan coating increased the liposome size to 120 ± 2.2 nm and the surface

charge to 24.8 ± 2.6 mV. Chitosomes formation was confirmed via FTIR spectroscopy and mucoadhesive analysis with anionic mucin dispersion. Blank liposomes and chitosomes showed no cytotoxic effect on human laryngeal stromal and cancer cells. Chitosomes were also internalized into the cytoplasm of human laryngeal cancer cells, indicating effective nanocarrier delivery. A higher cytotoxicity ($p<0.05$) of docetaxel-loaded chitosomes to human laryngeal cancer cells was observed compared to human stromal cells and control treatments. No hemolytic effect was observed on human red blood cells after 3h exposure, proving the proposed intra-arterial administration. Our *in vitro* results supported the potential of docetaxel-loaded chitosomes for locoregional chemotherapy delivery to laryngeal cancer cells.

4.1 Introduction

Head and neck cancer is one of the most aggressive cancers [1]. It is considered the sixth most common type of cancer [2], with more than 650,000 newly diagnosed head and neck cancer cases each year worldwide [3]. As a sub-type of head and neck cancer, laryngeal cancer has an annual incidence rate over 30% of the total number of head and neck cancers worldwide, second to oral cancer [4]. The 5-year survival rate of human papilloma virus-negative laryngeal cancer has been approximately 50% for the past three decades [1,5].

Induction chemotherapy is the standard-of-care treatment for head and neck cancer [6, 7]. In particular, docetaxel (DTX) is one common chemotherapy drug in the treatment of head and neck cancer [8–10] that is delivered via systemic intravenous [6,7,11–13] or locoregional intra-arterial [14–16] routes. Either delivery route has its own pros and cons that undermine the expected benefits of chemotherapy. Systemic intravenous delivery provokes highly toxic deleterious effects throughout the body because the chemotherapy concentration is similar in the tumor site as that present in the whole body [6,7,11–13]. Remarkably, about 1% of the chemotherapeutics reach solid tumors via the systemic route [17,18].

Alternatively, locoregional intra-arterial chemotherapy was proposed to overcome such systemic toxicities by infusing the drug into tumor-supplying arteries, rather than circulating the chemotherapeutics systemically [14–16]. However, the intra-arterial delivery may still cause toxic extravasation damage in the surrounding tumor region [15,16]. New advances in immunotherapy have been proposed to directly inject a gelatin biomaterial loaded with immune checkpoint

blockade drugs into the tumor [19]. However, considering the unique structure and immune environment of the upper airway, only a very small volume of drugs can be injected without causing breathing obstruction [20–22]. As such, reducing the unwanted toxic damage from either intra-venous or intra-arterial induction chemotherapy remains a major challenge in head and neck cancer treatment.

Nanocarriers have been proposed to protect chemotherapy drugs from early degradation and promote targeted delivery to the local tumor [23–25]. Among these nanocarriers, liposomes are FDA-approved drug vesicles with decreased dose concentrations providing a controlled and sustained drug release [25]. Liposomes are made of phospholipids and cholesterol [25,26] and have a similar phospholipid bilayer membrane as that of cells. Liposomes have been shown to protect lipophilic/water insoluble drugs, e.g., chemotherapy drugs such as DTX, from rapid degradation while they circulate the blood stream [26–29]. This feature can help the chemo drug to reach the tumor vasculature and reduce systemic toxicity [30–32] (**Figure 4-1**).

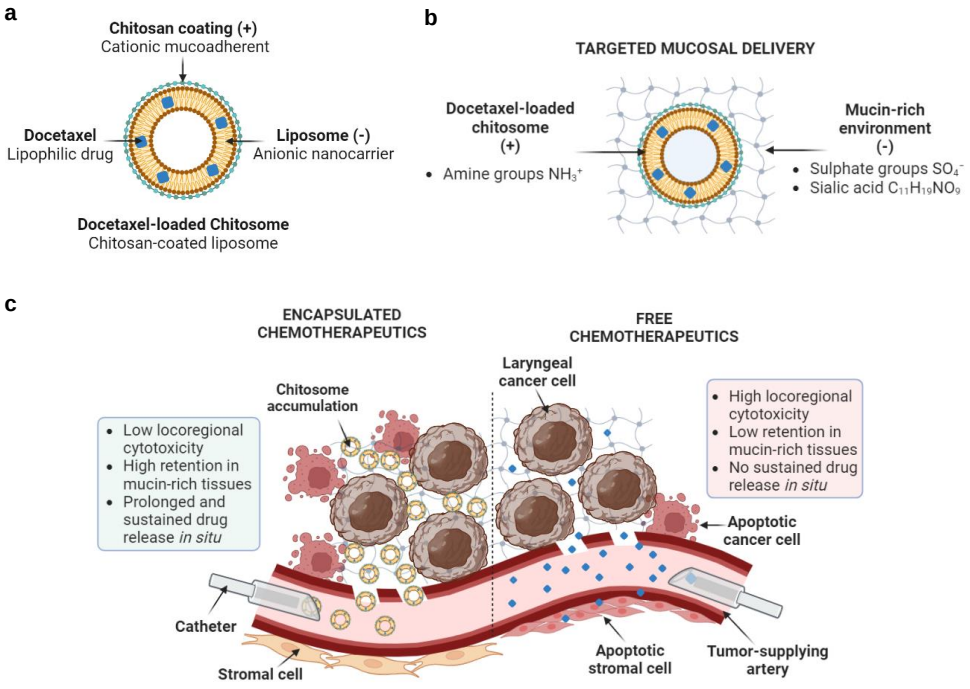

Figure 4-1. Schematic representation of chitosan-coated liposomes, namely 'chitosomes', as chemo drug nanocarriers. (a) Components of docetaxel-loaded chitosomes. (b) Mucin-chitosome electrostatic interactions. (c) Encapsulated versus free drugs comparison in mucin-rich tumors. Figure created with BioRender.com.

Multiple steps are implemented to synthesize DTX-loaded “chitosomes”, i.e., liposomes coated with chitosan [38,47-49]. Lipid components are first dissolved in organic solvents as ethanol [49] or chloroform [38,47,48] with an extra step to load DTX. The use of ethanol as organic solvent in liposome synthesis has been reported to increase reproducibility of liposome particle size and polydispersity index compared to those using other solvents [50]. In addition, the molecular weight of chitosan influences its effectiveness as a coating agent for nanoparticles in the process of mucosal adsorption [51]. A lower molecular weight is preferable in order to enhance mucoadhesion and drug permeation [51]. Chitosan with molecular weights ranging from low (110 KDa) [49] to high (10,000 KDa) [38] have been used to coat DTX-loaded liposomes. In addition, chitosan molecular weight lower than 4 KDa exhibits anti-tumor effects [52]. Therefore, based on a method previously used in our laboratory for one-step synthesis of liposomes [28], we used an ethanol injection method to fabricate our anionic liposomes coated with 1.5 KDa chitosan.

While several studies have investigated the use of DTX-loaded chitosome in breast cancer [38,47,49], none have investigated the use of such a drug delivery system in head and neck cancer. Also, existing DTX-loaded chitosomes are primarily designed for oral ingestion or intravenous injection [53]. However, as mentioned above, systemic intravenous [6,7,11-13] leads to unwanted high toxicities and extravasation. Thus, we designed a novel chitosome formulation to benefit from recent locoregional treatment, e.g., the intra-arterial administration [14-16], with the aim of reducing high toxic locoregional damage in the laryngeal mucosae.

In this study, we produced chitosomes and evaluated its applicability as nanocarriers of chemotherapy drugs for laryngeal cancer. We hypothesized that chitosomes would potentially circumvent chemotherapy drug solubility and attenuate the adverse side effects of systemic and locoregional chemotherapy deliveries. To demonstrate the feasibility of our approach, we first developed DTX-loaded chitosomes and performed a thorough physicochemical characterization, using nanoparticle tracking analysis and zeta potential measurements, FTIR spectroscopy, and electron and fluorescence microscopies. Then, mucoadhesive studies were performed by chitosome immersion in mucin-rich dispersions. *In vitro* studies were further performed to evaluate the DTX therapeutic effect on human vocal fold fibroblasts (HVFFs), laryngeal squamous cell carcinomas (LSCCs), and red blood cells.

4.2 Results and Discussion

4.2.1. DTX-loaded chitosomes possessed the expected physical properties

4.2.1.1. Size and surface charge analysis

Nanoparticle tracking analysis of the non-coated and blank liposomes indicated a size of 99.4 ± 1.5 nm for those nanocarriers (**Figure 4-2a**). Similar size (107 nm to 116 nm) and spherical morphology were also reported by Paun et al. [28] when the ethanol injection method was used for the fabrication of liposomes. Chitosan coating showed a significant increase in size of nanoliposomes from 99.4 ± 1.5 nm to 120 ± 3.1 nm (**Figure 4-2a**). Also, the polydispersity index (PDI) was below 0.2 denoting the consistent size distribution, which was similar to the 0.17 PDI (~140 nm) reported by Zafar et al. [49]. Ethanol injection method has been reported to provide more reproducible size in comparison to thin-film synthesis. Chitosome studies using chloroform as organic solvent yielded nano-liposomes with the PDI values ranging from 0.18 to 0.33 PDI (~90 nm) [38] and from 0.22 to 0.41 PDI (~240 nm) [47].

The chitosan coating was designed to create a positively-charged mucoadhesive surface on the liposomes to allow electrostatic interactions with the mucosal epithelial layer of the larynx. The shift in polarity from negative to positive was noted in anionic liposomes after the chitosan coating [23,40,47]. Further, our results showed that zeta potential shifted from -26 ± 2 mV for the blank liposomes to -8.5 mV immediately after the addition of 10 μL chitosan solution to liposomal dispersion. The addition of more chitosan solution, i.e., from 110 μL to 170 μL (0.4 to 0.7 mg/mL of chitosan), stabilized the surface charge of blank chitosome at 24.8 ± 2.6 mV and 28 ± 2 mV for DTX-loaded chitosomes (**Figure 4-2a**). For the zeta potential measurements, 130 μL of chitosan solution with a concentration of 0.5 mg/mL was used. The zeta value is an important parameter to take into consideration when developing nanoparticles, since it provides information about the colloidal stability and prone-to-aggregation of nanoparticles in suspension [54]. When zeta potential values exceed 25 mV, whether positive or negative, they provide repulsive forces for better dispersion of drug-loaded nanocarriers, and thus, for more efficient delivery of their cargo [55,56]. Our zeta values for both blank liposomes and chitosomes were higher than 20 mV, which confirms the colloidal stability of our nanocarriers.

The loading of the drug into chitosomes has changed the size and charge of liposo-mal systems. Compared to blank liposomes (99.4 ± 1.5 nm) and blank chitosomes (120 ± 3 nm), the drug loading significantly increased the nanocarrier size (DTX-loaded liposomes = 118 ± 1.4 nm; DTX-loaded chitosomes = 130.4 ± 0.9 nm) as expected. DTX-loaded chito-some and control groups (DTX-loaded liposome, blank chitosome, and blank liposome) showed a roughly spherical structure ranging from 120 nm to 150 nm in diameters ac-cording to transmission electron micrographs (**Figure 4-2b**), which corroborate with the size on these nanoparticles recorded by nanoparticle tracking analysis.

As expected, the addition of chitosan shifted the negative zeta potential values from - 27 mV for non-coated liposome groups to + 28 mV for chitosan-coated liposome groups (**Figure 4-2a**). To investigate the stability of the nanoliposomes, we further performed a 35-day stability evaluation on blank liposomes and chitosomes as well as their DTX-loaded versions. All groups maintained their baseline size for the first 28 days (***$p<0.001$) (**Figure 4-2c**). However, the zeta values showed differentiated trends across groups from day 1 to day 35. In particular, both DTX-loaded and blank chitosome groups showed significantly decreased in magnitude of the zeta values at day 35 (**Figure 4-2d**) (****$p<0.0001$). The decrease in zeta values of chitosome might be resulted from partial degradation of the chitosan coating. In contrast, the increased zeta values in blank liposomes may be resulted from the oxidation/hydrolysis of phospholipidic membrane of the liposomes. The blank, non-coated liposomes may become fused over extended time, resulting in an increase in zeta value [57].

Chitosomes' physical properties are key for the rational nanocarrier design, like sizes of 100 to 200 nm, tackling the enhanced permeability and retention effect [18]. When the lipoid S75 and S100 were used, chitosan coating has shown to increase the size of non-coated liposomes up to 18% [47]. In our case, the change in size of non-coated lipo-somes was about 10%, which may be due to the variation in anionic liposomal formula-tion. Nevertheless, this size is within the nanocarrier diameter ranges (100-200 nm) for proper circulating performance in the tumor vasculature [58]. The DTX-induced increases in size and in charge are consistent with those previously reported for chitosomes loaded with docetaxel (100-150 nm in size [43] and 29.8 ± 2.4 mV in surface charge [23]). Since in some of our investigations as described in section 2.3.2, we

used fluorescently labelled liposomes and chitosomes, we also measured their size and zeta potential, but the difference was not significant compared to unlabelled nanocarriers.

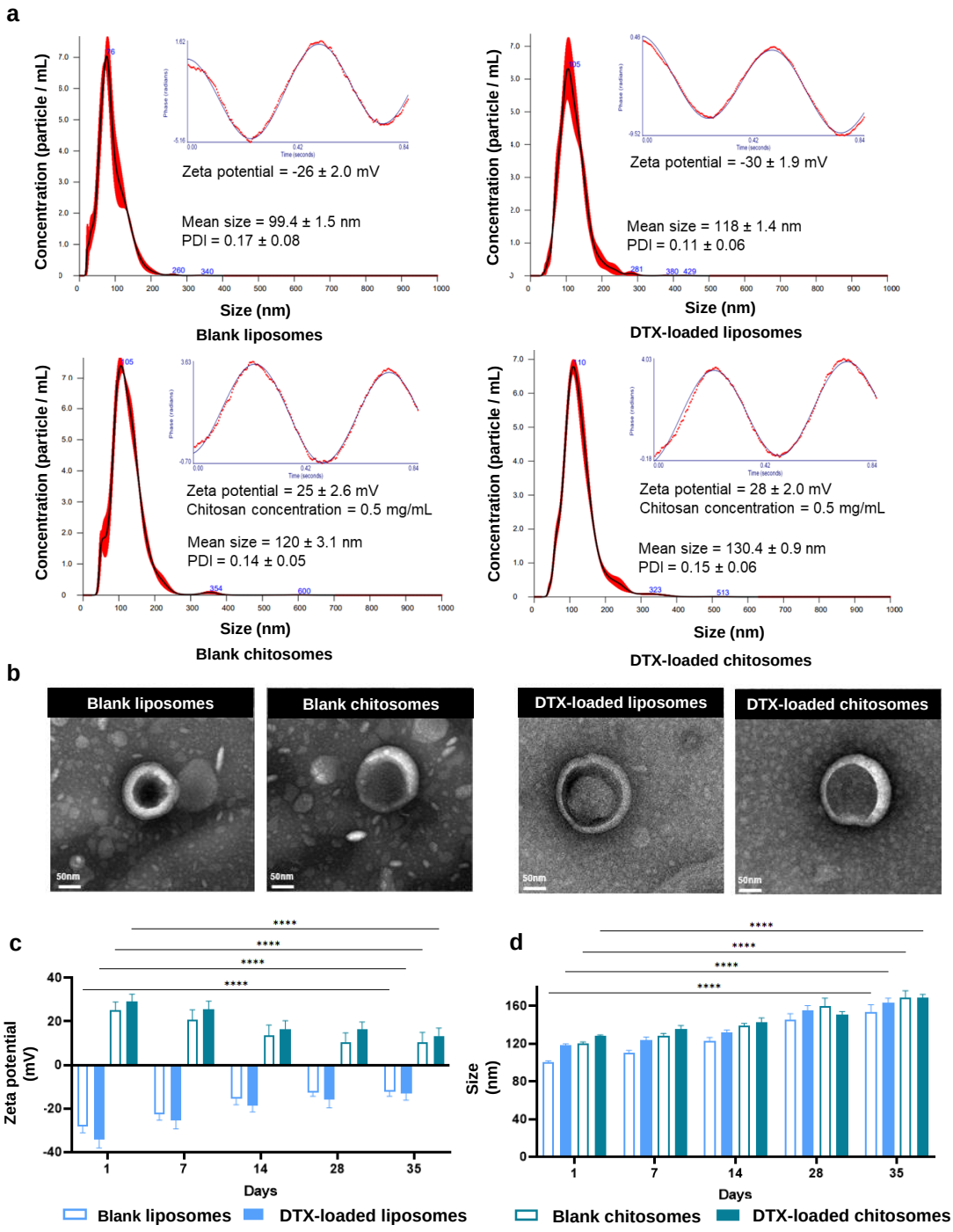

Figure 4-2. Size and charge of the blank and DTX-loaded liposomes coated with chitosan analyzed at neutral pH. (a) Optimized size and phase analysis light scattering plots of the blank and DTX-loaded liposomes coated with chitosan.

Chitosan concentration was calculated using the $C_1V_1 = C_2V_2$ dilution formula as (6mg/mL chitosan concentration)(10µL chitosan volume) = C_2(1.5mL liposomal suspension). (b) Morphology of the blank and DTX-loaded liposomes coated with chitosan via TEM. Scale bar = 50nm. The changes in size and charge of the DTX-loaded chitosomes were significant in comparison to all blank groups (c) Stability test at 37°C of DTX-loaded liposomal formulation. (d) Zeta potential of the DTX-loaded non-coated and coated liposomes after 5 weeks under 37°C and 5% CO_2. Size and zeta potential data are reported as mean ± SE and mean ± SD, respectively.

4.2.2. Chitosan-coating showed improved mucoadhesiveness and drug release profile of liposomes

4.2.2.1. FTIR spectroscopy

FTIR analysis was performed to characterize the chemical composition of the chitosomes. The chitosan coating on DTX-loaded liposomes was confirmed by the presence of the peaks at 753 cm-1 and 893 cm-1 corresponding to N-H bending and to the glycosidic C-O-C stretching of chitosan, respectively [59], which were absent in the blank liposome controls (**Figure 4-3, Table 4-1**). Blank liposomes spectrum was characterized by a peak at 1740 cm-1, representative of the C=O stretching of the ester bond of lipid components, which links the head group to the fatty acid tail of the phospholipids. Lipid-related peaks were also detected at 2800 cm-1 corresponding to CH2 symmetric stretch, and at 3400 cm-1 for the O-H and N-H stretching. The peak at 528 cm-1 was associated with the P-O asymmetrical bending of the PO4−3 molecule found in phospholipids [60]. The decrease in these peak intensities also confirmed a successful chitosan coating on liposomes. The DTX encapsulation in blank liposomes was also confirmed by the presence of a peak at 710cm-1, a fingerprint of the N-H bending of benzamide in the drug [61,62] (**Figure 4-3, Table 4-1**).

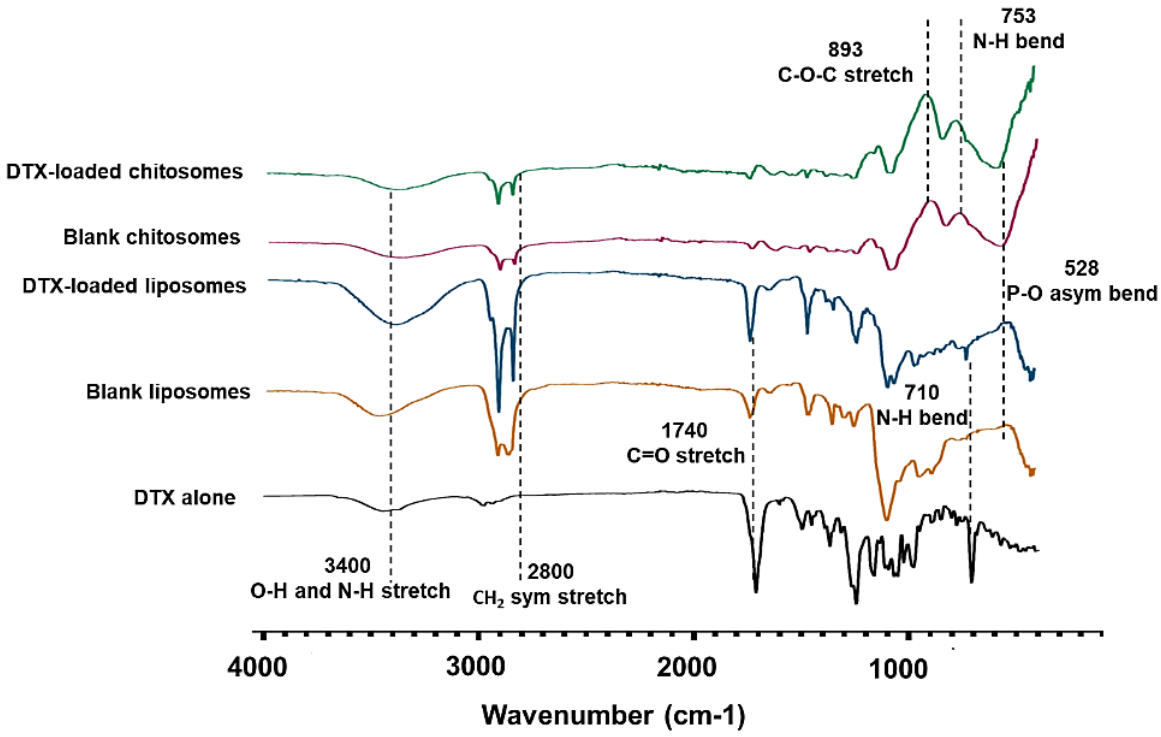

Figure 4-3. FTIR spectra of blank and DTX-loaded chitosomes. (a) FTIR spectra. Chemical fingerprint confirmation of chitosan presence and DTX loading on the liposomes.

Table 4-1. Identification of characteristic peaks of chitosomes compared to their constituent (controls) in their respective FTIR spectra.

Wavenumber (cm^{-1})	Vibrational mode	Biomolecular attributions
528	P-O asymmetrical bending	Phospholipids (PO_4^{-3} molecule)
710	Benzamide N-H bending	Docetaxel
753	N-H bending	Chitosan
893	Glycosidic C-O-C stretching	Chitosan
1740	C=O stretching	Lipids
2800	CH_2 stretching	Lipids
3400	O-H and N-H stretching	Lipids

4.2.2.2. Mucoadhesive studies

Results from the turbidity and surface charge tests confirmed the mucoadhesive properties of chitosan coating (**Figure 4-4a-c**). Chitosomes were exposed to mucin 1 originated from bovine submaxillary gland up to 3 hours. Submandibular gland mucosal environment has sero-mucinous similarities as that of the larynx [63]. Turbidity results showed an increased interaction between the mucin suspension and the chitosomes in comparison to the non-coated group recorded by an increased absorbance of the 2 h (***$p<0.001$) and 3 h (****$p<0.0001$) (**Figure 4-4b**). Similar turbidity trend was reported by Yamazoe et al. [64] with their system consisting of elcatonin-loaded chitosomes and the elcatonin-loaded liposomes.

The surface charge also decreased from 29.1 ± 3.3 mV to -16 ± 4.20 mV (****$p<0.0001$) in the DTX-loaded chitosomes after mucin exposure (**Figure 4-4c**). This positive-to-negative switch can be explained by the hydrophobic and hydrogen bonding as well as the electro-static and ionic interactions between the cationic chitosan coating and the anionic mucus suspension [64,65]. No significant changes in turbidity and surface charge were noted in the non-coated and blank liposomes, assumably owning to the anionic and repulsive interactions between anionic liposomal surface and mucin dispersion.

Mucoadhesive behavior of the DTX-loaded chitosomes may relate to increase the interstitial retention in the mucin-dominant tumors, as that found in the larynx [66]. The interactions between chitosomes and mucins are crucial for the intended use of these liposomal-based nanocarriers in head and neck cancers. Mucins, which are glycosylated proteins produced by epithelial cells to form mucus, are highly secreted by the head and neck squamous cell carcinomas [67,68] as LSCCs [66]. Particularly, overexpression of Mucin-1 was associated to worse prognosis in head and neck cancer [66–68].

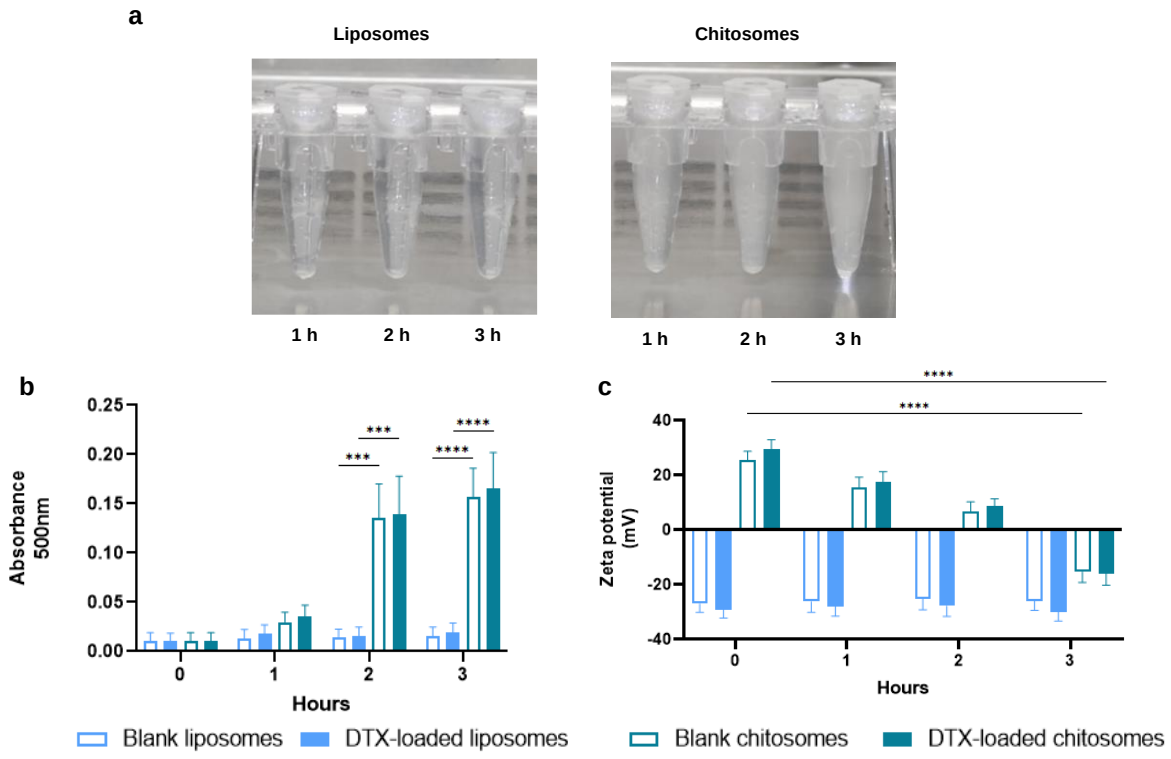

Figure 4-4. Mucoadhesive studies of DTX-loaded chitosomes. (a) Qualitative observation of turbidity as a result of the interaction between chitosomes or liposomes and mucin dispersion. Individual representative samples of DTX-loaded groups were chosen to properly visualize the turbidity of the samples. (b) Turbidity as a function of mucoadhesive behavior between chitosomes or liposomes and mucin at 500nm absorbance reading. (c) Zeta potential measurements of chitosomes or liposomes after mucin suspension exposure. Chitosomes' mucoadhesive behavior was confirmed in mucin-contained dispersion after 3 h immersion.

4.2.2.3. DTX entrapment and release studies

DTX entrapment efficiency in chitosomes was 82.6 ± 3.6% with regards to the DTX standardization curve (**Figure 4-5a-b**). As the chitosan coating was performed after the simultaneous fabrication and DTX loading of the liposomes, no significant difference was found in drug entrapment efficiency with non-coated liposomes (79.9 ± 3.1%). This entrapment efficiency was similar to those reported in other water insoluble drug encapsulation, such as copper (II) diethyldithiocarbamate [28].

The DTX solution release of ~80% from the dialysis membrane was similar to that reported by Sinhg et al. (2019) after 12h [44] (**Figure 4-5c**). Our results confirmed that the DTX release was

slower from the chitosomes than from the non-coated liposomes (**Figure 4-5c-d**). Both liposome groups showed a first-order DTX release profile as in previous reports [69]. As opposed to non-coated anionic liposomes, DTX release from chitosomes was expected to be prolonged due to the coating, in which providing an external physical barrier enveloping the liposomes [47,70].

Our results also revealed the effect of physiological environment on the drug retention. Exposing the liposomes and chitosomes to a release medium disrupted the liposomal bilayer, which resulted in a DTX escape from the nanocarriers. The incorporation of DSPC, cholesterol and DSPE into the liposomal formulation seemed to stabilize the liposomal membrane for DTX retention and release kinetics [71]. In addition, the DTX entrapment within the liposomal membrane might also help stabilize the bilayer by occluding the pores of the liposomal membrane. An increase drug retention of about ~12% on the coated group was observed compared to non-coated liposomes (18%) at 12-hour (**Figure 4-5c**). An increased drug retention of ~11% after 7 hours was noted for DTX-loaded liposomes coated with Eudragit, which is a cationic methacrylic acid-based polymer, com-pared to the non-coated liposomes [70]. Similarly, the DTX release from drug-loaded chitosomes was 20% lower after 24 hours at physiological pH 7 [38]. No longer time points were analyzed in these studies compared to ours where we investigated DTX released up to 28 days (**Figure 4-5d**). Furthermore, less than 40% of DTX was retained in the liposomal formulations after 72h (**Figure 4-5d**). This finding corroborates with a study where a similar phospholipid constituents was tested on breast cancer cells, and a DTX retention greater than 40% was obtained after 72h [72]. Nevertheless, our results indicate that the therapeutic window of our lipid nanocarriers would be up to day 3 after their local administration in the laryngeal mucosae of patients.

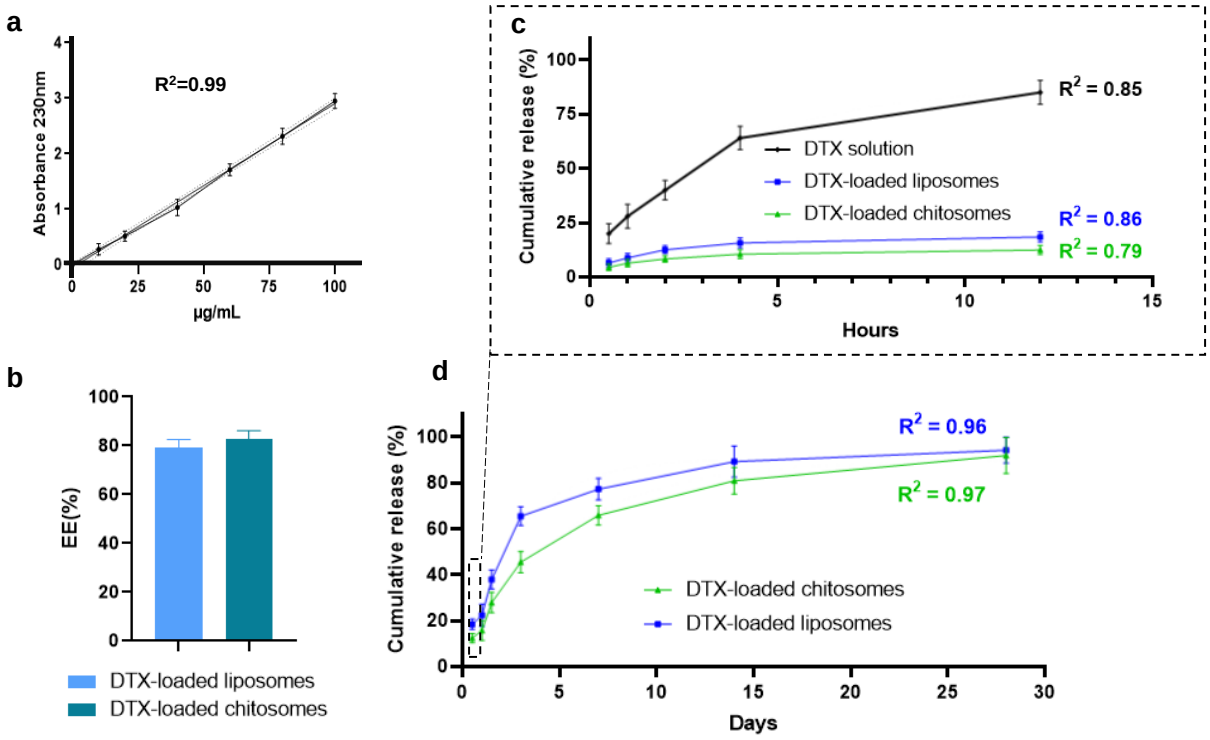

Figure 4-5. Drug release of DTX-loaded liposomes and chitosomes. (a) DTX standardization curve (Absorbance at 230 nm). (b) Docetaxel entrapment was about 81.9 ± 5.3% encapsulation efficacy after analysing the amount of the drug-released in supernatants. Drug release profile up to (c) 12 h and (d) 28 days.

4.2.3. Docetaxel-loaded chitosomes showed higher toxicity to cancer cells than healthy stromal and blood cells

4.2.3.1. HVFFs and LSCCs viability

In vitro cell viability analysis conducted with both liposomal and chitosomal nanocarriers without DXT showed no noticeable cytotoxicity to HVFFs and LSCCs up to 3 days (**Figure 4-6a-c**). Quantitative MTT assay confirmed no significance difference in cell viability on HVFFs and LSCCs in the absence of nanocarriers (**Figure 4-6d**). Using non-treated cells as a control group and setting their viability at 100% (*p>0.5) [73], we found that >95% of the HVFFs and LSCCs remained viable after exposure to nanocarriers, confirming the biocompatibility of chitosomes.

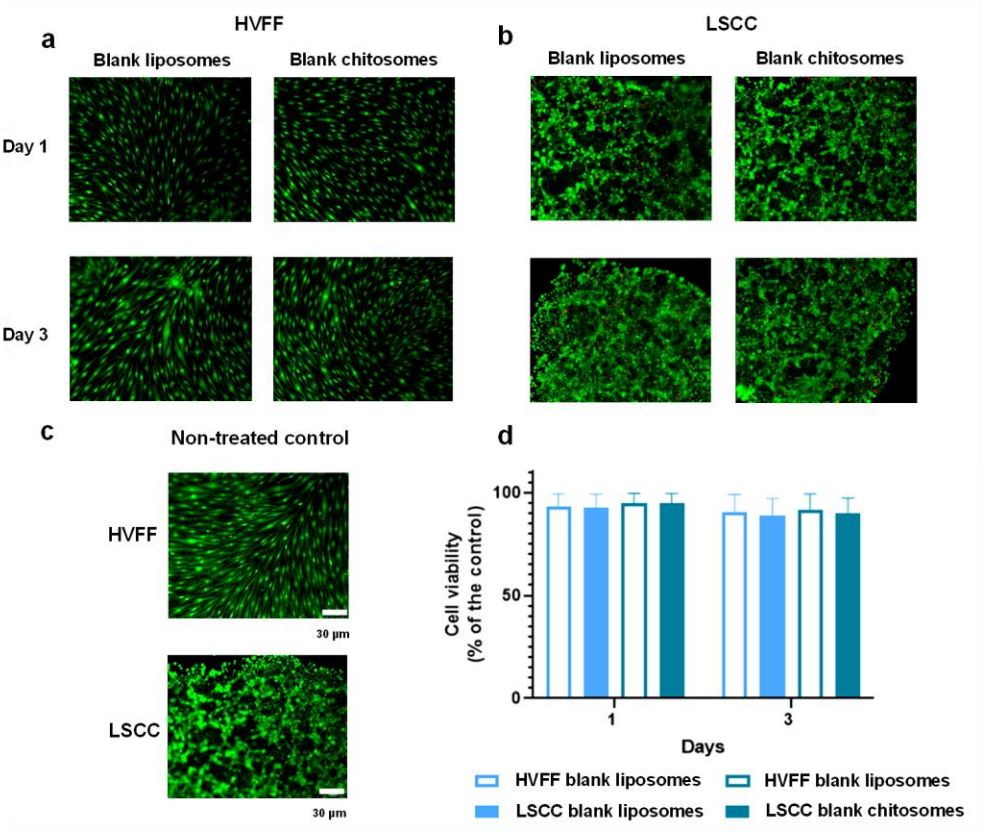

Figure 4-6. Blank liposome and chitosome effects on HVFFs and LSCCs. (a) Blank liposomes, (b) blank chitosomes, and (c) non-treated confluent control (Day 0). (d) MTT assay on the effect of blank liposomes and blank chitosomes on HVFFs and LSCCs. Non-treated HVFFs and LSCCs were set as the reference of 100% cell viability from confluency at Day 0. No significance difference was noticed among groups and culture time. Scale bar = 30µm.

4.2.3.2. Chitosome uptake by LSCCs

The chitosome uptake was observed in LSCCs during the first 4 hours of exposure (**Figure 4-7**), a timeframe very similar to other cell lines such as gastric and endothelial cells [43]. The EGFR staining on LSCCs surface showed an accumulation of nanocarrier within LSCCs, which serve as a spatial reference of the nanocarrier internalization (**Figure 4-7a**). The colocalization of chitosomes with lysosome/endosome was also observed in LSCCs (**Figure 4-7b**), indicating that the nanocarriers in endosomal compartment would disintegrate within its acidic environment. Overall, the cationic coating from chitosan seemed to result in more accumulation of nanocarriers in cancer cells. The electrostatic interaction of cationic nanocarriers with anionic cellular membrane may contribute to the following endocytosis [74]. Also, the ionisable/cationic chitosan

coating on anionic liposomes may provide an acid-dependent permeability for the diffusion of DTX entrapped after liposomal uptake by cells, leading to more effective drug release [38].

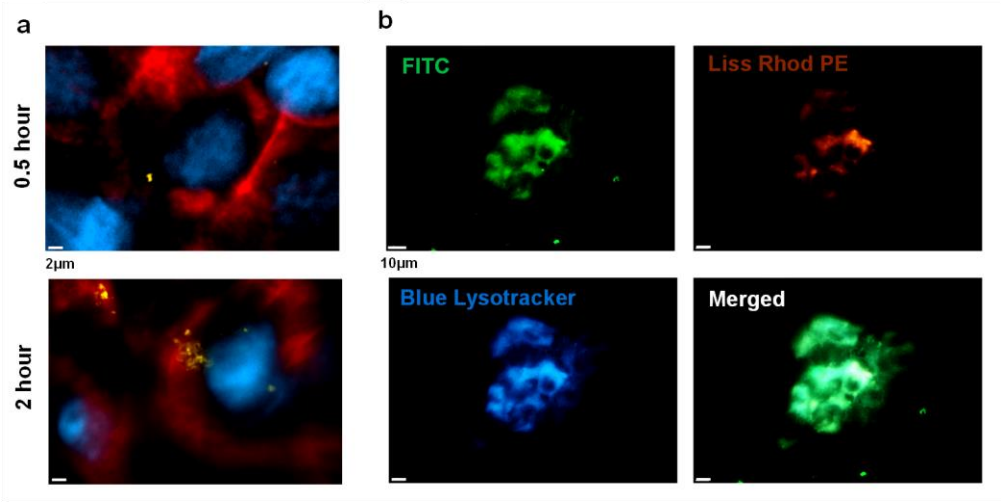

Figure 4-7. Chitosomes uptake by LSCCs. (a) Internalization of chitosomes after 0.5 hours and 2 hours of treatment respectively (bright orange, merged FITC/Liss Rhod PE). Immunofluorescence staining of cell membrane via EGFR (red) and DAPI as counterstaining was performed to visualize internal nanocarrier accumulation. Scale bar = 2μm. (b) Colocalization of chitosomes and endosomes/lysosomes immediately after a 4-hour chitosome exposure. The LSCC colony fluoresce showed the internalization of the FITC-labelled chitosomes via Blue Lysotracker. Scale bar = 10μm.

4.2.3.3. Docetaxel-loaded chitosome effectively reduces the LSCC and HVFF colony formation

From the LIVE/DEAD staining, LSCC and HVFF colony formation was reduced with increasing DTX concentration up to 10 μM after 3-day culture, in comparison to untreated confluent control (**Figure 4-6c**). To further verify DTX alone cytotoxicity on HVFFs and LSCCs, the MTT assay showed a decreasing trend in cell viability with increasing the DTX dose from 100 nM to 10 μM (**Figure 4-8a-c**). Based on IC50 dose-response curve as half maximal inhibitory drug concentration (**Figure 4-8c**), 1 μM (10-6) of DTX dose was sufficient to provide desired therapeutic effect on these cells after 3-day DTX exposure. As such, 1 μM DTX was used on consecutive cytotoxic analyses.

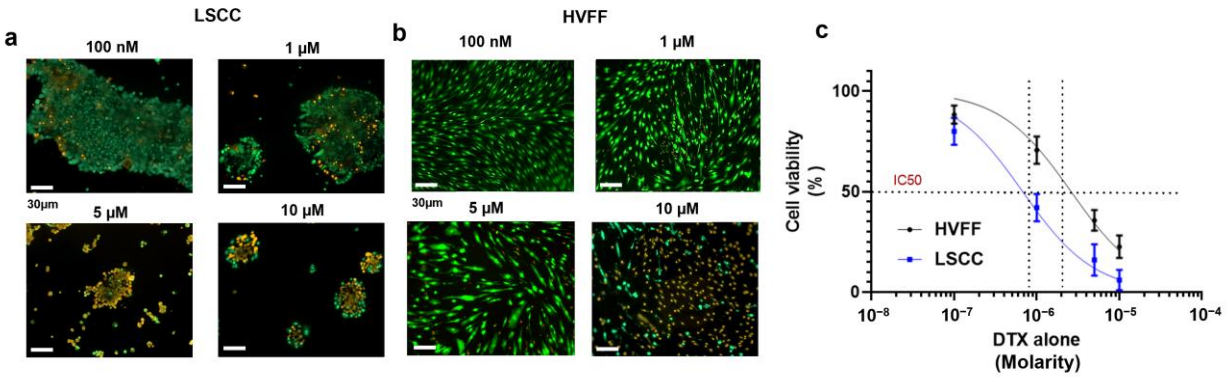

Figure 4-8. Docetaxel dose response of (a) LSCCs and (b) HVFFs. (c) MTT cytotoxicity assay of DTX on HVFFs and LSCCs after 3 days to determine IC50 inhibitor versus normalized response. A decreasing trend in LSCCs and HVFFs viability was noted with increasing molarity dose of DTX. Green = Live cells. Bright orange = Dead cells. Scale bar = 50µm

We further evaluated DTX cytotoxicity on LSCC and HVFFS for seven days. Increased cell death was observed on the LSCCs and HVFFs exposed to both DTX-loaded groups (**Figure 4-9a**) in comparison to non-treated controls (**Figure 4-6c**). Consequently, the quantitative decreasing trend in cell viability was also noted in cell-based MTT and supernatant-based LDH assays among all groups (**Figure 4-9c-d**). After day 3, the LSCC viability of the DTX-loaded chitosome group was below the IC50 threshold (~38% viability), whereas controls of DTX alone and DTX-loaded liposome exhibited ~50% and ~44% cell viability respectively. At day 7, DTX-loaded chitosome group showed significant difference in cancer cell death compared to DTX-loaded liposomes with ~8% increase (*$p<0.05$) and the DTX alone group with ~17% increase (****$p< 0.0001$). However, at day 7, HVFF viability remained above 20% after the exposure of the three treatments.

Cancer cells are known to form colonization especially during metastasis [75]. The biological activity of DTX-loaded chitosomes was further validated via colony formation analysis. Colony observation consisted of macroscopic staining using crystal violet (**Figure 4-10a-c**) and microscopic immunostaining of the cytoskeleton with β-tubulin III (ALEXA488/TUBIII) and counterstaining (DAPI) (**Figure 4-10d-f**). Such reductions support-ed the results described in **Figure 4-9**. Nevertheless, macroscopic crystal violet (**Figure 4-10a-b**) and microscopic immunostaining (**Figure 4-10d-e**) related experiments confirmed that DTX-loaded chitosomes inhibited the LSCC growth and proliferation after the 7-day study. In detail, absorbance at 590nm

measurements showed less clonogenic activity after 7-day treatment of DTX-loaded chitosomes (*p<0.05) compared to controls (**Figure 4-10c**). Nuclei counting also showed a decrease of cell number in LSCC colonies after DTX-loaded chitosome exposure (*p<0.05) compared to controls (**Figure 4-10f**). Further, the morphology of liposomes, i.e., round shape and ~100 nm size, is known to favor cellular intake and drug internalization [17,30–33,76]. To verify liposome's capacity of sustained drug re-lease, cytotoxicity was compared between the groups of DTX-loaded liposomes and DTX-alone over an extended 7 days of experiment. As expected, the DTX-loaded anionic liposome group showed significantly more cell death (i.e., cytotoxicity) (*p<0.05, **Figure 4-10**) over the course of the study, which confirmed the benefit of liposomes in anti-cancer therapeutics.

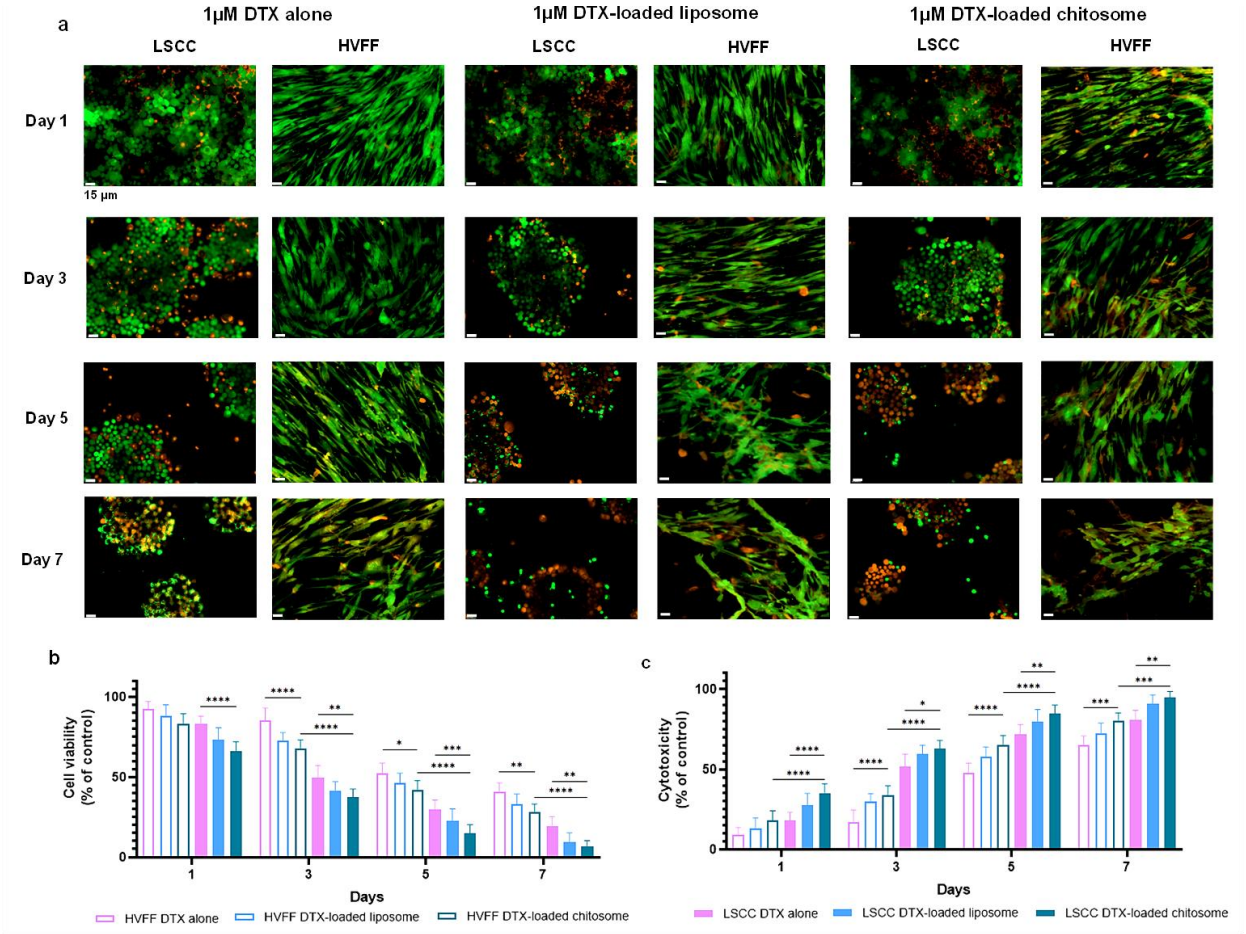

Figure 4-9. DTX-loaded chitosome effects on the viability of LSCCs and HVFFs. (a) Therapeutic exposures on LSCCs and HVFFs up to 7 days via LIVE/DEAD staining. Live cells fluoresce green, whereas dead cells fluoresce bright orange. Scale bar = 15μm. (b) MTT assay (c) LDH assay of the quantitative effect up to 7-day DTX exposure

on LSCCs and HVFFs. Cell viability was noted to reduce in the DTX alone and DTX encapsulated groups after the 7-day study.

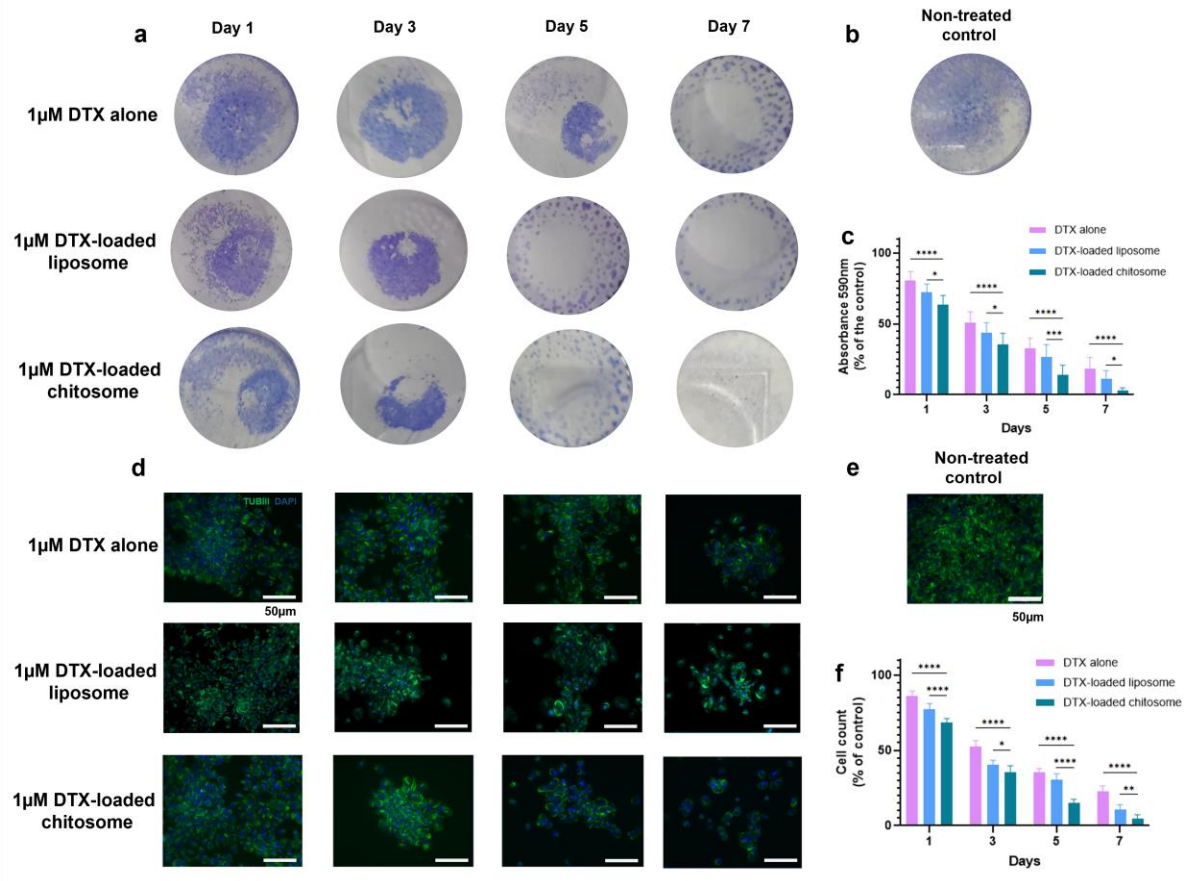

Figure 4-10. DTX-loaded chitosome effects on the colony formation of LSCC. (a), (b) Clonogenic assay via crystal violet staining. (c) Quantitative measurement of the crystal violet for clonogenic assessment at 590 nm absorbance. (d), (e) Colony observation of cytoskeleton via spot detection algorithm on DAPI channel. A decreasing trend in cancer colony size was observed following DTX alone and DTX encapsulated groups up to 7 days.

4.2.3.4. Chitosome did not induce hemolysis of human red blood cells

For intra-arterial locoregional delivery, the nanocarriers will inevitably interact with blood cells in the blood stream. It is thus imperative to assess the chitosome cytotoxicity in blood cells beside tumor and stromal cells. Hemolysis is defined by decomposition of blood cell membrane and hemoglobin release resulting in a red tint of solution. Released hemoglobin after oxidation becomes methemoglobin and then cyanmethemoglobin [65]. After 3h exposure of red blood cells

to DTX concentration of 1 μM in DTX-loaded nanocarrier, the observed hemolysis was less than 5%, indicating non-hemolytic behavior of DTX-loaded chitosome and other liposomal formulations of these nanocarriers (**Figure 4-11**). According to the American Society for Testing and Materials International (ASTM 2013), a value greater than 5%, a compound is considered hemolytic to red blood cells [65]. These result thus, together, prove that our drug delivery system is considered as non-hemolytic and suitable for intra-arterial administration. However, compared to non-coated lipid nanocarriers, chitosan-coated lipid nanocarriers have been reported to provide increased antiangiogenic effect as show in a chick embryo chorioallantoic membrane assay [49]. We anticipate a similar antiangiogenic behavior for our proposed chito-some nanocarriers.

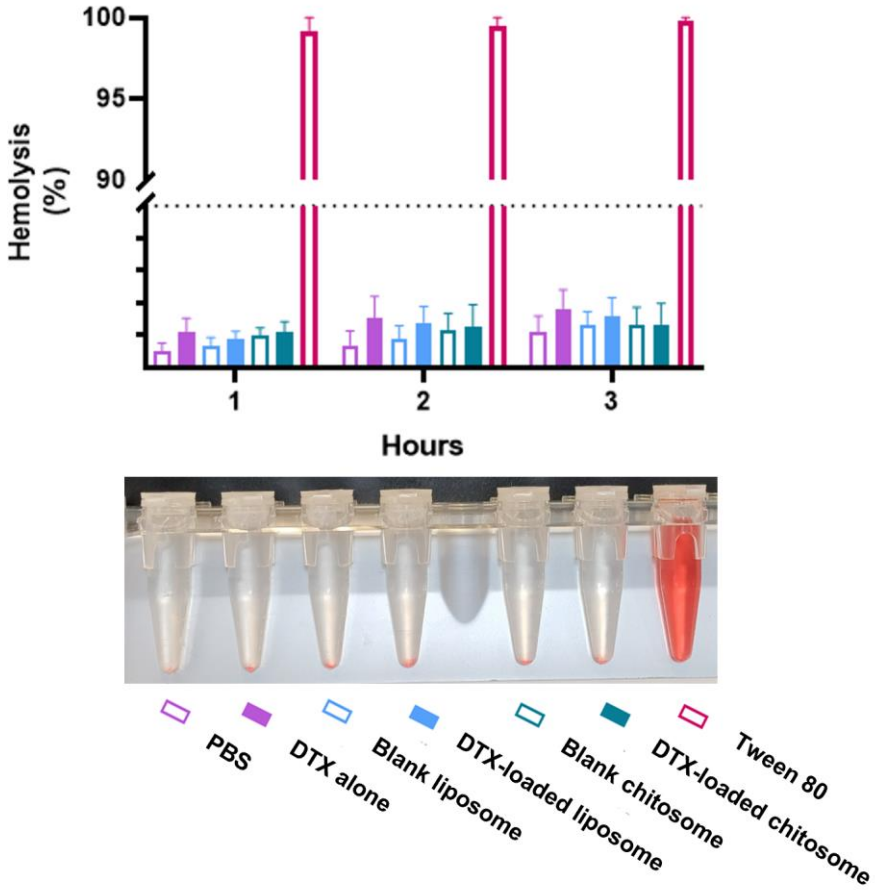

Figure 4-11. Hemolytic Analysis of DTX-loaded chitosomes up to 3h exposure. The hemolytic response was measured by the intensity of the red color in assay tubes. Absorbance of hemolytic effect of DTX-loaded chitosomes. Hemolysis of red blood cells was less than 5% indicating non-hemolytic behavior of either the DTX-loaded or blank liposomal and chitosomal formulations. Percentage over 5% is considered as hemolytic (ASTM 2013) [67].

Chitosan coating on drug-loaded liposomes has shown to increase cytotoxicity in terms of cancer cell death [23,24,38,39,43,47]. This is likely because the chitosan coating improves the mucoadhesive and permeability and retention properties of nanoliposomes. This would explain the increased DTX-loaded chitosomes cytotoxic effect towards LSCCs compared to DTX-loaded liposomes. Alongside the desired in vitro cytotoxicity towards LSCCs without compromising the viability of stromal cells, chitosomes showed no hemolytic effects on LSCCs and HVFFs.

Despite promising in vitro results, further preclinical investigation of the DTX-loaded chitosomes is still needed for the translational pipeline of this drug delivery system. For instance, in vivo experiments for laryngeal cancer may not be fully representative models because subcutaneous injection is used to induce carcinogenesis in flanks [77] or armpits [78] of mice instead of the laryngeal anatomical site, which may cause the subject to suffocate. For this reason, the implementation of advanced in vitro models that closely mimic in vivo conditions such as those found in the head and neck, are required to evaluate the translation potential of chitosomes prior to designing the in vivo experiments [1].

4.3 Materials and Methods

4.3.1. Materials

The Docetaxel (cat. # PHR1883), cholesterol (cat. # C8667), 1,2-distearoyl-sn-glycero-3-phosphocholine (DSPC, cat. # 850365P), 1,2-distearoyl-sn-glycero-3-phosphoethanolamine-N-[methoxy(polyethylene glycol)-2000]-ammonium salt (DSPE-PEG2000, cat. # 880120P), Liss Rhod PE (cat. # 810150P) and mucin from bovine submaxillary gland (cat. # M3895) from bovine submaxillary gland, human laryngeal cancer cell line (LSCC, cat. # UM-SCC-17A), FITC, UV-transparent 96 well plates, T-75 flasks, Dulbecco's modified Eagle's medium (DMEM), Fetal Bovine Serum (FBS), non-essential amino-acid, penicillin/streptomycin, and cyanmethemoglobin/Drabkin’s reagent were purchased from Millipore-Sigma (Burlington, MA, USA). Chitosan (cat. # 150597) with molecular weight of 1526.464 g/mol was purchased from MP Biomedicals. Dialysis membranes of 3.5-5kDa (cat. # 131204T) and 12-14kDa (cat. # 132703T) were purchased from Spectrum Chemical Mfg. Corp. (California, USA). The human vocal fold fibroblast immortalized cell line (HVFF) and 8-chamber culture slides (cat. # 154534 Lab-Tek®II) were obtained from University of Wisconsin-Madison (Madison, WI, USA) and Fisher Scientific (Ontario, Canada) respectively. Human red blood cells (cat. # IWB3ALS40ML)

were purchased from Innovation Research (Novi, MI, USA) and were used for hemolysis studies. LIVE/DEAD staining (cat. # L3224), MTT assay (cat. # V13154), and Blue LysoTracker (cat. # L7525) and cell dissociation reagent TrypLE (cat. # 12604013) were purchased from Thermo Fisher Scientific (Waltham, MA, USA). Crystal violet (cat. # C581-25) was bought from Fisher Scientific. LDH assay (cat. # ab65393), ALEXA647/EGFR (cat. # ab192982), ALEXA488/TUBIII (cat. # ab195879), and DAPI (cat. # ab228549), from Abcam (Cambridge, UK) were used to visualize cell membrane, cytoskeleton, and nucleus respectively. Trypan blue (cat. # 10702404) from Invitrogen (Waltham, MA, USA) was used for cell counting.

4.3.2. Fabrication of liposomes

Liposomal drug encapsulation is influenced by the phase transition temperatures (Tm) of the constituent phospholipids [79]. Phospholipids have specific Tm [71,79]. A Tm over the physiological temperature may be logically preferred for prolonged liposomal stabilization once inside the body. For instance, the 1,2-distearoyl-sn-glycero-3-phosphocholine (DSPC) has a Tm≈55°C [71]. This Tm above the physiological temperature was found to have a greater drug encapsulation efficacy in comparison to Tm lower than 37ºC [79]. In addition, PEG grafting is a common approach in designing liposomal-based drug delivery systems. The reason behind the strategy for using PEGylated lipids such as amphiphilic polymer consisting of hydrophilic 1,2-distearoyl-sn-glycero-3-phosphoethanolamine-N-[methoxy(polyethylene glycol)-2000] (DSPE-PEG2000), that has a Tm≈74°C [71] ensuring longer liposomal stabilization in body [79].

In contrast to previously reported DTX-loaded chitosome synthesis [23,24,38,39,43,47,49,53], our methodology modified a one-step liposome synthesis previously used in our laboratory [28], and DTX-loaded liposomes [72,80]. Briefly, DSPC, DSPE-PEG2000 and cholesterol with a molar ratio of 2/0.18/1 were dissolved in 2 mL of 100% ethanol by gentle stirring. For fluorescence microscopy visualization, 0.1 mg of Liss Rhod PE (orange colour) was added to the liposomal formulation.

For DTX loading, the formulation was heated at 50°C for 5 min. Ethanol injection was performed by pouring the lipid dispersion into a flask with 300 mL of MilliQ-water during 1200 rpm stirring. After 5 min stirring, the formulation was filtered using a coarse paper filter, and the solvent was removed by rotatory evaporation. The mixtures were dialyzed using 12-14 kDa membranes at

room temperature for 30 minutes against the 0.5% Tween 80 (pH 7.4) to remove free DTX from the DTX-loaded liposomes [81]. The liposomal dispersion was then stored at 4°C until use.

4.3.3. Fabrication of chitosomes

Firstly, 1.8 g of chitosan and 3 mL of 0.06 M HCL were added to 300 mL of MilliQ-water (6 mg/mL) [82]. The solution was stirred in a fume hood until the chitosan was completely dissolved. The chitosan solution was then filtered, and the pH was adjusted to 5 using 1 M NaHCO3 to protonate the amine groups in chitosan and obtain a polycationic behavior. The solution was again filtered by two successive filtration processes using 0.45 µm and 0.22 µm filters.

A volume of 0 µL to 170 µL chitosan solution were then added to 1.5 mL of either the DTX-loaded liposomal or blank liposomal dispersion and sonicated in a water-bath for 15 min (**Figure 3-12**). In detail, nine increasing concentrations from 0.4, 0.12, 0.2, 0.28, 0.36, 0.44, 0.52, 0.6, to 0.68 mg/mL of chitosan solution were used. Similar to non-coated liposomes loaded with DTX, the mixtures were dialyzed using 3.5-5 kDa membranes at room temperature for 30 minutes against the 0.5% Tween 80 (pH 7.4) to separate free chitosan from the liposomes. To obtain the fluorescent version of the chitosomes, Liss Rhod PE-liposomes and FITC-tagged chitosan (green colour) was used for coating on liposome. The chitosome formulation was then stored at 4ºC until use, or at 37°C for stability studies.

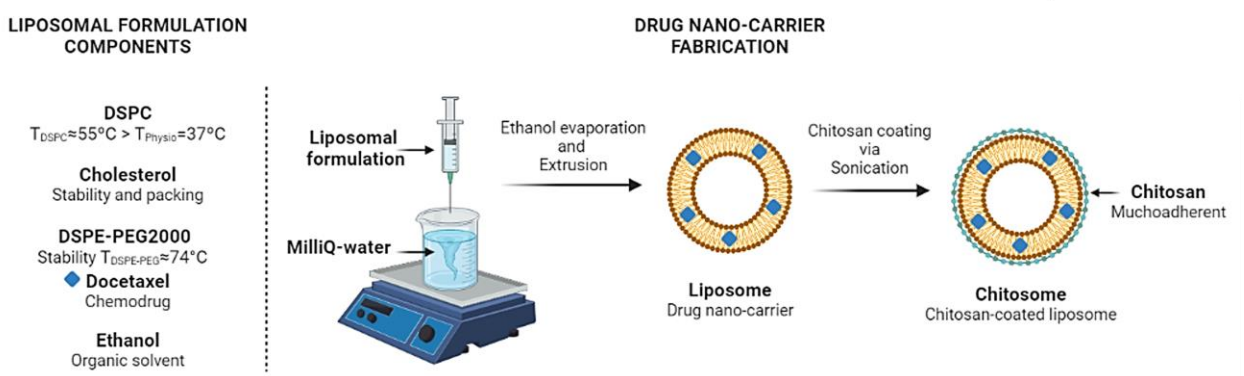

Figure 4-12. Schematic representation of DTX-loaded liposome and chitosome fabrication. Figure created with BioRender.com.

4.3.4. Size and Zeta potential analyses of chitosomes

10 µL of liposomal dispersion were placed in a 1.5 mL eppendorf tube containing 1 mL of MilliQ-water (pH = 7). After vortexing for 30 s, 1 mL of the dispersion (1:5000) was analysed by Nanoparticle Tracking Analysis (NTA, Nanosight NS300, UK) using a 640 nm laser, at T=25°C. Polydispersity index (PDI) was calculated by equation 1.

$$\mathrm{PDI} = \left(\frac{\text{standard deviation}}{\text{mean size}}\right)^2 \quad (1)$$

For Zeta potential measurements, 1.5 mL of the chitosome formulation (1:10) in distilled water was analyzed using a ZetaPALS zeta potential analyzer (Brookhaven Instruments Corp., USA). Stability of chitosome formulation was assessed at 37°C and 5% CO2 atmosphere for freshly prepared chitosomes and after 5 weeks of storage.

3.3.5. Transmission electron microscopy of chitosomes

The morphology of DTX-loaded chitosomes was examined by transmission electron microscope (TEM). 10 µL of DTX-loaded chitosome and liposome samples was placed on a carbon-coated copper grid. The negatively staining was performed on the formed thin film of samples on the grid by adding 2% filtered uranyl acetate (w/v) (pH 7.00). TEM images of samples were acquired using the Tecnai G2 F20 TEM (Hillsboro, USA) at a voltage of 120 kV.

4.3.6. FTIR characterization of chitosomes

FTIR spectra was acquired in transmission mode using a Spectrum II (PerkinElmer Inc, USA) spectrophotometer equipped with an Attenuated Total Reflection module, single bounce diamond crystal, and Spectrum software. Standard FTIR settings such as room-temperature, LiTaO3 (lithium tantalate) MIR detector, unique humidity shield design (OpticsGuardTM) system, Pearl Liquid Analyser – liquid transmission accessory, and ZnSe 200 µm windows were used for acquiring the spectra. The spectral resolution was at 4 cm−1 within a 4000–600 cm−1 range with background clearance. A total 128 scans were averaged for each testing sample. Baseline correction and atmospheric compensation was applied to all spectra.

4.3.7. Mucoadhesive behavior of chitosomes

Mucin-1 from bovine submaxillary gland was used to assess the mucoadhesive behavior of chitosomes compared to control blank liposomes. The mucin powder was suspended and stirred in 100 mM acetate buffer at a 0.5 mg/mL concentration, pH 4.4 overnight [64,65]. The mucin suspension was then centrifuged at 13,500 rpm for 20 min at 4°C. The supernatant was filtered through a 0.22 µm filter. A 1.5 mL aliquot of the mucin suspension was placed in a centrifuge tube, and then chitosomes and liposomes (1:10) were added into each corresponding individual tube and vortexed. The suspensions were then incubated for 1, 2, and 3 hours at 37°C. The turbidity of the suspension was measured using the Spectramax i3 plate reader (Molecular Devices, San Jose, CA, USA) at 500 nm along with recording the zeta potential for changes in surface charge after another water washing, centrifugation, and filtration steps.

4.3.8. Drug entrapment efficiency and release of chitosomes

The absorbance of DTX was first calibrated for different DTX concentrations using the Spectramax i3 plate reader at λ = 230 nm. To quantify the DTX entrapment efficiency, the nanocarriers supernatant containing unloaded drug was collected and diluted at various concentrations in 1×PBS and centrifuged at 2000 RCF for 5min to remove aggregates [28]. Samples were placed in UV-transparent 96 well plates and the absorbance of DTX at λ = 230 nm was recorded using the above-mentioned plate reader. The entrapment efficiency (EE) was then calculated according to the following equation (2).

$$\mathrm{EE}(\%) = \frac{\text{concentration of DTX detected in release medium (µg/mL)}}{\text{concentration of DTX added initially into chitosomes (µg/mL)}} \times 100 \quad (2)$$

For DTX release kinetic analysis, 2 mL of liposomal suspensions and 1 mg DTX solution were dialyzed using 12-14kDa membranes and poured into 400 mL of release medium containing 0.5% Tween 80 (pH 7.4) at 37°C [44]. The release profile of DTX was assessed after 0.5, 1, 2, 4, and 12 hours as well as after 1, 1.5, 3, 7, 14, and 28 days at 37°C. Cumulative release of DTX from chitosomes was then calculated as the percentage of DTX released at each time point compared to the amount encapsulated initially.

4.3.9. HVFFs and LSCCs culture protocol

Two cell lines were used for this study: (i) A non-chemoresistant human laryngeal cancer cell line (LSCC) isolated from primary laryngeal carcinoma located at the supraglottis in T2 or T3 stage assumable [83,84] of a 48-year-old female patient who did not benefit from radiotherapy; and (ii) a human vocal fold fibroblast (HVFF) immortalized cell line [85] (between passages 3 and 5) representing stromal cells in the laryngeal tumor. Both cell lines were grown in LSCC complete media consisting of high glucose DMEM, 10% FBS, 1% non-essential amino-acids and 1% penicillin/streptomycin in a humidified atmosphere of 5% CO2 at 37°C. After reaching 70-80% confluency in T-75 flasks at passage 3 to 5, cells were cultured in fresh Free-FBS media for 1 day to synchronize cell cycle, and were then harvested using TrypLE for 5 min. After adding LSCC media, cells were counted by a hemocytometer before being centrifuged at 900 rpm for 5 min. Media was discarded and cells were resuspended in fresh LSCC media with a working concentration of 1 × 106 cells/mL.

4.3.10. HVFFs and LSCCs viability analyses of liposomes and chitosomes

HVFFs and LSCCs viability assay was performed with approximately 1 × 104 cells seeded separately on 8-chamber slides. After reaching 100% confluency at Day 0 [86], non-drug loaded chitosomal and control liposomal dispersions were added to the culture media at a concentration (1/1000) [87]. At 1 and 3-day time points, cells were washed with 1x PBS before being stained, using a LIVE/DEAD viability/cytotoxicity assay kit following the manufacturer's instructions. The slides were incubated for 30 min in darkness at room temperature before being washed twice with 1x PBS. An inverted fluorescence microscope (Axiovert3, Zeiss, Germany) with a 10× objective was used to acquire cell images stained with FITC (LIVE, green) and Cy3 (DEAD, red/orange). Cells were considered as dead if LIVE/DEAD staining signals overlapped [22].

MTT analysis was also carried out to obtain quantitative data on cell viability. For this assay, about 5 × 103 cells were seeded in individual 96 well plates. A Spectramax i3 plate reader was used to determine the absorbance of MTT at $\lambda = 570$ nm. Percentage of cell viability was calculated using equation (3).

$$\text{Cell viability}(\%) = \frac{\text{Non-treated control} - \text{treated cells}}{\text{Non-treated control}} \times 100 \qquad (3)$$

4.3.11. Chitosome uptake by LSCCs

FITC-labelled chitosan was used to coat the Liss Rhod PE-liposomes as described in section 2.3. Approximately 1 × 104 LSCCs were seeded on 8-chamber slides and incubated with docetaxel-loaded FITC-labelled chitosomes and non-coated liposomal formulation (control) up to 4 h [88] with concentration (1/1000) [87]. The LSCCs chitosomal uptake was analyzed after 0.5- and 2-hours incubation via immunostaining following 4-hour inspection via cell tracker staining. ALEXA647/EGFR for cell membrane staining and DAPI as counterstaining along with Blue LysoTracker for lysosome staining were used to track the internalization of chitosomes lysosomes/endosomes. The immunostaining procedure was performed following the manufacturer's guidelines. The cells were then imaged with 40x and 63x magnification using the Zeiss Axiover3 (Zeiss, Germany) and retrieved using Imaris version 9.5.1 Software (Bitplane, South Windsor, CT).

4.3.12. DTX-loaded chitosome effect on LSCCs

To determine the therapeutic effect of DTX on LSCCs, first toxic effect of 100 nM, 500 nM, 1 µM and 10 µM DTX alone was assessed on HVFFs and LSCCs after 3 days via LIVE/DEAD staining, MTT analysis, and LDH assay. LSCCs were then exposed to DTX-loaded chitosomes up to 7 days. Approximately 1 × 104 cells were seeded on 8-chamber slides. After reaching 100% cell confluency, 1 µM DTX-loaded liposomal or chitosomal dispersions were added to the culture media at a 1/1000 dilution [87] in each of the slide's chambers. 1 µM DTX addition alone to cells was used as control. DTX formulation cytotoxicity was then investigated at day 1, 3, 5, and 7 by LIVE/DEAD assay. Furthermore, MTT assay was carried out as described in section 3.10 to obtain quantitative cell cytotoxicity data for each formulation treatment. In addition, LDH assay was performed to further corroborate the MTT results by analyzing the supernatant following manufacturer's guidelines. MTT and LDH percentages of cell viability were calculated using equation (3).

To investigate the colony formation after exposure of DTX alone, DTX-loaded liposomes, and DTX-loaded chitosomes, LSCCs were seeded in 24 well-plates at a density of 15 × 103 and incubated until full confluency up to 7 days. After treatments, the culture medium was removed, and the cells were washed twice with PBS. Then, cells were stained with 0.1% crystal violet (water 30%, ethanol 70%, crystal violet 0.1%) in sterile water (0.5 mL/well) for 30 min at room

temperature. After thorough washing, the colonies were analyzed via absorbance at 590 nm [89] with Spectramax i3 plate reader. Hampering of colony formation was analyzed via immunostaining of the cytoskeleton and nucleus using Axiovert3 microscope with a 20× objective and Cy3, ALEXA488, DAPI filters. Images were acquired using Imaris 9.5.1 Software, and cell nuclei (10 μm) were counted at the entire images with the spot detection algorithm via DAPI mean fluorescence intensity [90].

4.3.13. Hemolytic effect of chitosomes

The nanocarrier formulations at predetermined concentrations with and without DTX were added to the diluted (100x) red blood cells in PBS for a final volume of 12 mL. Tween 80 was used as a positive control. The samples were mildly shaken for 1, 2, and 3h at 37°C and centrifuged at 800 g for 15 min. Hemolysis was evaluated by mixing 100 μL of each supernatant with 100 μL of cyanmethemoglobin/Drabkin′s reagent into a 96-well plate and reading the absorbance at 540 nm using the Spectramax i3 plate reader. The percentage of hemolysis was calculated using equation (5).

$$\text{Hemolysis}(\%) = \frac{\text{absorbance sample} - \text{absorbance negative control}}{\text{absorbance positive control} - \text{absorbance negative control}} \times 100 \qquad (5)$$

4.3.14. Statistical analysis

Data are reported as mean ± SE or SD of at least three experiments. The statistical significance of the differences was analyzed by Two-way ANOVA and Tukey post-hoc tests using GraphPad Prism version 9.5.1 for Windows (GraphPad Software, San Diego, CA, USA).

4.4 Conclusion

In this study, we fabricated DTX-loaded chitosomes with optimal physical properties for enhanced permeability retention features. The DTX-loaded chitosomes are consisted of anionic nanoliposomes and a cationic chitosan coating to provide the nanoliposomes with mucoadhesive and increased drug retention properties. The overall in vitro results suggest that chitosomes loaded with docetaxel are a promising delivery system for laryngeal cancer via intra-arterial administration. DTX-loaded chitosomes showed indeed im-proved anti-cancer effects on a laryngeal cancer cell line with no signs of hemolysis. Further advanced in vitro studies are required

to better understand the fate and bioactivity as well as the targetability of DTX-loaded chitosomes in the laryngeal cancer tumor micro-environment.

Supplementary Materials: Not applicable

Author Contributions: CM-G: Conceptualization, visualization, writing-original draft, reviewing and editing. NL-J: Conceptualization, visualization, writing-original draft, reviewing and editing, supervision, funding acquisition, and project administration. MT: Conceptualization, visualization, writing-original draft, reviewing and editing, supervision, funding acquisition, and project administration. All authors have read and agreed to the published version of the manuscript.

Funding: This study was supported by the National Sciences and Engineering Research Council of Canada (RGPIN-2018–03843 and ALLRP 548623-19), Canada Research Chair research stipend (M.T., N.L.-J.) and the National Institutes of Health (R01 DC-018577-01A1). The presented content is solely the responsibility of the authors and does not necessarily represent the official views of the above funding agencies.

Institutional Review Board Statement: Not applicable.

Informed Consent Statement: Not applicable.

Data Availability Statement: Not applicable.

Acknowledgments: We thank our colleagues from both Voice and Upper Airway Research laboratory and Biomat'X research laboratory for their support and advice. We thank the contribution of Radu A. Paun for his help with the liposomal formulation and imaging the liposomes using transmission electron microscopy. We would also like to thank the McGill Facilities for Electron Microscopy Research (FEMR), Advanced BioImaging Facility (ABIF) and Chemistry Characterization Facility.

Conflicts of Interest: The authors declare no conflict of interest.

4.5 References

1. Moya-Garcia, C.R.; Okuyama, H.; Sadeghi, N.; Li, J.; Tabrizian, M.; Li-Jessen, N.Y.K. In vitro models for head and neck cancer: Current status and future perspective. Front. Oncol. 2022, 12, 3691.

2. Leemans, C.R.; Braakhuis, B.J.M.; Brakenhoff, R.H. The molecular biology of head and neck cancer. Nat. Rev. Cancer 2011, 11, 9–22.

3. Ferrari, D.; Ghi, M.G.; Franzese, C.; Codecà, C.; Gau, M.; Fayette, J. The Slippery Role of Induction Chemotherapy in Head and Neck Cancer: Myth and Reality. Front. Oncol. 2020, 10, 7.

4. Cramer, J.D.; Burtness, B.; Le, Q.T.; Ferris, R.L. The changing therapeutic landscape of head and neck cancer. Nat. Rev. Clin. Oncol. 2019, 16, 669–683.

5. Bose, P.; Brockton, N.T.; Dort, J.C. Head and neck cancer: From anatomy to biology. Int. J. Cancer 2013, 133, 2013–2023.

6. Vermorken, J.B.; Remenar, E.; Van Herpen, C.; Gorlia, T.; Mesia, R.; Degardin, M.; Stewart, J.S.; Jelic, S.; Betka, J.; Preiss, J.H.; et al. Cisplatin, fluorouracil, and docetaxel in unresectable head and neck cancer. N. Engl. J. Med. 2007, 357, 1695–1704.

7. Fabregas, J.C.; Loaiza-Bonilla, A.; Talebi, T.N.; Warsch, S.; Fernandez, G.; Raez, L.E.; Santos, E.S. Concurrent chemoradiotherapy versus induction chemotherapy followed by chemoradiotherapy (sequential approach) in the management of head and neck cancer. Expert Rev. Anticancer Ther. 2013, 13, 1065–1072.

8. Maloney, S.M.; Hoover, C.A.; Morejon-Lasso, L.V.; Prosperi, J.R. Mechanisms of taxane resistance. Cancers 2020, 12, 3323.

9. Bredell, M.G.; Ernst, J.; El-Kochairi, I.; Dahlem, Y.; Ikenberg, K.; Schumann, D.M. Current relevance of hypoxia in head and neck cancer. Oncotarget 2016, 7, 50781–50804.

10. Doktorova, H.; Hrabeta, J.; Khalil, M.A.; Eckschlager, T. Hypoxia-induced chemoresistance in cancer cells: The role of not only HIF-1. Biomed Pap. 2015, 159, 166–177.

11. Sadeghi, N.; Khalife, S.; Mascarella, M.A.; Ramanakumar, A.V.; Richardson, K.; Joshi, A.S.; Bouganim, N.; Taheri, R.; Fuson, A.; Siegel, R. Pathologic response to neoadjuvant chemotherapy in HPV-associated oropharynx cancer. Head Neck 2020, 42, 417–425.

12. Olusanya, T.O.B.; Ahmad, R.R.H.; Ibegbu, D.M.; Smith, J.R.; Elkordy, A.A. Liposomal drug delivery systems and anticancer drugs. Molecules 2018, 23, 907.

13. Li, R.; Ye, L.; Zhu, Y.; Ding, H.; Wang, S.; Ying, H.; Wu, C.; Zhou, L.; Wang, X.; Tian, S. Induction chemotherapy of modified docetaxel, cisplatin, 5-fluorouracil for laryngeal preservation in locally advanced hypopharyngeal squamous cell carcinoma. Head Neck 2022, 44, 2018–2029.

14. Aigner, K.R.; Selak, E.; Aigner, K. Short-term intra-arterial infusion chemotherapy for head and neck cancer patients maintaining quality of life. J. Cancer Res. Clin. Oncol. 2019, 145, 261–268.

15. Kuan, C.H.; Chung, M.J.; Hong, R.L.; Tseng, T.Y.; Tai, H.C.; Cheng, N.C.; Hsieh, J.H.; Horng, S.Y.; Lai, H.S. The impacts of intra-arterial chemotherapy on head and neck microvascular reconstruction. J. Formos. Med. Assoc. 2020, 119, 1524–1531.

16. Heianna, J.; Makino, W.; Hirakawa, H.; Agena, S.; Tomita, H.; Ariga, T.; Ishikawa, K.; Takehara, S.; Maemoto, H.; Murayama, S. Therapeutic efficacy of selective intra-arterial chemoradiotherapy with docetaxel and nedaplatin for fixed bulky nodal disease in head and neck cancer of unknown primary. Eur. Arch. Oto-Rhino-Laryngol. 2022, 279, 3105–3113.

17. de Lázaro, I.; Mooney, D.J. Obstacles and opportunities in a forward vision for cancer nanomedicine. Nat. Mater. 2021, 20, 1469–1479.

18. Bao, W.; Tian, F.; Lyu, C.; Liu, B.; Li, B.; Zhang, L.; Liu, X.; Li, F.; Li, D.; Gao, X.; et al. Experimental and theoretical explorations of nanocarriers' multistep delivery performance for rational design and anticancer prediction. Sci. Adv. 2021, 7, eaba2458.

19. Wu, Q.; Qu, M.; Kim, H.J.; Zhou, X.; Jiang, X.; Chen, Y.; Zhu, J.; Ren, L.; Wolter, T.; Kang, H.; et al. A Shear-Thinning Biomaterial-Mediated Immune Checkpoint Blockade. ACS Appl. Mater. Interfaces 2022, 14, 35309–35318.

20. Coburn, P.T.; Li, X.; Li, J.; Kishimoto, Y.; Li-Jessen, N.Y.K. Progress in Vocal Fold Regenerative Biomaterials: An Immunological Perspective. Adv. NanoBiomed Res. 2022, 2, 2100119.

21. Li-Jessen, N.Y.K.; Ridgway, C. Neurologic and Neurodegenerative Diseases ofthe Larynx; Springer: Berlin/Heidelberg, Germany, 2020; pp. 21–40.

22. Coburn, P.T.; Herbay, A.C.; Berrini, M.; Li-Jessen, N.Y.K. An in vitro assessment of the response of THP-1 macrophages to varying stiffness of a glycol-chitosan hydrogel for vocal fold tissue engineering applications. J. Biomed. Mater. Res.-Part A 2021, 109, 1337–1352.

23. Shukla, S.K.; Chan, A.; Parvathaneni, V.; Gupta, V. Metformin-loaded chitosomes for treatment of malignant pleural mesothelioma—A rare thoracic cancer. Int. J. Biol. Macromol. 2020, 160, 128–141.

24. Alomrani, A.; Badran, M.; Harisa, G.I.; ALshehry, M.; Alhariri, M.; Alshamsan, A.; Alkholief, M. The use of chitosan-coated flexible liposomes as a remarkable carrier to enhance the antitumor efficacy of 5-fluorouracil against colorectal cancer. Saudi. Pharm. J. 2019, 27, 603–611.

25. Liu, P.; Chen, G.; Zhang, J. A Review of Liposomes as a Drug Delivery System: Current Status of Approved Products, Regulatory Environments, and Future Perspectives. Molecules 2022, 27, 1372.

26. Bozzuto, G.; Molinari, A. Liposomes as nanomedical devices. Int. J. Nanomed. 2015, 10, 975–999.

27. Pereira, S.; Egbu, R.; Jannati, G.; Al-Jamal, W.T. Docetaxel-loaded liposomes: The effect of lipid composition and purification on drug encapsulation and in vitro toxicity. Int. J. Pharm. 2016, 514, 150–159.

28. Paun, R.A.; Dumut, D.C.; Centorame, A.; Thuraisingam, T.; Hajduch, M.; Mistrik, M.; Dzubak, P.; De Sanctis, J.B.; Radzioch, D.; Tabrizian, M. One-Step Synthesis of Nanoliposomal Copper Diethyldithiocarbamate and Its Assessment for Cancer Therapy. Pharmaceutics 2022, 14, 640.

29. Antimisiaris, S.G.; Marazioti, A.; Kannavou, M.; Natsaridis, E.; Gkartziou, F.; Kogkos, G.; Mourtas, S. Overcoming barriers by local drug delivery with liposomes. Adv. Drug Deliv. Rev. 2021, 174, 53–86.

30. Shinde, V.R.; Revi, N.; Murugappan, S.; Singh, S.P.; Rengan, A.K. Enhanced permeability and retention effect: A key facilitator for solid tumor targeting by nanoparticles. Photodiagnosis Photodyn. Ther. 2022, 39, 102915.

31. Kalyane, D.; Raval, N.; Maheshwari, R.; Tambe, V.; Kalia, K.; Tekade, R.K. Employment of enhanced permeability and retention effect (EPR): Nanoparticle-based precision tools for targeting of therapeutic and diagnostic agent in cancer. Mater. Sci. Eng. C 2019, 98, 1252–1276

32. Moradi Kashkooli, F.; Soltani, M.; Momeni, M.M.; Rahmim, A. Enhanced Drug Delivery to Solid Tumors via Drug-Loaded Nanocarriers: An Image-Based Computational Framework. Front. Oncol. 2021, 11, 655781.

33. Attia, M.F.; Anton, N.; Wallyn, J.; Omran, Z.; Vandamme, T.F. An overview of active and passive targeting strategies to improve the nanocarriers efficiency to tumour sites. J. Pharm. Pharmacol. 2019, 71, 1185–1198.

34. Blanco, E.; Shen, H.; Ferrari, M. Principles of nanoparticle design for overcoming biological barriers to drug delivery. Nat. Biotechnol. 2015, 33, 941–951.

35. Stevanovi´c, M. Biomedical Applications of Nanostructured Polymeric Materials. In Nanostructured Polymer Composites for Biomedical Applications; Elsevier: Amsterdam, The Netherlands, 2019; pp. 1–19.

36. Chauhan, V.P.; Stylianopoulos, T.; Martin, J.D.; Popovi´c, Z.; Chen, O.; Kamoun, W.S.; Bawendi, M.G.; Fukumura, D.; Jain, R.K. Normalization of tumour blood vessels improves the delivery of nanomedicines in a size-dependent manner. Nat. Nanotechnol. 2012, 7, 383–388.

37. Gabizon, A.A.; Shmeeda, H.; Zalipsky, S. Pros and cons of the liposome platform in cancer drug targeting. J. Liposome Res. 2006, 16, 175–183.

38. Sun, X.; Xu, H.; Huang, T.; Zhang, C.; Wu, J.; Luo, S. Simultaneous delivery of anti-miRNA and docetaxel with supramolecular self-assembled “chitosome” for improving chemosensitivity of triple negative breast cancer cells. Drug Deliv. Transl. Res. 2020, 11, 192–204.

39. Megahed, M.A.; El-sawy, H.S.; Reda, A.M.; Abd-Allah, F.I.; Abu, S.K.; Lila, A.E.; Ismael, H.R.; El-Say, K.M. Effect of nanovesicular surface-functionalization via chitosan and / or PEGylation on cytotoxicity of tamoxifen in induced-breast cancer model. Life Sci. 2022, 307, 120908.

40. Dawoud, M. Chitosan coated solid lipid nanoparticles as promising carriers for docetaxel. J. Drug Deliv. Sci. Technol. 2021, 62, 102409.

41. Lai, W.F.; Wong, W.T.; Rogach, A.L. Molecular design of layer-by-layer functionalized liposomes for oral drug delivery. ACS Appl. Mater. Interfaces 2020, 12, 43341–43351.

42. AlQahtani, S.A.; Harisa, G.I.; Alomrani, A.H.; Alanazi, F.K.; Badran, M.M. Improved pharmacokinetic and biodistribution of 5-fluorouracil loaded biomimetic nanoerythrocytes decorated nanocarriers for liver cancer treatment. Colloids Surf. B Biointerfaces 2021, 197, 111380.

43. Zhang, E.; Xing, R.; Liu, S.; Li, K.; Qin, Y.; Yu, H.; Li, P. Vascular targeted chitosan-derived nanoparticles as docetaxel carriers for gastric cancer therapy. Int. J. Biol. Macromol. 2019, 126, 662–672.

44. Singh, I.; Swami, R.; Jeengar, M.K.; Khan, W.; Sistla, R. p-Aminophenyl-α-d-mannopyranoside engineered lipidic nanoparticles for effective delivery of docetaxel to brain. Chem. Phys. Lipids 2015, 188, 1–9.

45. Pandey, M.; Choudhury, H.; Ying, J.N.S.; Ling, J.F.S.; Ting, J.; Ting, J.S.S.; Hwen, I.K.Z.; Suen, H.W.; Kamar, H.S.S.; Gorain, B.; et al. Mucoadhesive Nanocarriers as a Promising Strategy to Enhance Intracellular Delivery against Oral Cavity Carcinoma. Pharma- ceutics 2022, 14, 795.

46. Collado-González, M.; Espinosa, Y.G.; Goycoolea, F.M. Interaction between Chitosan and Mucin: Fundamentals and applications. Biomimetics 2019, 4, 32.

47. Alshraim, M.O.; Sangi, S.; Harisa, G.I.; Alomrani, A.H.; Yusuf, O.; Badran, M.M. Chitosan-coated flexible liposomes magnify the anticancer activity and bioavailability of docetaxel: Impact on composition. Molecules 2019, 24, 250.

48. Guo, X.; Zhang, J.; Cai, Q.; Fan, S.; Xu, Q.; Zang, J.; Yang, H.; Yu, W.; Li, Z.; Zhang, Z. Acetic acid transporter-mediated, oral, multifunctional polymer liposomes for oral delivery of docetaxel. Colloids Surf. B Biointerfaces 2021, 198, 111499.

49. Zafar, S.; Akhter, S.; Ahmad, I.; Hafeez, Z.; Rizvi, M.M.A.; Jain, G.K.; Ahmad, F.J. Improved chemotherapeutic efficacy against resistant human breast cancer cells with co-delivery of Docetaxel and Thymoquinone by Chitosan grafted lipid nanocapsules: Formulation optimization, in vitro and in vivo studies. Colloids Surf. B Biointerfaces 2020, 186, 110603.

50. Shah, S.; Dhawan, V.; Holm, R.; Nagarsenker, M.S.; Perrie, Y. Liposomes: Advancements and innovation in the manufacturing process. Adv. Drug Deliv. Rev. 2020, 154–155, 102–122.

51. Bruinsmann, F.A.; Pigana, S.; Aguirre, T.; Souto, G.D.; Pereira, G.G.; Bianchera, A.; Fasiolo, L.T.; Colombo, G.; Marques, M.; Pohlmann, A.R.; et al. Chitosan-coated nanoparticles: Effect of chitosan molecular weight on nasal transmucosal delivery. Pharmaceutics 2019, 11, 86.

52. Gonçalves, C.; Ferreira, N.; Lourenço, L. Production of low molecular weight chitosan and chitooligosaccharides (COS): A review. Polymers 2021, 13, 2466.

53. Ahmed, N.; Sohail, M.F.; Khurshid, Z.; Ammar, A.; Saeed, A.M.; Shazia, F.; Gul, S.; Zia, M. Synthesis, Characterization, and In Vivo Distribution of 99mTc Radiolabelled Docetaxel Loaded Folic Acid-Thiolated Chitosan Enveloped Liposomes. Bionanoscience 2023, 13, 134–144.

54. Lunardi, C.N.; Gomes, A.J.; Rocha, F.S.; De Tommaso, J.; Patience, G.S. Experimental methods in chemical engineering: Zeta potential. Can. J. Chem. Eng. 2021, 99, 627–639.

55. Assadpour, S.; Shiran, M.R.; Akhtari, J. Chitosan coating of anionic liposomes containing sumatriptan succinate: A candidate for nasal administration. Nanomed. J. 2021, 8, 132–139.

56. Shnoudeh, A.J.; Hamad, I.; Abdo, R.W.; Qadumii, L.; Jaber, A.Y.; Surchi, H.S.; Alkelany, S.Z. Synthesis, Characterization, and Applications of Metal Nanoparticles. In Biomaterials and Bionanotechnology; Elsevier Inc.: Amsterdam, The Netherlands, 2019; pp. 527–612.

57. Nakhaei, P.; Margiana, R.; Bokov, D.O.; Abdelbasset, W.K.; Jadidi Kouhbanani, M.A.; Varma, R.S.; Marofi, F.; Jarahian, M.; Beheshtkhoo, N. Liposomes: Structure, Biomedical Applications, and Stability Parameters With Emphasis on Cholesterol. Front. Bioeng. Biotechnol. 2021, 9, 748.

58. Mizrahy, S.; Peer, D. Polysaccharides as building blocks for nanotherapeutics. Chem. Soc. Rev. 2012, 41, 2623–2640. [CrossRef] 59. Rumengan, I.F.M.; Suryanto, E.; Modaso, R.; Wullur, S.; Tallei, T.E.; Limbong, D. Structural Characteristics of Chitin and Chitosan Isolated from the Biomass of Cultivated Rotifer, Brachionus rotundiformis. Int. J. Fish. Aquat. Sci. 2014, 3, 12–18.

60. Alinaghi, A.; Rouini, M.R.; Johari Daha, F.; Moghimi, H.R. The influence of lipid composition and surface charge on biodistribution of intact liposomes releasing from hydrogel-embedded vesicles. Int. J. Pharm. 2014, 459, 30–39.

61. Yang, M.; Ding, Y.; Zhang, L.; Qian, X.; Jiang, X.; Liu, B. Novel thermosensitive polymeric micelles for docetaxel delivery. J. Biomed. Mater. Res. Part A 2007, 81, 847–857.

62. Kulhari, H.; Pooja, D.; Shrivastava, S.; Naidu, V.G.M.; Sistla, R. Peptide conjugated polymeric nanoparticles as a carrier for targeted delivery of docetaxel. Colloids Surf. B Biointerfaces 2014, 117, 166–173.

63. Altman, K.W.; Kinoshita, Y.; Tan, M.; Burstein, D.; Radosevich, J.A. Western blot confirmation of the H+/K+-ATPase proton pump in the human larynx and submandibular gland. Otolaryngol.-Head Neck Surg. 2011, 145, 783–788.

64. Yamazoe, E.; Fang, J.Y.; Tahara, K. Oral mucus-penetrating PEGylated liposomes to improve drug absorption: Differences in the interaction mechanisms of a mucoadhesive liposome. Int. J. Pharm. 2021, 593, 120148.

65. Chatzitaki, A.T.; Jesus, S.; Karavasili, C.; Andreadis, D.; Fatouros, D.G.; Borges, O. Chitosan-coated PLGA nanoparticles for the nasal delivery of ropinirole hydrochloride: In vitro and ex vivo evaluation of efficacy and safety. Int. J. Pharm. 2020, 589, 119776.

66. Croce, M.V.; Price, M.R.; Segal-Eiras, A. Detection and isolation of MUC1 Mucin from larynx squamous cell carcinoma. Pathol. Oncol. Res. 2000, 6, 93–99.

67. Utispan, K.; Koontongkaew, S. Mucin 1 regulates the hypoxia response in head and neck cancer cells. J. Pharmacol. Sci. 2021, 147, 331–339.

68. Lu, H.; Liang, D.; Zhu, Y.; Xu, W.; Zhou, K.; Liu, L.; Liu, S.; Yang, W. Prognostic and clinicopathological significance of MUC expression in head and neck cancer: A systematic review and meta-analysis. Oncotarget 2017, 8, 96359–963772. Available online: https://www.ncbi.nlm.nih.gov/pmc/articles/PMC5707106/pdf/oncotarget-08-96359.pdf (accessed on 1 June 2023).

69. Wu, Y.; Wang, M.; Li, Y.; Xia, H.; Cheng, Y.; Liu, C.; Xia, Y.; Wang, Y.; Yue, Y.; Cheng, X.; et al. The Fabrication of Docetaxel- Containing Emulsion for Drug Release Kinetics and Lipid Peroxidation. Pharmaceutics 2022, 14, 1993.

70. Kim, J.H.; Shin, D.H.; Kim, J.S. Preparation, characterization, and pharmacokinetics of liposomal docetaxel for oral administration. Arch. Pharm. Res. 2018, 41, 765–775.

71. Avanti Polar Lipids. Phase Transition Temperature for Glycerophospholipids [Internet]; John Wiley & Sons, Inc.: Hoboken, NJ, USA, 2022; p. 2. Available online: https://avantilipids.com/wp-content/uploads/2015/11/Phase_Transition_Temps_for_ Glycerophospholipids_Table.pdf (accessed on 25 April 2023).

72. Li, N.; Fu, T.; Fei, W.; Han, T.; Gu, X.; Hou, Y.; Liu, Y.; Yang, J. Vitamin E D-alpha-tocopheryl polyethylene glycol 1000 succinate- conjugated liposomal docetaxel reverses multidrug resistance in breast cancer cells. J. Pharm. Pharmacol. 2019, 71, 1243–1254.

73. Hemmingsen, L.M.; Giordani, B.; Paulsen, M.H.; Vani´c, Ž.; Flaten, G.E.; Vitali, B.; Basnet, P.; Bayer, A.; Strøm, M.B.; Škalko-Basnet. Tailored anti-biofilm activity—Liposomal delivery for mimic of small antimicrobial peptide. Biomater. Adv. 2023, 145, 213238.

74. Saadat, M.; Zahednezhad, F.; Zakeri-Milani, P.; Heidari, H.R.; Shahbazi-Mojarrad, J.; Valizadeh, H. Drug targeting strategies based on charge dependent uptake of nanoparticles into cancer cells. J. Pharm. Pharm. Sci. 2019, 22, 191–220.

75. Pal, A.; Barrett, T.F.; Paolini, R.; Parikh, A.; Puram, S.V. Partial EMT in head and neck cancer biology: A spectrum instead of a switch. Oncogene 2021, 40, 5049–5065.

76. Bai, X.; Smith, Z.L.; Wang, Y.; Butterworth, S.; Tirella, A. Sustained Drug Release from Smart Nanoparticles in Cancer Therapy: A Comprehensive Review. Micromachines 2022, 13, 1623.

77. Bao, Y.Y.; Zhong, J.T.; Shen, L.F.; Dai, L.B.; Zhou, S.H.; Fan, J.; Yao, H.T.; Lu, Z.J. Effect of Glut-1 and HIF-1α double knockout by CRISPR/CAS9 on radiosensitivity in laryngeal carcinoma via the PI3K/Akt/mTOR pathway. J. Cell. Mol. Med. 2022, 26, 2881–2894.

78. Zhou, L.; Wu, J.; Sun, Z.; Wang, W. Oxidation and Reduction Dual-Responsive Polymeric Prodrug Micelles Co-delivery Precisely Prescribed Paclitaxel and Honokiol for Laryngeal Carcinoma Combination Therapy. Front. Pharmacol. 2022, 13, 934632.

79. Paolino, D.; Accolla, M.L.; Cilurzo, F.; Cristiano, M.C.; Cosco, D.; Castelli, F.; Sarpietro, M.G.; Fresta, M.; Celia, C. Interaction between PEG lipid and DSPE/DSPC phospholipids: An insight of PEGylation degree and kinetics of de-PEGylation. Colloids Surf. B Biointerfaces 2017, 155, 266–275.

80. Vakili-Ghartavol, R.; Rezayat, S.M.; Faridi-Majidi, R.; Sadri, K.; Jaafari, M.R. Optimization of Docetaxel Loading Conditions in Liposomes: Proposing potential products for metastatic breast carcinoma chemotherapy. Sci. Rep. 2020, 10, 5569.

81. Zhang, H.; Li, R.Y.; Lu, X.; Mou, Z.Z.; Lin, G.M. Docetaxel-loaded liposomes: Preparation, pH sensitivity, Pharmacokinetics, and tissue distribution. J. Zhejiang Univ. Sci. B 2012, 13, 981–989.

82. Jahan, K.; Mekhail, M.; Tabrizian, M. One-step fabrication of apatite-chitosan scaffold as a potential injectable construct for bone tissue engineering. Carbohydr. Polym. 2019, 203, 60–70.

83. Carey, T.E.; Bradford, C.R.; Schwartz, D.R.; Hsu, S.; Baker, S.R.; Van Dyke, D.L.; Hsu, S.; Baker, S.R. Characterization of Human Laryngeal Primary and Metastatic Squamous Cell Carcinoma Cell Lines UM-SCC-17A and UM-SCC-17B. Cancer Res. 1989, 49, 6098–6107.

84. Brenner, J.C.; Graham, M.P.; Kumar, B.; Saunders, L.; Kupfer, R.; Lyons, R.H.; Bradford, C.R.; Carey, T.E. Genotyping of 73 um-scc Head and Neck Squamous Cell Carcinoma Cell Lines. Head Neck 2010, 32, 417–426.

85. Chen, X.; Thibeault, S.L. Novel isolation and biochemical characterization of immortalized fibroblasts for tissue engineering vocal fold lamina propria. Tissue Eng.-Part C Methods 2009, 15, 201–212.

86. Risinger, A.; Dybdal-Hargreaves, N.F.; Mooberry, S.L. Breast Cancer Cell Lines Exhibit Differential Sensitivities to Microtubule- targeting Drugs Independent of Doubling Time. Anticancer Res. 2015, 35, 5845–5850.

87. Angius, F.; Floris, A. Liposomes and MTT cell viability assay: An incompatible affair. Toxicol. Vitr. 2015, 29, 314–319.

88. Yitayew, M.Y.; Tabrizian, M. Hollow microcapsules through layer-by-layer self-assembly of Chitosan/Alginate on E. coli. MRS Adv. 2020, 5, 2401–2407.

89. Soleimani, M.; Somma, A.; Kaoud, T.; Goyal, R.; Bustamante, J.; Wylie, D.C.; Holay, N.; Looney, A.; Giri, U.; Triplett, T.; et al. Covalent JNK Inhibitor, JNK-IN-8, Suppresses Tumor Growth in Triple-Negative Breast Cancer by Activating TFEB- and TFE3-Mediated Lysosome Biogenesis and Autophagy. Mol. Cancer Ther. 2022, 21, 1547–1560.

90. Doryab, A.; Taskin, M.B.; Stahlhut, P.; Groll, J.; Schmid, O. Real-Time Measurement of Cell Mechanics as a Clinically Relevant Readout of an In Vitro Lung Fibrosis Model Established on a Bioinspired Basement Membrane. Adv. Mater. 2022, 34, 2205083.

Preface to Chapter 5

In Chapter 5, we developed and characterized a DTX-resistant laryngeal cancer cell line (Aim 2) and assessed a chemosensitizing using a resistant laryngeal-tumor-on-a-chip model (Aim 3). We employed a 4-month stepwise dose strategy to induce DTX resistance in a commercial laryngeal cancer cell line. RNA-sequencing technique was used to compare transcriptomic profiles between non-resistant cells and the new in-house DTX-resistant cell line. Our analysis revealed the upregulation of pathways associated with PI3K/mTOR, autophagy, cytochrome P450, and mitochondrial processes in DTX-resistant laryngeal cancer cells (DR-LSCC). Additionally, specific genes related to DTX resistance, such as TUBB3, CYP24A1, and ABCC3, were found to be upregulated in DR-LSCC. To validate the phenotype of DR-LSCC, we proceeded with the *in vitro* evaluation of the resistant phenotype of DR-LSCC compared to non-resistance cell controls. We performed 2D flat monolayer cultures in terms of protein expression, signaling pathway analysis, autophagy and cell viability assessment after MTF/DTX combination therapy exposures. Results confirmed the expected phenotypes of chemoresistance in DR-LSCC.

To explore the potential possibility of chemosensitizing strategy, we co-cultured DR-LSCC with vocal fold fibroblasts using a tumor-on-a-chip device. This chip validated the tumor hypoxic core attributable to a hypoxic gradient. Also, combination therapies consisted of MTF-priming effect followed by DTX treatment (with and without encapsulation into chitosomes). DAPI analysis, cell counting, LDH supernatant analysis, and chitosome uptake were conducted to evaluate the treatment outcomes. For chip cultures receiving both MTF and DTX-loaded chitosomes, increased cell death was observed when compared to DTX alone treatment, implicating the potential benefits of adjuvant chemosensitizer priming in reducing DTX drug resistance. This study showed the successful development of DR-LSCC as chemoresistant cancer cell model, and the potential use of combination therapies in the treatment for resistant laryngeal cancer.

This work is in preparation for publication.

Chapter 5. Second original article

Establishment of a Chemoresistant Laryngeal Cancer Cell Model to Study Chemoresistance and Chemosensitization Responses Via Transcriptomic Analysis and a Tumor-On-A-Chip Platform

Christian R. Moya-Garcia, Meghana Munipalle, Alain Pacis, Nader Sadeghi, Maryam Tabrizian, Nicole Y. K. Li-Jessen**

Christian R. Moya-Garcia

Department of Biomedical Engineering, Faculty of Medicine and Health Sciences, McGill University, 3775 Rue University, Montreal, QC H3A 2B4, Canada

Meghana Munipalle

Department of Biomedical Engineering, Faculty of Medicine and Health Sciences, McGill University, 3775 Rue University, Montreal, QC H3A 2B4, Canada

Alain Pacis

Canadian Centre for Computational Genomics (C3G), Montréal Node, McGill University, 740 Dr. Penfield Avenue, Room 6103, Montreal, QC H3A 0G1, Canada

Nader Sadeghi

Department of Otolaryngology – Head and Neck Surgery, McGill University, MUHC (Royal Victoria Hospital), 1001 Decarie Blvd., Montreal, Quebec H4A 3J1, Canada

Maryam Tabrizian*

Department of Biomedical Engineering, Faculty of Medicine and Health Sciences, McGill University, 3775 Rue University, Montreal, QC H3A 2B4, Canada

Faculty of Dentistry and Oral Health Sciences, McGill University, 2001 Ave McGill College, Montreal, QC H3A 1G1, Canada

Nicole Y. K. Li-Jessen*

School of Communication Sciences and Disorders, McGill University, 2001 Av. McGill College #8, Montréal, QC H3A 1G1, Canada

Department of Biomedical Engineering, Faculty of Medicine and Health Sciences, McGill University, 3775 Rue University, Montreal, QC H3A 2B4, Canada

Department of Otolaryngology – Head and Neck Surgery, McGill University, MUHC (Royal Victoria Hospital), 1001 Decarie Blvd., Montreal, Quebec H4A 3J1, Canada

Research Institute of the McGill University Health Centre, 1001 Decarie Blvd., Montreal, QC H4A 3J1, Canada

* Equal contribution as senior authors

***** E-mail: maryam.tabrizian@mcgill.ca; nicole.li@mcgill.ca

Keywords: chemoresistance, laryngeal cancer, metformin, docetaxel, transcriptomics, microfluidics, combination therapy

Abstract: Tumor resistance to chemotherapy is a common cause of cancer recurrence in patients with head and neck squamous cell carcinoma. The goal of this study was to establish a chemoresistant laryngeal cancer cell model and to test a chemosensitizing agent as an adjunct to standard chemotherapy. A stepwise dose-escalation continuous exposure method was used to induce chemoresistance to docetaxel in a laryngeal cancer cell line. At the genotypic level, RNA sequencing confirmed that the cells acquired putative resistance with upregulated docetaxel-resistant genes (e.g., TUBB3, CYP24A1) and signaling pathways (e.g., PI3K/mTOR, autophagy). For phenotypic analysis, docetaxel-resistant cells were co-cultured with laryngeal fibroblasts in a 2-channel microfluidic chip that mimics a hypoxic tumor core as *in vivo*. Stromal fibroblasts were observed to migrate towards docetaxel-resistant cancer cells expressing nitroreductase, an intracellular maker indicative of hypoxia. In addition, a drug sensitivity test with a chemosensitizer, metformin, was performed on the drug-resistant tumor-on-a-chip. Compared to untreated controls, metformin-primed cancer cells exhibit higher sensitivity to docetaxel, i.e., cell death. Collectively, this resistance-acquired cell model displayed presumed genotypic and phenotypic profiles of chemoresistance, which will provide a viable option for testing new therapeutic strategies of restoring tumor sensitivity to docetaxel.

***Translational impact statement*:**

Incomplete understanding of chemoresistance in locally-advanced mucosal laryngeal carcinoma leads to overtreatment. Here, we develop docetaxel-resistant laryngeal cancer cells to understand key molecular mechanisms and chemosensitizing strategies. From such resistant-acquired cells, molecular targets for inhibition are identified regarding upregulated genes and signaling pathways including PI3K/mTOR and autophagy associated with docetaxel resistance. Tumor-on-a-chip cultures emulate the hypoxic laryngeal tumor core for chemosensitizing evaluation. Metformin is used to sensitize chemoresistant cells to docetaxel encapsulated into mucoadhesive chitosomes causing increased cytotoxicity with prospect clinical target of mucin-overexpressing tumors.

.

5.1 Introduction

The global burden of head and neck cancer (HNC) is estimated as $535 billion USD from cases between 2018 and 2030.[1] HNC encompasses squamous cell carcinoma in the mucosal tissue found in the oral cavity, nasal cavity, pharynx, larynx, and salivary glands.[2] The 5-year overall survival rate for patients with locally-advanced HNC remains to be 50% for the last three decades.[3,4] About 65% of patients with locally-advanced stage of HNC develop metastatic/recurrent cancer with a 15% rate of developing a second primary tumor in the head and neck anatomical site.[5] Resistance to treatment is a common cause of cancer recurrence and metastasis, leading to treatment failure.[6] As a sub-type of HNC with up to a 40% case load,[7] laryngeal cancer affects critical functions such as speaking, swallowing, and breathing.[8] Laryngeal cancer had an annual incidence rate of 177,422 worldwide in 2019.[9] This incidence rate is expected to increase 43% by 2035 due to attributable risk factors as smoking and drinking.[10]

In standard treatment of HNC, taxanes, platinum-based, and 5-fluoruoracil (TPF) are common chemotherapeutic agents, typically used concomitantly with radiotherapy either in definitive or adjuvant setting.[7] Docetaxel (DTX) is a taxane drug that was approved by US FDA for head and neck cancers since 1996.[11] When administering DTX as a single agent, positive response rates were found as low as 10% in HNC unrelated to human papilloma virus infection.[12] This low response rate is primarily attributed to tumor resistance to the drugs used in chemotherapy.[2,12–14]

Multiple molecular pathways are plausibly associated with HNC progression and therapeutic resistance, such as alterations in drug efflux transporters, disruptions in apoptotic pathways, augmentation of DNA repair mechanisms, and dysregulation of survival signaling pathways.[15,16] Specific to DTX, upregulation of β-III tubulin,[17–19] cytochrome P450 (CYP),[17] and ATP-binding cassette (ABC) transporters[17,20,21] were linked to its anti-cancer effects. DTX hampers microtubule dynamics by binding to the β-subunit of microtubules like β-III tubulin, which causes inhibition of mitotic processes.[22] Upregulated β-III tubulin with TUBB3 as an encoding gene is associated with reducing the DTX-related mitotic arrest on microtubule dynamics, leading to treatment resistance.[17–19] With regards to DTX drug metabolic breakdown, its enzymatic degradation relates to Cytochrome P450 (CYP) family.[17] CYP24A1 is a CYP family gene that encodes 24-hydroxylase enzymes helping regulate vitamin D activity.[23] Upregulated CYP24A1 is associated

with DTX resistance,[24] and poor overall survival of oral cancer patients.[23,25] Concerning ABC transporters, ABCB1 encodes the P-glycoprotein that is commonly known as multidrug resistance protein 1.[17,20,21] These efflux transporters play critical roles in reducing the intracellular accumulation of DTX by pumping the drug out of cancer cells.[17,20,21] In addition to ABCB1, increased resistance to DTX is correlated to an upregulated expression of the ABCC3 ATP binding cassette gene, in which ultimately diminish the efficacy of cancer treatment.[26,27]

Combination therapy, often involving two or more drugs or treatment modalities, have been explored to circumvent chemoresistance in head and neck oncology.[14] For instance, PI3K/mTOR pathway is the most aberrantly activated cancer-associated signaling pathway with more than a 90% prevalence in head and neck malignancy.[28] Their upregulation is linked to taxane resistance with downstream effects on regulation of cell survival, metabolism, and proliferation.[17,20,29–32] Monotherapy or combination treatments of the mammalian target of rapamycin (mTOR) inhibitors are also proposed to sensitize resistant cells that may help improve treatment outcome. In particular, metformin (MTF), which is an antihyperglycemic agent and first-line treatment for diabetes, was found to inhibit mTOR pathway on several cancer types.[33–35] When used as an adjuvant treatment to chemotherapy, MTF decreased resistance to taxane therapies in ovarian tumors, with 20% more epithelial cancer cell death compared to taxane alone after 2-day inspection.[33] In gastric cancer, MTF in combination with DTX or 5-fluororuacil showed more than 80% reduction in gastric cancer colony number after a 10-day clonogenic inspection.[34] A randomized clinical trial study also suggested a favorable impact of MTF on enhancing the sensitivity of DTX treatment in patients with metastatic prostate cancer.[35]

In HNC, *in vitro* evidence became available for possible anti-tumor effects of MTF[36] from ongoing clinical trials[37,38] (e.g., phase I,[4] phase I/II[39]). In oral cancer, an *in vitro* study reported that MTF inhibits cell proliferation and regulates cancer-associated pathways affecting mTOR and mitochondrial activity.[36] Also, MTF has shown regulation of resistant mechanisms during curcumin chemotherapy treatment.[40] In laryngeal cancer, MTF in combination with 5-fluororacil was showed to upregulate genes associated with protein metabolism, cytochrome P450, endoplasmic reticulum stress, DNA damage and apoptosis; as well as to reduce cell proliferation and migration *in vitro*.[41] In locally advanced stage III of squamous cell carcinoma of the oral

cavity, oropharynx, hypopharynx and larynx, adjuvant MTF has shown improved overall survival and progression-free survival in phase I/II clinical studies.[4,39]

One issue with low therapeutic effect of the anti-cancer drugs, particularly for HNC, is related to the route of drug administration. Systemic intravenous delivery of chemotherapy induces highly toxic effects throughout the body because the chemotherapy concentration in the tumor site is like that found in the entire body, with only approximately 1% of the chemotherapy reaching solid tumors via this route.[42,43] Although locoregional intra-arterial chemotherapy is proposed as a means of mitigating systemic toxicities by directing the drug into tumor-supplying arteries rather than through systemic circulation, this administration still carries the risk of causing toxic extravasation damage in the surrounding tumor region.[13,44] In our previous work, we encapsulated DTX into anionic liposomes coated with cationic chitosan, i.e., mucoadhesive chitosomes, for quasi-targeted local controlled and sustained release of drugs.[13] We then administered DTX-loaded chitosomes to non-resistant laryngeal cancer cells (mucosal carcinoma) targeted via mucin-chitosan interactions. After a week, DTX-loaded chitosomes exhibited about 20% more laryngeal cancer cell death compared to DTX alone.[13]

At present, most laryngeal cancer studies rely on animal models.[45,46] When laryngeal carcinogenesis is studied by subcutaneous injection into the flank[45] or armpits[46] of mice, animal models fell short to accurately mimic the disease, as it does not target the anatomical site of the laryngeal mucosa. There remains a need for advancing cell culture model for pre-clinical assessment in laryngeal cancer research. Meanwhile, existing *in vitro* laryngeal cancer models are limited to fully characterizing the tumor microenvironment and the tumor response, both sensitivity and resistance, to chemotherapy.[2,47,48] In this study, we aimed to develop a DTX-resistant laryngeal cancer cell model that would help advance the understanding of chemoresistance and the evaluation of new drug design. We implemented an escalating intermittent dose protocol to successfully induce DTX resistance in a commercially available laryngeal cancer cell line. RNA sequencing analysis was performed with the aim of evaluating DTX-exposed cells resistance through measuring the upregulation of DTX-resistant genes (e.g., TUBB3, CYP24A1, ABCC3, etc.) and signaling pathways (e.g., PI3K/mTOR, autophagy, mucin, endocytosis, etc.) compared to healthy laryngeal epithelial cells and laryngeal cancer cells with no DTX exposure. To emulate chemosensitization therapies, DTX-resistant cells were co-cultured

with vocal fold stromal fibroblasts on a tumor-on-a-chip device, in which was then exposed to a combined MTF/DTX drug treatment with free DTX or encapsulated into chitosomes compared to monotherapy controls.

5.2 Results

5.2.1. Inducing and Genotyping Docetaxel Resistance in Laryngeal Cancer Cells.c

5.2.1.1. Stepwise dose-escalation exposure induced chemoresistance in laryngeal cancer cells.

DTX-resistance was induced in laryngeal squamous cell carcinoma (DR-LSCC) by applying a stepwise dose-escalation exposure protocol, namely, a 3-day exposure of complete media followed by 3-day DTX enriched media for 4 months (**Figure 5-1a**). Chemoresistance was confirmed based on the analyses of apoptosis, autophagy, cell migration, protein and gene expressions (**Figure 5-1b**).[17] The docetaxel resistance analysis was performed to assess the viability of DR-LSCC, in comparison with a non-resistant LSCC group and a healthy laryngeal squamous epithelial cell (LSEC) control groups. After a 72-hour of 1μM DTX exposure, the MTT cell viability assay showed that DR-LSCC were more resistant to the DTX treatment after a 3-day inspection. Less cell death was observed in DR-LSCC than that of LSCCs and LSEC (~36% vs ~15%; **Figure 5-1c**). After confirming an increased resistance on DR-LSCC, monodansylcadaverine staining was carried out for the detection of autophagy (**Figure 5-1d**). Tamoxifen, an autophagy inducer, was used as the positive control.[49] A significant increase in basal autophagy activity was noted in DR-LSCC compared to controls ($p < 0.05$), indicating that DR-LSCC have an increased metabolic activity than LSCC and LSEC (**Figure 5-1e**).

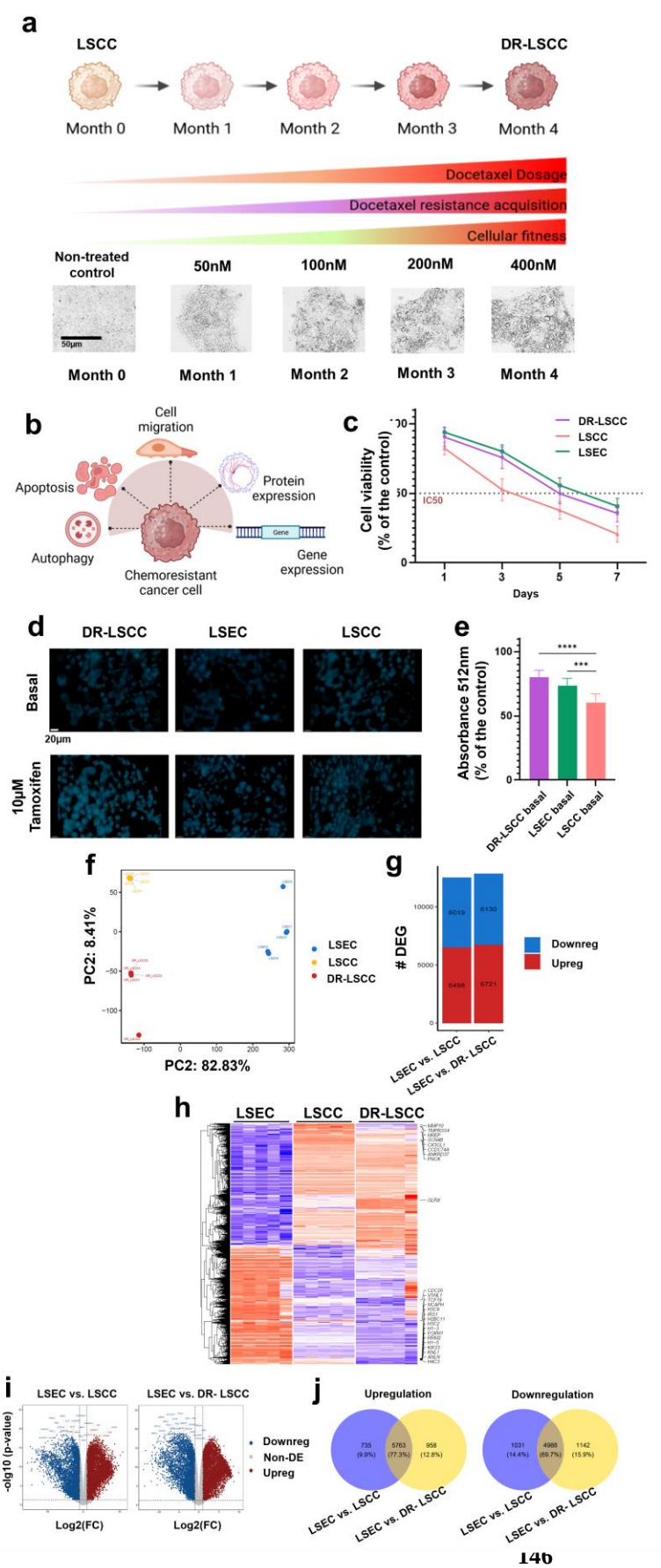
a
LSCC
DR-LSCC
Month 0
Month 1
Month 2
Month 3
Month 4
Docetaxel Dosage
Docetaxel resistance acquisition
Cellular fitness
Non-treated control
50nM
100nM
200nM
400nM
50μm
Month 0
Month 1
Month 2
Month 3
Month 4
b
Cell migration
Apoptosis
Protein expression
Autophagy
Gene
Gene expression
Chemoresistant cancer cell
c
DR-LSCC
LSCC
LSEC
Cell viability (% of the control)
IC50
Days
d
DR-LSCC
LSEC
LSCC
Basal
20μm
10μM Tamoxifen
e
Absorbance 512nm (% of the control)
****
***
DR-LSCC basal
LSEC basal
LSCC basal
f
PC2: 8.41%
PC2: 82.83%
LSEC
LSCC
DR-LSCC
g
DEG
6010
6130
6496
6721
Downreg
Upreg
LSEC vs. LSCC
LSEC vs. DR- LSCC
h
LSEC
LSCC
DR-LSCC
i
LSEC vs. LSCC
LSEC vs. DR- LSCC
-olg10 (p-value)
Log2(FC)
Log2(FC)
Downreg
Non-DE
Upreg
j
Upregulation
Downregulation
735 (9.9%)
5763 (77.3%)
958 (12.8%)
1031 (14.4%)
4988 (69.7%)
1142 (15.9%)
LSEC vs. LSCC
LSEC vs. DR- LSCC
LSEC vs. LSCC
LSEC vs. DR- LSCC

Figure 5-1. Chemoresistance in laryngeal cancer cells with distinct genotypic profile. (a) Illustration of the protocol for inducing chemoresistance in laryngeal cancer cells. Brightfield images show the progression of chemoresistance (4x magnification). (b) Chemoresistance can induce autophagy, apoptosis, cell migration, protein expression, gene expression and so on. (c) Drug resistance analysis of DTX cytotoxicity effect on non-resistant (LSEC and LSCC) and resistant (DR-LSCC) cells. (d) Autophagy staining of DR-LSCC, LSCC, and LSEC with positive controls of tamoxifen. Blue = monodansylcadaverine. Scale bar = 20μm. (e) Normalized autophagy absorbance to positive controls. *** $p < 0.001$, **** $p < 0.0001$. (f) Principal component analysis (PCA) of the transcriptomic data for each cell group sample (n = 5). (g) Total identified differentially expressed genes (DEG) depicted as heat maps with a Z-core (-2 to 2). Individual DEG are represented on the y axis and the sample regions along the x axis. (h) Number of upregulated and downregulated DEG (# DEG) of comparison between cell groups. (i) A volcano plot of LSEC vs. LSCC, and LSEC vs. DR-LSCC comparisons. (j) Differentially expressed gene Venn diagram of comparison between cell groups. LSEC = laryngeal squamous epithelial cell; LSCC = laryngeal squamous cell carcinoma; DR-LSCC = docetaxel-resistant laryngeal squamous cell carcinoma.

5.2.1.2. DR-LSCC and LSCC presented overall distinct genotypic profile compared to LSEC.

More than 150ng/μL of RNA was obtained for all sequencing sample of LSEC, LSCC, and DR-LSCC (**Table 5-S1**). Principal component analysis (**Figure 5-1f**) was implemented to observe the data in terms of their first dimension (PC1) and second dimension (PC2) of variation between cell groups. PC1 axis was greater than the comparable distances observed along the PC2 axis. PC1 and PC2 accounted for 83% and 8% of variability, respectively, and the three groups of cells were clearly separated from each other. From the 23,922 expressed genes among the three cell groups, differentially expressed genes (DEG) were identified and depicted as heatmaps to visualize data clustering as entities through a dendrogram and assess the logical coherence of this structure (**Figure 5-1g**). Heatmap analysis exhibited distinct genotypic profiles from DR-LSCC, LSCC, and LSEC of the identified DEG. Healthy LSEC control presented over 12,000 DEG, either upregulated or downregulated, when compared to either LSCC or DR-LSCC with P-adjusted < 0.05 and $|\log2FC| > 1$ (**Figure 5-1h**). In total, there were 12,517 DEG between healthy control and cancerous group (LSEC vs. LSCC), and 12,851 DEG between healthy control and resistant cancerous group (LSEC vs. DR-LSCC).

Volcano plots analysis confirmed the distinctive genotypic profile of both cancerous groups (**Figure 5-1i**). Compared to non-cancerous LSEC, both cancerous groups exhibited statistically significant downregulated (~40%, displayed as blue dots) and upregulated (~60%, shown as red

dots) genes. To understand the correlation of these data, overlap analysis of up- and downregulated DEG from **Figure 5-1g** and **5-1i** was depicted in Venn diagrams (**Figure 5-1j**). About 77% (5,763/7,456) of upregulated DEG and 70% of downregulated DEG (4,988/7,161) were shared in both cancerous groups compared to non-cancerous LSEC. Overall, both cancerous groups (LSCC and DR-LSCC) displayed distinctive genotypic profiles from that of non-cancerous (LSEC) and subsequent analysis would focus on the comparison of the two cancerous groups.

5.2.2. DR-LSCC Oncogene Profiling of Metastasis and Resistance

Based on the analysis of 45 oncogenes known to head and neck squamous cell carcinomas[17,26,32,50–57], DR-LSCC presented a differentially expressed genotypic profile with respect to metastasis cytokine, apoptosis, proliferation, drug transporters, enzymatic, and vitamin D-related markers compared to LSEC (**Figure 5-S1**). Of these 45 oncogenes, 21 genes were selected for further investigation herein (**Figure 5-2a**) as their expression patterns were distinctive from other related work.[32,51] Compared to non-cancerous LSEC, markers of metastasis, namely (wild type) SLC16A1 and COL4A1, were significantly downregulated in DR-LSCC as anticipated. Such outcome may refer to the constant DTX exposure caused a greater effect on cytokine gene expression as MMP-3 ($p < 0.05$), CXCL5 (n.s.), and CXCL11 ($p < 0.05$). An explanation may relate to MMP expression being part of the development of metastasis in HNC,[32,51,58] rather than the lymph node metastatic gene expression of COL4A1 and SLC16A1 as suggested in Jin et al.'s paper.[51]

Further in comparison to LSEC, apoptosis-related expression of (wild type) TP53 was downregulated (n.s.) and TNFRSF11A was significantly upregulated ($p < 0.05$) in DR-LSCC. Genes related to cancer proliferation including NOTCH1 ($p < 0.05$), EP300 (n.s.), and PTCH1 ($p < 0.05$) were all upregulated in DR-LSCC. Upregulation of the drug transporter ABCC3 (n.s.) and downregulation of microtubule binding protein FRY ($p < 0.05$) were observed in DR-LSCC. With respect to autophagy-related genes, DR-LSCC showed upregulation of CFLAR ($p < 0.05$) and ZFYVE26 (n.s.). A non-significant upregulation of the chromatin remodeling gene KMT2D was observed in DR-LSCC.

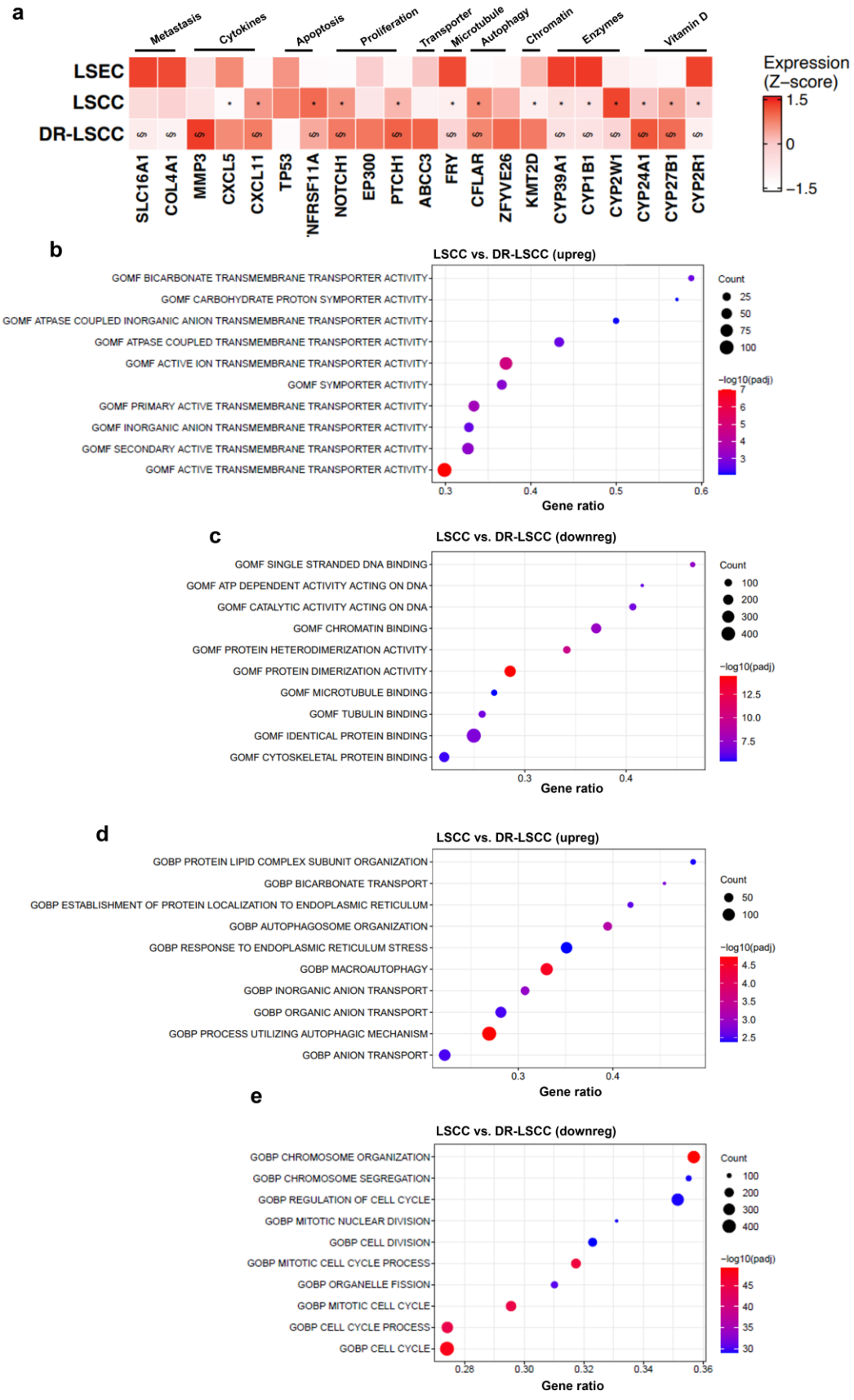
a
Metastasis
Cytokines
Apoptosis
Proliferation
Transporter
Microtubule
Autophagy
Chromatin
Enzymes
Vitamin D
LSEC
LSCC
DR-LSCC
SLC16A1
COL4A1
MMP3
CXCL5
CXCL11
TP53
NFRSF11A
NOTCH1
EP300
PTCH1
ABCC3
FRY
CFLAR
ZFYVE26
KMT2D
CYP39A1
CYP1B1
CYP2W1
CYP24A1
CYP27B1
CYP2R1
Expression (Z−score)
1.5
0
−1.5
b
LSCC vs. DR-LSCC (upreg)
GOMF BICARBONATE TRANSMEMBRANE TRANSPORTER ACTIVITY
GOMF CARBOHYDRATE PROTON SYMPORTER ACTIVITY
GOMF ATPASE COUPLED INORGANIC ANION TRANSMEMBRANE TRANSPORTER ACTIVITY
GOMF ATPASE COUPLED TRANSMEMBRANE TRANSPORTER ACTIVITY
GOMF ACTIVE ION TRANSMEMBRANE TRANSPORTER ACTIVITY
GOMF SYMPORTER ACTIVITY
GOMF PRIMARY ACTIVE TRANSMEMBRANE TRANSPORTER ACTIVITY
GOMF INORGANIC ANION TRANSMEMBRANE TRANSPORTER ACTIVITY
GOMF SECONDARY ACTIVE TRANSMEMBRANE TRANSPORTER ACTIVITY
GOMF ACTIVE TRANSMEMBRANE TRANSPORTER ACTIVITY
0.3
0.4
0.5
0.6
Gene ratio
Count
25
50
75
100
−log10(padj)
7
6
5
4
3
c
LSCC vs. DR-LSCC (downreg)
GOMF SINGLE STRANDED DNA BINDING
GOMF ATP DEPENDENT ACTIVITY ACTING ON DNA
GOMF CATALYTIC ACTIVITY ACTING ON DNA
GOMF CHROMATIN BINDING
GOMF PROTEIN HETERODIMERIZATION ACTIVITY
GOMF PROTEIN DIMERIZATION ACTIVITY
GOMF MICROTUBULE BINDING
GOMF TUBULIN BINDING
GOMF IDENTICAL PROTEIN BINDING
GOMF CYTOSKELETAL PROTEIN BINDING
0.3
0.4
Gene ratio
Count
100
200
300
400
−log10(padj)
12.5
10.0
7.5
d
LSCC vs. DR-LSCC (upreg)
GOBP PROTEIN LIPID COMPLEX SUBUNIT ORGANIZATION
GOBP BICARBONATE TRANSPORT
GOBP ESTABLISHMENT OF PROTEIN LOCALIZATION TO ENDOPLASMIC RETICULUM
GOBP AUTOPHAGOSOME ORGANIZATION
GOBP RESPONSE TO ENDOPLASMIC RETICULUM STRESS
GOBP MACROAUTOPHAGY
GOBP INORGANIC ANION TRANSPORT
GOBP ORGANIC ANION TRANSPORT
GOBP PROCESS UTILIZING AUTOPHAGIC MECHANISM
GOBP ANION TRANSPORT
0.3
0.4
Gene ratio
Count
50
100
−log10(padj)
4.5
4.0
3.5
3.0
2.5
e
LSCC vs. DR-LSCC (downreg)
GOBP CHROMOSOME ORGANIZATION
GOBP CHROMOSOME SEGREGATION
GOBP REGULATION OF CELL CYCLE
GOBP MITOTIC NUCLEAR DIVISION
GOBP CELL DIVISION
GOBP MITOTIC CELL CYCLE PROCESS
GOBP ORGANELLE FISSION
GOBP MITOTIC CELL CYCLE
GOBP CELL CYCLE PROCESS
GOBP CELL CYCLE
0.28
0.30
0.32
0.34
0.36
Gene ratio
Count
100
200
300
400
−log10(padj)
45
40
35
30

Figure 5-2. HNC biomarker expression on analyzed laryngeal cells. (a) Heatmap of specific differences on HNC biomarkers, drug metabolism, oncogenes, and tumor suppressors with Z-score (-1.5 to 1.5). Top 10 gene ontology molecular functions (GOMF) of (b) upregulated and (c) downregulated DEG between LSCC and DR-LSCC. Top 10 gene biological process (GOBP) of (d) upregulated and (e) downregulated DEG between LSCC and DR-LSCC. * $p < 0.05$, § $p < 0.01$ in comparison to LSEC.

5.2.2.1 Gene ontology analysis revealed unique molecular pathways between LSCC and DR-LSCC

To gain a better understanding of the functional differences between the two cancerous groups, we performed differential expression analysis of DR-LSCC relative to LSCC (**Figure 5-S2, 5-S3**). We next applied gene set enrichment analysis (GSEA) using gene ontology (GO) annotations. Based on GO molecular functions (GOMF), DR-LSCC showed significant upregulation on transmembrane transporter and symporter activities than LSCC (**Figure 5-2b**) while molecular functions including DNA activity, protein dimerization, and cytoskeleton binding are downregulated (**Figure 5-2c**). For GO biological processes (GOBP), the most upregulated gene sets in DR-LSCC compared to LSCC were involved in autophagic mechanism, anion transport, endoplasmic reticulum responses (**Figure 5-2d**), while cell cycle is the top downregulated process (**Figure 5-2e**). These biological processes are known to implicate in the metabolism and differentiation of laryngeal cancer development and progression,[62] confirming the acquired chemoresistance of DR-LSCC at the gene transcription level. The ability of cancer cells to alter their metabolism has been associated with their resistance to anti-cancer drugs. In particular, resistant cells were able to adapt to oxidative stress and balance their internal redox levels by boosting the production of glutathione.[63] Such metabolic adaptation can be attributed to the mutation or deregulation of some genes that control microtubule stabilization, cancer senescence, hypoxia and antioxidant capacity, and adaptive mitochondrial reprogramming as described next.

5.2.3. Chemoresistance-Related Genes and Pathways: *in vitro* verification.

5.2.3.1. DR-LSCC expressed chemoresistant-associated genotypes.

Overall, compared to those of LSEC and LSCC, DR-LSCC showed upregulated expression of microtubule stabilization genes like ALK gene, metabolic gene GSK3B and slight increase of hypoxia gene HIF1A in the KEGG hsa05200 cancer pathway (**Figure 5-S2, 5-S3**). The result is in

concordance with a presumed highly metabolic and hypoxic phenotype of resistant cells reported in literature.[17] A set of chemoresistance-related markers,[15,17,20,28,29,64–68] namely βIII-tubulin (TUBIII), EGFR, Ki-67, E-Cadherin, vimentin, α-Smooth Muscle Actin (α-SMA), Oct-4, P53, and PIK3CA were further profiled and verified in this study. (**Figure 5-3, S4**).

For microtubule marker of TUBIII, both transcriptomic and staining results showed increased expression in DR-LSCC, attributable to DTX microtubule-binding effect.[22] For HNC oncogene of EGFR, immunostaining showed strong expression on the cell surface of DR-LSCC and LSCC but in opposite expression from the transcriptomic results. It is possible that continuous exposure of DTX may have a plateau effect on EGFR expression at the gene level. These results were unexpected since EGFR overexpression is often associated with taxane drug resistance.[16] For the proliferation marker of Ki-67, both cancerous groups showed strong stains but their encoding gene MKI67 was significantly downregulated compared to LSEC ($p < 0.05$). Although low levels of Ki-67 are associated with cancer senescence,[69] DR-LSCC exhibited proliferative activity via Ki-67 immunofluorescent inspection contradicting the MKI67 gene results.

For a cell adhesion marker of CDH1 gene and its encoding epithelial cadherin (E-cad), both cancerous groups showed significantly stronger expression than LSEC (p <0.05). For a mesenchymal marker of vimentin, both gene and staining data showed a low expression of this focal adhesion marker in DR-LSCC and LSCC. Another mesenchymal marker of ACTA2 gene and its α-smooth muscle actin, both cancerous groups also showed downregulation compared to LSEC (p <0.05); whereas DR-LSCC had significantly higher ACTA2 expression compared to LSCC. Therapy-induced cancer senescence reprograms metabolic activity resulting in promotion of the epithelial-mesenchymal transition,[70] which has been associated with oral squamous cell carcinoma promotion and invasiveness.[71]

For stemness markers of POU5F1 gene and its Oct-4, all cell types had comparable expressions. With respect to the tumor suppressor marker of TP53 gene and its P53, DR-LSCC showed significantly lower expression than the other two cell groups (p <0.05). Such results were anticipated considering that reduced expression of P53 manifested the process of cancer senescence.[69] For a metabolic mTOR-related marker of PIK3CA encoding gene and its P13K, DR-LSCC showed higher expression than LSEC. Collectively, these results suggested the genotypic

senescent state of DR-LSCC could be linked to a higher possibility of survival from drug challenges.

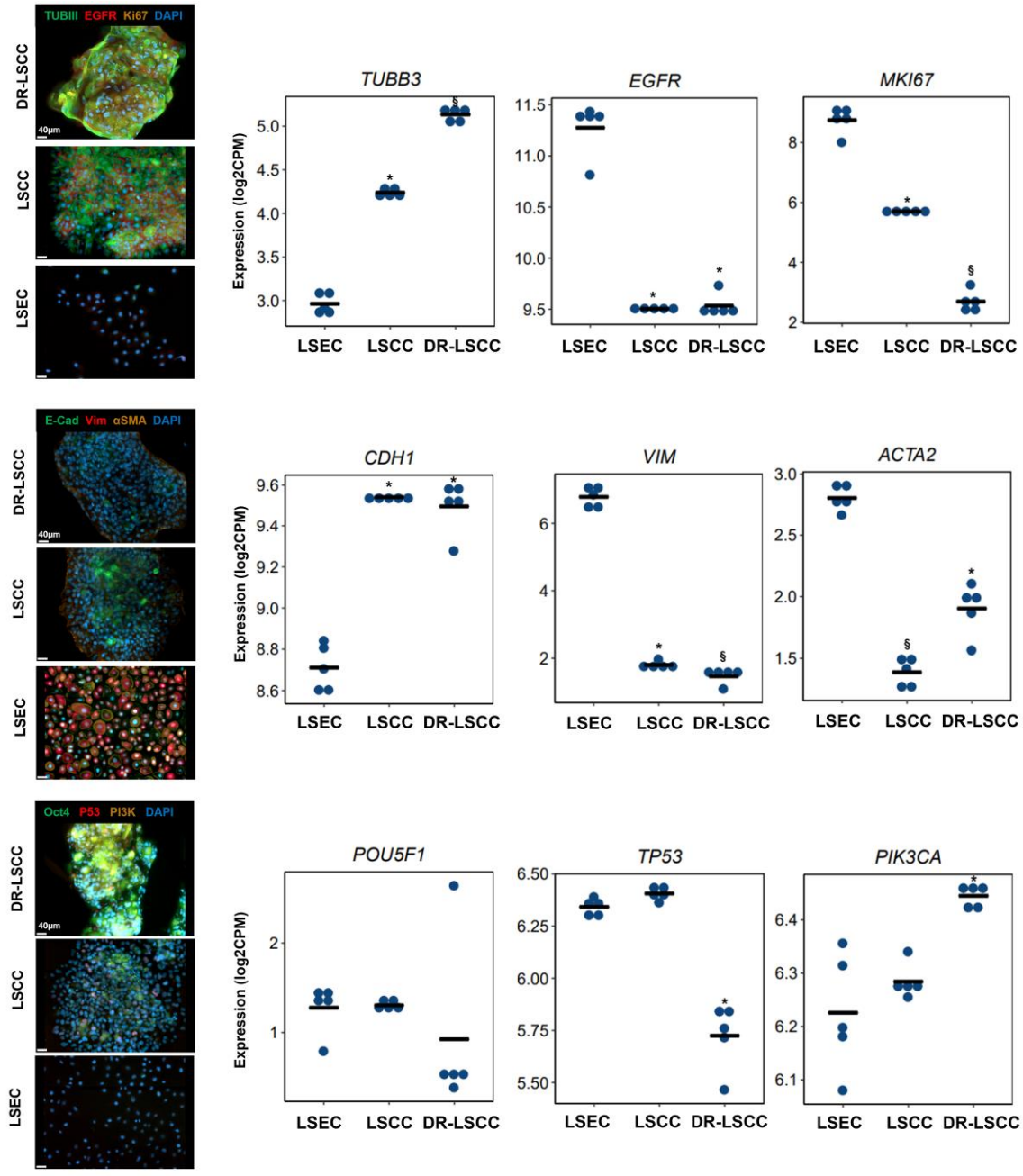

Figure 5-3. Immunostaining and corresponding transcriptomic data of chemoresistance markers. Immunofluorescence of βIII-tubulin (TUBIII), EGFR, Ki-67, E-cadherin, Vimentin, α-Smooth Muscle Actin (αSMA), OCT4, P53 and PI3K with their specific gene expression. Scale bar = 40µm. * $p < 0.05$, § $p < 0.01$ in comparison to LSEC.

5.2.3.2. DR-LSCC showed upregulated mTOR-signaling pathways and functional processes.

Upregulation of the mTOR complex[17,72–76] is associated with resistance to taxane drugs.[17] Compared to LSEC and LSCC, DR-LSCC showed respective 0.5-fold and 2.2-fold increases in the upstream DEPTOR based on the KEGG Pathway analysis [hsa04150 mTOR signaling] (**Figure 5-4a, S5a**). CASTOR1 was also upregulated in DR-LSCC, compared to both LSEC (~3.8 fold-change) and compared to LSCC (~1 fold-change). In contrast, DR-LSCC showed downregulation of IRS1 in comparison to both controls (>2.2 fold-change). Meanwhile, RNF152 exhibited a ~0.2-fold increase and ~1.5-fold decrease in DR-LSCC compared to LSEC and LSCC respectively.

For mTOR transcriptional activators, DR-LSCC showed upregulation for RRAGD compared to LSEC (~4 fold-change) and LSCC (~0.7 fold-change). For RRAGB, DR-LSCC showed about 1-fold increase and 0.8-fold decrease compared to LSEC and LSCC respectively. PRKCA is an mTOR downstream target, which showed a ~1-fold decrease and ~0.5-fold increase in DR-LSCC compared to LSEC and LSCC respectively. SGK1 showed a decreased expression (~1.5 fold-change) in DR-LSCC in comparison to the other two cell groups. SKG1 dysregulation is tumor specific, being upregulated in oral squamous cell carcinomas and downregulated in colorectal cancer.[77]

Intracellular mTOR proteins were quantified to verify the mTOR ontology results using enzyme-linked immunosorbent assays (ELISA). Compared to LSCC and LSEC, DR-LSCC showed significant protein levels of pan-mTOR but not phosphorylated ones, indicating higher metabolic activity and acquired chemoresistance (**Figure 5-4b**). One downstream effect of mTOR signaling is to regulate cytokine production in cancer cells.[51] For instance, matrix metalloproteinase-3 (MMP3) cytokine is a HNC oncogene that is involved in tumor remodeling.[51] DR-LSCC showed significant increases of MMP3 in both secreted and intracellular protein levels from media and lysate samples respectively, compared to LSCC and LSEC ($p < 0.05$, **Figure 5-4c**). Together, these results may relate to the DR-LSCC's upregulation of PI3K/mTOR-related (i.e., PIK3CA: 0.2-fold increase; PRKCA: 0.3-fold increase) as well as cytokine-related (i.e., STAT1-4 complex: varied between 1.7 and 0.7-fold increase; NOS1: 2.7-fold increase) pathways (**Figure 5-4, 5-S2, 5-S3**).

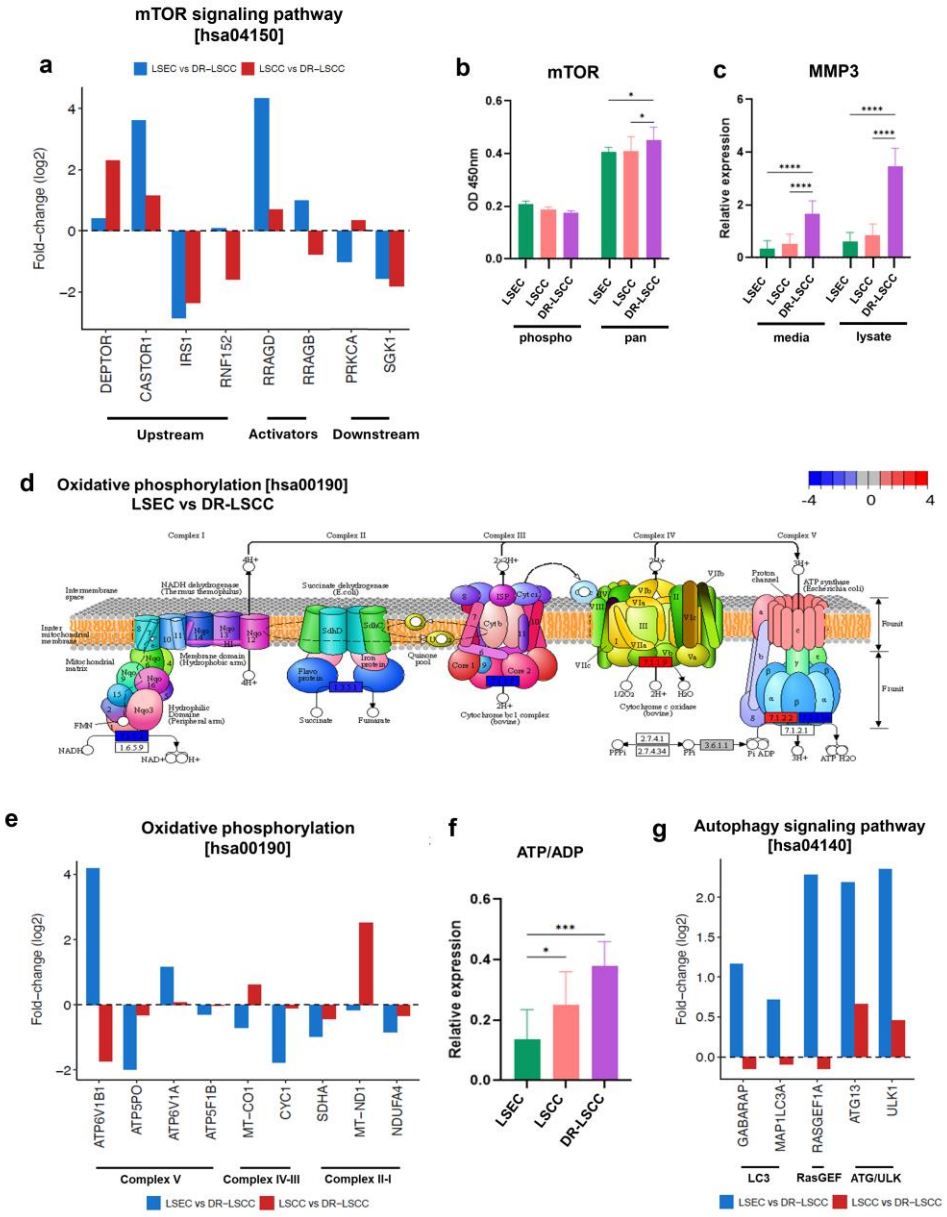

Figure 5-4. mTOR, oxidative phosphorylation, and autophagy signaling pathways. (a) Genes of interest from mTOR pathway [hsa04150]. Blue = LSEC vs. DR-LSCC; Red = LSCC vs DR-LSCC. (b, c) ELISA data of mTOR and MMP3 expressions of the cell groups LSEC, LSCC and DR-LSCC. (d) KEGG oxidative phosphorylation pathway [hsa00190] on non-resistant and resistant cells (LSEC vs. DR-LSCC) with color of fold-change (-4 to 4). Red = upregulation; Blue = downregulation. Genes of interest from KEGG oxidative phosphorylation pathway [hsa00190]. Blue = LSEC vs. DR-LSCC; Red = LSCC vs DR-LSCC (f) Luminescent data on ATP/ADP ratio of LSEC, LSCC, and DR-LSCC (g) Genes of interest from KEGG autophagy pathway [hsa04140]. Blue = LSEC vs. DR-LSCC; Red = LSCC vs DR-LSCC. * $p < 0.05$, **** $p < 0.0001$.

5.2.3.3 DR-LSCC showed upregulated mitochondrial and autophagy pathways.

Pathway analysis of mitochondrial activity as oxidative phosphorylation [hsa00190] was evaluated between resistant and non-resistant cells in terms of ATPase, ATP synthase, hydrogenase, oxidase, and reductase expressions (**Figure 5-4d, e**). For Complex V ATPase ATP6V1B1, DR-LSCC showed about 4-fold increase and 2-fold decrease compared to LSEC and LSCC respectively. For F-type ATPase ATP5PO, DR-LSCC showed downregulation than those of LSEC (~2 fold-change) and LSCC (~0.3 fold-change) controls. Regarding H+ ATPase ATP6V1A, DR-LSCC exhibited upregulation compared to LSEC (~1.2 fold-change) and LSCC (~0.2 fold-change). For membrane ATP synthase ATP5F1B, DR-LSCC showed < 0.5-fold downregulation compared to the other two groups. With regards to the mitochondria's Complex IV and III, these cytochrome c-related genes may play a role in the modification of energetic metabolism in DR-LSCC. For the oxidase MT-CO1, DR-LSCC showed about ~0.6-fold decrease and ~0.5-fold increase compared to LSEC and LSCC respectively. For reductase CYC1, DR-LSCC exhibited about 2-fold and 0.3-fold decreases than those of LSEC and LSCC.

Complex II-related SDHA, Complex I-related MT-ND1 and NDUFA4 are the genes that may mediate dehydrogenase and oxidoreductases in chemoresistance[37,78] (**Figure 5-4e**). For succinate dehydrogenase SDHA, DR-LSCC showed downregulation when compared to LSEC (~1 fold-change) and LSCC (~0.5 fold-change). For Complex I oxidoreductase MT-ND1, DR-LSCC showed about 0.4-fold decrease and about ~2.5-fold increase compared to LSEC and LSCC respectively. The upregulation of MT-ND1 may affect encoding-enzyme groups of mitochondria's Complex I for cancer cell respiratory capacity. For oxidoreductase NDUFA4, DR-LSCC showed downregulation of this oxidative-stress related gene, when compared to LSEC (~0.9 fold-change) and LSCC (~0.4 fold-change) controls. The metabolic activity of DR-LSCC was confirmed at the intracellular protein level. By implementing a bioluminescent assay on cell lysates, DR-LSCC showed a significant increase in relative expression of baseline ATP/ADP ratio ($p < 0.05$, 1-fold), compared to those of LSCC and LSEC (**Figure 5-4f**). This intracellular protein data confirmed the likely association of increases in metabolic genes (e.g., PI3KCA, GSK3B, CYP24A1, etc.) and ATP/ADP energy activity (ATP6V1A) in DR-LSCC.

Besides metabolic reprogramming, autophagy is also associated with taxane chemoresistance.[15,17,20,79,80] Based on the pathway analysis of autophagy [hsa04140] (**Figure 5-4g, 5-S5b**), when compared to healthy cells (i.e., LSEC), the five autophagy genes (GARABAP, MAP1LC3A, RASGEF1A, ATG13 and ULK1) were all upregulated in DR-LSCC. However, when compared to non-resistant cancer cells (i.e., LSCC), only two of them, namely, ATG3 and ULK1 were upregulated whereas the other three were downregulated in DR-LSCC. Resistance often involves aberrations in apoptosis regulation. Downregulation of pro-apoptotic elements (e.g. MDM2), and upregulation of anti-apoptotic proteins (e.g., BCL2) may confer a survival advantage to cancer cells[66] in response to DTX (**Figure 5-S2, 5-S3**).

5.2.4 An mTOR-inhibitor exposure study further confirmed the phenotype of DR-LSCC.

Metformin (MTF) is a rapamycin agent that inhibits mTOR that has demonstrated the ability to enhance the sensitivity of tumor cells to chemotherapy drugs.[33–35,81] MTF also inhibits the mitochondrial oxidative phosphorylation by targeting the Complex I NADH dehydrogenase,[37,78] such as upregulated MT-ND1 (**Figure 5-4e**). MTF was thus chosen to validate the phenotype of DR-LSCC via a cell sensitization analysis.

DR-LSCC, LSEC, LSCC and stromal human vocal fold fibroblasts (HVFF) were exposed to 500mM, 1mM, 5mM and 10mM MTF for three days. MTF cytotoxic activity was evaluated via mitochondrial-related MTT assay (**Figure 5-5a**) and LIVE/DEAD staining (**Figure 5-5b**). Results showed a decreasing trend in cell viability after exposing the cell with higher concentration of MTF after the 3-day inspection. Based on the results above, 1mM MTF treatment was selected for subsequent experiments due to its therapeutic effect below IC50 for the cancerous groups, but above IC50 threshold for non-cancerous LSEC and stromal HVFF.

ELISA data showed that 1mM of MTF treatment significantly ($p < 0.05$) enhanced the presence of phosphorylated mTOR on the four cell groups, suggesting that an inhibitory effect on mTOR synthesis (**Figure 5-5c**). Autophagy evaluation using monodansylcadaverine and propidium iodide stain showed noticeable increase of autophagy in MTF-treated DR-LSCC and compared to HVFF and LSEC (**Figure 5-5d**).

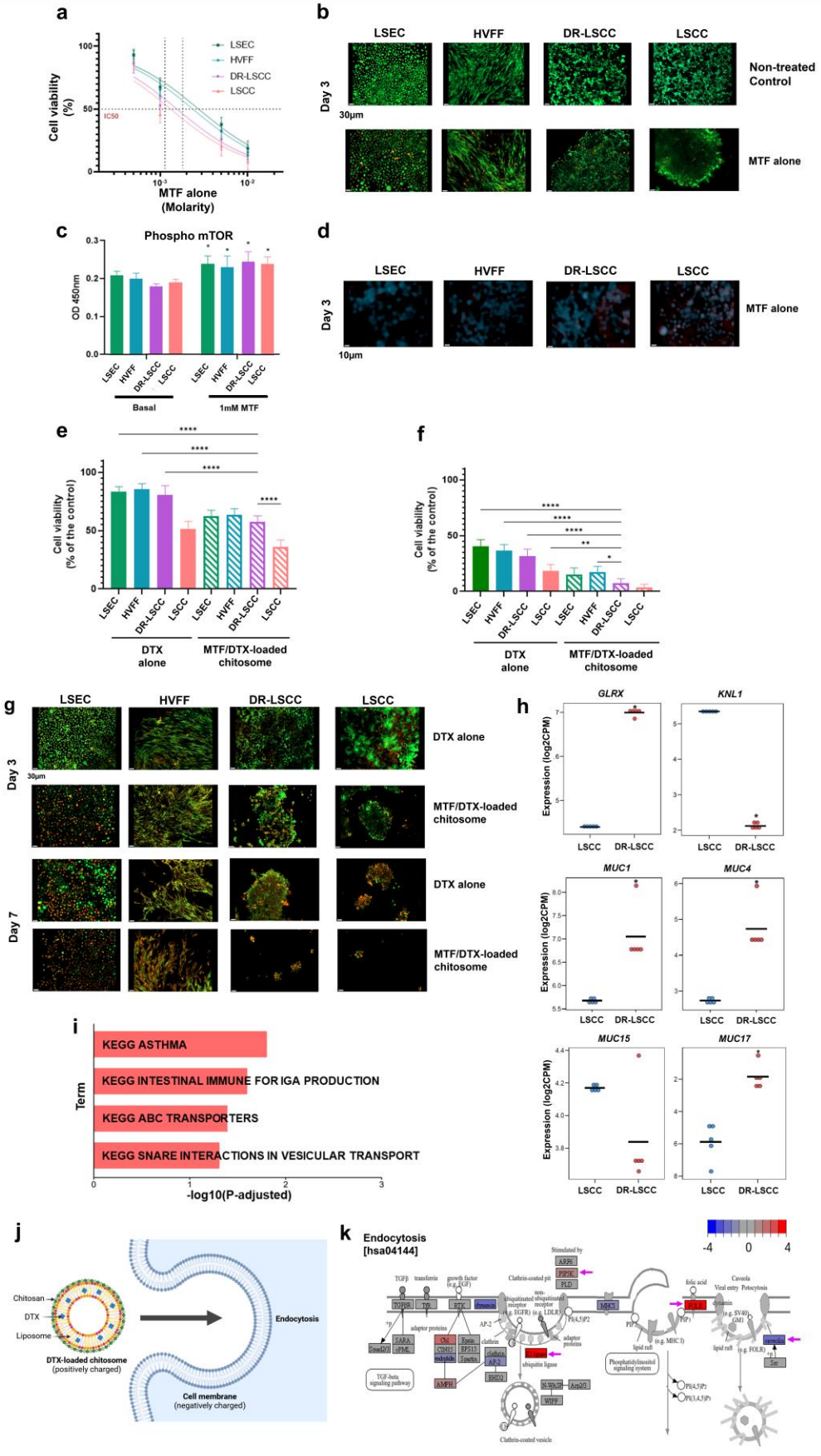
a
Cell viability (%)
LSEC
HVFF
DR-LSCC
LSCC
IC50
MTF alone (Molarity)
b
LSEC
HVFF
DR-LSCC
LSCC
Day 3
30μm
Non-treated Control
MTF alone
c
Phospho mTOR
OD 450nm
Basal
1mM MTF
d
LSEC
HVFF
DR-LSCC
LSCC
Day 3
10μm
MTF alone
e
Cell viability (% of the control)
DTX alone
MTF/DTX-loaded chitosome
f
Cell viability (% of the control)
DTX alone
MTF/DTX-loaded chitosome
g
LSEC
HVFF
DR-LSCC
LSCC
Day 3
30μm
DTX alone
MTF/DTX-loaded chitosome
Day 7
DTX alone
MTF/DTX-loaded chitosome
h
GLRX
KNL1
MUC1
MUC4
MUC15
MUC17
Expression (log2CPM)
LSCC
DR-LSCC
i
KEGG ASTHMA
KEGG INTESTINAL IMMUNE FOR IGA PRODUCTION
KEGG ABC TRANSPORTERS
KEGG SNARE INTERACTIONS IN VESICULAR TRANSPORT
Term
-log10(P-adjusted)
j
Chitosan
DTX
Liposome
DTX-loaded chitosome
(positively charged)
Endocytosis
Cell membrane
(negatively charged)
k
Endocytosis
[hsa04144]
-4
0
4
TGF-beta signaling pathway
Phosphatidylinositol signaling system
Clathrin-coated vesicle

Figure 5-5. Effects of MTF alone and its combination with DTX on non-resistant and resistant cells. (a) Dose response curve of the MTF dosage on non-resistant cells and DR-LSCC. Relative-Absolute IC50 threshold expressed as vertical dotted lines. (b) Cytotoxic evaluation of MTF dosage via LIVE/DEAD staining. Green = live cells; Orange = dead cells. Scale bar = 30µm. (c) Phospho-mTOR levels after 1mM metformin. (d) Autophagy activity after1mM metformin. Blue = autophagy activity; Red = dead cells. Scale bar = 10µm. MTT analysis on cell viability after 3-Day (e) and 7-Day (f) treatment exposures. (g) Cytotoxic evaluation of DTX alone, and MTF/DTX-loaded chitosomes via LIVE/DEAD staining. Green = live cells; Orange = dead cells. Scale bar = 30µm. (h) Genes associated with antioxidant, microtubule binding, and mucus glycosylation activities. (i) KEGG analysis of DR-LSCC upregulated genes compared to LSCC. (j) Schematic representation of DTX-loaded chitosome internalization by cells. (k) Representative KEGG endocytosis pathway [hsa05200] LSCC vs. DR-LSCC, with genes of interest PIP5K1A, E3 ligase/UBR3, FOLR1, CAV1/caveolin (pointed at with magenta arrows) with color of fold-change (-4 to 4). Red = upregulation; Blue = downregulation. * $p < 0.05$, ** $p < 0.01$, **** $p < 0.0001$.

Upon cells were sensitized with MTF chemosensitizer followed by DTX-loaded mucoadhesive chitosomes (**Figure 5-5e-g, 5-S6**), MTF-primed DR-LSCC showed more cell death (<25% viable cells, $p<0.05$) at Day 3 and Day 7, compared to DTX alone groups (**Figure 5-5e-g**). Similar patterns were also observed in LSCC and non-cancerous cells, indicative of restoring drug sensitivity from MTF.

5.2.3.5 DR-LSCC showed upregulated antioxidant, vesicle transport and mucin-related genes that may facilitate treatment and chitosome internalization.

Compared to LSCC, DR-LSCC showed upregulated antioxidant-associated GLRX[82] gene, downregulated microtubule-related KNL1 gene,[83] as well as upregulated biological processes related to ABC transporters and SNARE interactions in vesicular transport (**Figure 5-5h, i**). These genes and biological processes were related to drug sensitivity and retention of the encapsulated DTX in chitosomes.

Further, in comparison with LSCC, mucosal glycosylation[84] MUC1, MUC4 and MUC17 along with MUCL1, MUC2, and MUC5AC were significantly overexpressed ($p < 0.05$, >1-fold increase) whereas MUC15 was the only mucin-related gene downregulated ($p > 0.05$, 0.2-fold decrease) in DR-LSCC (**Figure 5-5h, 5-S7**). Upregulation of membrane genes associated to endocytosis, i.e., PIP5K1A, E3 ligase/UBR3, FOLR1, and mucosal barrier formation were also observed in DR-LSCC, which are likely favorable for the mucoadhesive chitosome internalization by DR-LSCC (**Figure 5-5j, k**). The observed enhanced drug sensitivity may relate to clathrin-

dependent endocytic internalization, being CAV1/caveolin downregulated (**Figure 5-5k**), of quasi-targeted mucoadhesive chitosomes (**Figure 5-5j, k**) as potentially explained by the transcriptomic profile.

Further, our DR-LSCC cell model showed the preservation of resistant phenotype after one freeze-thaw cycle. DTX alone and combination therapy were exposed to both DR-LSCC and thawed DTX-resistant cells (tDR-LSCC). LIVE/DEAD staining (**Figure 5-S8a**), MTT readouts (**Figure 5-S8b**) and clonogenic analyses (**Figure 5-S8c-d**) showed that tDR-LSCC displayed similar percentage of cell death and colonies as DR-LSCC after Day 3 and Day 7 of both DTX alone and MTF/DTX treatments. Specifically, the combination therapy exhibited 15% more cell death in DR-LSCC and tDR-LSCC after 3-day and more than 20% of cell death was observed after 7 days, compared to DTX alone ($p < 0.0001$; **Figure 5-S8b, d**). Autophagy activity and propidium iodide staining showed both DR-LSCC and tDR-LSCC had an increased autophagy with decreased cell death compared to LSCC after DTX alone and DTX-loaded chitosome treatments after 7 days (**Figure 5-S8e**).

5.2.4. DR-LSCC Sensitization with Laryngeal Tumor-on-a-chip Platform

Hypoxic tumor core, which is an important resistant-related tumor microenvironment feature, was not represented in the prior 2D monolayer study. To emulate the hypoxic laryngeal tumor core,[2] we cultured DR-LSCC with HVFF under a diffusion/hypoxic gradient in a microfluidic platform. The chip cultures were then subjected to a new set of chemosensitizing study for 5 days.

5.2.4.1. Tumor-on-a-chip co-culture cells presented a hypoxic marker.

The DR-LSCC/HVFF co-culture was performed on a microfluidic device with two microchannels and one central chamber (**Figures 5-6a**). On Day 0, results of phenotypic markers confirmed the co-culture of DR-LSCC (green/TUBIII$^+$, red/Vimentin$^-$) and HVFF (green/TUBIII$^-$, red/Vimentin$^+$) in their shared distinct compartments (**Figure 5-6b**). The diffusion/hypoxic gradient was set up by blocking the inlets/outlets of the stromal chamber and cancer channel after cell seeding (**Figure 5-6c**). By doing that, the oxygen/nutrients diffused from the drug-media channel towards the co-culture setup. After 5 days of co-culture **(Figure 5-6d)**, HVFF were observed to migrate towards the cancer channel when a hypoxia inducer (deferoxamine) was

introduced as positive controls. In the negative control group, MTF was used to inhibit HVFF migration owing to its antiproliferative effect on stromal cells known in the literature.[85] In our experimental group, HVFF were observed to migrate toward DR-LSCC, similar to the positive control groups. Also, a slight DR-LSCC growth into the stromal channel was observed, along with the HVFF migrating into the cancer channel (**Figure 5-6d**). This could be related to a slight increase in nitroreductase activity of hypoxic DR-LSCC and a more oxidative stress on HVFF (**Figure 5-6e**), owing to the hypoxia gradient in the microfluidic device.

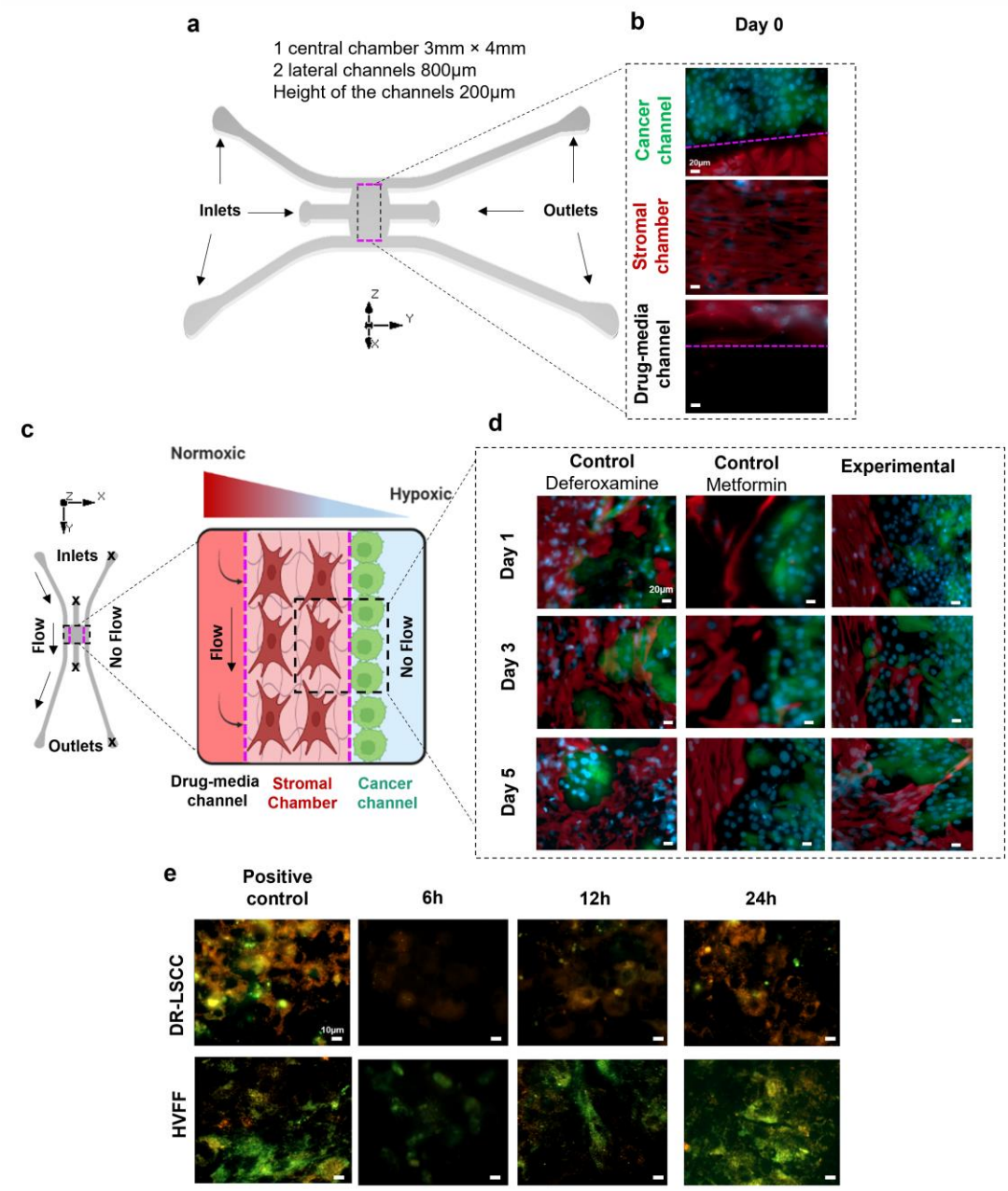

Figure 5-6. Hypoxia and migration analyses within the microfluidic device. (a) CAD design of the BEOnChip Gradient device. DR-LSCC were seeded on mucin-coated cancer channel whereas HVFF embedded in a collagen I gel were placed in Stromal chamber. (b) Phenotypic markers of the co-culture at Day 0. DR-LSCC (green/TUBIII^{+}, red/Vimentin^{-}) and HVFF (green/TUBIII^{-}, red/Vimentin^{+}). Magenta line = Collagen I gel limit. (c) Schematic representation of the co-culture setup within the microfluidic device mimicking the hypoxic tumor core by blocking inlets/outlets (represented as ×) after cell seeding to create an oxygen/nutrient gradient flow. (d) Migration analysis of the stromal cells (red, vimentin) towards the cancer channel (green, TUBIII), scale bar = 20 µm. Controls of Deferoxamine as hypoxia inducer and MTF as proliferation inhibitor (e) Hypoxia and oxidative stress analyses on DR-LSCC and HVFF at 24h (Day 0). Orange = hypoxia; Green = oxidative stress. Positive controls: Deferoxamine as hypoxia inducer and Pyocyanin as oxidative stress inducer.

5.2.4.2. DR-LSCC/HVFF co-culture showed increased sensitivity to combination therapy.

Chip cultures with DR-LSCC and HVFF were exposed to a combined MTF/DTX treatment for up to 5 days. The administration of the drugs was a 6-hr MTF priming and then 12-min perfusion of DTX or DTX-loaded chitosomes, followed by 18 hours of MTF perfusion. Overall, cell count analysis based on DAPI showed that HVFF and DR-LSCC decreased by number after treatment (**Figure 5-7a, b, Figure 5-S9**). The LDH results further showed that the total number of viable cells (HVFF + DR-LSCC) was in a decreasing trend in both groups of DTX-chitosome (27%) only and MTF/DTX-chitosomes (15%) but not for other non-capsulated drug groups (MTF: 85%, DTX: 68%, MTF/DTX: 55%; $p < 0.05$) (**Figure 5-7c**). At Day 5, LIVE/DEAD staining for each cell type further confirmed that the MTF/DTX-chitosome group showed more cell death in both stromal and cancer cells, compared to the non-capsulated MTF-DTX group and no treatment controls (**Figure 5-7d**).

To estimate the amount of chitosomes taken up by the cells, the difference between the amount of chitosomes injected into the device and the amount retrieved at the outlet was first determined. It was found that approximately 40% of the total amount of injected chitosomes was retained within the microfluidic device for a 6-hour treatment (**Figure 5-7e**, **Video 5-S1**). This retention result was then compared with absorbance measurements and NTA of the supernatant collected from the stromal and cancer channels (**Figure 5-S10**), showing that 60% of the chitosomes were present in the analyzed supernatant. The uptake of bare liposomes by HVFF and LSCC (**Figure 5-S10**) and of DTX-loaded chitosomes (**Figure 5-7e**) by HVFF and DR-LSCC was also confirmed by immunostaining, both indicating similar uptake regardless the presence or absence of the drug.

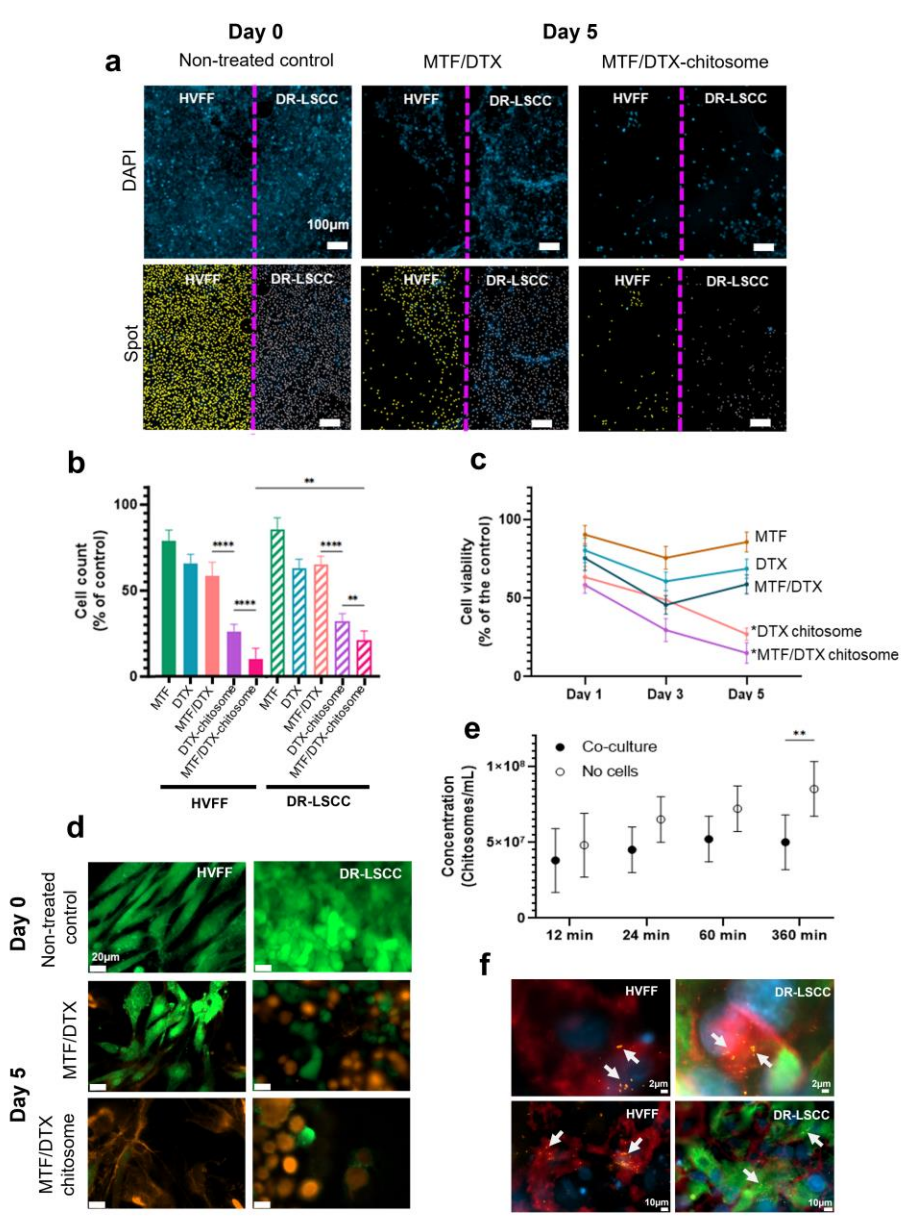

Figure 5-7. MTF/DTX combination therapy tested on the tumor-on-a-chip. (a) Cytotoxic effect via DAPI inspection, and Spot detection algorithm at Day 5. Yellow spots = HVFF; Gray spots = DR-LSCC; Magenta line = collagen gel limit. Scale bar = 100 µm. (b) Cell count using Spot detection algorithm on DAPI images at 5-day inspection. (c) LDH co-culture supernatant analysis. (d) LIVE/DEAD images at Day 5. Green = live cells; Orange = dead cells. Scale bar = 20µm. (e) Chitosome retention analysis, and (f) fluorescent chitosome uptake. Immunostaining of HVFF (red/EGFR$^+$, green/CK5$^-$) and cancer (red/EGFR$^+$, green/CK5$^+$) cells showed the internalization of the orange-fluorescent chitosomes (pointed at with white arrows) with DAPI as counterstaining after 6h inspection. Cancer-associated fibroblast behaviour characterized by EGFR expression could have been activated by DR-LSCC/HVFF crosstalk (cytokine pathway).[86,87] Scale bars = 5 µm (top images), 10 µm (below images). * $p < 0.05$, ** $p < 0.01$.

5.3 Discussion

Acquired drug resistance is a significant challenge to laryngeal cancer treatments. One strategy might involve the use of chemosensitizers like MTF to enhance the efficacy of chemotherapeutic agents by inhibiting the mTOR pathway.[88] The lack of preclinical *in vitro* model of chemoresistant laryngeal cancer has, however, impeded the progression of testing new treatment strategies for restoring tumor sensitivity. Using a stepwise intermittent protocol, we successfully developed a DTX-resistant laryngeal cancer cell model as shown by distinct gene expression. Genes were downregulated with regards to mucous expression (MUC15), microtubule (FRY and KNL1), apoptosis (TP53, TNFRSF11A, and BCL2), proliferation (MKI67), metabolism (IRS1 and SGK1), endocytosis (CAV1/caveolin) and metastasis (SLC16A1 and COL4A1). However, our main focus of study was the upregulation of genes associated with ABC transporters (ABCC3), mucosa glycosylation (MUC1, MUCL1, MUC2, MUC4, MUC5AC, MUC17), endocytosis (PIP5K1, UBR3, FOLR1), microtubules (TUBB3, ALK), receptors (PDGFR, NOTCH1), metabolism (PIK3CA, DEPTOR, CASTOR1, GSK3B, CYP24A1), hypoxia (HIF1A), apoptosis (NTRK1, MDM2), cytokine production (STAT1, IL6, GM-CSF/CSF2RA) and autophagy (CFLAR-AS1, ATG13, ULK1). Our overall findings are corroborated with other studies in HNC,[32,50] and DTX-related studies in carcer (**Table 5-S2**). For example, with regards to DTX-resistance genes in pancreatic cancer, the drug efflux ABBC3,[89] metabolic PIK3CA[90] and CYP24A[91] were upregulated in our DR-LSCC compared to their non-resistant counterparts. Our transcriptomic data revealed additional genes of mucin MUCL1, MUC4, MUC15 and MUC17, endocytic UBR3, mitotic FRY, metabolic CASTOR1, IRS1, and SGK1, apoptotic NTRK1, metastatic SLC16A1, and autophagic CFLAR-AS1, ATG13 and ULK1 that were mutated in our DTX-resistant laryngeal cancer cells, which have not been identified to be associated with DTX resistance in other types of cancer before.

Besides, genes from molecular pathways of autophagy (ULK/ATG complex), drug efflux (ABC transporters), mitochondrial activity (V-ATP synthase), hypoxia (HIF1A), and PI3K/mTOR (PIK3CA, CASTOR1, and DEPTOR) were upregulated in resistant laryngeal cancer cells. Autophagy maintains cellular homeostasis by degrading intracellular molecules and damaged organelles, which have an impact on drug degradation once internalized by cancer cells.[92] Increased autophagy activity protects cells from the therapeutic effects of drugs as shown by our

resistant laryngeal cancer cell model. Another common contributor of chemoresistance is the upregulation of the ABC transporters, like ABCC3, whose role is to export drugs out of the tumor cells via transmembrane ATP pumps.[93] Such a drug efflux process diminishes drug cytotoxic effects due to the remaining scarce drug concentration inside cells. Thus, the highly expressed transmembrane transporter and symporter activities may reflect the increased drug efflux of the resistant laryngeal cancer cell model and its associated cytotoxic resistance to drug free forms.

The proposed encapsulation of DTX into mucoadhesive chitosan-coated liposomes[13] could improve drug bioavailability inside and surrounding cancer cells that potentially enhance drug sensitivity via mucin-chitosan interaction. The mucin-related genes, MUC1 and MUC4, are overexpressed in treatment-resistant laryngeal carcinoma.[94] DR-LSCC showed over 1-fold increase in multiple mucin-related genes (e.g., MUC1, MUCL1, MUC2, MUC4, MUC5A, MUC17) compared to both non-resistant controls. However, DR-LSCC exhibited a non-significant 0.2-fold downregulation of MUC15 compared to non-resistant LSCC. As note, downregulated MUC15 expression is associated with poor clinical prognosis in hepatocellular carcinoma.[95] Anionic carboxyl groups in mucins, i.e., MUC1 encoding Mucin 1 transmembrane protein, interact electrostatically with the cationic amine groups in chitosan, which forms protein–polysaccharide complexes.[96] In our previous study,[13] cationic chitosome mucoadhesiveness was confirmed by turbidimetry and absorbance readouts using an anionic Mucin 1-riched dispersion. In turn, DTX-loaded chitosomes exhibited increased cytotoxic effect in LSCC compared to non-encapsulated DTX exposure. Our chitosome system could be compatible for the local delivery of DTX to mucin-overexpressing tumors such as by intra-arterial delivery, i.e., drug to be delivered into tumor's supplying artery.[44] Intra-arterial delivery can help limit deleterious systemic side effects and likely targeting metastatic tumor cells especially for locally-advanced laryngeal cancer, i.e., stage III and IV. We anticipate that by targeting mucin-overexpressing laryngeal cancer cells, the chitosan-coated liposomes will electrostatically bind to transmembrane mucins like MUC1, MUC4, MUC17 and thus enhance the drug intake and retention process.[95,96]

Encapsulated drugs are often internalized by cells via endocytosis mechanisms rather than transmembrane transporter activity.[97] In endocytosis, the internalized substance interacts with cell membrane via plasma membrane vesicles. For nanoparticle carriers like liposomes, the related endocytosis processes are still in debate that may relate to dependent or independent mechanisms

of the transmembrane protein clathrin.[98] In our study, DR-LSCC exhibited upregulation of the PIP5K1A (**Table 5-S2**), an upstream PI3K/mTOR pathway actuator[99] present in clathrin endocytic mechanisms. Interestingly, both clathrin-dependent gene (UBR3) and clathrin-independent gene (FOLR1) were also upregulated in DR-LSCC, suggesting that chitosomes may be uptaken primarily via clathrin-dependent endocytic processes since the caveolin gene (CAV1) related to the clathrin-independent mechanism was downregulated by DR-LSCC (**Table 5-S2**).

In our chemosensitizing study, DR-LSCC primed with MTF showed higher cell death than non-resistant LSCC in 2D cultures. To demonstrate the physiological relevance of our DR-LSCC model, a resistant tumor-on-a-chip was developed to emulate the hypoxic tumor core by co-culturing laryngeal fibroblast embedded in a collagen gel with laryngeal cancer cells. Compared to DR-LSCC, stromal cells showed ~10% more cell death after treatment of encapsulated drugs. This result may be attributed to the fact that the stromal chamber had greater exposure to the drug agents because of its immediate proximity to the drug-media channel. Another explanation could be owing to the sustained and controlled released of DTX from the mucoadhesive chitosomes[13] entrapped within the microfluidic device. This chip design may have trapped the chitosomes within the microfluidic device. Non-encapsulated DTX, MTF, and MTF/DTX treatments showed a ~15% recovery in cell viability considering the co-culture cell number on Day 5, which is attributable to drugs being washed away with less than 40% retention rate. Low drug retention gave time for the cells to recover from treatment cytotoxic effects. Interestingly, such recovery in cell viability was not observed in the treatment groups of the DTX-loaded chitosomes with or without MTF.

For this very first laryngeal-tumor-on-a-chip, the hypoxic-driven setups corroborated the interplay between increased oxidative stress and reduced oxygen levels.[100] DR-LSCC was housed in a presumably less oxygen tension than HVFF in the chip. Interestingly, DR-LSCC showed strong intracellular hypoxia but low oxidative stress signals, whereas HVFF showed strong signals in these two intracellular markers. This observation may be likely caused by the antioxidant behavior of DR-LSCC, marked by their dysfunctional mitochondrial activity leading to an increased GLRX expression that consequently regulates intracellular hypoxia (HIF-1, nitroreductase).

As noted in lung cancer cells, the antioxidant gene of GLRX, a regulator of the HIF-1,[101] is associated with treatment resistance, in which their overexpression may result in treatment

failure.[102] Also, chemoresistance-associated mitochondrial oxidative phosphorylation[103–105] may implicate the oxidative stress and intracellular respiratory processes in DR-LSCC. From our transcriptomic findings, DR-LSCC showed upregulated MT-ND1 and downregulated mitochondrial-related genes including ATP5PO, ATP5F1B, CYC1, SDHA, NDUFA4, and COX6B1. In this case, increased GLRX expression and impaired mitochondrial activity may collectively regulate the oxidative and hypoxic behavior (i.e., increased HIF1A) exhibited by the resistant laryngeal cancer cells (**Figure 5-S11**).

In this study, the design of the tumor-on-a-chip remains simple with only two cell types of a heterogeneous laryngeal tumor. More complex models to include multiple cell types, mimicking local tumor microenvironment, will render these models more representative of in vivo tumor environment. Further advancement closely resembling the tumor microenvironment could include tumor-associated macrophages, known for being tumor scavenger/immunosuppressive cells. DTX was reported to promote monocyte polarization into the tumor-associated phenotype as part of acquiring DTX resistance.[106] A denser stroma,[42] i.e., denser collagen gel, could be used to represent the laryngeal tumor cores for the analysis of liposome/nanocarrier sequestration. Denser stroma of tumor microenvironment is considered as a prognostic biomarker of metastasis and treatment failure[107] in laryngeal cancer. By including tumor-associated macrophages and denser stroma into chip cultures, a more physiological-relevant *in vitro* models of laryngeal tumor chemoresistance can be achieved.

5.4 Conclusion

In sum, chemoresistance is an incalcitrant clinical challenge in laryngeal cancer treatment. A physiology-representative *in vitro* model is warranted to decipher critical molecular mechanisms associated with chemoresistance. We developed a chemoresistant laryngeal cancer cell model whose genotypic and phenotypic profiles were collaborated to those known in the literature as HNC and other cancer studies. This resistant cell model can be applied to help elucidate tumor-stromal interaction in chemoresistance and evaluate new drug strategies in the reduction of chemoresistance for laryngeal cancer.

5.5 Experimental Methods

Table 5-1. Key resources.

REAGENT	SOURCE	IDENTIFIER
Materials for transcriptomic and functional analysis		
RNeasy Micro Kit (50)	QIAGEN, Toronto, Canada	74004
TruSeq Stranded Total RNA kits	Illumina, San Diego, USA	20020597
Qubit RNA HS Assay	Thermo Fisher Scientific, Waltham, USA	Q32855
High sensitivity RNA screen tape	Agilent, Santa Clara, USA	5067-5579
qPCR Library quantification kit	Roche Diagnostics, Laval, Canada	7960140001
mTOR ELISA kit	Abcam, Cambridge, UK	ab279869
LDH assay kit	Abcam, Cambridge, UK	ab65393
ADP/ATP assay kit	Abcam, Cambridge, UK	ab83359
Autophagy kit	Abcam, Cambridge, UK	ab133075
MMP-3 Activity Assay Kit	Abcam, Cambridge, UK	ab118972
DAPI	Abcam, Cambridge, UK	ab228549
ALEXA647/EGFR	Abcam, Cambridge, UK	ab192982
ALEXA488/TUBIII	Abcam, Cambridge, UK	ab195879
ALEXA594/PI3KCA	Abcam, Cambridge, UK	ab282113
ALEXA647/p53	Abcam, Cambridge, UK	ab224942
ALEXA555/αSMA	Abcam, Cambridge, UK	ab202509
ALEXA647/Vim	Abcam, Cambridge, UK	ab194719
ALEXA488/CK5	Abcam, Cambridge, UK	ab193894
eFluor615/ki-67	Thermo Fisher Scientific, Waltham, USA	42-5698-82
ALEXA488/OCT3/4	Thermo Fisher Scientific, Waltham, USA	53-5841-82
LIVE/DEAD staining	Thermo Fisher Scientific, Waltham, USA	L3224
MTT assay	Thermo Fisher Scientific, Waltham, USA	V13154
ROS-ID® Hypoxia/Oxidative stress detection kit	Enzo life sciences, NY, USA	ENZ-51042-0125
DAPI	Abcam, Cambridge, UK	ab228549
Materials for cell culture experiments		
LSEC	ATCC, Manassas, USA	CRL-3342

Dermal Cell Basal Medium	ATCC, Manassas, USA	PCS-200-030
LSCC	MilliPore-Sigma, Burlington, USA	UM-SCC-17A
HVFF	University of Wisconsin-Madison	Thibeault Lab
Collagen I	Thermo Fisher Scientific, Waltham, USA	A1048301
Mucin 1 powder	MilliPore-Sigma, Burlington, USA	M3895
BEGradient Barrier Free	BEOnChip, Zaragoza, Spain	1000320
Pooled Human Plasma	Innovative Research Inc, Novi, USA	IPLAWBNAE50ML
8-chamber slides	Lab-Tek®II	154534
Docetaxel	MilliPore-Sigma, Burlington, USA	PHR1883
Metformin	MilliPore-Sigma, Burlington, USA	PHR1084
Materials for chitosome experiments		
Cholesterol	MilliPore-Sigma, Burlington, USA	C8667
DSPC	MilliPore-Sigma, Burlington, USA	850365P
DSPE-PEG2000	MilliPore-Sigma, Burlington, USA	880120P
Liss Rhod PE	MilliPore-Sigma, Burlington, USA	810150P
Pacific Hemostasis™ APTT	Thermo Fisher Scientific, Waltham, USA	100309
EQUIPMENT/SOFTWARE	**SOURCE**	**IDENTIFIER**
Zeiss Axiover3	Zeiss, Germany	Florescence microscope
Spectramax i3	Molecular Devices, San Jose, USA	Plate reader
LightCycler® 480	Roche Diagnostics, Laval, Canada	4729749001
DNA High Sensitivity LabChip	PerkinElmer, Waltham, USA	CLS760672
Tecnai G2 F20 200kV	Fei, Hillsboro, USA	TEM
Imaris version 9.5.1 Software	Bitplane, South Windsor, CT	Image processing software
BioRender	BioRender, Toronto, Canada	Scientific illustration software
GraphPad Prism version 9.5.1	GraphPad Software, San Diego, CA, USA	Scientific data analysis software

5.5.1 Cell Culture

Three cell lines were used for this study: (1) A non-chemoresistant human laryngeal cancer cell line (LSCC) isolated from primary laryngeal carcinoma located at the supraglottis in T2 or T3 stage assumable[108,109] of a 48-year-old female patient who did not benefit from radiotherapy; (2) a human immortalized vocal fold fibroblast cell line (HVFF)[110] representing stromal cells in the

laryngeal tumor; and (3) a human laryngeal epithelial cell line (LSEC) representing healthy laryngeal epithelia. LSCC and HVFF cell lines were grown in LSCC complete media consisting of high glucose DMEM, 10% FBS, 1% non-essential amino-acids and 1% enicillin/streptomycin in a humidified atmosphere of 5% CO_2 at 37°C. LSEC were grown in ATCC dermal cell basal media. After reaching 70-80% confluency in T-75, cells were cultured in fresh Free-FBS media for 1 day to synchronize cell cycle, and were then harvested using TrypLE for 5 to 15 min. After adding fresh media, cells were counted by a hemocytometer before being centrifuged at 900 rpm for 5 min. Media was discarded and cells were resuspended in fresh media with a working concentration of 1×10^6 cells/mL. Both HVFF and LSEC between passage 3 to 5 were used for this study.

5.5.2 Experimentally Inducing Cell Resistance to Docetaxel Drugs

LSCC were monthly exposed to escalating doses of DTX. LSCC were exposed to increasing doses (50nM, 100nm, 200nM and 400nM) for up to 4 months to induce the DTX-resistant phenotype on cancer cells. LSCC were exposed to DTX-enriched LSCC media for 3 days followed by a 3-day exposure of regular LSCC media. Experiments were performed on docetaxel-resistant LSCC (DR-LSCC) after the escalating 4-month exposure of DTX.

5.5.3 RNA-sequencing of Transcriptomic Profiles

RNA-sequencing analysis was performed at the McGill Genome Centre. Transcriptomic profiling was performed on three cell groups cultured in conventional 2D flat monolayers: (1) the docetaxel-resistant laryngeal cancer cells (DR-LSCCs), (2) non-treated laryngeal cancer cells (LSCCs), and (3) non-treated laryngeal epithelial cells (LSEC). The RNeasy® mini Kit was used to isolate and purify the RNA from cells according to the manufacturer's guidelines. Such an analysis was carried out on LoBind tubes containing isolated RNA. A total of 5 replicates per group x 3 cell groups = 15 in total, and 150M reads per sample were conducted. For initial RNA quality check, concentrations were measured using the Qubit RNA HS Assay. Then, the RNA integrity profile was verified using a High sensitivity RNA screen tape. RNA libraries were constructed using the TruSeq Stranded Total RNA from Illumina following the manufacturer's protocol. Library QC was measured by qPCR with the library quantification kit and LightCycler® 480 from Roche Diagnostics. Finally, the library profile was measured with a DNA High Sensitivity LabChip. Only

samples that met the RNA quantity and quality concentration of about 150ng/L were subjected to subsequent sequencing (**Table 5-S1**).

5.5.4 RNA-sequencing Data Analysis

RNA sequencing was processed using the TruSeq Stranded Total RNA With Illumina Ribo-Zero Plus rRNA Depletion workflow to obtain the LibQC results (**Table 5-S1**). Adaptor sequences and low quality score bases (Phred score < 30) were first trimmed using Trimmomatic.[111] The resulting reads were aligned to the GRCh38 human reference genome assembly, using STAR.[112] Read counts were obtained using HTSeq[113] with parameters -m intersection-nonempty-stranded=reverse. For all downstream analyses, we excluded lowly-expressed genes with an average read count lower than 10 across all samples. Raw counts were normalized using edgeR's TMM algorithm[114] and were then transformed to log2-counts per million (logCPM) using the voom function implemented in the limma R package.[115] To assess differences in gene expression levels, we fitted a linear model using limma's lmfit function. Nominal p-values were corrected for multiple testing using the Benjamini-Hochberg method. Gene set enrichment analysis (GSEA) based on pre-ranked gene list by t-statistic was performed using the R package fgsea (http://bioconductor.org/packages/fgsea/). In GSEA, scoring process was repeated 1000 times and *p*-value was determined by comparing how frequently the Enrichment score from the actual ranking surpassed that obtained from random permutations. Padj values were computed by evaluating the distribution of Normalized Enrichment Scores across numerous gene sets. KEGG pathway diagrams were generated using the visualization tools Pathview[116] and KEGGscape.[117] The RNA sequencing data generated in this study have been deposited to the National Center for Biotechnology Information Gene Expression Omnibus (GEO) with accession codes GSE248302.

5.5.5 Cell Cytotoxicity

Cell viability assay was performed on LSEC, LSCC, and DR-LSCC with approximately 1×10^4 cells seeded separately on 8-chamber slides. After reaching 100% confluency, 1μM DTX was added to the culture media in each of the slide's chambers. At Day 3, cells were washed with 1x PBS before being stained, using a LIVE/DEAD viability/cytotoxicity assay kit with green-fluorescent calcein-AM and red-fluorescent ethidium homodimer-1 dyes following the manufacturer's instructions. The slides were incubated for 30 min in darkness at room temperature

before being washed twice with 1x PBS. Zeiss Axiovert3 inverted fluorescence microscope with 10× objective was used to acquire cell images with FITC (LIVE, green) and Cy3 (DEAD, red/orange) filters.

MTT analyses were also carried out to obtain quantitative data on cell viability. For this assay, about 5×10^3 cells were seeded in individual 96 well plates following manufactures' guidelines. A Spectramax i3 plate reader was used to determine the absorbance of MTT at λ = 570 nm. Percentage of cell viability was calculated using equation (1).

$$\text{Cell viability}(\%) = \frac{(\text{Non-treated control}) - (\text{treated celss})}{\text{Non-treated control}} \times 100 \quad (1)$$

The therapeutic effect of MTF on cells was determined using LIVE/DEAD staining and MTT readouts to obtain qualitative and quantitative cell cytotoxicity data. First, the effect of MTF (500 µM, 1mM, 5mM and 10 mM) was assessed on HVFF, LSEC, LSCC and DR-LSCC after 3 days of exposure. Second, cytotoxic effect of the combination therapy MTF/DTX-loaded chitosomes were evaluated up to 7 days on the same groups and freeze-thawed DR-LSCC. Lastly, the morphology of the DTX-loaded chitosomes was examined by transmission electron microscopy using a FEI Tecnai G2 F20 Transmission Electron Microscope (TEM) at a voltage of 120 kV. The coagulation effect of DTX-loaded chitosomes was evaluated using the Activated Partial Thromboplastin Time (APTT) method[118] up to 15min exposure.

5.5.6 Autophagy Analysis

Autophagy analysis was performed on LSEC, LSCC, and DR-LSCC following similar experimental conditions as that of the cell cytotoxicity analysis described above. By following manufacturer's protocol, we discarded the media and added 100 µL of the Cell-Based Propidium Iodide solution in each well and cells were incubated for two minutes at room temperature. A washing step was proceeded with 100 µL of Cell-Based Assay Buffer. A 100 µL of the Cell-Based MDC solution was then added to each well and cells were incubated for ten minutes at 37°C. After another washing step, cells were imaged with a fluorescent microscopy at 63x magnification with Zeiss Axiovert3. 10µM tamoxifen was used as positive control. Dead cells were stained by propidium iodide and detected with a Texas Red filter. Autophagic vacuoles were stained by Monodansylcadaverine (MDC) and detected with a DAPI filter. Absorbance readouts were

conducted using the Spectramax i3 plate reader with UV-DAPI and Texas red wavelengths as specified by manufacturer guidelines.

5.5.7 Immunocytochemistry Analysis

DR-LSCC, LSCC, and LSEC were fixed with 4% paraformaldehyde in PBS for 10 min at room temperature. Then cells were blocked with 0.1% Triton X-100 in PBS (blocking solution) for 30 min at room temperature. Followed by blocking with 10% normal goat serum with 0.5% Triton X-100 in PBS (blocking solution) for 30min at room temperature. Fluorochrome-conjugated primary antibodies with a 1/150 ratio: ALEXA488/TUBIII, eFluor615/ki-67, ALEXA647/EGFR, ALEXA488/OCT3-4, ALEXA594/PI3KCA, ALEXA647/p53, ALEXA488/ECAD, ALEXA555/αSMA, and ALEXA647/Vim were diluted in blocking solution and incubated at 37°C for 1h. DAPI was applied for 10 min at room temperature. The cells were then imaged with 10x magnification using the Zeiss Axiover3 using filters corresponding to the conjugated antibody and retrieved using Imaris version 9.5.1 Software.

5.5.8 mTOR Enzyme-linked Immunosorbent Assay (ELISA)

Expression of pan-mTOR and phospho-mTOR was analyzed on DR-LSCC, LSCC, and LSEC, ELISA was used to quantify the intracellular mTOR expression. In brief, cells were washed with PBS, followed by adding the lysis buffer. Cells were solubilized at about 4 x 10^7 cells/mL in prepared Cell Lysate Buffer by gently pipetting up and down to resuspend the pellet. Lysates were incubated with shaking at 4°C for 30 minutes. Microcentrifuge at 13,000 rpm for 10 minutes at 4°C and transfer the supernatants into a clean test tube. Lysates were 80-fold diluted with Assay Diluent. We continued following manufacturer's guidelines and read at 450nm using the Spectramax i3 plate reader.

5.5.9 MMP3 Activity Assay

MMP3 Activity Assay was performed to measure MMP3 activity in cell culture media (secreted protein, 40-fold diluted) and cell lysates (intracellular protein, 100-fold diluted) from DR-LSCC, LSCC, and LSEC at 4 x 10^7 cells/mL. To directly measure MMP3 activity,[119] cells (1 x 10^6) were homogenized in 200 µL ice-cold MMP3 Assay Buffer then centrifuged to remove insoluble material at 13,000 x g for 10 minutes. Sample volumes of 50 µL/well were mixed with Assay

Buffer in a 96-well plate. After reacting with the MMP3 substrate (prepared according to the protocol), the plate was read at Ex/Em = 325/393 nm twice in 2h using the Spectramax i3 plate reader. Read R1 at T1. Read R2 again at T2 after incubating the reaction at room temperature for 60 min, protected from light. The RFU of fluorescence generated by hydrolyzation of the substrate is (2):

$$\Delta RFU = R2 - R1 \qquad (2)$$

5.5.10 ATP/ADP Assay

To evaluate metabolic activity, intracellular ATP/ADP ratios were measured via ATP and ADP assays. DR-LSCC, LSCC, and LSEC at 4 x 10^7 cells/mL were washed twice in cold PBS before harvesting and diluted 80-folds. Cells were resuspended and homogenized in 100 µL of Assay Buffer IV/ADP Assay Buffer. Then, cells were incubated on ice for 10 min. Samples were centrifuged for 5 minutes at 4°C at top speed to remove any insoluble material. Supernatant were collected and kept on ice. 50 µL of Reaction Mix was added to each standard, sample, and background control wells. Plate was incubated at room temperature for 30 minutes protected from light, followed by measuring the output using the Spectramax i3 plate reader at OD 570nm.

5.5.11 Clonogenic Assay

Colony formation was analyzed after exposure of DTX alone, DTX-loaded liposomes, and DTX-loaded chitosomes, LSCCs were seeded in 24 well-plates at a density of 15 × 10^3 and incubated until full confluency up to 7 days. After treatments, the culture medium was removed, and the cells were washed twice with PBS. Then, cells were stained with 0.1% crystal violet (water 30%, ethanol 70%) in sterile water (0.5 mL/well) for 30 min at room temperature. After thorough washing, the colonies were analyzed via images taken with a cellphone camera.

5.5.12 Microfluidic Analyses

The microfluidic device Gradient Barrier-Free from BEOnChip (Zaragoza, Spain) was used for this analysis because of the desired representation of hypoxic tumor models. The device comprised two lateral channels, referred to drug-media and cancer channels in this study, interconnected via a central chamber referred to as stromal chamber. For cell seeding, microfluidic devices were warmed at 37°C for 24 hours, to prevent massive bubble formation. HVFF were embedded in a

2mg/mL collagen I gel following the gel preparation protocol of the manufacturer. After encapsulating HVFF in the collagen I gel, 7 µL of HVFF-containing gel was injected into the central chamber (stromal chamber). The central chamber inlet and outlet were sealed with adhesive tape provided by the BEOnchip. After 4h, cancer channel was coated with 0.5 mg/mL oral mucin 1 solution to emulate a mucosal tumor as *in vivo*.[84] After 1h, one wash with culture media was performed before injecting 15 µL cancer cells into the mucin-coated lateral channels (cancer channel). Cancer channel inlet and outlet were also sealed with plugs to create a diffusion gradient. After 1h, culture media was infused in the remaining lateral channel (drug-media channel) at a 0.65 µL/min rate simulating interstitial flow using an Ismatec peristaltic pump (**Figure 5-S12, Video 5-S1**). The whole system was placed inside the Biosafety Cabinet to maintain sterile conditions.

5.5.13 Functional Verification of Tumor-on-a-Chip

5.5.13.1 Phenotypic Markers and Migration Assay

DR-LSCC and HVFF were expected to overexpress βIII-tubulin[13] and vimentin,[120] respectively. Phenotypic markers were evaluated at Day 0 that occurred 24h after seeding cells into the microfluidic device with immunostating of ALEXA488/TUBIII and ALEXA647/Vim. Migration of HVFFs into the cancer channel were assessed after 1, 3, and 5 days. Controls comprised 4h exposures of (1) 10 mM MTF to hinder hypoxia/proliferation and (2) 200 µM deferoxamine to induce hypoxia/proliferation, respectively. Cells were imaged by 40x magnification using the Zeiss Axiovert3 using ALEXA488 and ALEXA647 filters and retrieved using Imaris version 9.5.1 Software.

5.5.13.2 Hypoxia/ Oxidative Stress Assay

Nitroreductase activity in hypoxic cells was measured using a hypoxia detection kit. Briefly, DR-LSCC and HVFF microfluidic cultures were evaluated during Day 0 at 6, 12, and 24 h. Deferoxamine (200 µM, hypoxia inducer) and Pyocyanin (200 µM, oxidative stress inducer) were used as positive control after 4h exposure. Cells were washed twice with PBS, and incubated with the hypoxia/oxidative stress detection mix for 30 min. Next, detection mix was discarded, and cells were washed twice with PBS. Cells were imaged by 63x magnification using the Zeiss Axiovert3 with ALEXA488 and ALEXA594 filters and retrieved using Imaris version 9.5.1 Software.

5.5.14 Microfluidic Evaluation Combined MTF/DTX Strategy

The set up of the chemosensitivity study was to mimic a 12 min intra-arterial injection of chemotherapeutics[121,122] *in vitro*. A treatment of 1mM MTF was administered by 1-day continuously flowing in the drug-media microchannel. After the first 6h of MTF chemosensitizing infusion, 1μM DTX-loaded chitosomes (about 1×10^8 nanocarriers) or 1μM DTX were infused once for 12 min in the drug-media channel at 5μL/min to match the interstitial tumor injection rates.[123] Then, MTF was infused for the rest of the day, i.e., 18 hrs. Drug-free media was flown afterwards until the end point of the study.

Controls of 1mM MTF, 1μM DTX alone, and 1μM DTX-loaded chitosomes on DR-LSCC and HVFF were evaluated at Day 0 (100% confluent control) and time points for 1, 3, and 5 days in the co-culture setup. DAPI staining was used to image the cells after treatments at 10× magnification using the Zeiss Axiovert3 and Imaris version 9.5.1 Software. For cell counting, cell nuclei (10 μm) in two regions of interest (stromal chamber and cancer channel) were counted using the spot detection algorithm and DAPI mean fluorescence intensity. LIVE/DEAD staining was adapted from **Section 5.5.5** to evaluate the combination therapies (MTF/DTX, and MTF/DTX-loaded chitosomes) in the co-culture setup on Day 0 and 5. Zeiss Axiovert3 inverted fluorescence microscope with 40× objective was used to acquire cell images with FITC (LIVE, green) and Cy3 (DEAD, red/orange) filters.

In addition, LDH assay was performed to analyze cytotoxicity and verify the qualitative DAPI images. Supernatant was collected from drug-media outlets at 6, 12, 24, 60, 360 min after starting infusing nanoparticle (a 12-min injection). LDH percentages of cell viability were calculated using equation (1). To estimate drug retention within the microfluidic device, residual levels of nanoparticles and combination therapy MTF/DTX were measured in spent cell media. Nanoparticle retention was analyzed using the Nanosight NS300 nanoparticle tracking analyzer[124] whereas estimated drug retention of combined MTF/DTX was measured at OD 230nm (MTF OD = 233nm[125] and DTX OD = 230nm[13]). Moreover, fluorescent chitosomes uptake[13] after 6h inspection with the inverted microscope Zeiss Axiovert 3. DR-LSCC was anticipated to express EGFR considering that LSCC is known to stain positively with EGFR (ALEXA647/EGFR).[126,127] Considering the 24-hr co-culturing, HVFF was also expected to exhibit a transition to cancer-associated fibroblast phenotype with positive EGFR stain.[86,87] Cytokeratin 5 (ALEXA488/CK5)

is a squamous differentiation marker and is exclusively expressed on DR-LSCC.[128] Cytokeratin 5 would thus be used to differentiate DR-LSCC ($CK5^+$) from HVFF ($CK5^-$).

5.5.15 Statistical Analysis

The data are reported as mean ± SD. The statistical significance of the differences was analyzed by one-way or two-way ANOVA (all assumptions were met) and Tukey as post hoc test to assess difference between pair groups using GraphPad Prism version 9.5.1.

Data Availability Statement

The RNA-seq data generated in this study are available at the National Center for Biotechnology Information Gene Expression Omnibus (GEO) with accession codes GSE248302. All other included data in this study are available from the corresponding authors upon reasonable request.

Supporting Information

Supporting Information is available at **subsection 5.7**.

Acknowledgements

We thank our colleagues from both the Voice and Upper Airway Research laboratory and Biomat'X research laboratory for their support and advice. We appreciate the donation of the BEGradient Barrier Free microfluidic devices from BEOnChip (Zaragoza, Spain). We thank the contribution of Bryan Daniel Herrera Lozada for his help with the videos of the microfluidic device. We would also like to thank the McGill Facilities for Advanced BioImaging (ABIF), Applied Genomics Innovation Core (MAGIC), and Canadian Centre for Computational Genomics (C3G) Montréal Node.

Funding Support

This study was supported by the National Sciences and Engineering Research Council of Canada (RGPIN-2018–03843, RGPIN-2024-04235 and ALLRP 548623-19), Canada Research Chair research stipend (M.T. and N.Y.K.L.-J.) and the National Institutes of Health (R01 DC-018577-01A1). The presented content is solely the responsibility of the authors and does not necessarily represent the official views of the above funding agencies.

Conflict of interest

The authors declare no conflict of interest.

Author Contributions

C.R.M.-G.: conceptualization, data plotting, visualization, writing-original draft, and writing-reviewing and editing.

M.M: reviewing and editing.

A.P: data plotting, visualization, reviewing and editing.

N.S. reviewing and editing.

M.T.: conceptualization, visualization, writing-original draft, reviewing and editing, supervision, funding acquisition, and project administration.

N.Y.K.L.-J.: conceptualization, visualization, writing-original draft, writing-reviewing and editing, supervision, funding acquisition, and project administration.

5.6 References

1. Patterson RH, Fischman VG, Wasserman I, et al. Global Burden of Head and Neck Cancer: Economic Consequences, Health, and the Role of Surgery. *Otolaryngol - Head Neck Surg (United States)*. 2020;162(3):296-303. doi:10.1177/0194599819897265

2. Moya-Garcia CR, Okuyama H, Sadeghi N, Li J, Tabrizian M, Li-Jessen NYK. In vitro models for head and neck cancer : Current status and future perspective. *Front Oncol*. 2022;12:3691. doi:10.3389/fonc.2022.960340

3. Schutte HW, Heutink F, Wellenstein DJ, et al. Impact of Time to Diagnosis and Treatment in Head and Neck Cancer: A Systematic Review. *Otolaryngol - Head Neck Surg (United States)*. 2020;162(4):446-457. doi:10.1177/0194599820906387

4. Gulati S, Desai J, Palackdharry SM, et al. Phase 1 dose-finding study of metformin in combination with concurrent cisplatin and radiotherapy in patients with locally advanced head and neck squamous cell cancer. *Cancer*. 2020;126(2):354-362. doi:10.1002/cncr.32539

5. Schepens EJA, Al-Mamgani A, Karssemakers LHE, van den Broek D, van den Brekel MWM, Lopez-Yurda M. Squamous Cell Carcinoma Antigen in the Follow-up of Patients With

Head and Neck Cancer. *Otolaryngol - Head Neck Surg (United States)*. 2023. doi:10.1002/ohn.510

6. Haring CT, Kana LA, Dermody SM, et al. Patterns of recurrence in head and neck squamous cell carcinoma to inform personalized surveillance protocols. *Cancer*. 2023;129(18):2817-2827. doi:10.1002/cncr.34823

7. Lee MY, Belfiglio M, Zeng J, et al. Primary Total Laryngectomy versus Organ Preservation for Locally Advanced T3/T4a Laryngeal Cancer. *Laryngoscope*. 2023;133(5):1122-1131. doi:10.1002/lary.30254

8. Obid R, Redlich M, Tomeh C. The Treatment of Laryngeal Cancer. *Oral Maxillofac Surg Clin North Am*. 2019;31(1):1-11. doi:10.1016/j.coms.2018.09.001

9. Cramer JD, Burtness B, Le QT, Ferris RL. The changing therapeutic landscape of head and neck cancer. *Nat Rev Clin Oncol*. 2019;16(11):669-683. doi:10.1038/s41571-019-0227-z

10. Lin C, Cheng W, Liu X, Li H, Song Y. The global, regional, national burden of laryngeal cancer and its attributable risk factors (1990–2019) and predictions to 2035. *Eur J Cancer Care (Engl)*. 2022;31(6):1-10. doi:10.1111/ecc.13689

11. U.S. Food and Drug Administration. HIGHLIGHTS OF PRESCRIBING INFORMATION. Docetaxel Injection. https://www.accessdata.fda.gov/drugsatfda_docs/label/2021/022534s012lbl.pdf. Published 1996. Accessed February 15, 2024.

12. Gu Z, Yao Y, Yang G, et al. Pharmacogenomic landscape of head and neck squamous cell carcinoma informs precision oncology therapy. *Sci Transl Med*. 2022;14(661):eabo5987. doi:10.1126/scitranslmed.abo5987

13. Moya-Garcia CR, Li-jessen NYKL, Tabrizian M. Chitosomes Loaded with Docetaxel as a Promising Drug Delivery System to Laryngeal Cancer Cells : An In Vitro Cytotoxic Study. *Int J Mol Sci*. 2023;24(12):9902. doi:10.3390/ijms24129902

14. Sadeghi N, Khalife S, Mascarella MA, et al. Pathologic response to neoadjuvant chemotherapy in HPV-associated oropharynx cancer. *Head Neck*. 2020;42(3):417-425. doi:10.1002/hed.26022

15. Marquard FE, Jücker M. PI3K/AKT/mTOR signaling as a molecular target in head and neck cancer. *Biochem Pharmacol*. 2020;172:113729. doi:10.1016/j.bcp.2019.113729

16. Galstyan A, Cho J, Johnson DE, Grandis JR. Modulation of the PI3K/mTOR pathways. *Improv Ther Ratio Head Neck Cancer*. 2020:89-105. doi:10.1016/b978-0-12-817868-3.00005-6

17. Maloney SM, Hoover CA, Morejon-Lasso L V., Prosperi JR. Mechanisms of taxane resistance. *Cancers (Basel)*. 2020;12(11):1-57. doi:10.3390/cancers12113323

18. Das T, Anand U, Pandey SK, et al. Therapeutic strategies to overcome taxane resistance in cancer. *Drug Resist Updat*. 2021;55(February):100754. doi:10.1016/j.drup.2021.100754

19. Nienstedt JC, Gröbe A, Clauditz T, et al. High-level βIII-tubulin overexpression occurs in most head and neck cancers but is unrelated to clinical outcome. *J Oral Pathol Med*. 2017;46(10):986-990. doi:10.1111/jop.12607

20. Zheng HC. The molecular mechanisms of chemoresistance in cancers. *Oncotarget*. 2017;8(35):59950-59964. doi:10.18632/oncotarget.19048

21. Azharuddin M, Roberg K, Dhara AK, et al. Dissecting multi drug resistance in head and neck cancer cells using multicellular tumor spheroids. *Sci Rep*. 2019;9(1):1-12. doi:10.1038/s41598-019-56273-6

22. Kanno Y, Chen CY, Lee HL, Chiou JF, Chen YJ. Molecular Mechanisms of Chemotherapy Resistance in Head and Neck Cancers. *Front Oncol*. 2021;11(May):1-13. doi:10.3389/fonc.2021.640392

23. Izreig S, Hajek M, Edwards HA, et al. The role of vitamin D in head and neck cancer. *Laryngoscope Investig Otolaryngol*. 2020;5(6):1079-1088. doi:10.1002/lio2.469

24. Zeng Z, Zheng W, Hou P. The role of drug-metabolizing enzymes in synthetic lethality of cancer. *Pharmacol Ther*. 2022;240:108219. doi:10.1016/j.pharmthera.2022.108219

25. Zeljic K, Supic G, Stamenkovic Radak M, Jovic N, Kozomara R, Magic Z. Vitamin D receptor, CYP27B1 and CYP24A1 genes polymorphisms association with oral cancer risk and survival. *J Oral Pathol Med*. 2012;41(10):779-787. doi:10.1111/j.1600-0714.2012.01164.x

26. Kadioglu O, Saeed MEM, Munder M, Spuller A, Greten HJ, Efferth T. Effect of ABC transporter expression and mutational status on survival rates of cancer patients. *Biomed Pharmacother*. 2020;131:110718. doi:10.1016/j.biopha.2020.110718

27. Dai Y, Xie C-H, Neis JP, Fan C-Y, Vural E, Spring PM. MicroRNA EXPRESSION PROFILES OF HEAD AND NECK SQUAMOUS CELL CARCINOMA WITH DOCETAXEL-INDUCED MULTIDRUG RESISTANCE. *Head Neck*. 2011;36(6):786-791. doi:10.1002/hed.21540

28. Li Q, Tie Y, Alu A, Ma X, Shi H. Targeted therapy for head and neck cancer: signaling pathways and clinical studies. *Signal Transduct Target Ther*. 2023;8(1). doi:10.1038/s41392-022-01297-0

29. da Silva SD, Morand GB, Alobaid FA, et al. Epithelial-mesenchymal transition (EMT) markers have prognostic impact in multiple primary oral squamous cell carcinoma. *Clin Exp Metastasis*. 2015;32(1):55-63. doi:10.1007/s10585-014-9690-1

30. Doktorova H, Hrabeta J, Khalil MA, Eckschlager T. Hypoxia-induced chemoresistance in cancer cells: The role of not only HIF-1. *Biomed Pap*. 2015;159(2):166-177. doi:10.5507/bp.2015.025

31. Jawa Y, Yadav P, Gupta S, et al. Current Insights and Advancements in Head and Neck Cancer: Emerging Biomarkers and Therapeutics with Cues from Single Cell and 3D Model Omics Profiling. *Front Oncol*. 2021;11(August):1-31. doi:10.3389/fonc.2021.676948

32. Cheng H, Yang X, Si H, et al. Genomic and Transcriptomic Characterization Links Cell Lines with Aggressive Head and Neck Cancers. *Cell Rep*. 2018;25(5):1332-1345.e5. doi:10.1016/j.celrep.2018.10.007

33. dos Santos Guimarães I, Ladislau-Magescky T, Tessarollo NG, et al. Chemosensitizing effects of metformin on cisplatin- and paclitaxel-resistant ovarian cancer cell lines. *Pharmacol Reports*. 2018;70(3):409-417. doi:10.1016/j.pharep.2017.11.007

34. Fatehi-Agdam M, Vatankhah MA, Panahizadeh R, Jeddi F, Najafzadeh N. Efficacy of Metformin and Chemotherapeutic Agents on the Inhibition of Colony Formation and Shh/Gli1 Pathway: Metformin/Docetaxel Versus Metformin/5-Fluorouracil. *Drug Res (Stuttg)*. 2021;71(1):17-25. doi:10.1055/a-1248-9008

35. Zaidi S, Gandhi J, Joshi G, Smith NL, Khan SA. The anticancer potential of metformin on prostate cancer. *Prostate Cancer Prostatic Dis*. 2019;22(3):351-361. doi:10.1038/s41391-018-0085-2

36. Rêgo DF, Elias ST, Amato AA, Canto GDL, Guerra ENS. Anti-tumor effects of metformin on head and neck carcinoma cell lines: A systematic review. *Oncol Lett*. 2017;13(2):554-566. doi:10.3892/ol.2016.5526

37. Bouland C, Eynden X Vanden, Lalmand M, et al. Preventive and Therapeutic Effect of Metformin in Head and Neck Cancer : A Concise Review. *J Clin Med*. 2023;12(9):6195.

38. Gaertner F, Preissner S, Heiland M, Preissner R, Wüster J. Beneficial Effect of Metformin on the Five-Year Survival in about 40,000 Patients with Head and Neck Cancer. *Cancers (Basel)*. 2024;16(5):982.

39. Kemnade JO, Florez M, Sabichi A, et al. Phase I / II trial of metformin as a chemo-radiosensitizer in a head and neck cancer patient population. *Oral Oncol*. 2023;145(December 2022):106536. doi:10.1016/j.oraloncology.2023.106536

40. Siddappa G, Kulsum S, Ravindra DR, et al. Curcumin and metformin-mediated chemoprevention of oral cancer is associated with inhibition of cancer stem cells. *Mol Carcinog*. 2017;56(11):2446-2460. doi:10.1002/mc.22692

41. Barlak N, Sanli F, Capik O, et al. Metformin Treatment Sensitizes Human Laryngeal Cancer Cell Line Hep- 2 to 5-Fluorouracil. *Clin Cancer Drugs*. 2019;7(1):16-24. doi:10.2174/2212697x06666190906165309

42. de Lázaro I, Mooney DJ. Obstacles and opportunities in a forward vision for cancer nanomedicine. *Nat Mater*. 2021;20(11):1469-1479. doi:10.1038/s41563-021-01047-7

43. Li R, Ye L, Zhu Y, et al. Induction chemotherapy of modified docetaxel, cisplatin, 5-fluorouracil for laryngeal preservation in locally advanced hypopharyngeal squamous cell carcinoma. *Head Neck*. 2022;44(9):2018-2029. doi:10.1002/hed.27119

44. Heianna J, Makino W, Hirakawa H, et al. Therapeutic efficacy of selective intra-arterial chemoradiotherapy with docetaxel and nedaplatin for fixed bulky nodal disease in head and neck cancer of unknown primary. *Eur Arch Oto-Rhino-Laryngology*. 2022;279(6):3105-3113. doi:10.1007/s00405-021-07121-9

45. Bao YY, Zhong JT, Shen LF, et al. Effect of Glut-1 and HIF-1α double knockout by CRISPR/CAS9 on radiosensitivity in laryngeal carcinoma via the PI3K/Akt/mTOR pathway. *J Cell Mol Med*. 2022;26(10):2881-2894. doi:10.1111/jcmm.17303

46. Zhou L, Wu J, Sun Z, Wang W. Oxidation and Reduction Dual-Responsive Polymeric Prodrug Micelles Co-delivery Precisely Prescribed Paclitaxel and Honokiol for Laryngeal Carcinoma Combination Therapy. *Front Pharmacol*. 2022;13(July):1-12. doi:10.3389/fphar.2022.934632

47. Ingber DE. Human organs-on-chips for disease modelling, drug development and personalized medicine. *Nat Rev Genet*. 2022;0123456789. doi:10.1038/s41576-022-00466-9

48. Pillai S, Kwan JC, Yaziji F, Yu H, Tran SD. Mapping the Potential of Microfluidics in Early Diagnosis and Personalized Treatment of Head and Neck Cancers. *Cancers (Basel)*. 2023;15(15). doi:10.3390/cancers15153894

49. You K, Parikh P, Khandalavala K, et al. Moderate hyperoxia induces senescence in developing human lung fibroblasts. *Am J Physiol Lung Cell Mol Physiol*. 2019;317:L525-L536.

50. Farah CS. Molecular landscape of head and neck cancer and implications for therapy. *Ann Transl Med*. 2021;9(10):915-915. doi:10.21037/atm-20-6264

51. Jin Y, Qin X. Comprehensive analysis of transcriptome data for identifying biomarkers and therapeutic targets in head and neck squamous cell carcinoma. *Ann Transl Med*. 2020;8(6):282-282. doi:10.21037/atm.2020.03.30

52. Zhang L, Peng M. Integrated bioinformatic analysis identified a novel prognostic pan-programmed cell death signature for bladder cancer. *Front Immunol*. 2022;13(November):1-16. doi:10.3389/fimmu.2022.1030097

53. Shah PA, Huang C, Li Q, et al. NOTCH1 Signaling in Head and Neck Squamous Cell Carcinoma. *Cells*. 2020;9(12). doi:10.3390/cells9122677

54. Zhang D, Peng Y, Lin G, et al. TGF-βRII / EP300 /Smad4 cascade signaling pathway promotes invasion and glycolysis in oral squamous cell carcinoma . *J Oral Pathol Med*. 2023;(January):1-10. doi:10.1111/jop.13424

55. Chakraborty B, Basu M, Mukhopadhyay D, et al. Differential promoter usages of PTCH1 and down regulation of HHIP are associated with HNSCC progression. *Pathol Res Pract*. 2022;232(February):153827. doi:10.1016/j.prp.2022.153827

56. Nagai T, Ikeda M, Chiba S, Kanno SI, Mizuno K. Furry promotes acetylation of microtubules in the mitotic spindle by inhibition of SIRT2 tubulin deacetylase. *J Cell Sci*. 2013;126(19):4369-4380. doi:10.1242/jcs.127209

57. Kang X, Chen Y, Yi B, et al. An integrative microenvironment approach for laryngeal carcinoma: The role of immune/methylation/autophagy signatures on disease clinical prognosis and single-cell genotypes. *J Cancer*. 2021;12(14):4148-4171. doi:10.7150/JCA.58076

58. Mastronikolis NS, Spyropoulou D, Kyrodimos E, et al. The interplay between tumor and nodal microenvironments for the formation of nodal premetastatic niche in head and neck cancer. *Am J Physiol - Cell Physiol*. 2023;325(6):C1516-C1531. doi:10.1152/ajpcell.00337.2023

59. Melchardt T, Hufnagl C, Magnes T, et al. CYP39A1 polymorphism is associated with toxicity during intensive induction chemotherapy in patients with advanced head and neck cancer. *BMC Cancer*. 2015;15(1):1-7. doi:10.1186/s12885-015-1776-x

60. Choudhary A, Anitha P, Balachander K, Girija ASS, Paramasivam. A, Vijayshree Priyadharsini J. Aberrations in genes coding for cytochrome P450 family 2 and its putative association with HNSCC. *J Surv Fish Sci*. 2023;10(1S):538-553.

61. Morgan ET, Skubic C, Lee C, Cokan KB, Rozman D. Regulation of cytochrome P450 enzyme activity and expression by nitric oxide in the context of inflammatory disease. *Drug Metab Rev*. 2020;52(4):455-471. doi:10.1080/03602532.2020.1817061.Regulation

62. Lian M, Shi Q, Fang J, et al. In vivo gene expression profiling for chemosensitivity to docetaxel-cisplatin-5-FU (TPF) triplet regimen in laryngeal squamous cell carcinoma and the effect of TPF treatment on related gene expression in vitro. *Acta Otolaryngol*. 2017;137(7):765-772. doi:10.1080/00016489.2016.1272001

63. Chen X, Chen S, Yu D. Metabolic reprogramming of chemoresistant cancer cells and the potential significance of metabolic regulation in the reversal of cancer chemoresistance. *Metabolites*. 2020;10(7):1-15. doi:10.3390/metabo10070289

64. Bredell MG, Ernst J, El-Kochairi I, Dahlem Y, Ikenberg K, Schumann DM. Current relevance of hypoxia in head and neck cancer. *Oncotarget*. 2016;7(31):50781-50804. doi:10.18632/oncotarget.9549

65. Yazdani J, Ghavimi MA, Jabbari Hagh E, Ahmadpour F. The Role of E-Cadherin as a Prognostic Biomarker in Head and Neck Squamous Carcinoma: A Systematic Review and Meta-Analysis. *Mol Diagnosis Ther*. 2018;22(5):523-535. doi:10.1007/s40291-018-0351-y

66. Cui D, Qu R, Liu D, Xiong X, Liang T, Zhao Y. The Cross Talk Between p53 and mTOR Pathways in Response to Physiological and Genotoxic Stresses. *Front Cell Dev Biol*. 2021;9(November):1-11. doi:10.3389/fcell.2021.775507

67. Xie W, Yu J, Yin Y, Zhang X, Zheng X, Wang X. OCT4 Promotes Ovarian Cancer Progression by Regulating the PI3K / AKT / mTOR Pathway. 2021. doi:10.21203/rs.3.rs-1055810/v1

68. Peltanova B, Liskova M, Gumulec J, et al. Sensitivity to cisplatin in head and neck cancer cells is significantly affected by patient-derived cancer-associated fibroblasts. *Int J Mol Sci*. 2021;22(4):1-13. doi:10.3390/ijms22041912

69. Park SS, Lee YK, Choi YW, et al. Cellular senescence is associated with the spatial evolution toward a higher metastatic phenotype in colorectal cancer. *Cell Rep*. 2024;43(3):113912. doi:10.1016/j.celrep.2024.113912

70. Xiao S, Qin D, Hou X, et al. Cellular senescence: a double-edged sword in cancer therapy. *Front Oncol*. 2023;13(September):1-10. doi:10.3389/fonc.2023.1189015

71. Niklander SE, Aránguiz P, Faunes F, Martínez-Flores R. Aging and oral squamous cell carcinoma development: the role of cellular senescence. *Front Oral Heal*. 2023;4(October). doi:10.3389/froh.2023.1285276

72. Zhang Q, Zhang Y, Chen Y, Qian J, Zhang X, Yu K. A Novel mTORC1/2 Inhibitor (MTI-31) inhibits tumor growth, epithelial-mesenchymal transition, metastases, and improves antitumor immunity in preclinical models of lung cancer. *Clin Cancer Res*. 2019;25(12):3630-3642. doi:10.1158/1078-0432.CCR-18-2548

73. Ashrafizadeh M, Mirzaei S, Hashemi F, et al. New insight towards development of paclitaxel and docetaxel resistance in cancer cells: EMT as a novel molecular mechanism and

therapeutic possibilities. *Biomed Pharmacother*. 2021;141:111824. doi:10.1016/j.biopha.2021.111824

74. Chamarthy S, Angirekula HS, Kutala VK, Mekala JR. *Phospholipase Signaling Network in Cancer Metastasis and Chemoresistance*. Vol 2. Elsevier Inc.; 2023. doi:10.1016/b978-0-323-95696-3.00015-6

75. Ozdemir Kutbay N, Biray Avci C, Sarer Yurekli B, et al. Effects of metformin and pioglitazone combination on apoptosis and AMPK/mTOR signaling pathway in human anaplastic thyroid cancer cells. *J Biochem Mol Toxicol*. 2020;34(10):1-11. doi:10.1002/jbt.22547

76. Goul C, Peruzzo R, Zoncu R. The molecular basis of nutrient sensing and signalling by mTORC1 in metabolism regulation and disease. *Nat Rev Mol Cell Biol*. 2023;24(12):857-875. doi:10.1038/s41580-023-00641-8

77. Sang Y, Kong P, Zhang S, et al. SGK1 in Human Cancer: Emerging Roles and Mechanisms. *Front Oncol*. 2021;10(January):1-17. doi:10.3389/fonc.2020.608722

78. Curry JM, Johnson J, Mollaee M, et al. Metformin clinical trial in HPV+ and HPV-head and neck squamous cell carcinoma: Impact on cancer cell apoptosis and immune infiltrate. *Front Oncol*. 2018;8(OCT):1-8. doi:10.3389/fonc.2018.00436

79. Akbari Dilmaghani N, Safaroghli-Azar A, Pourbagheri-Sigaroodi A, Bashash D. The PI3K/Akt/mTORC signaling axis in head and neck squamous cell carcinoma: Possibilities for therapeutic interventions either as single agents or in combination with conventional therapies. *IUBMB Life*. 2021;73(4):618-642. doi:10.1002/iub.2446

80. Zamame Ramirez JA, Romagnoli GG, Kaneno R. Inhibiting autophagy to prevent drug resistance and improve anti-tumor therapy. *Life Sci*. 2021;265(November 2020):118745. doi:10.1016/j.lfs.2020.118745

81. Mayer MJ, Klotz LH, Venkateswaran V. Evaluating Metformin as a Potential Chemosensitizing Agent when Combined with Docetaxel Chemotherapy in Castration-resistant Prostate Cancer Cells. *Anticancer Res*. 2017;37(12):6601-6607. doi:10.21873/anticanres.12117

82. Farley JH, Brady WE, O'Malley D, et al. A phase II evaluation of temsirolimus with carboplatin and paclitaxel followed by temsirolimus consolidation in clear cell ovarian cancer: An NRG oncology trial. *Gynecol Oncol*. 2022;167(3):423-428. doi:10.1016/j.ygyno.2022.10.006

83. Sarkar S, Sahoo PK, Mahata S, et al. Mitotic checkpoint defects: en route to cancer and drug resistance. *Chromosom Res*. 2021;29(2):131-144. doi:10.1007/s10577-020-09646-x

84. Reynolds IS, Fichtner M, McNamara DA, Kay EW, Prehn JHM, Burke JP. Mucin glycoproteins block apoptosis; promote invasion, proliferation, and migration; and cause chemoresistance through diverse pathways in epithelial cancers. *Cancer Metastasis Rev*. 2019;38(1-2):237-257. doi:10.1007/s10555-019-09781-w

85. Mostafavi S, Zalpoor H, Hassan ZM. The promising therapeutic effects of metformin on metabolic reprogramming of cancer-associated fibroblasts in solid tumors. *Cell Mol Biol Lett*. 2022;27(1). doi:10.1186/s11658-022-00356-2

86. Alsahafi E, Begg K, Amelio I, et al. Clinical update on head and neck cancer: molecular biology and ongoing challenges. *Cell Death Dis*. 2019;10(8). doi:10.1038/s41419-019-1769-9

87. Su L, Wu S, Huang C, et al. Chemoresistant fibroblasts dictate neoadjuvant chemotherapeutic response of head and neck cancer via TGFα-EGFR paracrine signaling. *npj Precis Oncol*. 2023;7(1):1-17. doi:10.1038/s41698-023-00460-2

88. Mosca L, Ilari A, Fazi F, Assaraf YG, Colotti G. Taxanes in cancer treatment: Activity, chemoresistance and its overcoming. *Drug Resist Updat*. 2021;54(November 2020):100742. doi:10.1016/j.drup.2020.100742

89. Wang S, Han L, Li J, Liu Y, Wang S. Inflammatory molecules facilitate the development of docetaxel-resistant prostate cancer cells in vitro and in vivo. *Fundam Clin Pharmacol*. 2022;36(5):837-849. doi:10.1111/fcp.12773

90. Liu Z, Zhu G, Getzenberg RH, Veltri RW. The upregulation of PI3K/Akt and MAP kinase pathways is associated with resistance of microtubule-targeting drugs in prostate cancer. *J Cell Biochem*. 2015;116(7):1341-1349. doi:10.1002/jcb.25091

91. Yin H, Qin H, Yang L, et al. circCYP24A1 promotes Docetaxel resistance in prostate Cancer by Upregulating ALDH1A3. *Biomark Res*. 2022;10(1):1-20. doi:10.1186/s40364-022-00393-1

92. Qin Y, Ashrafizadeh M, Mongiardini V, et al. Autophagy and cancer drug resistance in dialogue: Pre-clinical and clinical evidence. *Cancer Lett*. 2023;570(June). doi:10.1016/j.canlet.2023.216307

93. Ramírez-Cosmes A, Reyes-Jiménez E, Zertuche-Martínez C, et al. The implications of ABCC3 in cancer drug resistance: can we use it as a therapeutic target? *Am J Cancer Res*. 2021;11(9):4127-4140. http://www.ncbi.nlm.nih.gov/pubmed/34659880%0Ahttp://www.pubmedcentral.nih.gov/articlerender.fcgi?artid=PMC8493376.

94. Sipaul F, Birchall M, Corfield A. What role do mucins have in the development of laryngeal squamous cell carcinoma? A systematic review. *Eur Arch Oto-Rhino-Laryngology*. 2011;268(8):1109-1117. doi:10.1007/s00405-011-1617-8

95. Jonckheere N, Vincent A, Neve B, Van Seuningen I. Mucin expression, epigenetic regulation and patient survival: A toolkit of prognostic biomarkers in epithelial cancers. *Biochim Biophys Acta - Rev Cancer*. 2021;1876(1):188538. doi:10.1016/j.bbcan.2021.188538

96. Collado-González M, Espinosa YG, Goycoolea FM. Interaction between Chitosan and Mucin: Fundamentals and applications. *Biomimetics*. 2019;4(2):1-20. doi:10.3390/biomimetics4020032

97. Wang X, Qiu Y, Wang M, et al. Endocytosis and organelle targeting of nanomedicines in cancer therapy. *Int J Nanomedicine*. 2020;15:9447-9467. doi:10.2147/IJN.S274289

98. Chitty JL, Skhinas JN, Filipe EC, et al. The Mini-Organo: A rapid high-throughput 3D coculture organotypic assay for oncology screening and drug development. *Cancer Rep*. 2020;3(1):1-15. doi:10.1002/cnr2.1209

99. Sarwar M, Syed Khaja AS, Aleskandarany M, et al. The role of PIP5K1α/pAKT and targeted inhibition of growth of subtypes of breast cancer using PIP5K1α inhibitor. *Oncogene*. 2019;38(3):375-389. doi:10.1038/s41388-018-0438-2

100. D'Aiuto N, Hochmann J, Millán M, et al. Hypoxia, acidification and oxidative stress in cells cultured at large distances from an oxygen source. *Sci Rep*. 2022;12(1):1-9. doi:10.1038/s41598-022-26205-y

101. Matsui R, Ferran B, Oh A, et al. Redox regulation via glutaredoxin-1 and protein S-glutathionylation. *Antioxid Redox Signal*. 2020;32(10):677-700. doi:10.1089/ars.2019.7963

102. Wang L, Liu J, Liu J, et al. GLRX inhibition enhances the effects of geftinib in EGFR-TKI-resistant NSCLC cells through FoxM1 signaling pathway. *J Cancer Res Clin Oncol*. 2019;145(4):861-872. doi:10.1007/s00432-019-02845-y

103. Guerra F, Arbini AA, Moro L. Mitochondria and cancer chemoresistance. *Biochim Biophys Acta - Bioenerg*. 2017;1858(8):686-699. doi:10.1016/j.bbabio.2017.01.012

104. do Carmo Greier M, Runge A, Dudas J, et al. Mitochondrial dysfunction and epithelial to mesenchymal transition in head neck cancer cell lines. *Sci Rep*. 2022;12(1):1-9. doi:10.1038/s41598-022-16829-5

105. Frederick M, Skinner HD, Kazi SA, Sikora AG, Sandulache VC. High expression of oxidative phosphorylation genes predicts improved survival in squamous cell carcinomas of the head and neck and lung. *Sci Rep*. 2020;10(1):1-14. doi:10.1038/s41598-020-63448-z

106. Gupta, R., Kadhim, M.M., Jalil, A.T., Alasheqi, M.Q., Alsaikhan, F., Mukhamedova, N.K., Ramírez-Coronel, A.A., Jawhar, Z.H., Ramaiah, P. and Najafi M. The interactions of docetaxel with tumor microenvironment. *Int Immunopharmacol*. 2023;119:110214.

107. Alessandrini L, Ferrari M, Taboni S, et al. Tumor-stroma ratio, neoangiogenesis and prognosis in laryngeal carcinoma. A pilot study on preoperative biopsies and matched surgical specimens. *Oral Oncol*. 2022;132(June):105982. doi:10.1016/j.oraloncology.2022.105982

108. Carey TE, Bradford CR, Schwartz DR, et al. Characterization of Human Laryngeal Primary and Metastatic Squamous Cell Carcinoma Cell Lines UM-SCC-17A and UM-SCC-17B. *Cancer Res*. 1989;49(21):6098-6107.

109. Brenner JC, Graham MP, Kumar B, et al. GENOTYPING OF 73 UM-SCC HEAD AND NECK SQUAMOUS CELL CARCINOMA CELL LINES. *Head Neck*. 2010;32(4):417-426.

110. Chen X, Thibeault SL. Novel isolation and biochemical characterization of immortalized fibroblasts for tissue engineering vocal fold lamina propria. *Tissue Eng - Part C Methods*. 2009;15(2):201-212. doi:10.1089/ten.tec.2008.0390

111. Bolger AM, Lohse M, Usadel B. Trimmomatic: A flexible trimmer for Illumina sequence data. *Bioinformatics*. 2014;30(15):2114-2120. doi:10.1093/bioinformatics/btu170

112. Dobin A, Davis CA, Schlesinger F, et al. STAR: Ultrafast universal RNA-seq aligner. *Bioinformatics*. 2013;29(1):15-21. doi:10.1093/bioinformatics/bts635

113. Anders S, Pyl PT, Huber W. HTSeq-A Python framework to work with high-throughput sequencing data. *Bioinformatics*. 2015;31(2):166-169. doi:10.1093/bioinformatics/btu638

114. Robinson MD, McCarthy DJ, Smyth GK. edgeR: A Bioconductor package for differential expression analysis of digital gene expression data. *Bioinformatics*. 2009;26(1):139-140. doi:10.1093/bioinformatics/btp616

115. Ritchie ME, Phipson B, Wu D, et al. Limma powers differential expression analyses for RNA-sequencing and microarray studies. *Nucleic Acids Res*. 2015;43(7):e47. doi:10.1093/nar/gkv007

116. Luo W, Pant G, Bhavnasi YK, Blanchard SG, Brouwer C. Pathview Web: User friendly pathway visualization and data integration. *Nucleic Acids Res*. 2017;45(W1):W501-W508. doi:10.1093/nar/gkx372

117. Nishida K, Ono K, Kanaya S, Takahashi K. KEGGscape: A Cytoscape app for pathway data integration. *F1000Research*. 2014;3:1-10. doi:10.12688/f1000research.4524.1

118. Lira AL, Mina N, Bonturi CR, et al. Anionic Ultrasmall Gold Nanoparticles Bind to Coagulation Factors and Disturb Normal Hemostatic Balance. *Chem Res Toxicol*. 2022;35(9):1558-1569. doi:10.1021/acs.chemrestox.2c00190

119. Deng Y, Miki Y, Nakanishi A. Estradiol/GPER affects the integrity of mammary duct-like structures in vitro. *Sci Rep*. 2020;10(1):1-15. doi:10.1038/s41598-020-57819-9

120. Chu Y, Fang Y, Wu H, Cheng L, Chen J. Establishment and characterization of immortalized human vocal fold fibroblast cell lines. *Biotechnol Lett*. 2023;45(3):347-355. doi:10.1007/s10529-023-03350-6

121. Aigner KR, Selak E, Aigner K. Short-term intra-arterial infusion chemotherapy for head and neck cancer patients maintaining quality of life. *J Cancer Res Clin Oncol*. 2019;145(1):261-268. doi:10.1007/s00432-018-2784-4

122. Yabuuchi H, Kuroiwa T, Tajima T, Tomita K, Ochiai N, Kawamoto K. Efficacy of intra-arterial infusion therapy using a combination of cisplatin and docetaxel for recurrent head and neck cancers compared with cisplatin alone. *Clin Oncol*. 2003;15(8):467-472. doi:10.1016/j.clon.2003.07.003

123. Yang Y, Zhan W. Role of Tissue Hydraulic Permeability in Convection-Enhanced Delivery of Nanoparticle-Encapsulated Chemotherapy Drugs to Brain Tumour. *Pharm Res*. 2022;39(5):877-892. doi:10.1007/s11095-022-03261-7

124. Paun RA, Dumut DC, Centorame A, et al. One-Step Synthesis of Nanoliposomal Copper Diethyldithiocarbamate and Its Assessment for Cancer Therapy. *Pharmaceutics*. 2022;14(3):640.

125. Lal JS, Radha D, Devaky KS. Drug release studies of metformin hydrochloride from chitosan - Mango leaf extract microspheres. *J Drug Deliv Sci Technol*. 2023;84(April):104524. doi:10.1016/j.jddst.2023.104524

126. Ren K, Wang B, Qi Q. Development of a new EGFR antibody antagonist which exhibits potential biological effects against laryngeal cancer. *Ann Transl Med*. 2021;9(12):964-964. doi:10.21037/atm-21-1839

127. Tuo H, Li X, Du H, et al. FOLR1-stabilized β-catenin promotes laryngeal carcinoma progression through EGFR/AKT/GSK-3β pathway. *Mol Carcinog*. 2024;63(1):34-44. doi:10.1002/mc.23634

128. Samuels TL, Zimmermann MT, Zeighami A, et al. RNA Sequencing Reveals Cancer-Associated Changes in Laryngeal Cells Exposed to Non-Acid Pepsin. *Laryngoscope*. 2021;131(1):121-129. doi:10.1002/lary.28636

5.7 Supplementary Information

Table 5-S1. RNA quality and quantity of DR-LCC, LSCC, and LSEC.

Sample Name	Conc. (ng/ul)	Volume (ul)	Total (ng)	Plate coor.	Conc.(ng/ul) dil. 1/5	Conc. (ng/ul)	Volume (ul)	Total RNA (ng)	RIN
DR-LSCC1	176.2	15	2643	A01	12.3	61.5	13	799.5	7.9
DR-LSCC2	268.8	15	4032	B01	38	190	13	2470	6.3
DR-LSCC3	172.3	15	2585	C01	10.6	53	13	689	8.6
DR-LSCC4	175.8	15	2637	D01	37.2	186	13	2418	8.2
DR-LSCC5	167.5	15	2513	E01	41.8	209	13	2717	8.5
LSCC1	475.6	15	7134	F01	61.6	308	13	4004	8.5
LSCC2	461	15	6911	G01	78.6	393	13	5109	8.4
LSCC3	471	15	7064	H01	82.6	413	13	5369	8.9
LSCC4	466	15	6984	A02	75.4	377	13	4901	8.6
LSCC5	471	15	7068	B02	83.6	418	13	5434	8.6
LSEC1	204	15	3065	C02	55.2	276	13	3588	8.3
LSEC2	191	15	2858	D02	51.8	259	13	3367	8.3
LSEC3	201	15	3012	E02	44.8	224	13	2912	8.2
LSEC4	185	15	2778	F02	46.8	234	13	3042	8
LSEC5	166	15	2487	G02	40.8	204	13	2652	9

Table 5-S2. Transcriptomic-related altered biological functions associated with docetaxel resistance. Adjusted p-values (P_{adj}) were based on gene set enrichment analysis (Section 5.4. RNA-sequencing Data Analysis).

OUR DATA (LSCC vs. DR-LSCC)			LITERATURE		
Altered function	**Gene**	**Mutation Padj**	**Cancer**	**Chemoresistance Promotion**	**Ref.**
Drug efflux	ABBC3	Upregulated 4.53E-06	Pancreatic cancer cell lines PC3, DU145, and murine pancreatic cancer cells	PI3K/Akt pathway	1
Mucous barrier/ glycosylation	MUC1	Upregulated 0.0006312	Pancreatic cancer cell lines LNCaP, PC3, and DU145, and xenografts mice models	AR, and cancer stemness pathways	2
	MUCL1	Upregulated 3.54E-08	Not available	Not available	Not available
	MUC2	Upregulated 0.003701156	Patient-derived breast cancer xenograft mice model	Metastasis pathway	3
	MUC4	Upregulated 5.02E-05	Not available	Not available	Not available
	MUC5AC	Upregulated 1.55E-06	Gastric cancer clinical samples, in-house cell line, and mice models	Cancer stemness pathways	4
	MUC17	Upregulated 0.000135	Not available	Not available	Not available
	MUC15	Downregulated 0.0814225	Not available	Not available	Not available
Endocytosis	PIP5K1A	Upregulated 4.55E-07	Breast cancer cell line MDA-MB-231, and mice xenograft tumors	PI3K/Akt pathway	5
	UBR3	Upregulated 0.000112078	Not available	Not available	Not available
	FOLR1	Upregulated 0.004237585	Prostate cancer cell lines PC3; C4-2 B and LNCaP	ABC transporters	6
	CAV1	Downregulated 2.52E-10	Breast cancer cell lines BT474, Hs578T, and MDA-MB-468	Multidrug resistance and apoptosis pathways	7
Mitosis	TUBB3	Upregulated 2.65E-10	Tongue squamous cell carcinoma HSC-3 cells	PI3K/Akt pathway	8
	ALK	Upregulated 5.15E-05	Non-small Cell Lung Cancer Patients	EML4-ALK fusion gene	9
	FRY	Downregulated 0.008727047	Not available	Not available	Not available
	KNL1	Downregulated 2.72E-15	Breast cancer cell line MDA-MB-231, and mice xenografts models	Spindle assembly checkpoint kinase TTK	10

Receptors	PDGFR	Upregulated 0.001021801	Human HNSCC of the oropharynx (11A) and larynx (14C)	Platelet-derived growth factor receptor α, β. Angiogenic and cytokines pathways	11
	NOTCH1	Upregulated 0.000739924	Tongue squamous cell carcinoma CAL27 Pharynx squamous cell carcinoma FaDu	NOTCH pathway participates in EMT	12
Metabolism	PIK3CA	Upregulated 0.006980052	Pancreatic cancer DU145 human cell lines	PI3K/Akt/mTOR pathway	13
	DEPTOR	Upregulated 4.06E-10	Esophageal squamous cell carcinoma patients, and cell lines TE-1, TE-13, EC109, KYSE510	IRS1/PI3K/Akt/mTOR pathway	14
	CASTOR1	Upregulated 9.73E-09	Not available	Not available	Not available
	GSK3B	Upregulated 1.11E-05	Human breast cancer cell lines MDA-MB-231, and MCF-7	GSK-3β/β-Catenin Signaling Pathway	15
	CYP24A1	Upregulated 1.58E-07	Pancreatic cancer patients, and HEK293T, DU145 and 22Rv1 cell lines	PI3K/AKT/mTOR pathway	16
	IRS1	Downregulated 5.28E-16	Not available	Not available	Not available
	SGK1	Downregulated 5.63E-12	Not available	Not available	Not available
Hypoxia	HIF1A	Upregulated 3.44E-05	Human breast cancer patients, and cell lines MB-231 and MB-468	HIF-1α/miR-494/Survivin signaling pathway	17
Apoptosis	NTRK1	Upregulated 2.77E-06	Not available	Not available	Not available
	MDM2	Upregulated 2.64E-09	Mice-derived prostatic carcinoma cells	Apoptosis and EMT pathway	18
	TP53	Downregulated 5.29E-08	Non-small cell lung cancer A549, H460 and H1355 cells, and mice xenografts models	Apoptosis pathway	19
	TNFRS11A	Downregulated 6.19E-07	Lung adenocarcinoma H1299 and A549 cell lines	mTOR pathway and correlation with GPI gene expression	20
	BCL2	Downregulated 7.64E-11	Prostate cancer cell lines PC-3	Apoptosis pathway	21
Cytokine production	STAT1	Upregulated 2.06E-08	Colon carcinoma cell lines HCT116, DLD1, MCF7, SKOV-3 hTERT-BJ	Interferon-related genes	22
	IL6	Upregulated 1.79E-05	Prostate cancer PC3 cell line	STAT pathway	23
	CSF2RA	Upregulated 1.07E-08	Pharynx carcinoma-monocyte coculture FaDu–THP 1 coculture	Autophagy/IL-1β-associated pathways	24
Autophagy	CFLAR-AS1	Upregulated 0.000536234	Not available	Not available	Not available
	ATG13	Upregulated 6.57E-09	Not available	Not available	Not available

	ULK1	Upregulated 4.75E-06	Not available	Not available	Not available
Metastasis	SLC16A1	Downregulated 0.005262002	Not available	Not available	Not available
	COL4A1	Downregulated 3.28E-07	Ovarian cancer cell line NCI/ADR-RES	MAPK–Akt, Wnt, and Notch pathways	25

References

1. Wang S, Han L, Li J, Liu Y, Wang S. Inflammatory molecules facilitate the development of docetaxel-resistant prostate cancer cells in vitro and in vivo. *Fundam Clin Pharmacol*. 2022;36(5):837-849. doi:10.1111/fcp.12773

2. Wong N, Major P, Kapoor A, et al. Amplification of MUC1 in prostate cancer metastasis and CRPC development. *Oncotarget*. 2016;7(50):83115-83133. doi:10.18632/oncotarget.13073

3. Astashchanka A, Shroka TM, Jacobsen BM. Mucin 2 (MUC2) modulates the aggressiveness of breast cancer. *Breast Cancer Res Treat*. 2019;173(2):289-299. doi:10.1007/s10549-018-4989-2

4. Fujita T, Chiwaki F, Takahashi RU, et al. Identification and characterization of CXCR4-positive gastric cancer stem cells. *PLoS One*. 2015;10(6):1-19. doi:10.1371/journal.pone.0130808

5. Sarwar M, Syed Khaja AS, Aleskandarany M, et al. The role of PIP5K1α/pAKT and targeted inhibition of growth of subtypes of breast cancer using PIP5K1α inhibitor. *Oncogene*. 2019;38(3):375-389. doi:10.1038/s41388-018-0438-2

6. Singh SK, Lillard JW, Singh R. Reversal of drug resistance by planetary ball milled (PBM) nanoparticle loaded with resveratrol and docetaxel in prostate cancer. *Cancer Lett*. 2018;427:49-62. doi:10.1016/j.canlet.2018.04.017

7. Jung H, Kim D, Kang YY, Kim H, Lee JB, Mok H. CpG incorporated DNA microparticles for elevated immune stimulation for antigen presenting cells. *RSC Adv*. 2018;8(12):6608-6615. doi:10.1039/c7ra13293j

8. Cui J, Wang H, Zhang X, Sun X, Zhang J, Ma J. Exosomal miR-200c suppresses chemoresistance of docetaxel in tongue squamous cell carcinoma by suppressing TUBB3 and PPP2R1B. *Aging (Albany NY)*. 2020;12(8):6756-6773. doi:10.18632/AGING.103036

9. Morodomi Y, Takenoyama M, Inamasu E, et al. Non-small cell lung cancer patients with EML4-ALK fusion gene are insensitive to cytotoxic chemotherapy. *Anticancer Res*. 2014;34(7):3825-3830.

10. Maia ARR, De Man J, Boon U, et al. Inhibition of the spindle assembly checkpoint kinase TTK enhances the efficacy of docetaxel in a triple-negative breast cancer model. *Ann Oncol*. 2015;26(10):2180-2192. doi:10.1093/annonc/mdv293

11. Aderhold, C., Umbreit, C., Faber, A., Sauter, A., Sommer, J.U., Birk, R., Erben, P., Hofheinz, R.D., Stern-Straeter, J., Hoermann, K. and Schultz J. Chemotherapeutic Alteration of VEGF, PDGF and PDGFRα/β Expression Under 5-FU vs. Docetaxel in HPV-transformed Squamous Cell Carcinoma Compared To HPV-negative HNSCC In Vitro. *Oncol ReportsAnticancer Res*. 2013;33(5):1951-1961. doi:10.3892/or.2011.1499

12. Zhao ZL, Zhang L, Huang CF, et al. NOTCH1 inhibition enhances the efficacy of conventional chemotherapeutic agents by targeting head neck cancer stem cell. *Sci Rep*. 2016;6(March):1-12. doi:10.1038/srep24704

13. Liu Z, Zhu G, Getzenberg RH, Veltri RW. The upregulation of PI3K/Akt and MAP kinase pathways is associated with resistance of microtubule-targeting drugs in prostate cancer. *J Cell Biochem*. 2015;116(7):1341-1349. doi:10.1002/jcb.25091

14. Dong X, Wang L, Han Z, Zhou L, Shan L, Ding Y. Different functions of DEPTOR in modulating sensitivity to chemotherapy for esophageal squamous cell carcinoma. *Exp Cell Res*. 2017;353(1):35-45. doi:10.1016/j.yexcr.2017.03.003

15. Zhang X, Zhong S, Xu Y, et al. MicroRNA-3646 contributes to docetaxel resistance in human breast cancer cells by GSK-3β/β-catenin signaling pathway. *PLoS One*. 2016;11(4):1-14. doi:10.1371/journal.pone.0153194

16. Yin H, Qin H, Yang L, et al. circCYP24A1 promotes Docetaxel resistance in prostate Cancer by Upregulating ALDH1A3. *Biomark Res*. 2022;10(1):1-20. doi:10.1186/s40364-022-00393-1

17. Li H, Su X, Li J, et al. Hypoxia induces docetaxel resistance in triple-negative breast cancer via the HIF-1α/miR-494/Survivin signaling pathway. *Neoplasia (United States)*. 2022;32(C):100821. doi:10.1016/j.neo.2022.100821

18. Slabáková E, Kharaishvili G, Smejová M, et al. Opposite regulation of MDM2 and MDMX expression in acquisition of mesenchymal phenotype in benign and cancer cells. *Oncotarget*. 2015;6(34):36156-36171. doi:10.18632/oncotarget.5392

19. Kuo WT, Tu DG, Chiu LY, Sheu GT, Wu MF. High pemetrexed sensitivity of docetaxel-resistant A549 cells is mediated by TP53 status and downregulated thymidylate synthase. *Oncol Rep*. 2017;38(5):2787-2795. doi:10.3892/or.2017.5951

20. Yang Z, Zhu J, Yang T, et al. Comprehensive analysis of the lncRNAs-related immune gene signatures and their correlation with immunotherapy in lung adenocarcinoma. *Br J Cancer*. 2023;129(9):1397-1408. doi:10.1038/s41416-023-02379-8

21. Cao W, Shiverick KT, Namiki K, et al. Docetaxel and bortezomib downregulate Bcl-2 and sensitize PC-3-Bcl-2 expressing prostate cancer cells to irradiation. *World J Urol*. 2008;26(5):509-516. doi:10.1007/s00345-008-0289-5

22. Kolosenko I, Fryknäs M, Forsberg S, et al. Cell crowding induces interferon regulatory factor 9, which confers resistance to chemotherapeutic drugs. *Int J Cancer*. 2015;136(4):E51-E61. doi:10.1002/ijc.29161

23. Mahon KL, Lin HM, Castillo L, et al. Cytokine profiling of docetaxel-resistant castration-resistant prostate cancer. *Br J Cancer*. 2015;112(8):1340-1348. doi:10.1038/bjc.2015.74

24. Hsieh CY, Lin CC, Huang YW, et al. Macrophage secretory IL-1β promotes docetaxel resistance in head and neck squamous carcinoma via SOD2/CATICAM1 signaling. *JCI Insight*. 2022;7(23):1-19. doi:10.1172/jci.insight.157285

25. Vert A, Castro J, Ribó M, Vilanova M, Benito A. Transcriptional profiling of NCI/ADR-RES cells unveils a complex network of signaling pathways and molecular mechanisms of drug resistance. *Onco Targets Ther*. 2018;11:221-237. doi:10.2147/OTT.S154378

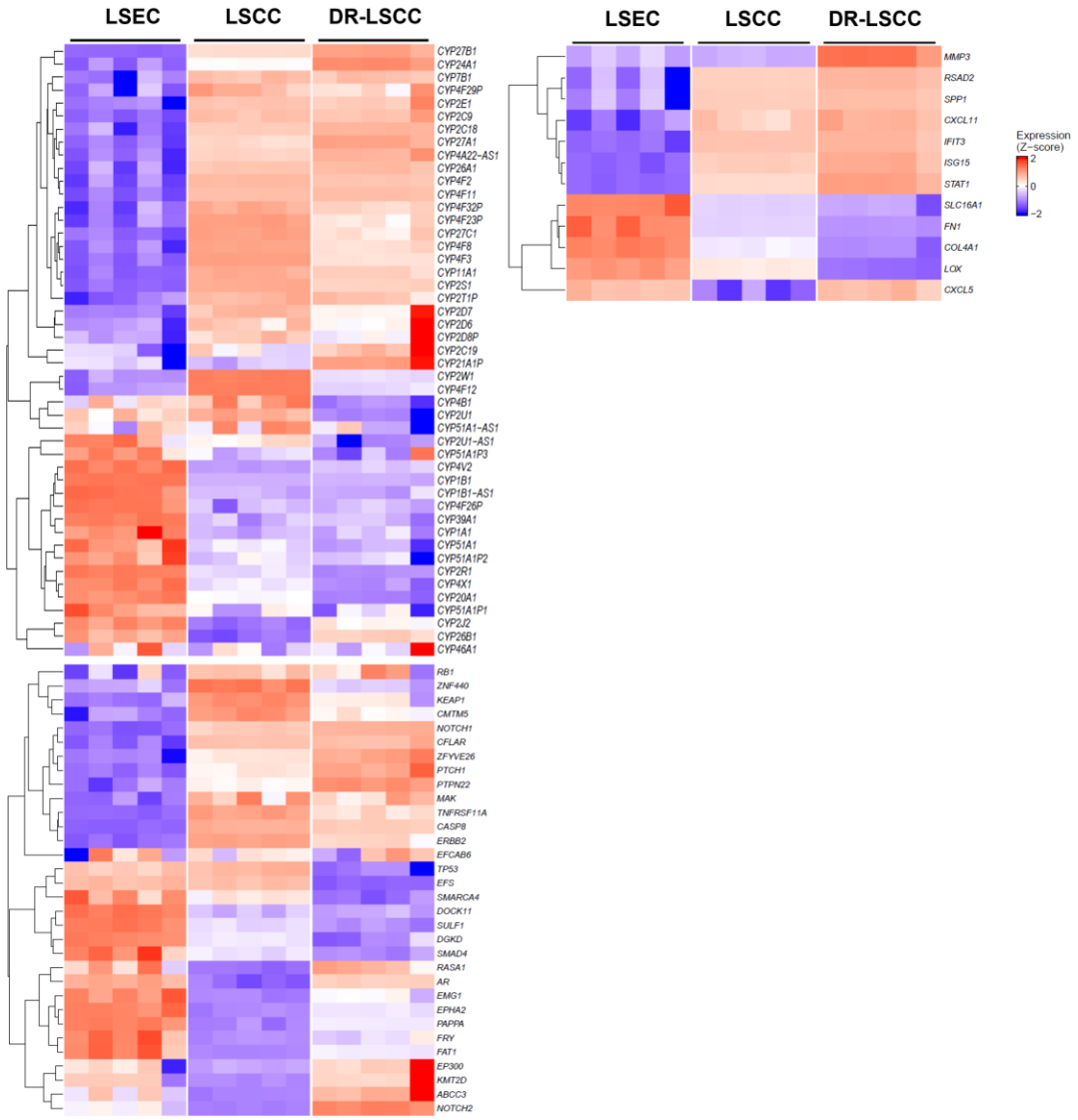

Figure 5-S1. Heatmap of specific differences on drug metabolism (CYP family), HNC biomarkers, oncogenes, and tumor suppressors wit Z-score (-2 to 2). Red = upregulation, Blue = downregulation.

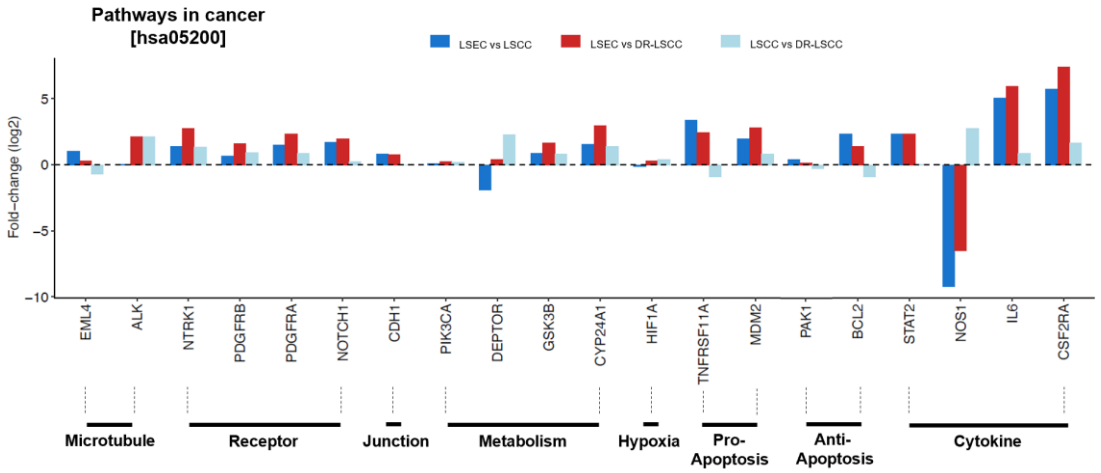

Figure 5-S2. Genes of interest from cancer pathway [hsa05200]. Blue = LSEC vs. LSCC; Red = LSEC vs. DR-LSCC; Light blue = LSCC vs DR-LSCC. Bars represent fold changes in gene expression (log 2).

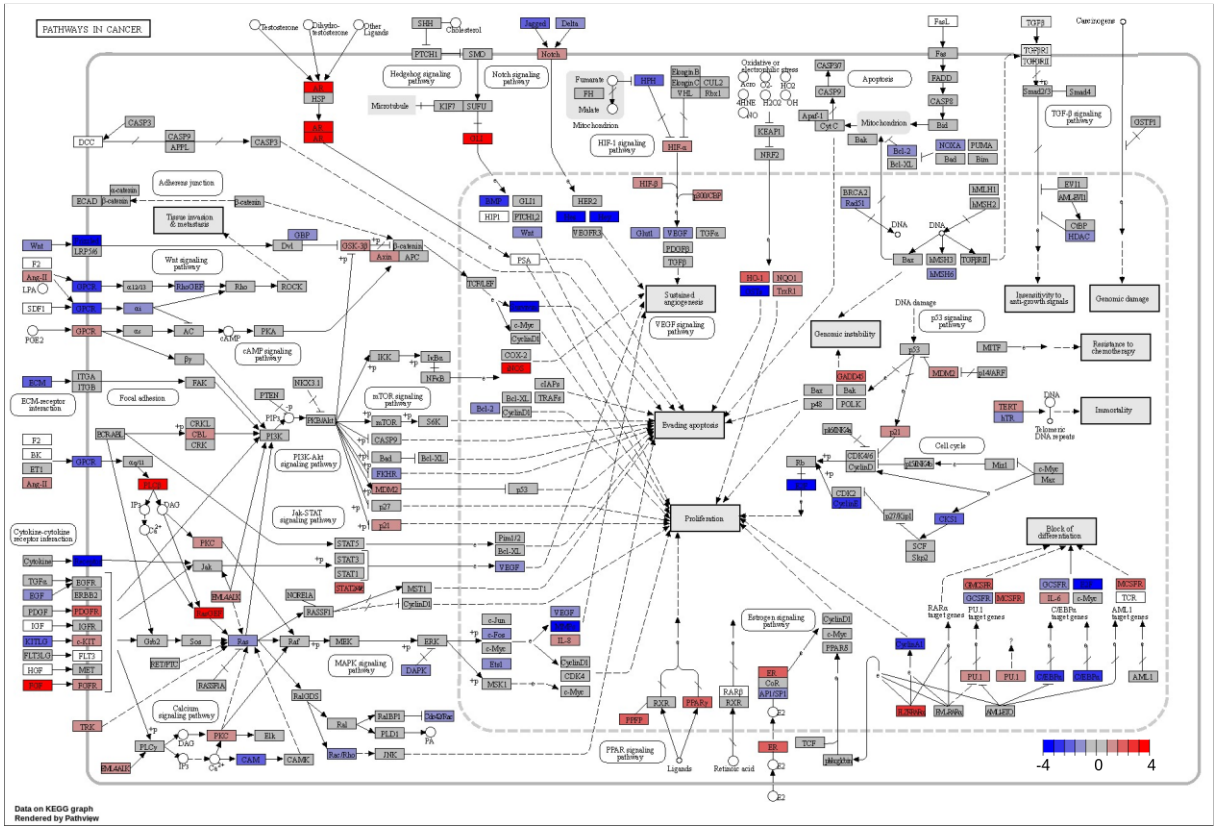

Figure 5-S3. Cancer pathway [hsa05200] LSCC vs DR-LSCC. Red = upregulation, Blue = downregulation. Color represents fold changes in gene expression.

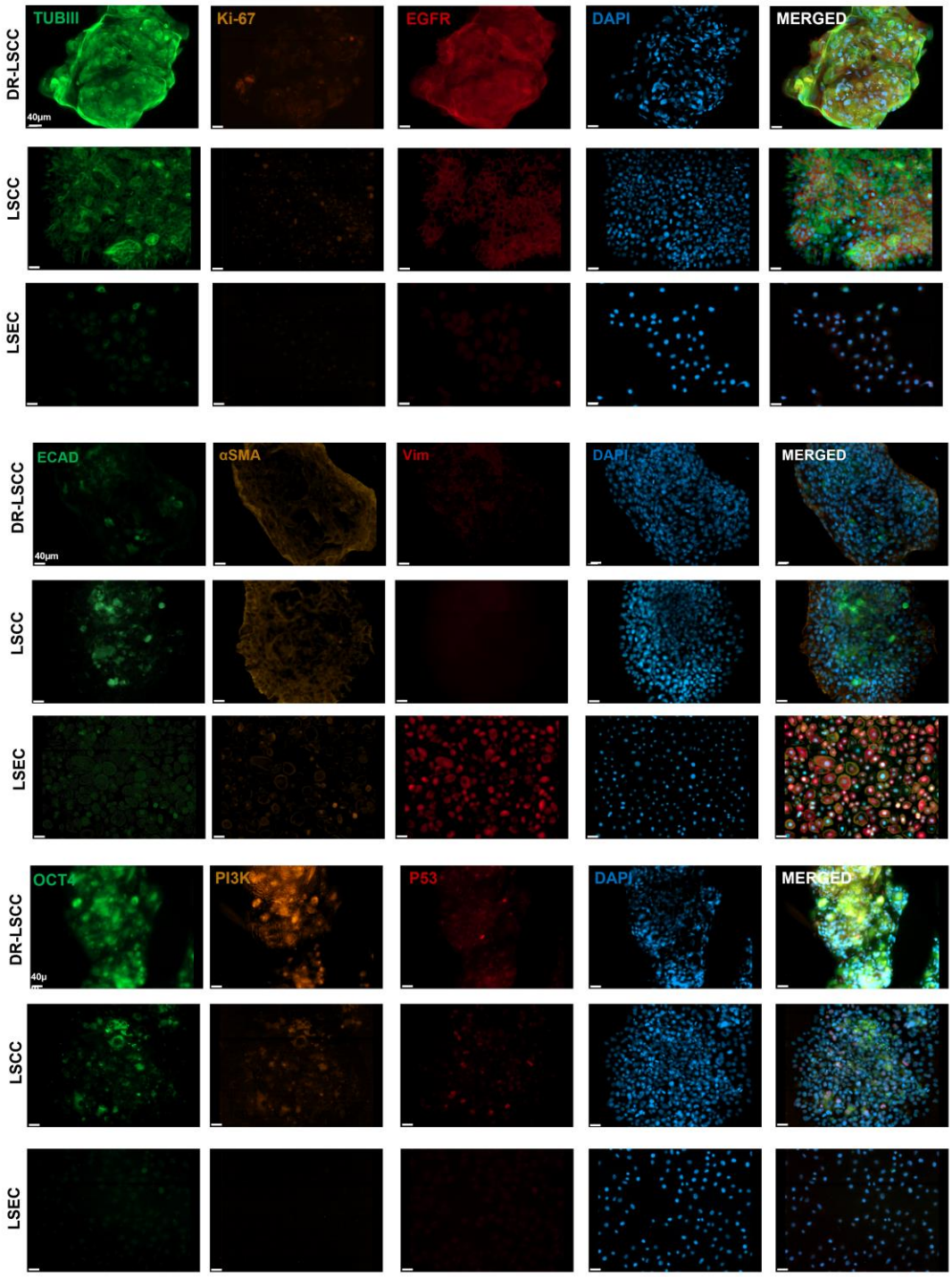

Figure 5-S4. Chemoresistance marker expressions of LSEC, LSCC, and DR-LSCC was carried out via the staining of βIII-tubulin (referred as TUBIII), ki-67, EGFR, vimentin, E-Cadherin, α-Smooth Muscle Actin, PI3KCA, P53, and Oct-4. Scale bar = 40 μm.

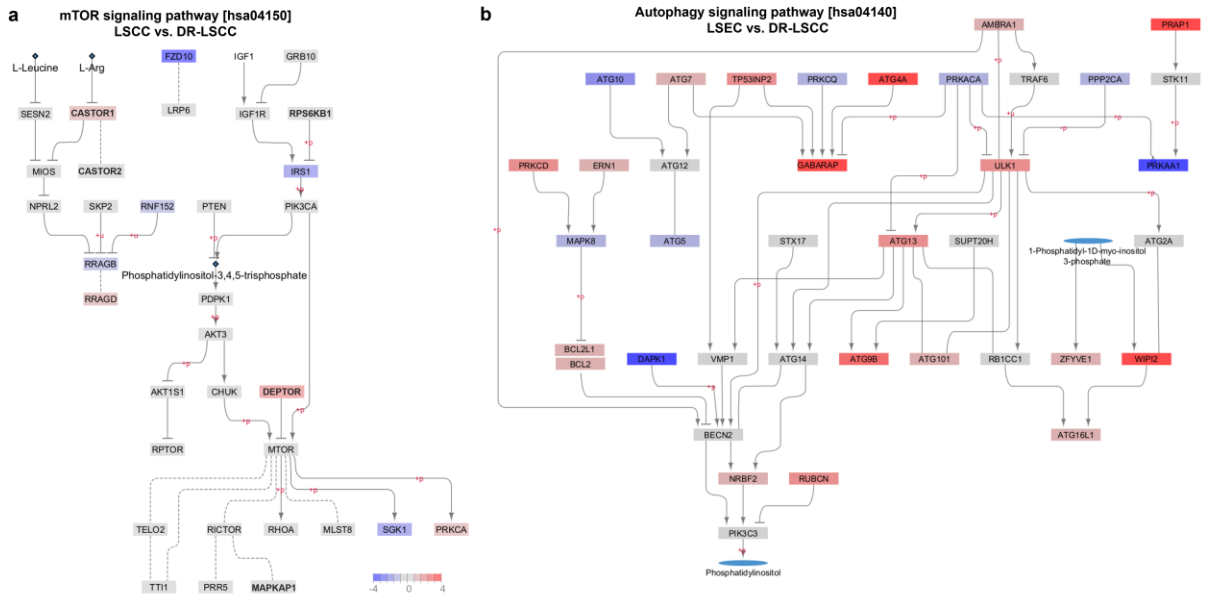

Figure 5-S5. Simplified KEGG signaling pathways. (a) Representative LSCC vs. DR-LSCC mTOR pathway [hsa04150], and LSEC vs. DR-LSCC autophagy pathway [hsa4140]. Color bar of fold-change (-4 to 4). Red = upregulation; Blue = downregulation.

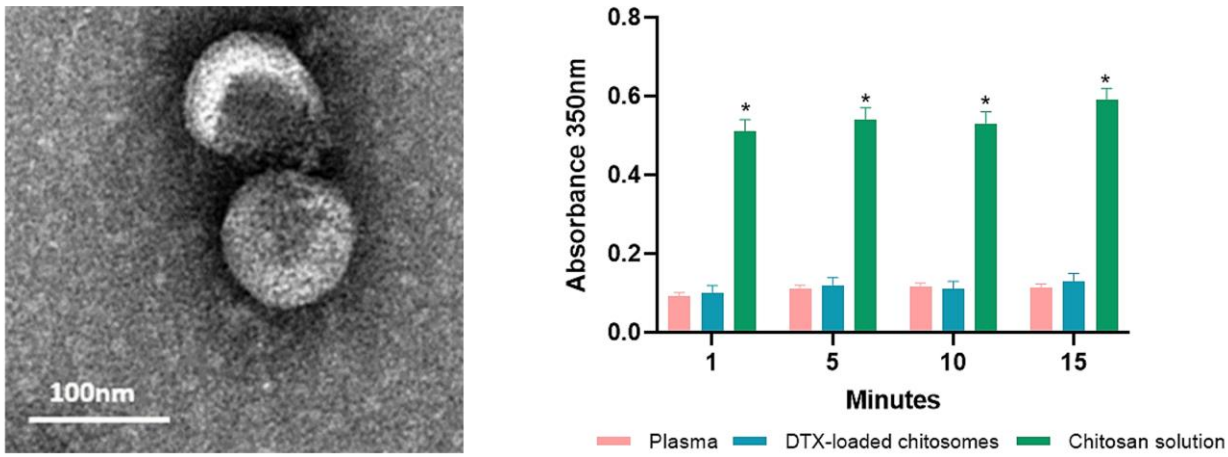

Figure 5-S6. Transmission electron images of the DTX-loaded chitosomes along with ATPP coagulation assay. DTX-loaded chitosomes showed absence of coagulation effect in comparison to 6mg/mL chitosan solution. Analyzed groups comprised APTT reagent added to (1) human plasma, (2) human plasma/DTX-loaded chitosomes, and (3) human plasma/chitosan solution. * $p < 0.05$.

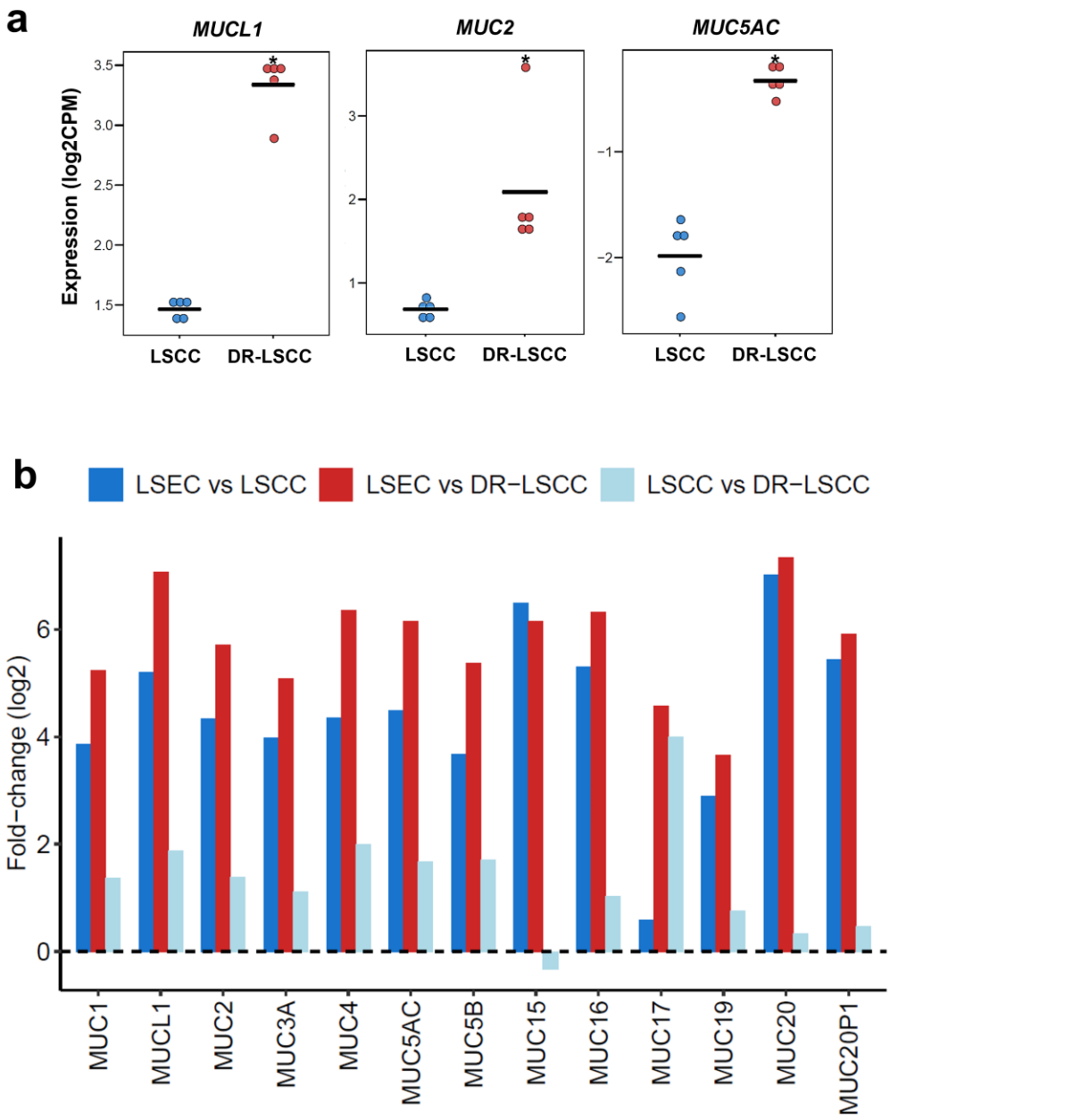

Figure 5-S7. Mucin-related genes. (a) Representative upregulated mucin-associated genes LSCC vs. DR-LSCC. (b) Genes of interest from the mucin pathway. Blue = LSEC vs. LSCC; Red = LSEC vs. DR-LSCC; Light blue = LSCC vs DR-LSCC. Bars represent fold changes in gene expression (log 2). * $p < 0.05$.

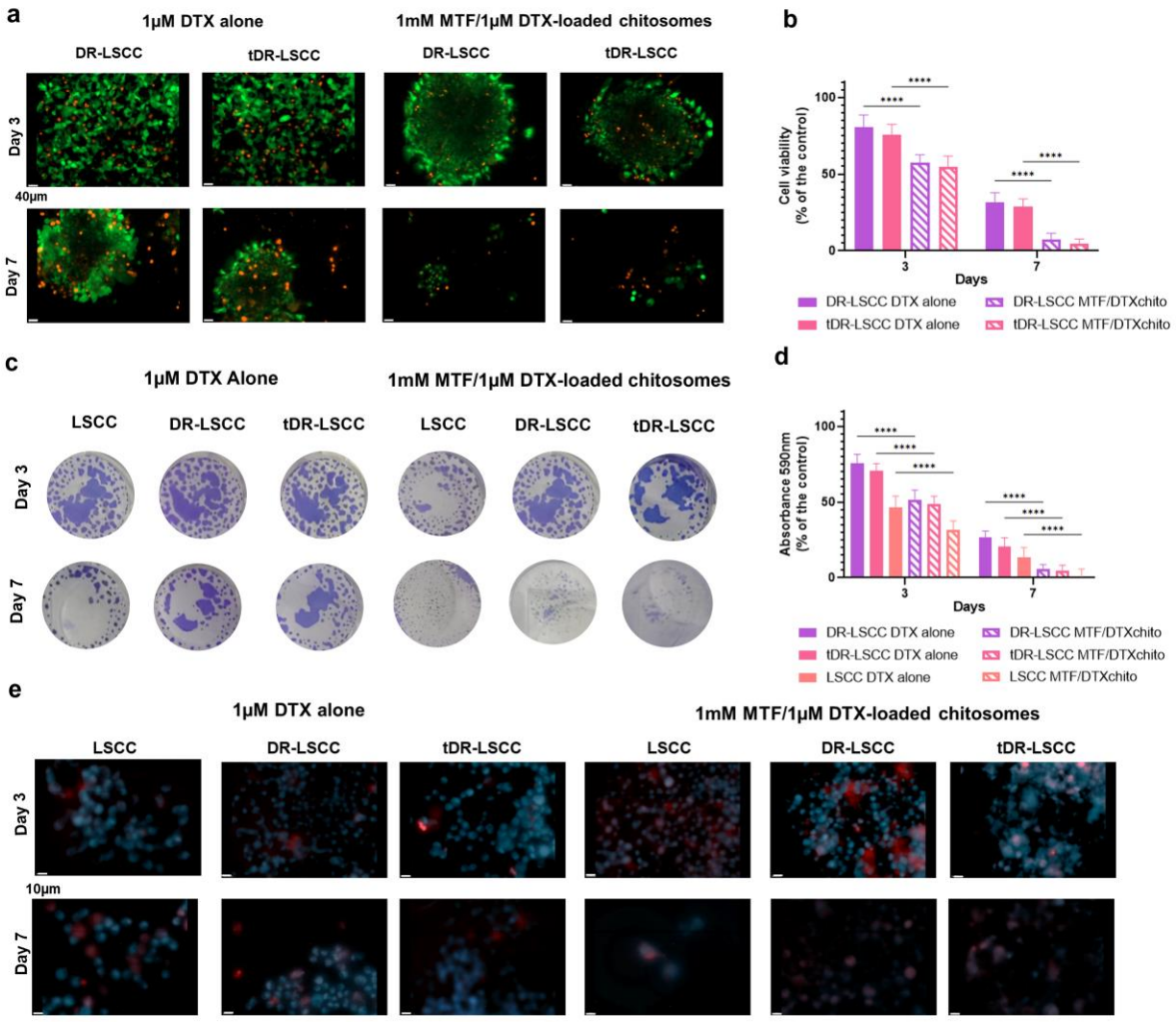

Figure 5-S8. Combined metformin/docetaxel treatment with resistant laryngeal cancer cells after a single freeze/thaw cycle. Cytotoxic evaluation via (a) LIVE/DEAD staining. Green = live cells; Orange = dead cells. Scale bar = 40μm (b) MTT cytotoxic analysis. DR-LSCC data from Figure 8c was included for cell viability comparisons. (c-d) Clonogenic studies, and (e) Autophagy studies on laryngeal cancer cells with scale bar = 10μm. Blue = autophagy activity; Red = dead cells. * $p < 0.05$, **** $p < 0.0001$. tDR-LSCC = thawed DR-LSCC.

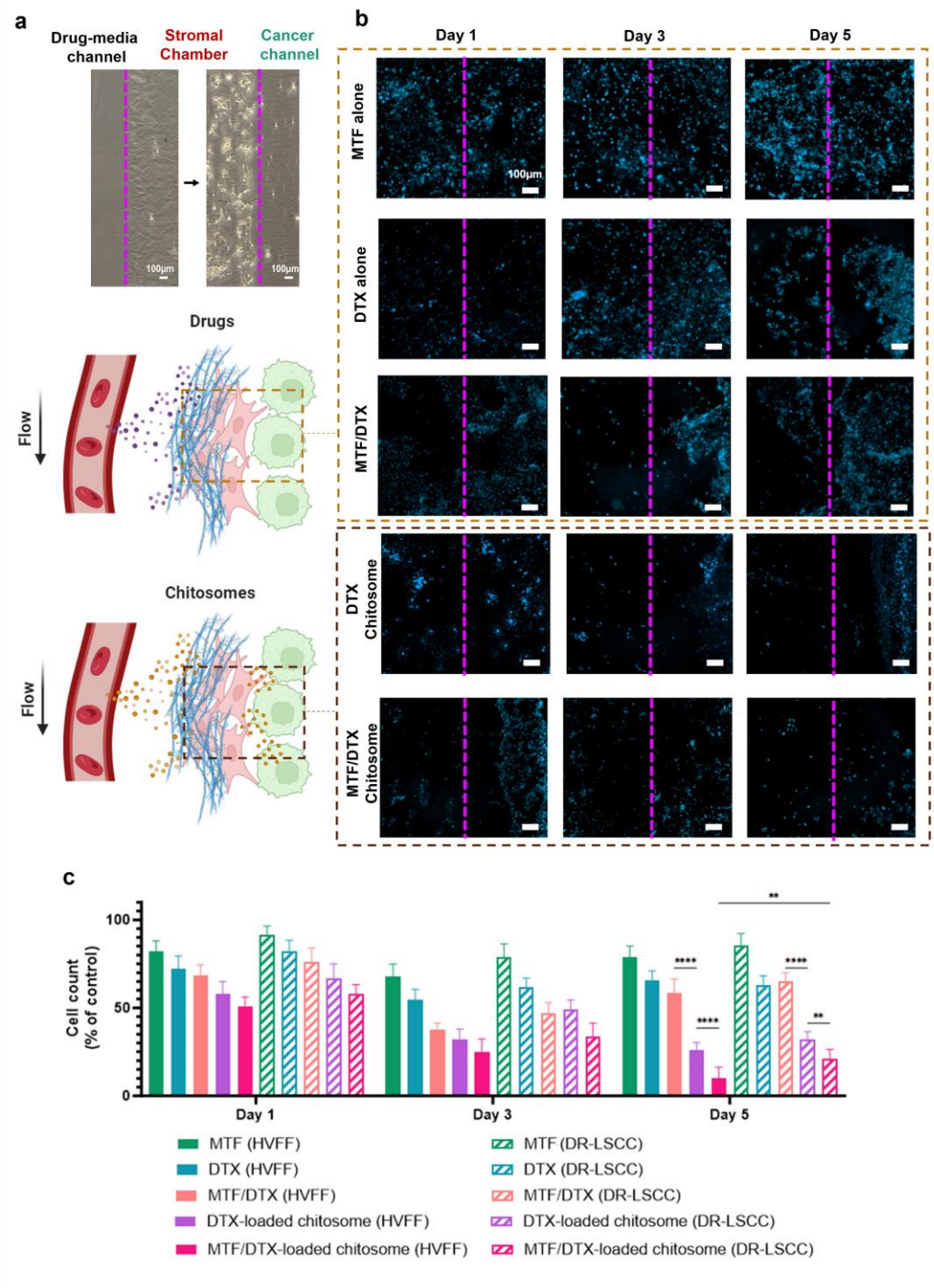

Figure 5-S9. Cytotoxic effect of the combination MTF/DTX therapy of the tumor-on-a-chip. (a) Brightfield images of the microfluidic device and schematic representation of the drug uptake. Cytotoxic effect via (b) DAPI inspection up to 5 days. Scale bar = 100 μm. Magenta line = collagen gel limit. (c) Cell count using Spot detection algorithm on DAPI images up to 5-day inspection. * $p < 0.05$, ** $p < 0.01$, **** $p < 0.0001$.

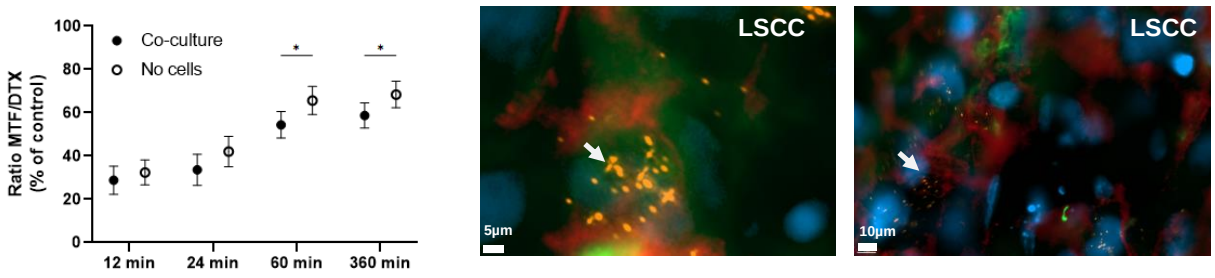

Figure 5-S10. Drug uptake of the MTF/DTX combination therapy within the microfluidic device, and fluorescent chitosome (orange) uptake by LSCC (red/EGFR, green/CK5) after 6h analysis.

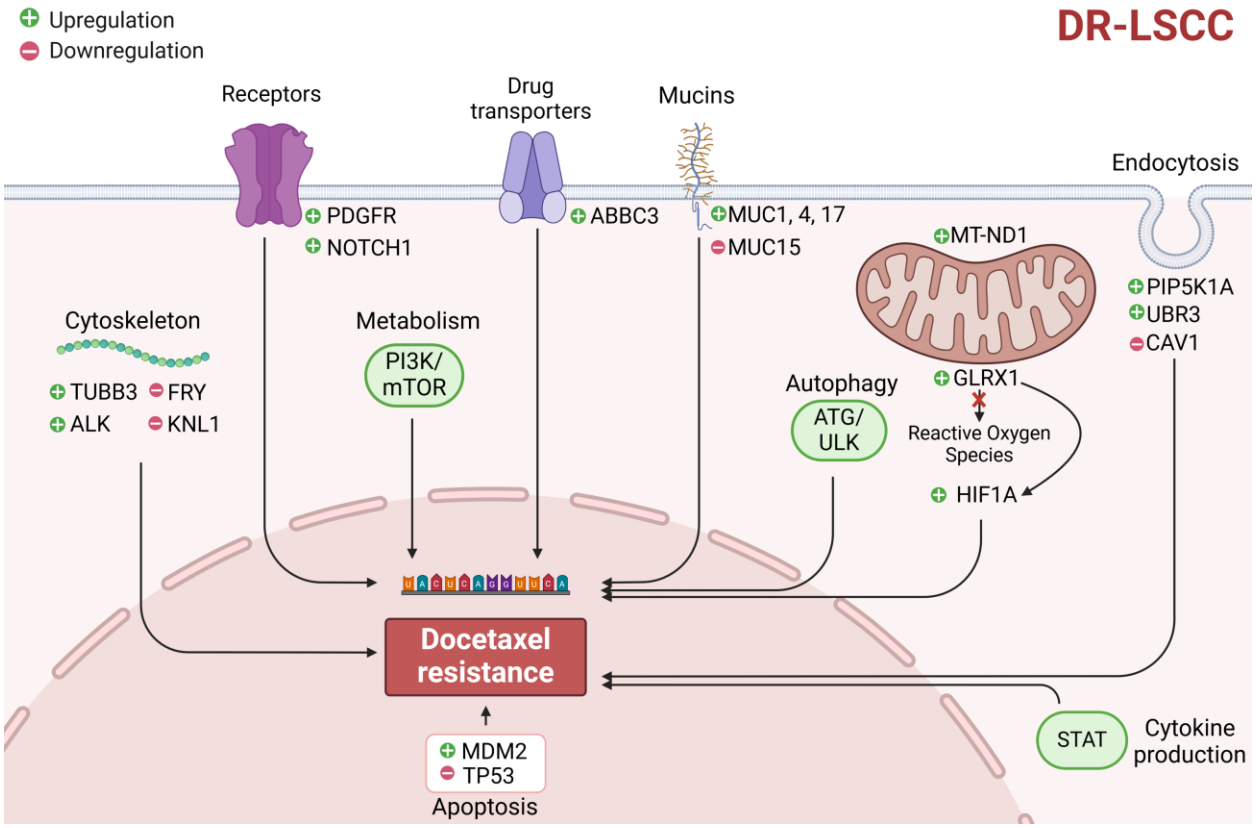

Figure 5-S11. Representative genes associated with docetaxel resistance in DR-LSCC. Figure created with BioRender.com.

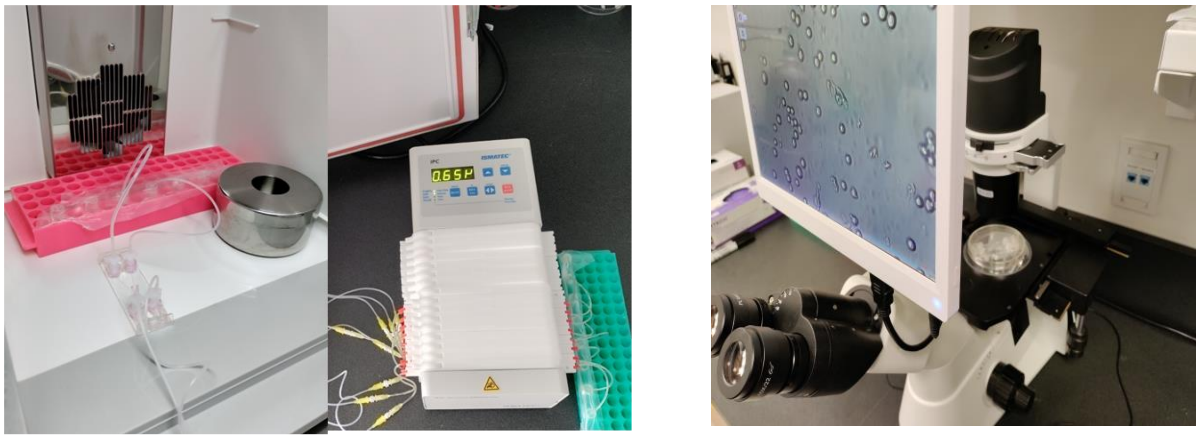

Figure 5-S12. Microfluidic setup of the cancer/stromal co-culture and cell seeding evaluation.

Video 5-S1. Supplementary video of microfluidic setup and injection of fluorescent chitosomes. Provisional link prior publication: Video S1.mp4

Chapter 6. Discussion

This thesis focused on the *in vitro* evaluation of a combination therapy to improve the treatment of DTX-resistant laryngeal carcinoma. Such combination therapy was intended to treat mucin 1-overexpressing primary tumors of locally-advanced head and neck cancer or secondary tumors (stage III/IV). A promising strategy for delivery of DTX to laryngeal cancer cells was provided by the DTX-loaded chitosome. The developed chemoresistant laryngeal cancer cells offered a model to study genotypic features in experimentally induced DTX resistance. Laryngeal-tumor-on-a-chip models were used to evaluate a potential chemosensitizing strategy with MTF in a physiological fashion. This work will expand our ability to understand the molecular nature of chemoresistance. Study limitations and future prospects of this thesis are described below.

6.1 Chitosomes as DTX drug carriers

The proposed cationic chitosome systems to deliver DTX was devoted as a mucoadhesive platform to adhere onto anionic laryngeal mucosae [1]. However, the current DTX delivery system was only tested on an *in vitro* phantom comprised of an anionic mucin dispersion. Further quantitative techniques can be implemented to study the expected mucoadhesive behavior of the chitosomes. For example, Scurti *et al*. investigated the interaction between chitosomes and intestinal cells in real time using wide-angle surface plasmon resonance (SPR) spectroscopy [2]. Compared to non-coated nanocarriers, a 10-time greater cell interaction was observed with chitosome. By implementing SPR technique, electrostatic interactions of cationic chitosomes with anionic membrane of laryngeal cancer cells would be depicted as an additional proof of the mucoadhesive properties of chitosome.

One study limitation is related to an overlook of Enhanced Permeability and Retention (EPR) effect in the proposed chitosome delivery system. Our system design was expected to allow for passive targeting and accumulation of the nanocarriers when they reach the tumor and pass through fenestrae of the 380 to 780 nm at the tumor vasculature, owning to the EPR effect [1,3]. Thus, DTX-loaded chitosomes were designed to have a nanocarrier size within the range of 100-130nm for passive targeting [1]. However, recent findings challenge the EPR notion, indicating that the process of delivering nanoparticles into tumors is more intricate. Specifically, nanoparticles could be transported into the tumor tissue by a specific subtype of endothelial cells, known as

nanoparticle transport endothelial cells, through an active transport mechanism [3,4]. In our work, we only examined the biological effect of DTX-loaded chitosomes on laryngeal cancer cells, stromal fibroblasts, and red blood cells, but not endothelial cells. A study involving the endothelial cells would further elucidate the delivery mechanism of DTX by chitosomes to laryngeal tumors and provide a more holistic approach to the complexity of the tumor microenvironment in order to formulate more effective nano-based therapeutics.

6.2 mTOR inhibitor metformin as a potential chemosensitizing agent to DTX

A significant challenge in the treatment of laryngeal cancer is the development of resistance to chemotherapy [5], particularly to the DTX. To better understand the development of the DTX-resistant treatment, we devised a DTX-resistant laryngeal cancer cell model using 4-month stepwise intermittent cell exposures to DTX. We also characterized the presumed resistant profile via transcriptomic analysis, cytotoxicity assay, and protein expression. The chemoresistant behavior of DR-LSCC was marked by the upregulation of genes associated with autophagy, microtubules, receptors, epithelial adherence, mitochondrial activity, hypoxia, cytokine production and PI3K/mTOR-related metabolism. This finding identified a pool of candidate genes, namely ATG13, TUBB3, ABCC3, CDH1, V-type, ATP6V1A, MT-ND1, HIF1A, MMP3, and DEPTOR that can be used to benchmark future preclinical chemoresistant laryngeal tumor models, through our intermittent drug exposure, CRISPR/Cas 9 technology or other gene editing strategies.

In this thesis, mTOR pathway was chosen as a DTX-resistant cell sensitization target to improve laryngeal cancer treatment. At this end, MTF was chosen given its inhibition effects on the mTOR pathway [6]. MTF is a first-line drug in the treatment of type II diabetes; however, MTF as adjuvant chemosensitizing treatment for non-diabetics cancer patients is still on debate because of its specificity to increase insulin levels when it is not needed debate [7]. The strategy of using MTF was also that this drug induces several metabolic changes in cancer cells, including a reduction in glucose oxidation and an increased reliance on reductive glutamine metabolism [8].

Other mTOR inhibitors can be considered to sensitize laryngeal cancer cells to DTX, repurposing other types of FDA-approved mTOR inhibitors may be beneficial for cancer overtreatment. For example, sensitizing effect of everolimus, a rapamycin analogue used as an immunosuppressant in organ transplantation, has been investigated for head and neck cancer [9–11]. To date, phase

I/II clinical trial data support the use of everolimus as adjuvant therapy for cisplatin, docetaxel, and cetuximab in locally advanced squamous cell carcinomas of head and neck [9–11]. These results provide some evidence that everolimus may be another potential candidate to inhibit mTOR and sensitize cells to DTX treatment, avoiding the controversy of the MTF's effect on non-diabetic cancer patients.

6.3 Tumor-on-a-chip as a biomimetic *in vitro* system for drug testing

We used a 2-channel microfluidic device to co-culture stromal laryngeal cells and DR-LSCC as a laryngeal tumor-on-a-chip model in this study. By using this chip model, we could mimic the tumor hypoxic core, in which cells showed hypoxic and oxidative stress behaviors. We were able to control the delivery of the MTF/DTX-loaded chitosomes through the microchannel. In this study, we only implemented two cell types and two drugs sequentially flowing in the same channel. However, multicellular and multidrug studies have been explored in organ-on-a-chip research of lung, breast, liver, colorectal, and thyroid cancers [12]. For example, Riley *et al* [13] investigated a combined JNK inhibitor and etoposide drugs on cultured patient-derived thyroid carcinoma tumor slices in a single tissue well for up to 4 day-inspection. Head and neck tumors are heterogenous with a unique tumor microenvironment and have strong immune-stromal-tumor interactions (cell-cell crosstalk) [5]. For example, patient-derived tumor slices from thyroid carcinoma were cultured in a single tissue well to study a combined JNK inhibitor and etoposide drugs up to 4 days [13]. Their roles in drug sensitivity and resistance are under-studied for laryngeal cancer. For that reason, culturing laryngeal-tumor slices on chip models may support the analysis of multi-cellular thick biological samples.

Further, this study has only focused on the cancer-stromal interface to echo the laryngeal tumor core. However, microfluidic platforms facilitate the concurrent compartmentalization of various cell populations while maintaining a continuous flow of culture media [5,14]. To further emulate the tumor core, different cell types can be incorporated into the tumor-on-a-chip model. Tumor-associated macrophages are found in the tumor core where sequester nanoparticles [3,15]. For example, in a pancreatic cancer-on-a-chip study that focused on the triculture of cancer, stellate, and macrophages in a 2-chamber device [16]. A 3-day multidrug immunostaining evaluation involves a perfusion of gemcitabine, liposomal clodronate, and all-trans retinoic acid. Results

showed a significant 2-fold increase in the chemotherapy effect on the tumor-on-a-chip model compared to no treatment controls. Macrophage incorporation within the microfluidic setup would then improve our laryngeal tumor-on-a-chip model to further study preclinical multidrug cytotoxicity.

6.4 Translational potential

Overtreatment in laryngeal cancer is a pressing issue due to the considerable physical and emotional side effects experienced by patients. A study conducted by Saghafi *et al.* [17] elucidated patients' experiences during the treatment of head and neck cancer, revealing the adverse symptoms and emotional challenges encountered. Overly aggressive treatments, such as extensive surgery and high-dose chemotherapy, contribute to these difficulties. De-escalation of treatment is essential to minimize adverse effects while maintaining therapeutic efficacy [18]. Current approaches to de-escalation involve refining the selection of patients for aggressive treatment and optimizing therapies [18]. Strategies such as elective nodal volume and dose de-escalation have already been explored in clinical trials [19]. These efforts aim to strike a balance between effective cancer control and preserving patients' quality of life [17].

Laryngeal cancer patients may benefit from the use of chemosensitizers and drug delivery systems. To sensitize cells, we evaluated 1mM of the metformin [20,21] as performed in our *in vitro* studies. The implemented dose of 1mM to sensitize laryngeal cells is less than the 500-2500mg MTF daily prescription for diabetic patients [22]. Oral intake of MTF is hypothesized as chemosensitizing treatment, but further animal and clinical studies are required to validate MTF administration route. Our proposed delivery systems would allow to convey necessary therapeutic doses, and reduce exposure to adjacent healthy tissues and minimize the likelihood of side effects [23]. We proposed the use of lipid nanoparticles to encapsulate 1µM of docetaxel as performed in our *in vitro* cytotoxic studies [1]. Such concentrations are lower than those reported in systemic delivery (75mg/m^2 docetaxel every 3 weeks [24]) to reduce the risk of overtreatment. In contrast to non-coated anionic liposomes, the presence of a chitosan coating on the chitosomes acted as an external physical barrier, which resulted in a prolonged release of DTX [1] as reported in the literature [25,26]. This release serves as a slow and constant therapy to avoid frequent reinjection of the drug within tumor via the proposed locoregional intra-arterial delivery [1] or systemic delivery

potentially targeting Mucin 1-overexpressing metastatic tumors. The reason of the presumed metastatic targeting relates to our DTX-loaded chitosomes showing electrostatic interaction with Mucin 1-rich dispersion via turbidimetry and absorbance respective analyses [1], which may result in the chitosomes being internalized by secondary tumors, i.e., metastasized tumors.

In addition, since liver and renal impairment influence docetaxel pharmacokinetics [27,28] a locoregional administration of drug-loaded chitosome would circumvent that treatment impediment and potential systemic overtreatment by reducing systemic delivery. Research indicates that after intravenous administration, a significant portion of nanoparticles, ranging from 30% to 99%, is retained in the liver and spleen [3,29], and only as few as 1 in 100,000 of the injected nanoparticles reach tumor cancer cells [3,29]. Since our DTX-loaded chitosome is designed for locoregional delivery of chemotherapeutics attributed to its mucoadhesive properties, it could serve a viable option to support localized treatments of laryngeal cancer. Further, considering intravenous approaches for our chitosome delivery system, *in vivo* models would be required to assess the biodistribution of the DTX-loaded chitosomes, where liver and spleen would be the target organs for such analysis. Taken into consideration intra-arterial delivery, organ toxicity in the liver and spleen must be analyzed to determine nonspecific accumulation of nanoparticles and pharmacokinetics since treatment may circulate throughout the body until clearance [3,28,29].

6.5 Future prospects

Ample opportunities exist to further customize and engineer proposed biomaterials and devices that will enhance their practicality and benefits in clinical applications. Examples include chitosome delivery approaches, engineered chemoresistance cell lines, and air-liquid microfluidic devices (**Figure 6-1**). A high-level summary and key hypotheses of these ongoing and future works are detailed below.

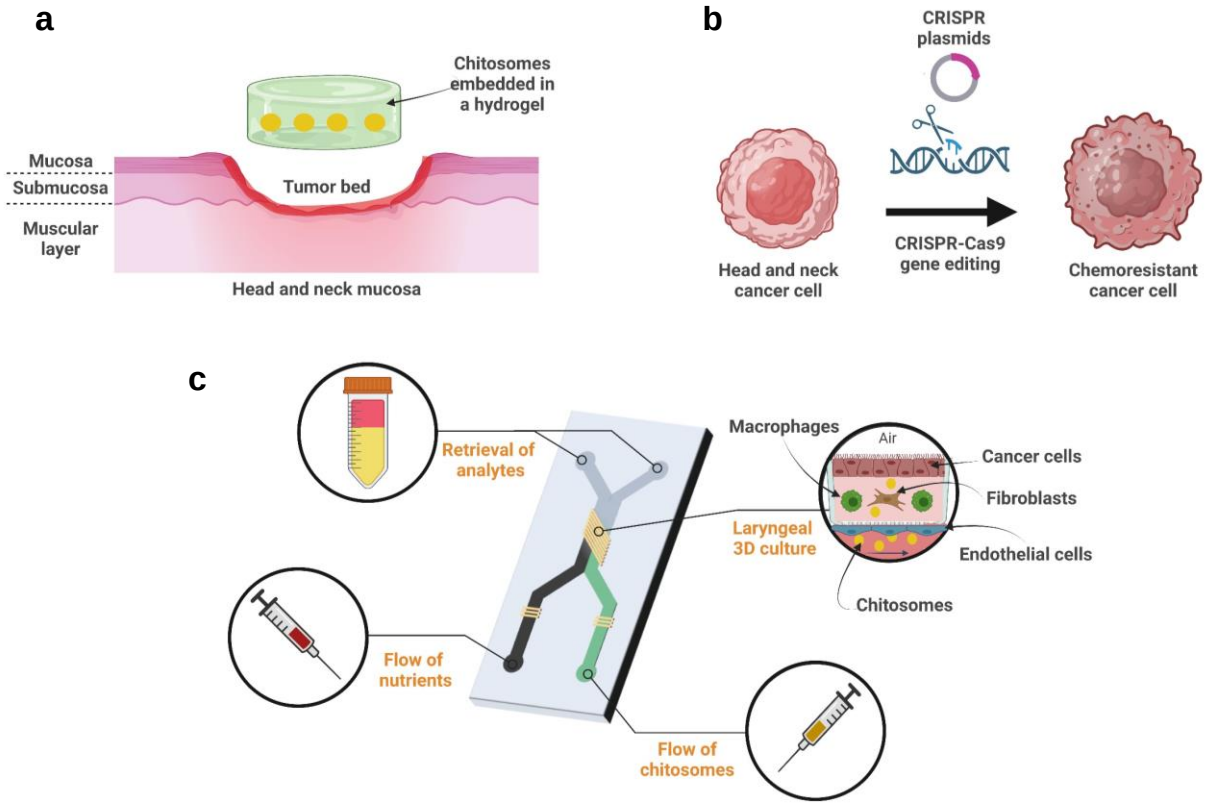

Figure 6-1. Future prospects of this thesis work. (a) Postoperative administration of chemotherapy-loaded chitosomes embedded in a hydrogel. (b) CRISPR-Cas 9 system for chemoresistant gene editing on head and neck cancer cells. (c) Laryngeal-on-a-chip with an air-liquid interface. Image created using BioRender.com.

6.5.1 Administration of chemotherapy-loaded chitosomes

Nano-based drug delivery systems are proposed to improve the biodistribution, pharmacokinetics and pharmacodynamics of chemotherapy agents [30–32] like DTX. We expect the volume of the DTX-loaded chitosomes in solution would be up to 1cc [33–35] to keep the airway patency and reduce the tumor size for further surgical intervention. By administering the chitosome locoregionally at the laryngeal site, this rapid entry of nanoparticles may result in a faster onset of therapeutic effects with reduced systemic side effects. Ongoing nanocarriers studies are exploring localized systems that bypass systemic circulation, thereby mitigating the associated drug toxicities throughout the body [36].

Postoperative tumor therapy may also be an alternative administration for chitosomes [37–39]. Chitosomes may be loaded into hydrogel/nanocomposites for local application after tumor

resection (**Figure 6-1a**). Inhibition of cancer relapse may be facilitated by adhering chitosome-containing hydrogels on the defect after tumor resection, in which has been proposed in tumor-bearing mice studies of cervical [38] and breast [37] cancers. In our study, we restrained from using animal models concerning the hurdles of laryngeal carcinogenesis that may lead the animal subject to asphyxiate. However, having an ideal laryngeal cancer animal model, the postoperative tumor approach of chitosome delivery could be further investigated, where the expected therapeutic effect of the chitosome-containing hydrogels would last in the tumor bed between 21 and 24 days [38, 37].

6.5.2 Development of novel chemoresistant cancer cell models

In this thesis, a stepwise intermittent method was implemented to induce DTX resistance on laryngeal cancer cells. Methods for preserving cell lines resistant to drugs are delineated, encompassing strategies such as sustained exposure to chemotherapy, intermittent chemotherapy pulse treatments, or reverting to original drug-resistant cell models [40,41]. The variability observed in drug-resistant models derived from identical parent cell lines treated with the same chemotherapy agent is investigated, particularly in relation to ABC subfamily [40,41]. The diversity within drug-resistant cell lines mirrors the heterogeneity observed in clinical drug resistance [40]. However, techniques other than our intermittent methods could be implemented to induce drug resistance in cancer cells.

Gene editing techniques like CRISPR/Cas 9 can be used to induce genotypical changes in cells [5], which can be applied for chemoresistance induction (**Figure 6-1b**). CRISPR/Cas9 genome editing comprises the deployment of a single-effector Cas9 protein for inducing double-stranded breaks in the designated DNA target, and a single guide RNA to direct the Cas9 complex to the specific genomic region of interest [5,42,43]. Nevertheless, identifying molecular targets for inducing chemoresistance is crucial to develop resistant cell models using CRISPR/Cas 9 technology. For chemoresistant induction in HNC cells, gene editing can be directed towards the EGFR/PI3K/mTOR pathway [5]. Another potential marker for inducing chemoresistance is Ly6D [44]. The surface marker Ly6D is associated with laryngeal chemoresistance through the miR-509/β-catenin signaling pathway [44], making it a potential target for inducing treatment resistance via gene editing on laryngeal cancer.

6.5.3 Incorporation of air-liquid interface in laryngeal tumor-on-a-chip models

Recent microfluidic platforms designed to mimic airways, especially those incorporating an air-liquid interface feature [45–48], are well-suited for modeling HNC [5] (**Figure 6-1c**). This suitability arises from the laryngeal anatomical site that represents a constant air exposure to laryngeal mucosae [5]. Implementing a microfluidic platform that incorporates an air-liquid interface for multidrug drug screening [5] may be a valuable to laryngeal-tumor-on-a-chip model. The presence of air-liquid interface is essential to study cancer biology [49]. The therapeutic effect of drugs may have a different impact considering if cells are exposed to air-liquid interfaces or just conventional media-related cultures.

The air-liquid interface epithelial culture model may exhibit different therapy response when compared to the *in vivo* epithelium [50]. Considering that air-liquid interface cultures mimic essential structural, biochemical, and operational aspects of the natural epithelium, such as the production of mucus and the movement of cilia [50]. However, chip cultures may approximate the emulation of such *in vivo* epithelial conditions in a monitorable fashion. To accomplish such a task, for example, an air-liquid interface methodology was described to culture 3D tumoroids of lung adenocarcinoma cells using transwell inserts in 24-well plates [51]. In a study for pulmonary effect of manufactured nanomaterials, a similar transwell-based methodology was implemented to develop a pulmonary air-liquid interface to test nanoparticle doses [52]. Results from the 30min nanoparticle exposure showed that a 0.17μg/cm^2 dose of TiO_2 nanoparticles caused a 5-fold increased cytotoxicity in the pulmonary air-liquid interface compared to controls exposed to humidified clean air. With that in mind, such transwell-based epithelial cultures may be adapted using microfluidic devices to test chitosome-driven therapies for laryngeal cancer treatment.

Chapter 7. Conclusion

The overall objective of the presented thesis was to evaluate a de-escalation strategy for chemoresistant laryngeal cancer. Chitosan-coated liposomes was developed as a drug delivery system for DTX. The application of cationic chitosan coating on anionic nanoliposomes enabled them to improve the DTX retention and mucoadhesiveness in comparison to non-coated nanocarriers. We also developed a cell line of DTX-resistant laryngeal squamous cell carcinoma, namely, DR-LSCC, using a step-wise drug escalating approach. Our DR-LSCC showed comparable transcriptomic and phenotypic profiles as known in head and neck cancer literature. We then evaluated the cytotoxicity effects of MTF and DTX-loaded chitosomes on resistant laryngeal cancer cells and stromal vocal fold fibroblasts that were co-cultured on microfluidic chips. This laryngeal-tumor-on-a-chip emulated hypoxic tumor core that was known as one key factor affecting drug sensitivity in cancer cells. We observed that in combination with MTF, DTX-encapsulated in chitosomes exhibited sustained and controlled release, leading to higher cell death in DR-LSCC and stromal vocal fold fibroblasts compared to non-encapsulated drug treatments. In summary, overcoming chemoresistance is a vital step towards improving laryngeal cancer treatment outcomes and patient's quality of life. In this thesis project, the proposed drug delivery systems, a chemoresistant cell line and a laryngeal-tumor-on-a-chip platform will serve as useful experimental tools for basic research in understanding chemoresistance, as well as, translated research in novel drug design for restoring tumor sensitivity in future.

References

1. Moya-Garcia CR, Li-jessen NYKL, Tabrizian M. Chitosomes Loaded with Docetaxel as a Promising Drug Delivery System to Laryngeal Cancer Cells : An In Vitro Cytotoxic Study. Int J Mol Sci. 2023;24(12):9902.

2. Scurti E, Martins JP, Celia C, Palumbo P, Lombardi F, Iannotta D, et al. In Vitro Characterization and Real-Time Label-Free Assessment of the Interaction of Chitosan-Coated Niosomes with Intestinal Cellular Monolayers. Langmuir. 2023;39(23):8255–66.

3. Paun RA, Jurchuk S, Tabrizian M. A landscape of recent advances in lipid nanoparticles and their translational potential for the treatment of solid tumors. Bioeng Transl Med. 2023;(September):1–34.

4. Kingston BR, Lin ZP, Ouyang B, Macmillan P, Ngai J, Syed AM, et al. Specific Endothelial Cells Govern Nanoparticle Entry into Solid Tumors. ACS Nano. 2021;15(9):14080–94.

5. Moya-Garcia CR, Okuyama H, Sadeghi N, Li J, Tabrizian M, Li-Jessen NYK. In vitro models for head and neck cancer : Current status and future perspective. Front Oncol. 2022;12:3691.

6. Jin Y, Qin X. Comprehensive analysis of transcriptome data for identifying biomarkers and therapeutic targets in head and neck squamous cell carcinoma. Ann Transl Med. 2020;8(6):282–282.

7. Bouland C, Eynden X Vanden, Lalmand M, Buset T, Yanni A, Javadian R, et al. Preventive and Therapeutic Effect of Metformin in Head and Neck Cancer : A Concise Review. J Clin Med. 2023;12(9):6195.

8. Hua Y, Zheng Y, Yao Y, Jia R, Ge S, Zhuang A. Metformin and cancer hallmarks: shedding new lights on therapeutic repurposing. J Transl Med [Internet]. 2023;21(1):1–20.

9. Marquard FE, Jücker M. PI3K/AKT/mTOR signaling as a molecular target in head and neck cancer. Biochem Pharmacol [Internet]. 2020;172:113729.

10. Patel J, Nguyen SA, Ogretmen B, Gutkind JS, Nathan C, Day T. mTOR inhibitor use in head and neck squamous cell carcinoma: A meta-analysis on survival, tumor response, and toxicity. Laryngoscope Investig Otolaryngol. 2020;5(2):243–55.

11. Nathan CAO, Hayes DN, Karrison T, Harismendy O, Flores JM, Moore-Medlin T, et al. A Randomized Multi-institutional Phase II Trial of Everolimus as Adjuvant Therapy in Patients with Locally Advanced Squamous Cell Cancer of the Head and Neck. Clin Cancer Res. 2022;28(23):5040–8.

12. Dsouza VL, Kuthethur R, Kabekkodu SP, Chakrabarty S. Organ-on-Chip platforms to study tumor evolution and chemosensitivity. Biochim Biophys Acta - Rev Cancer [Internet]. 2022;1877(3):188717.

13. Riley A, Green V, Cheah R, McKenzie G, Karsai L, England J, et al. A novel microfluidic device capable of maintaining functional thyroid carcinoma specimens ex vivo provides a new drug screening platform. BMC Cancer. 2019;19(1):1–13.

14. Fitzgerald AA, Li E, Weiner LM. 3D culture systems for exploring cancer immunology. Cancers (Basel). 2021;13(1):1–19.

15. Lin ZP, Nguyen LNM, Ouyang B, Macmillan P, Ngai J, Kingston BR, et al. Macrophages Actively Transport Nanoparticles in Tumors after Extravasation. ACS Nano. 2022;16(4):6080–92.

16. Haque MR, Wessel CR, Leary DD, Wang C, Bhushan A, Bishehsari F. Patient-derived pancreatic cancer-on-a-chip recapitulates the tumor microenvironment. Microsystems Nanoeng. 2022;8(1).

17. Saghafi E, Andås CA, Bernson J, Kjeller G. Patients' experiences of adverse symptoms, emotions, and coping strategies in connection to treatment of head and neck cancer - an interview study. BMC Oral Health. 2023;23(1):1–13.

18. Rosenberg AJ, Vokes EE. Optimizing Treatment De-Escalation in Head and Neck Cancer: Current and Future Perspectives. Oncologist. 2021;26(1):40–8.

19. Sher DJ, Sen N, Shah JL, Pham NL, Subramaniam R, Moore W, et al. Recurrence and Quality-of-Life Following Elective Nodal Volume and Dose De-Escalation for Oropharyngeal and Laryngeal Cancer: Initial Results from the Infield Trial. Int J Radiat Oncol [Internet]. 2019;105(1):S53–4.

20. Mayer MJ, Klotz LH, Venkateswaran V. Evaluating Metformin as a Potential Chemosensitizing Agent when Combined with Docetaxel Chemotherapy in Castration-resistant Prostate Cancer Cells. Anticancer Res. 2017;37(12):6601–7.

21. Zhang P, Zhao S, Lu X, Shi Z, Liu H, Zhu B. Metformin enhances the sensitivity of colorectal cancer cells to cisplatin through ROS-mediated PI3K/Akt signaling pathway. Gene [Internet]. 2020;745(November 2019):144623.

22. Chung H, Oh J, Yoon SH, Yu KS, Cho JY, Chung JY. A non-linear pharmacokinetic-pharmacodynamic relationship of metformin in healthy volunteers: An open-label, parallel group, randomized clinical study. PLoS One. 2018;13(1):1–11.

23. Laracuente ML, Yu MH, McHugh KJ. Zero-order drug delivery: State of the art and future prospects. J Control Release [Internet]. 2020;327(September):834–56.

24. Sadeghi N, Khalife S, Mascarella MA, Ramanakumar A V., Richardson K, Joshi AS, et al. Pathologic response to neoadjuvant chemotherapy in HPV-associated oropharynx cancer. Head Neck. 2020;42(3):417–25.

25. Alshraim MO, Sangi S, Harisa GI, Alomrani AH, Yusuf O, Badran MM. Chitosan-coated flexible liposomes magnify the anticancer activity and bioavailability of docetaxel: Impact on composition. Molecules. 2019;24(2):1–14.

26. Kim JH, Shin DH, Kim JS. Preparation, characterization, and pharmacokinetics of liposomal docetaxel for oral administration. Arch Pharm Res [Internet]. 2018;41(7):765–75.

27. Clarke SJ, Rivory LP. Clinical pharmacokinetics of docetaxel. Clin Pharmacokinet. 1999;36(2):99–114.

28. Nieuweboer AJM, de Morrée ES, de Graan AJM, Sparreboom A, de Wit R, Mathijssen RHJ. Inter-patient variability in docetaxel pharmacokinetics: A review. Cancer Treat Rev [Internet]. 2015;41(7):605–13.

29. Dai Q, Wilhelm S, Ding D, Syed AM, Sindhwani S, Zhang Y, et al. Quantifying the Ligand-Coated Nanoparticle Delivery to Cancer Cells in Solid Tumors. ACS Nano. 2018;12(8):8423–35.

30. Kalaydina RV, Bajwa K, Qorri B, Decarlo A, Szewczuk MR. Recent advances in "smart" delivery systems for extended drug release in cancer therapy. Int J Nanomedicine. 2018;13:4727–45.

31. Mehrotra N, Gupta M, Kovar A, Meibohm B. The role of pharmacokinetics and pharmacodynamics in phosphodiesterase-5 inhibitor therapy. Int J Impot Res. 2007;19(3):253–64.

32. Singh G, Pai RS. Pharmacokinetics and in vivo biodistribution of optimized PLGA nanoparticulate drug delivery system for controlled release of emtricitabine. Drug Deliv. 2014;21(8):627–35.

33. Zeleník K, Formánek M, Walderová R, Formánková D, Komínek P. Five-year results of vocal fold augmentation using autologous fat or calcium hydroxylapatite. Eur Arch Oto-Rhino-Laryngology [Internet]. 2021;278(4):1139–44.

34. Zeleník K, Walderová R, Kučová H, Jančatová D, Komínek P. Comparison of long-term voice outcomes after vocal fold augmentation using autologous fat injection by direct microlaryngoscopy versus office-based calcium hydroxylapatite injection. Eur Arch Oto-Rhino-Laryngology. 2017;274(8):3147–51.

35. Wang CC, Wu SH, Tu YK, Lin WJ, Liu SA. Hyaluronic Acid Injection Laryngoplasty for Unilateral Vocal Fold Paralysis-A Systematic Review and Meta-Analysis. Cells. 2020;9(11).

36. Hariharan A, Tran SD. Localized Drug Delivery Systems: An Update on Treatment Options for Head and Neck Squamous Cell Carcinomas. Pharmaceutics. 2023;15(7).

37. Li R, Lin Z, Zhang Q, Zhang Y, Liu Y, Lyu Y, et al. Injectable and in Situ-Formable Thiolated Chitosan-Coated Liposomal Hydrogels as Curcumin Carriers for Prevention of in Vivo Breast Cancer Recurrence. ACS Appl Mater Interfaces. 2020;12(15):17936–48.

38. Xiao L, Xu W, Huang L, Liu J, Yang G. Nanocomposite pastes of gelatin and cyclodextrin-grafted chitosan nanoparticles as potential postoperative tumor therapy. Adv Compos Hybrid Mater [Internet]. 2023;6(1):1–14.

39. Kefayat A, Vaezifar S. Biodegradable PLGA implants containing doxorubicin-loaded chitosan nanoparticles for treatment of breast tumor-bearing mice. Int J Biol Macromol [Internet]. 2019;136:48–56.

40. McDermott M, Eustace AJ, Busschots S, Breen L, Crown J, Clynes M, et al. In vitro development of chemotherapy and targeted therapy drug-resistant cancer cell lines: A practical guide with case studies. Front Oncol. 2014;4 MAR(March).

41. Abdelmaksoud NM, Abulsoud AI, Doghish AS, Abdelghany TM. From resistance to resilience: Uncovering chemotherapeutic resistance mechanisms; insights from established models. Biochim Biophys Acta - Rev Cancer [Internet]. 2023;1878(6):188993.

42. Uddin F, Rudin CM, Sen T. CRISPR Gene Therapy: Applications, Limitations, and Implications for the Future. Front Oncol. 2020;10(August).

43. Asmamaw M. Biologics : Targets and Therapy Mechanism and Applications of CRISPR / Cas-9-Mediated Genome Editing. 2021;353–61.

44. Wang J, Sheng N, Li Y, Fan Y, Nan X, Fu R. Ly6D facilitates chemoresistance in laryngeal squamous cell carcinoma through miR-509 / β-catenin signaling pathway. 2023;13(5):2155–71.

45. Park JY, Ryu H, Lee B, Ha DH, Ahn M, Kim S, et al. Development of a functional airway-on-a-chip by 3D cell printing. Biofabrication. 2019;11(1).

46. Si L, Bai H, Rodas M, Cao W, Oh CY, Jiang A, et al. A human-airway-on-a-chip for the rapid identification of candidate antiviral therapeutics and prophylactics. Nat Biomed Eng [Internet]. 2021;5(8):815–29.

47. Si L, Prantil-Baun R, Benam KH, Bai H, Rodas M, Burt M, et al. Discovery of influenza drug resistance mutations and host therapeutic targets using a human airway chip. BioRxiv. 2019;685552.

48. Benam KH, Villenave R, Lucchesi C, Varone A, Hubeau C, Lee HH, et al. Small airway-on-a-chip enables analysis of human lung inflammation and drug responses in vitro. Nat Methods. 2016;13(2):151–7.

49. Cristo L Di, Sabella S. Cell Cultures at the Air–Liquid Interface and Their Application in Cancer Research. In: Cancer Cell Culture Methods in Molecular Biology. New York, NY: Springer US.; 2023. p. 41–64.

50. Lee RE, Reidel B, Nelson MR, Macdonald JK, Kesimer M, Randell SH. Air-Liquid interface cultures to model drug delivery through the mucociliary epithelial barrier. Adv Drug Deliv Rev [Internet]. 2023;198:114866.

51. Movia D, Prina-Mello A. A Method for Culturing 3D Tumoroids of Lung Adenocarcinoma Cells at the Air–Liquid Interface. In: Cancer Cell Culture: Methods and Protocols. New York, NY: Springer US.; 2023. p. 173–8.

52. Diabaté S, Armand L, Murugadoss S, Dilger M, Fritsch-Decker S, Schlager C, et al. Air–liquid interface exposure of lung epithelial cells to low doses of nanoparticles to assess pulmonary adverse effects. Nanomaterials. 2021;11(1):1–23.